FEDERAL UNIVERSITY OF CEARÁ

CENTER OF TECHNOLOGY

DEPARTAMENT OF HYDRAULICS AND ENVIRONMENTAL ENGINEERING

DOCTORAL DEGREE IN CIVIL ENGIREERING: WATER RESOURCES

UDINART PRATA RABELO

MODELING HYDROLOGICAL DYNAMICS IN A DRYLAND CATCHMENT WITH DENSE RESERVOIR NETWORKS

FORTALEZA

2025

UDINART PRATA RABELO

MODELING HYDROLOGICAL DYNAMICS IN A DRYLAND CATCHMENT WITH DENSE RESERVOIR NETWORKS

Thesis submitted to the Graduate Program in Civil Engineering: Water Resources of the Center of Technology of the Federal University of Ceará, as partial requirement for obtaining the title of Doctor in Civil Engineering. Concentration Area: Water Resources.

Advisor: Prof. Iran Eduardo Lima Neto, Ph.D.

Co-advisor: Prof. Alexandre Cunha Costa, Ph.D.

Co-advisor: Prof. Jörg Dietrich, Ph.D.

FORTALEZA
2025

Dados Internacionais de Catalogação na Publicação
Universidade Federal do Ceará
Sistema de Bibliotecas
Gerada automaticamente pelo módulo Catalog, mediante os dados fornecidos pelo(a) autor(a)

R114m Rabelo, Udinart Prata.
Modeling Hydrological Dynamics in a Dryland Catchment with Dense Reservoir Networks / Udinart Prata Rabelo. – 2025.
189 f. : il. color.

Tese (doutorado) – Universidade Federal do Ceará, Centro de Tecnologia, Programa de Pós-Graduação em Engenharia Civil: Recursos Hídricos, Fortaleza, 2025.
Orientação: Prof. Dr. Prof. Dr. Iran Eduardo Lima Neto.
Coorientação: Prof. Dr. Alexandre Cunha Costa.

1. dryland modeling. 2. SWAT model. 3. high-density reservoir network. 4. hydrological connectivity. 5. extended droughts. I. Título.

CDD 627

UDINART PRATA RABELO

MODELING HYDROLOGICAL DYNAMICS IN DRYLAND CATCHMENTS WITH SOIL AND WATER ASSESSMENT TOOL (SWAT)

Thesis submitted to the Water Resources and Environmental Sanitation Post-Graduate Program of the Technology Center at the Federal University of Ceará, as partial requirement for the doctor degree in Civil Engineering. Concentration Area: Water Resources.

Approved on: 01/17/2025

EXAMINING COMMITTEE

Prof. Dr. Iran Eduardo Lima Neto (Advisor)
Federal University of Ceará (UFC)

Prof. Dr. Alexandre Cunha Costa (Co-advisor)
University of International Integration of the Afro-Brazilian Lusophony (UNILAB)

Prof. Dr. Jörg Dietrich (Co-advisor)
Leibniz University Hannover (LUH)

Prof. Dr. Danielle de Almeida Bressiani
Federal University of Pelotas (UFPel)

Dr. Germano Gondim Ribeiro Neto
University of Bristol (UB)

Prof. Dr. Paulo Tarso Sanches de Oliveira
Federal University of Mato Grosso do Sul (UFMS)

Prof. Dr. Walter Collischonn
Federal University of Rio Grande do Sul (UFRGS)

To God.

To my parents, Ticiana and Flávio.

To my brother, Flávio Filho.

To my wife, Dalila.

ACKNOWLEDGEMENTS

To God, for the gift of life.

I would like to thank my wife, Dalila, my parents, Ticiana and Flávio, my brother, Flávio Filho, my grandmother, Conceição, and my aunts, Renata and Tatiana for all their love and affection, for their support and encouragement throughout the years.

I am very grateful to my supervisors Prof. Dr. Iran Eduardo Lima Neto and Prof. Dr. Alexandre Cunha Costa for their great help and contribution, for the encouragement they has given me over the last six years. Their support throughout the entire course of my studies helped me overcome many obstacles. It was a privilege to work under their supervision.

I would like to thank my professors in the Ph.D. program in Water Resources at Department of Hydraulic and Environmental Engineering (DEHA), who have provided me with a solid foundation and a deep understanding of water-related issues, sharing their knowledge with great dedication.

I would like to express my gratitude to Prof. Dr. Jörg Dietrich, for welcoming me to Leibniz University Hannover (LUH) for six months, where I had the opportunity to further my understanding of hydrological modeling. It was a pleasure to work with him and other researchers and to share this invaluable experience at LUH.

I would also like to thank the teams at the Ceará Water Resources Management Company (COGERH) and at the National Agency of Water and Sanitation (ANA), who generously provided assistance with river flow data and reservoir volumes in Ceará.

My sincere thanks to my colleagues at the Federal Institute of Ceará (IFCE), who supported me in fulfilling my teaching responsibilities and allowed the flexibility needed to complete the coursework and participate in the sandwich Ph.D. program in Germany.

Lastly, I would like to acknowledge my friends from both graduate and post-graduate studies, who have accompanied me on this journey and motivated me to continue striving for my goals.

“Success is born of desire, determination and persistence in reaching a goal. Even if you don't reach the target, those who seek it out and overcome obstacles will at the very least do admirable things.” (José de Alencar)

ABSTRACT

Drylands represent some of the most vulnerable ecosystems to climate change and anthropogenic activities. Hydrological modeling, particularly through tools like the Soil and Water Assessment Tool (SWAT), serves as an essential instrument for addressing practical challenges such as supporting decision-making in water resource management and hydrological forecasting for drylands. However, there remains substantial scope for evaluating the performance of such models in dryland watersheds, especially those characterized by dense reservoir networks, and assessing their behavior during consecutive years of drought as well as during years with extreme rainfall events. Furthermore, during periods of extreme aridity, particularly severe droughts, the models face significant challenges in accurately representing crucial processes, including runoff transmission losses, evapotranspiration rates, and anthropogenic influences. This thesis aims to advance the application of the SWAT model in dryland catchments by addressing its ability to simulate the hydrological processes of these regions, particularly in the context of dense reservoir networks and their impact on water retention across interannual drought and flood scenarios. Additionally, the thesis evaluates the model's performance during an extended drought and their hydrological recovery period in a more arid and warmer climate decade, subsequent to a previously calibrated time series. The study was conducted in the Conceição River Catchment (3,347 km²), located in Ceará, northeastern Brazil. This catchment contains 230 reservoirs (0.068 reservoirs per km²), with storage capacities ranging from less than 0.01 hm³ to 52 hm³. The analysis was based on a 40-year dataset of climate and observed runoff, with 30 years used for model calibration and an additional 10 years for extending the time series to include an extreme drought period. The key findings of this research are as follows: (i) The model's daily performance was found to be acceptable (Nash-Sutcliffe Efficiency = 0.63, Kling-Gupta Efficiency = 0.81 and Percent BIAS = 0.53%), demonstrating reliability in representing peak flows during wet years, periods of no flow, and the rising limb of the hydrograph. While small reservoirs (less than 0.01 hm³) were found to reduce streamflow, their overall impact on catchment retention was minimal, with water retention rates of 2% in wet years and 9% in dry years; (ii) The reduction in runoff due to the increased number of small reservoirs was more pronounced during dry years (up to 30%) compared to wet years (up to 8%). This reduction also escalated over consecutive years of drought, a result obtained in the scenario analysis, considering reservoir densities ranging from 0 to 3 reservoirs per km² within the catchment, potentially exacerbating the effects of prolonged droughts; (iii) Despite the model's strong performance over a 30-year climatic series, which

included periods of severe drought, it struggled to accurately predict streamflow during the extreme drought and the subsequent recovery phase, showing a marked decline in performance during these critical periods. Even after adjusting the most sensitive parameters related to key hydrological processes, the model's performance did not significantly improve. The SWAT model proves to be an acceptable model in dryland modeling for non-extreme drought events, and the methodology proposed in this study is highly transferable for different catchments worldwide. Overall, this thesis provides valuable insights into enhancing dryland modeling, bridging the gap between scientific research, modeling, and water resource management. These advancements are critical for improving the accuracy of scenario predictions and, consequently, for enhancing strategies to manage water resources in regions vulnerable to scarcity.

Keywords: dryland modeling; SWAT model; high-density reservoir network; hydrological connectivity; extended droughts.

RESUMO

As regiões áridas e semiáridas representam alguns dos ecossistemas mais vulneráveis às mudanças climáticas e às atividades antropogênicas. A modelagem hidrológica, especialmente por meio de ferramentas como o SWAT (Soil and Water Assessment Tool), serve como um instrumento essencial para enfrentar desafios práticos, como a previsão hidrológica e o suporte à tomada de decisões no gerenciamento dos recursos hídricos nessas regiões. No entanto, importantes questões científicas ainda são alvo de estudos, relativos ao desempenho desses modelos em bacias hidrográficas de regiões áridas e semiáridas, especialmente aquelas caracterizadas por redes densas de reservatórios, sendo analisado ainda o comportamento dos modelos durante anos consecutivos de seca e em anos com eventos extremos de precipitação. Além disso, durante períodos de secas severas, os modelos enfrentam desafios na representação de processos importantes nas regiões áridas e semiáridas, como perdas por transmissão, taxas de evapotranspiração e a inclusão das influências antropogênicas. Esta tese tem como objetivo avançar no entendimento da modelagem em bacias hidrográficas de regiões secas, abordando a capacidade do modelo SWAT em simular os processos hidrológicos dessas regiões, especialmente no contexto de redes densas de reservatórios e seu impacto na retenção de água em cenários interanuais de secas e enchentes. Adicionalmente, os estudos buscam avaliar o desempenho do modelo na representação de secas prolongadas e período posterior de recuperação hidrológica, ambas em uma década mais seca e quente, subsequente a uma série temporal previamente calibrada. O estudo foi realizado na bacia hidrográfica do Rio Conceição (3.347 km²), localizada no Ceará, nordeste do Brasil. Essa bacia contém 230 reservatórios (0,068 reservatórios por km²), com capacidades de armazenamento variando de menos de 0,01 hm³ a 52 hm³. A análise foi baseada em uma série de 40 anos de dados climáticos e de vazão observada, sendo 30 anos utilizados para a calibração do modelo e 10 anos adicionais para a extensão da série, incluindo um período de seca extrema. Os principais resultados desta pesquisa são os seguintes: (i) O desempenho diário do modelo foi considerado aceitável (*Nash-Sutcliffe Efficiency* = 0,63, *Kling-Gupta Efficiency* = 0,81 and *Percent BIAS* = 0,53%), demonstrando confiabilidade na previsão de picos de vazão durante anos úmidos, na previsão de períodos sem vazão e no aspecto de subida dos hidrogramas de cheia. Embora os pequenos reservatórios (menores que 0,01 hm³) tenham atuado na retenção das vazões, seu impacto geral foi pequeno, com taxas médias de retenção de água de 2% em anos úmidos e 9% em anos secos; (ii) A redução no escoamento devido ao aumento do número de pequenos reservatórios foi mais acentuada durante anos secos (até 30%) em comparação aos anos úmidos (até 8%). Essa

retenção também se intensificou ao longo de anos consecutivos de seca, um resultado obtido na análise de cenários, considerando densidades de reservatórios variando de 0 a 3 reservatórios por km² na bacia hidrográfica, sugerindo um aumento potencial de retenção devido aos pequenos reservatórios durante secas prolongadas; (iii) Apesar do bom desempenho do modelo ao longo de uma série climática de 30 anos, que incluiu períodos de seca severa, ele apresentou dificuldades para prever com precisão o escoamento durante uma posterior seca extrema (prolongada) e sua subsequente recuperação hidrológica, mostrando uma queda acentuada no desempenho durante esses períodos críticos. Mesmo após ajustes nos parâmetros mais sensíveis relacionados aos processos hidrológicos chave o desempenho do modelo não foi considerado aceitável. O modelo SWAT se provou como um modelo aceitável para modelagem de regiões secas com densas redes de reservatórios e as metodologias aplicadas nessse trabalho podem ser replicadas para diferentes bacias hidrográficas em outras regiões secas ao redor do mundo. De modo geral, esta tese oferece valiosas contribuições para o aprimoramento da modelagem de regiões áridas e semiáridas, conectando a pesquisa científica, a modelagem e o gerenciamento de recursos hídricos. Esses avanços são fundamentais para melhorar a precisão das previsões de cenários e, consequentemente, para fortalecer as estratégias de gestão dos recursos hídricos em regiões vulneráveis à escassez de água.

Palavras-chave: modelagem de terras secas; modelo SWAT; redes densas de reservatórios; conectividade hidrológica; secas prolongadas.

LIST OF FIGURES

LIST OF TABLES

TABLE OF CONTENTS

1 INTRODUCTION

1.1 General Introduction

Drylands are regions characterized by average rainfalls less than the potential moisture losses through evaporation and transpiration. The aridity index (AI) is a numerical value that measures how dry a climate is at a specific location. It is calculated by dividing the long-term average of water supply by the long-term average of water demand. The term "dryland" encompasses a wide range of environments, usually categorized in the literature as hyper-arid (AI < 0.05 and average rainfall < 200 mm), arid (0.05 < AI < 0.20 and average rainfall < 400 mm), semi-arid (0.20 < AI < 0.50 and average rainfall < 600 mm), and dry-subhumid regions (0.50 < AI < 0.65 and average rainfall < 800 mm) (Huang et al., 2017). The combination of limited rainfall and high evaporation rates results in minimal chemical weathering, contributing to generally poor soil development in these areas (Qader et al., 2021). The vegetation in drylands is typically adapted to low water availability, manifesting as scattered plant clumps in arid regions or scrubby vegetation and grasslands in semi-arid zones (Abel et al., 2023). These inherent characteristics pose significant challenges to agricultural development and food production (Chimwamurombe and Mataranyika, 2021). Drylands cover approximately 40% of the Earth's surface and are home to over 2 billion people, predominantly in developing countries, who are frequently vulnerable to water scarcity and food insecurity (Stavi et al., 2021; Wang et al., 2023). Figure 1.1 illustrates the global distribution of drylands.

Drylands are among the most sensitive ecosystems to climate change and anthropogenic activities. The rate of warming in these regions is 20% to 40% higher than in humid areas, despite greenhouse gas emissions being approximately three times higher in humid regions. This heightened warming rate suggests an accelerated expansion of drylands, accompanied by an increased risk of desertification. Consequently, many regions worldwide are likely to face significant challenges in water resource management, with growing uncertainties in their ability to meet water demands (Guan et al., 2016; Huang et al., 2016; Sun et al., 2022).

Figure 1.1 – Distribution of drylands around the world

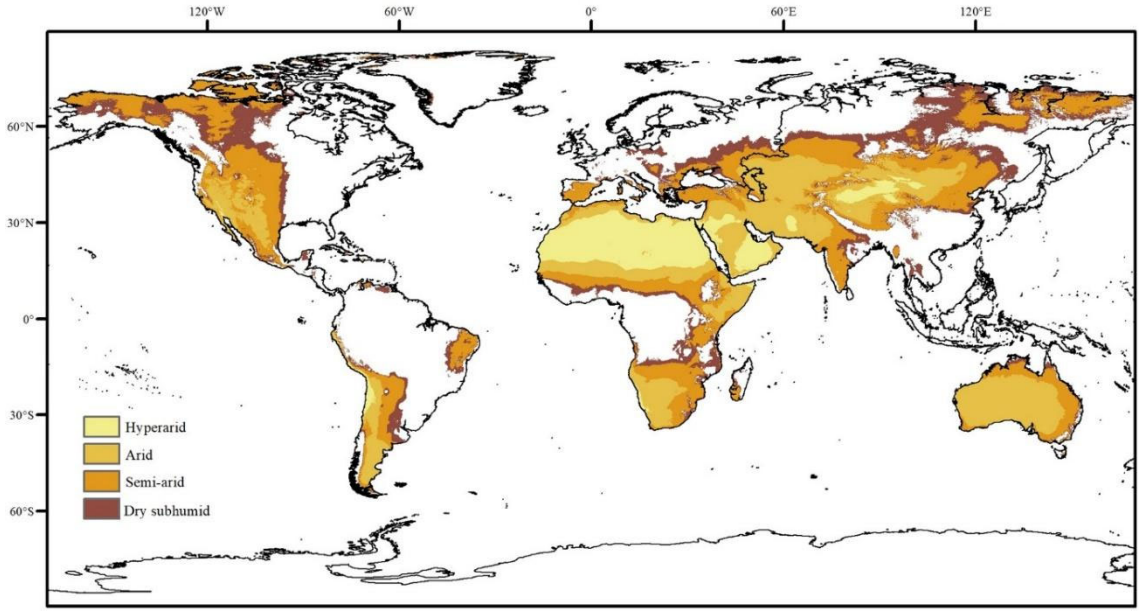

Source: Wang et al. (2023)

Human activities have profoundly impacted dryland environments through processes such as population growth, urbanization, agricultural expansion, and overgrazing. These activities have led to significant alterations in landscape patterns, which in turn affect the water cycle, carbon cycle, thermal processes, and biodiversity. As a result, the study of land cover change, soil characteristics, biodiversity, vegetation dynamics, and patterns of temperature, precipitation, potential evapotranspiration, and streamflows in drylands has become essential for understanding global environmental change (Wang et al., 2023; Huang et al., 2017; Zhang et al., 2024). Hydrological models are an efficacious instrument for water resources management, solving practical problems such as hydrological forecasting, hydrological analysis, and calculation (Cai et al., 2023; Duethmann et al., 2022).

The combination of climatic characteristics and human intervention in the catchments increases the challenges in understanding the hydrological dynamics of drylands. Due to the importance of these ecosystems, much recent research has been carried out in the area of hydrological modeling, using software to represent the main processes of rainfall-runoff transformation, groundwater movement, sediment transport and nutrient propagation, such as WASA/WASA-SED (Model of Water Availability in Semi-Arid), MODFLOW, QUAL2E, CE-QUAL-W2, MGB, and SWAT/SWAT+ (Soil and Water Assessment Tool), helping improve knowledge about impacts of climate change, water-efficient irrigation, changes in crop pattern, water management to meet water demand, water and sediment retention, and nutrients

routine from soil to rivers and reservoirs, as well as many other areas of study in drylands (Cai et al., 2023; Rabelo et al., 2022; Rocha et al., 2023). The primary challenges in hydrological modeling include the scarcity of observational data, the poor quality of available data, concerns regarding simulation accuracy, and the inherent technical limitations of the models (Samimi et al., 2020). Furthermore, many of these software tools were initially developed for humid or temperate regions and were subsequently adapted for application in dry regions, often necessitating the incorporation of additional modules to account for the distinct processes occurring in different climatic conditions. Moreover, in standard hydrological model calibration methods, the calibration process often relies on a single variable, typically runoff, which can introduce parameter uncertainty and cast significant doubt on the accuracy of subprocess calculations and simulations (Cai et al., 2023; López-Ramírez et al., 2021).

In recent years, many authors have conducted research on dryland topics. A search on the Web of Science for the term “dryland” identified 8,270 articles and review papers published between 2005 and 2024 in fields related to dryland in water related areas. Figure 1.2 illustrates the annual evolution of published articles, highlighting the growing research interest in dryland regions. A refined search further revealed that 558 of these articles explicitly mentioned dryland modeling in their keywords. Figure 1.3 presents the distribution of these 252 articles across predefined categories, including hydrology, ecohydrology, agriculture, climate change, climate and atmosphere, carbon cycle, droughts, floods, nutrient cycle, remote sensing, sediments, and surface and groundwater hydrology.

A growing research focus in dryland hydrology is the modeling of dense reservoir networks, with studies employing models such as ResNetM (Peter et al., 2014), WASA-SED (Medeiros et al., 2010; Malveira et al., 2012; Araújo and Medeiros, 2013; Medeiros et al., 2018), mass balance approaches (Fowe et al., 2015; Nascimento et al., 2019), and even field-based models (Lima Neto et al., 2011). These studies have identified key effects, including water retention in upstream reservoirs, reduced sedimentation in large strategic reservoirs, decreased soil erosion, and lower energy demand for pumping. However, most of these models employ lumped approaches to represent dense reservoir networks, often relying on monthly or annual time steps. One of the challenges of this study is to improve the representation of dense reservoir networks by incorporating their horizontal connectivity, enabling a more detailed analysis of dryland hydrology at a daily time step and capturing all aspects of the hydrographs.

Figure 1.2 – Number of publications identified by the Web of Science Core Collection for drylands from 2005 to 2024

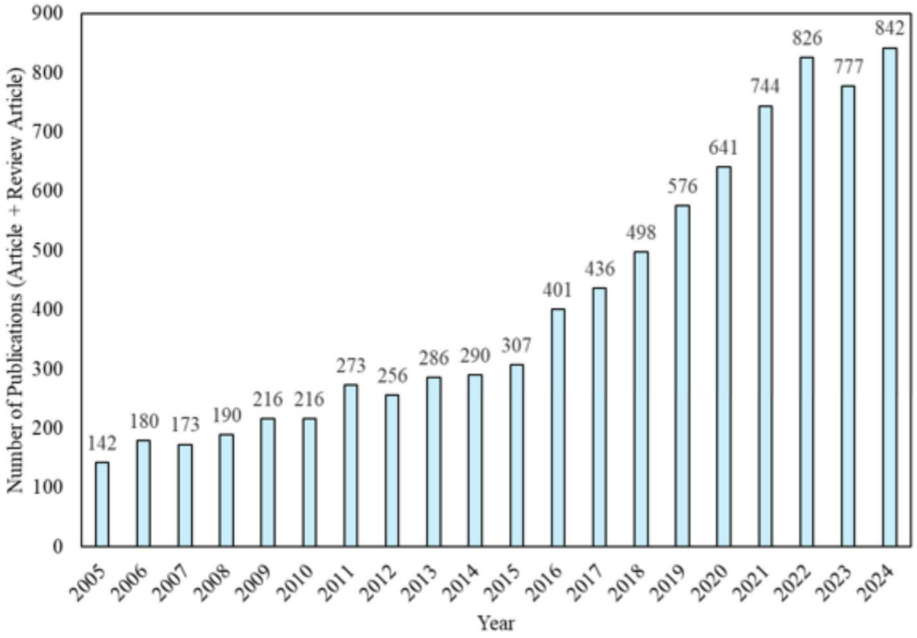

Source: Web of Science (2025)

Figure 1.3 – Distribution of categories for dryland modeling publications which is explicitly highlighted in the keywords identified by the Web of Science from 2005 to 2024

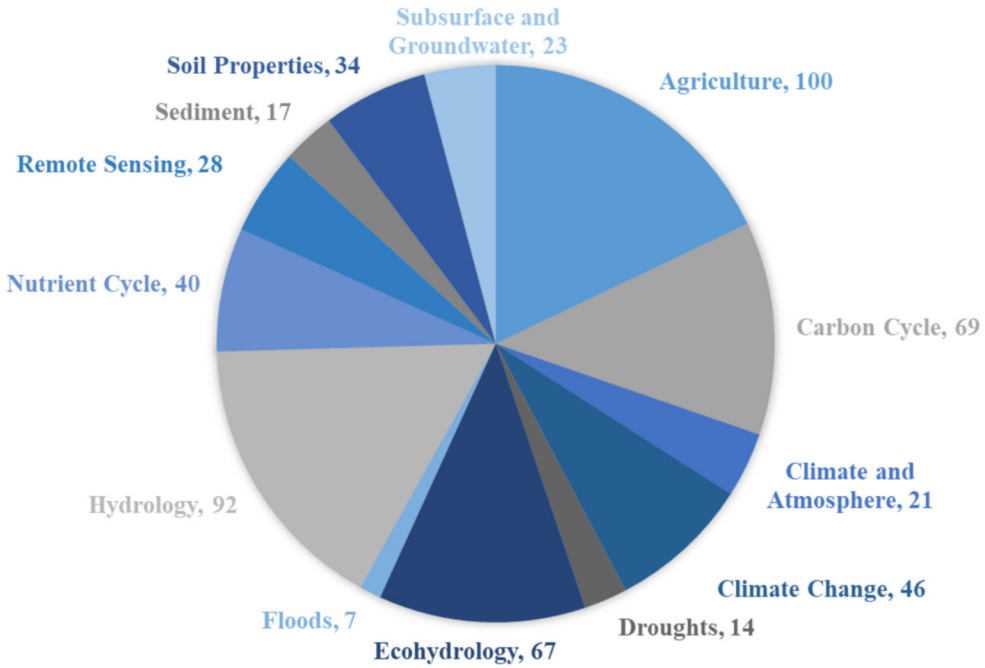

Source: Web of Science (2025)

Additionally, the modeling of severe drought periods is another crucial area for drylands. During severe and multi-annual droughts, the use of conceptual models tend to exhibit a decline in performance, especially in catchments where shifts in the rainfall-runoff relationship are observed (Saft et al., 2016; Trotter et al., 2023). In this context, there is an opportunity to analyze the performance of distributed and semi-distributed models that represent catchments with dense reservoir networks and their hydrological connectivity during extreme drought years.

Hydrological models have obtained satisfactory results in reproducing wet and dry periods in different catchments. Among the hydrological models, SWAT has considerable advantages and application potential in water resources evaluation and is diffusely applied in different catchments all over the world (Rabelo et al., 2022; Samimi et al., 2020; Song et al., 2022). SWAT is a semi-distributed model whose calculation basis is the hydrological cycle in the watershed, with its main elements shown in Figure 1.4, and works as follows: the catchment is initially divided into sub-basins after its delimitation; files with information on land use, soil type and slope are inserted; these three pieces of information are combined to generate the fundamental unit of the model: the hydrologic response unit (HRU) – Figure 1.5; within each sub-basin, HRUs are generated that have the same combination of land use, soil and slope; hydrological calculations are carried out for each HRU, and then processed for the rivers, ponds, wetlands and reservoirs in each sub-basin. Figure 1.6 shows a flowchart with the chain of command executed by the program to simulate the hydrological processes in the HRUs. In addition to the basic model structure, many modelers deal with the challenges of dryland modeling by combining data from different sources, using supplementary tools to estimate missing data and evaluate model performance, trading off simulation accuracy when the main objective of the study has not been undermined, and developing modular codes, tools and algorithms to expand model capabilities and improve process representations (Rabelo et al., 2021; Samimi et al., 2020).

Exploring the uncertainties within the SWAT model is pivotal for enhancing the precision and predictive capabilities of hydrological simulations. The SWAT model stands as a robust tool for simulating and replicating regional ecological and hydrological processes. It effectively forecasts the impacts of diverse land use and cover scenarios, management practices, and soil conditions on regional hydrological dynamics, even in the face of complex subsurface conditions and limited regional data availability (Cai et al., 2023; Serrão et al., 2022; Zahabiyoun et al., 2013). However, there remains considerable scope for evaluating the performance of the SWAT model in dryland watersheds characterized by dense reservoir

networks, as well as its behavior during consecutive years of drought and in years with extreme rainfall events, which result in significant river discharge peaks. Moreover, during periods of extreme aridity, particularly severe droughts, the model encounters significant challenges in accurately representing critical processes such as runoff transmission losses, evapotranspiration rates, and the anthropogenic influences (Bruno et al., 2024; Kumar et al., 2022; Wada et al., 2017).

This work seeks to contribute to the use of the SWAT model to advance modeling in dryland watersheds, evaluating points such as the model's ability to represent the hydrological processes of semi-arid lands, the inclusion of dense networks of reservoirs and their impact on water retention for interannual scenarios of droughts and floods, as well as evaluating the model's performance in representing extended droughts and their hydrological recovery periods.

Figure 1.4 – Main elements of hydrological cycle in the SWAT model

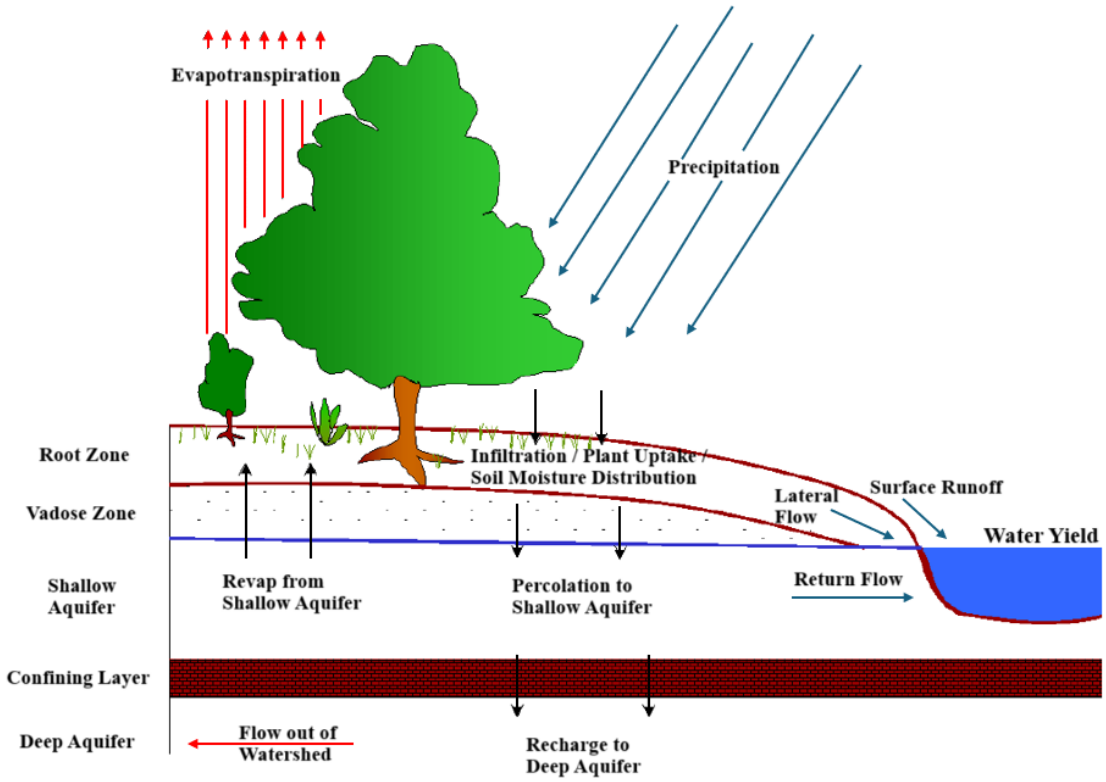

Source: SWAT Reference Manual (Adapted by the Author)

Figure 1.5 – Schematic representation of the combination of subbasin, land use, soil type, and slope maps for HRU generation in the SWAT Model

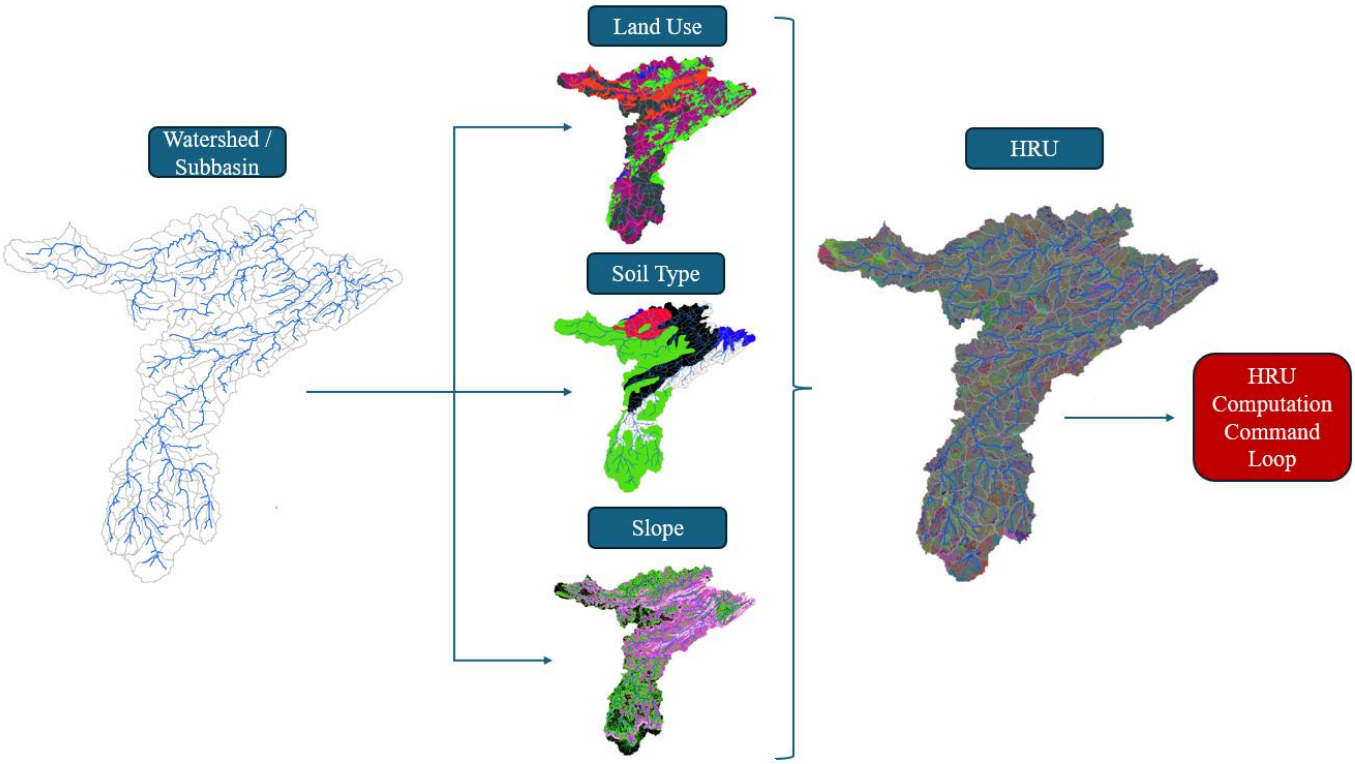

Source: The author

Figure 1.6 – Flowchart of HRU command computation

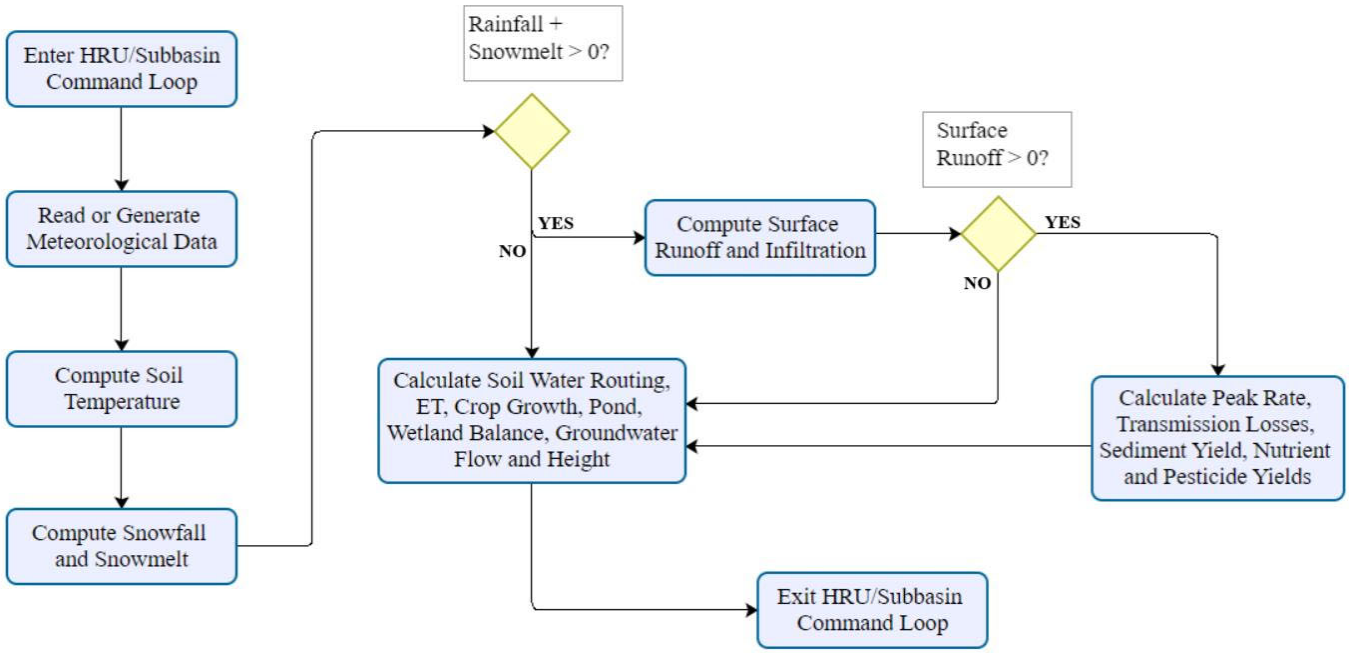

Source: The author

1.2 Objectives

1.2.1 General Objective

The main objective of this thesis is to advance in the hydrological modeling for dryland catchments as well as to improve the understanding of high-density reservoir networks influence and the impact of severe droughts on the performance of the model for streamflow estimation in the watershed.

1.2.2 Specific Objectives

- To develop a modeling methodology with detailed representation of large and small reservoirs in the SWAT model.
- To carry out an extensive analysis about the cumulative impact of small reservoirs on the horizontal hydrological connectivity for large-scale dryland catchments.
- To assess the influence of high-density reservoir network on the interannual runoff variability.
- To evaluate model performance during extreme droughts and its hydrological recovery afterwards.

1.3 Thesis Organization

This thesis is composed of three contributions in dryland modeling, based on the SWAT model of a semiarid meso-scale catchment in northeast of Brazil. Each contribution is presented in a separate chapter. Following is a brief introduction to each chapter.

Chapter 2 describes the potential of SWAT to model dense reservoir networks (DRN) for dryland catchments, presenting an innovative way of implementing the DRN, with detailed representation of large and small reservoirs, and an extensive analysis about the cumulative impact of small reservoirs on the horizontal hydrological connectivity. The efforts in the parameterization of reservoirs and aggregation of ponds allowed a better analysis of the hydrological processes and their impacts in the catchment, and the results of the cumulative impact of small reservoirs were relevant for a better understanding of hydrology in dryland

catchments, and can be applied to catchments in similar climatic and socio-economic environments.

Chapter 3 describes the impact of the augmentation in the number of small reservoirs in dryland catchment, evaluating the annual flows generated at the outlet for the dryland watershed for scenarios with different densities of small reservoirs (number of reservoirs per area). This study enhanced the understanding of the interannual variability of flow retention and the potential impacts of future increases in the number of small reservoirs, particularly concerning DRN in dryland catchments.

Chapter 4 describes the performance of the model to simulate a severe drought and its hydrological recovery afterwards. The model calibration developed in chapter 2 (from 1979 to 2010) was utilized to simulate streamflow in a later drier and warmer climate decade (2011 to 2022), encompassing the record drought from 2012 to 2017 in the study region. There is a knowledge gap regarding the reliability of hydrological models in simulating severe droughts and this chapter provided a broader scientific discussion on the need to improve hydrological modeling of streamflow during extreme drought events.

Chapter 5 presents some general conclusions and recommendations for future research.

2 REPRESENTING A DENSE NETWORK OF PONDS AND RESERVOIRS IN A SEMI-DISTRIBUTED DRYLAND CATCHMENT MODEL[1]

2.1 Introduction

Dryland environments are home to the world's water poorest populations and, during recent decades, have been subjected to increases in population, partial rise in living standards, development of irrigated agriculture, and new activities – especially tourism – that have drastically changed water and land use. These populations are vulnerable to the adverse consequences of environmental changes and in need of regional hydrological studies for better water resources management and water-scarcity risk reduction (Gutiérrez et al., 2014; AghaKouchak et al., 2015; Mallakpour et al., 2018; Samimi et al., 2020; Yao et al., 2020). To overcome the mismatch between natural water availability and demand, dams of different sizes have been built with the purpose of storing large amounts of water during the wet season, which may then be used during the dry season and dry years (Simmers, 2003; Mamede et al., 2012; Mady et al., 2020).

The increase in population in dryland regions and the consequent growth in water demand for human activities expanded the number of large, medium and small dams distributed along the catchments (Mady et al., 2020; Samimi et al., 2020). The federal and state governments of dryland regions have promoted the construction of large reservoirs, which mainly serve to provide for the water demand of industries, urban regions and large-scale irrigation agriculture (Araújo and Medeiros, 2013). Additionally, small-scale reservoirs have been used for a long time, mainly in dryland regions, as a complement to meet the water demand of small municipalities, rural communities and farmers. The small-sized and seasonal freshwater system play an important role in reducing inequalities for rural populations, providing sustainable development for rural communities and farmers. Due to their reduced cost and availability of many favourable locations, the number of small reservoirs has increased in recent decades (Araújo and Medeiros, 2013; Berhane et al., 2016; Yaeger et al., 2017; Habets et al., 2018).

[1]A paper based on the content of this chapter has been accepted for publication in the Journal of Hydrology, ScienceDirect, as Rabelo et al. (2021), and is available online at: https://doi.org/10.1016/j.jhydrol.2021.127103.

The spatial density of small reservoirs varies across different regions, with catchments in India with 4.2 reservoirs per km², Northeastern Brazil with 0.2 reservoir per km² and Australia with values between 0.15 to 6.1 reservoirs per km², for example. The advances of remote sensing techniques in obtaining important information from satellite images have allowed a better identification of the dimensions and uses of small reservoirs and assessing their global distribution (Lima Neto et al., 2011; Carluer et al., 2016; Mady et al, 2020; Paredes-Beltran et al., 2021). The small reservoirs (medium to micro-dams) are usually built disregarding the potential impact on the water availability of downstream communities. This has led to the generation of a chaotic system, which is referred to as a high-density reservoir network (Lima Neto et al., 2011; Mamede et al., 2012; Abouabdillah et al., 2014). On the one hand, such a reservoir network ensures a more equally distributed use of the water resources among the population of the river basin, as it reduces the concentration of water in large downstream reservoirs and enhances an even spatial distribution (Mamede et al., 2012; Fowe et al., 2015; Zhang et al., 2016). This has also positive effects such as decreasing sedimentation in the large strategic reservoirs (Lima Neto et al., 2011; Berg et al., 2016; Mamede et al., 2018), decreasing soil erosion (Abouabdillah et al., 2014) and decreasing the energy demand for pumping (Nascimento et al., 2019). On the other hand, as the smaller dams are also designed to maximize storage and the flow in tributaries is rare, the spilling frequency of the reservoirs is low, increasing hydrological discontinuity (Araújo and Medeiros, 2013; Abouabdillah et al., 2014; Peter et al., 2014).

The cumulative impact of the small reservoirs on downstream water availability are not simple to estimate because they are not necessarily the sum of individual effects of each small reservoir. These reservoirs may be inter-dependent and the cumulative effect can be greater or less than the sum of the individual effects, depending on their dimensions, uses and locations (Habets et al., 2018). However, there is evidence that the cumulative impact of the small reservoirs can be considerable, as the inflow to the large downstream reservoirs is reduced (Malveira et al., 2012; Araújo and Medeiros, 2013; Fowler et al., 2016). Some modeling approaches have been developed to assess the effects of small reservoirs in a basin. Most of them reported a decrease on the annual stream discharge, with a wide range from 0.2% to 36% and decreases in low flow and peak flow (Neal et al., 2002; Schreider et al., 2002; Nathan et al., 2015; Callow and Smettem, 2009; Hughes and Mantel, 2010; Nathan and Lowe, 2012; Fowe et al., 2015; Ayalew et al., 2017; Habets et al., 2018; Zhang et al., 2020a).

Most of those models are, however, based on simple mass balance methods developed for dryland environments. Thus, their application in a scenario of increase in the

number of small reservoirs should be done with caution, due to specific water use and hydraulic infrastructure patterns. Moreover, despite the importance of the small reservoirs for local needs and their impact on water availability at catchment scale, the small reservoirs have been neglected by water authorities, providing little technical information about them (Fowe et al., 2015; Habets et al., 2018). Reservoir data scarcity hampers, therefore, successful hydrological model application to drylands and semi-arid environments with high-density reservoir networks, which already face both poor monitoring of streamflow and extreme precipitation variation from year to year. The lack of information on small reservoirs characteristics and the difficulty to estimate cumulative impact is a challenge to assess and to model the hydrology in dryland environments.

The incorporation of reservoirs in hydrological models was carried out using simplified approaches in several other studies to assess their impact in streamflow. In WASA (Model of Water Availability in Semi-arid Environments) the reservoirs are grouped into size classes according to their storage capacity, with reservoirs of a smaller size class located upstream of reservoirs of a higher size class, and arranged in a cascade system, with only reservoirs of the largest size class regarded explicitly in the model in daily or hourly steps (Güntner, 2002; Güntner et al., 2004; Medeiros et al., 2018). The TEDI (Tool for Estimating Dam Impacts) model also uses as model input the dam size distribution, subdivided into classes, with computations on a monthly basis. TEDI assumes that reservoirs are connected in parallel, and the excess water spilling from each reservoir is directly routed to the outlet of the catchment, disregarding the spatial arrangement of the single reservoirs. Subsequently, the CHEAT (Complex Hydrological Evaluation of the Assumptions in TEDI) tool was developed by Nathan et al. (2015) and included information on the location of the reservoirs on the river network and the network topology, thus differentiating between sequential and parallel arrangement of single reservoirs (Nathan and Lowe, 2012; Fowler et al., 2016). However, the horizontal connectivity of reservoir networks is often less investigated in large-scale catchment models.

The eco-hydrological model SWAT (Soil and Water Assessment Tool, Arnold et al., 2012) has been applied worldwide for the simulation of catchments, in particular where water extractions and agricultural water management are of major relevance (e.g., Uniyal et al., 2019 with study areas in India, Chile, Vietnam and Germany). Various SWAT applications regarding the hydrology of dryland areas in China, Mongolia, Azerbaijan, Pakistan, Tunisia, Algeria, Mexico and Brazil have been published (Abouabdillah et al., 2014; Bressiani et al., 2015a, 2015b; Ghoraba, 2015; Molina-Navarro et al., 2015; Luo et al., 2016; Siqueira et al., 2016; Sukhbaatar et al., 2017; Sun et al., 2017; Zettam et al., 2017; Santos et al., 2018a;

Andaryani et al., 2019; Andrade et al., 2019). Despite this, there are few examples of studies (e.g., Zhang et al., 2012; Liu et al., 2014; Nguyen et al., 2017) that investigate the impacts of the combination of reservoirs of different types and levels of operation on catchment runoff using SWAT. In fact, approaches that mimic the effects of a large number of reservoirs in hydrological model structures have rarely been published. To achieve acceptable model performance in dryland watersheds for daily time steps modeling, the implementation of the reservoir network and its horizontal connectivity can be a key factor for or a more in-depth analysis, with the detailed representation of large and small reservoirs enabling a better analysis of their cumulative effects.

This paper investigates capabilities of the eco-hydrological catchment model SWAT to represent dense networks of large and small reservoirs as common for many dryland regions, as well as to gain in-depth understanding of hydrological processes and reservoir storage for meso-scale dryland catchments. To accomplish this goal, a detailed approach for dense networks of reservoirs is modeled for daily time steps in the eco-hydrological model SWAT. A new modeling and parameterization strategy of ponds and reservoirs is developed with detailed representation, focusing on the horizontal hydrological connectivity and the cumulative impact of small reservoirs, together with the parameterization of transmission losses and flood routing based on a modified SWAT version (Nguyen et al., 2018), with a corrected Muskingum subroutine suggested by the authors. The catchment in the SWAT model is evaluated using streamflow and reservoir water level series by a two-fold cross-validation approach. Moreover, a reservoir scenario approach is performed to assess the impact of the large and small reservoirs on the streamflow and storage volume, including different combinations of small reservoir dimensions. The present study not only improves the understanding of the hydrology of dense reservoir networks but also proposes a modeling approach that can be applied to water resources management in dryland catchments.

2.2 Materials and methods

2.2.1 Study area: catchment

The region for application of the model is a dryland meso-scale catchment in Brazil. The Conceição River (catchment area: 3,347 km²) is located in the state of Ceará in the Northeast of Brazil (Figure 2.1). The discharge from the watershed outlet is monitored daily at the Malhada gauging station (ANA, 2024). The Conceição River is a tributary of the Upper

Jaguaribe (Alto-Jaguaribe) River Basin (UJB), which is itself a sub-catchment of the Jaguaribe River watershed. The Jaguaribe River flows through the entire state of Ceará disemboguing into the Atlantic Ocean. The study area sits between the latitudes of -6.5° and -7.5°. The altitudes in the region vary from approximately 300 to 870 m, with an average elevation of 550 m.a.s.l.

Figure 2.1 - Location of the study catchment with the main rivers and reservoirs. The numbers 17 and 123 represent the largest main private reservoirs for Benguê catchment and Poço da Pedra catchment, respectively. The numbers 46 and 146 represent the two main private reservoirs with the largest drainage area and the largest storage volume, respectively.

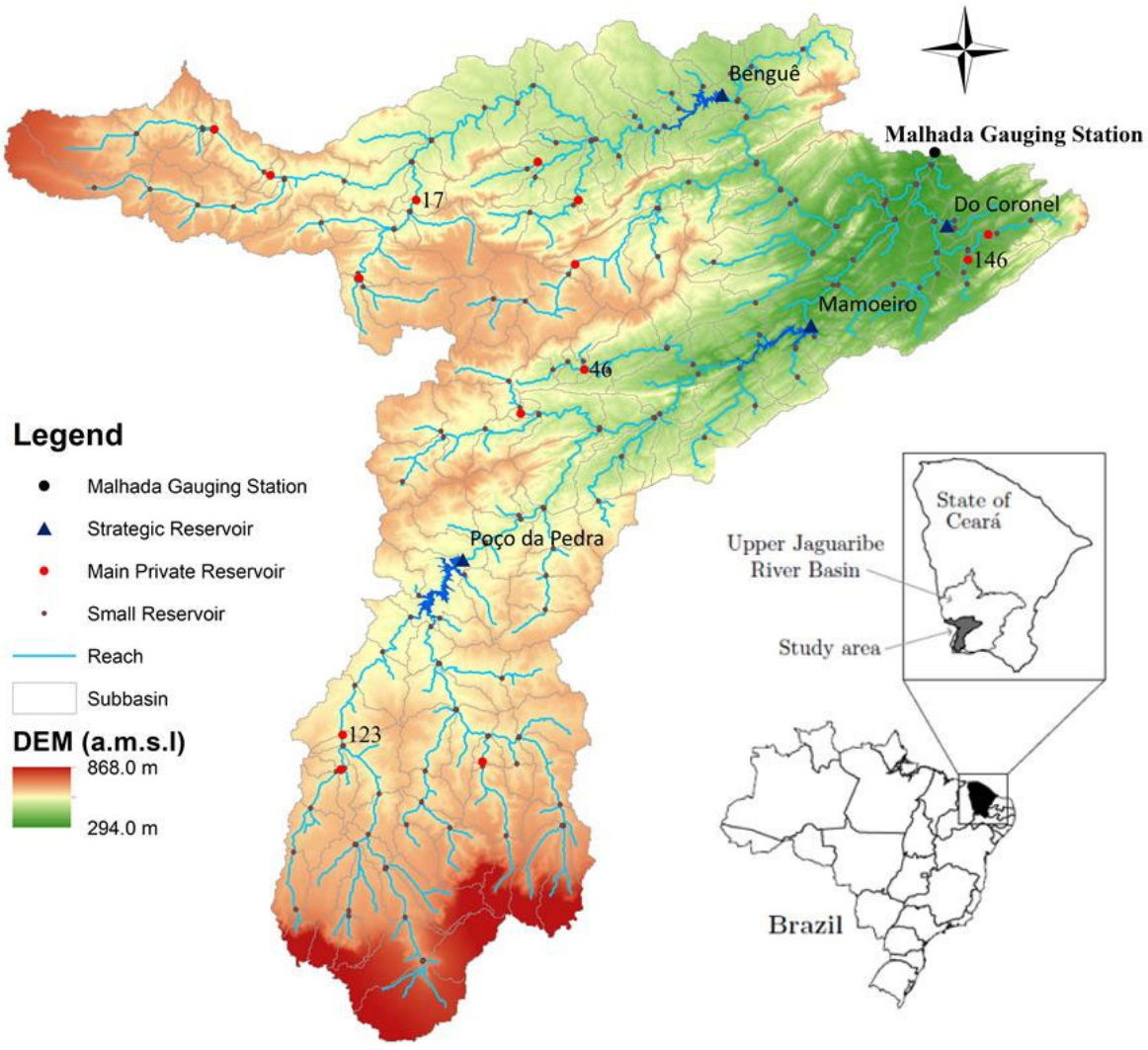

Source: Adapted by the author (DEM – FUNCEME, 2021; Malhada Gauging Station – ANA, 2021; Strategic Reservoirs – COGERH, 2021; Private and Small Reservoirs – GOOGLE EARTH, 2021)

According to Köppen the climate of the region is defined as semi-arid dry and hot ("Bsh") (Araújo and Medeiros, 2013). It is characterized by a clear distinction between a rainy and a dry season. The rain period lasting from January through May accounts for about 80% of the total annual precipitation. The annual precipitation ranges from 500 to 1000 mm (Araújo and Medeiros, 2013), amounting to 700 to 800 mm on average (Malveira et al., 2012). The dry season, however, is characterized by water scarcity as the potential evaporation exceeds precipitation by up to four times annually (Gatto, 1999). The prevailing climatic conditions with high interannual precipitation variability cause regular droughts, which may even occur in several consecutive years. Climate data and its pre-processing are presented in the Appendix A.

The vast majority of the region is covered by steppe-like savannah (Gatto, 1999). The predominant natural flora is the so called arboreal caatinga, a vegetation type found only in the Northeast of Brazil being composed of trees, shrubs and cacti, which are characterized as tropical xerophytic deciduous broadleaved plants (Malveira et al., 2012; Gatto, 1999). The caatinga presents a spatially rather continuous vegetation cover only with slight variations in density. The trees have densely branched stems and firm foliage, which dries out and falls off shortly after the rainy season (Güntner, 2002).

Geologically, 80% of the UJB is composed of crystalline bedrock (Eudoro, 2009), which is characterized by shallow overlying soils with low hydraulic conductivity and porosity (Silva et al., 2007). Therefore, the subsurface water storage (vadose zone and groundwater) in the catchment is limited (Eudoro, 2009). Along the principal rivers and tributaries, alluvial depositions may be found composed by young sandy-clayey sediments. These alluvial bodies present rather high permeability (Feitosa, 1998; Feitosa and Oliveira, 1998; Colares and Feitosa, 1998). Soil mapping and its physical parameters derivation are presented in the Appendix B.

The spatial and temporal variability in rainfall, combined with the low groundwater storage capacity and high evaporation, creates an adverse environment with regard to natural water availability, which is characterized by intermittent rivers and low runoff coefficients (Araújo and Medeiros, 2013; Malveira et al., 2012). Surface runoff generated in higher parts of the hillslopes is likely to infiltrate into the soil when reaching lower unsaturated areas. If produced at all, streamflow in upstream tributaries is of ephemeral nature, lasting only for short periods (in the range of minutes). Only after several consecutive rainy days, the soil water content is increased so that hydraulic connectivity is established on a catchment-scale and streamflow occurs in the main rivers, continuing over longer periods (in the range of weeks)

(Araújo and Medeiros, 2013; de Figueiredo et al., 2016). In river reaches embedded in an alluvium the flow regime is additionally influenced by channel transmission losses as a consequence of infiltration through the river bed and banks (Costa et al., 2012, 2013).

2.2.2 Study area: reservoir system

Reservoirs were distinguished between the large so-called strategic reservoirs, constructed and managed by the state government, and the privately built, unmanaged reservoirs of different sizes and shapes (Figure 2.1). The latter ones will be generally referred to as small reservoirs.

2.2.2.1 Strategic reservoirs

Four strategic reservoirs, namely Poço da Pedra, Benguê, Mamoeiro and Do Coronel, are located within the catchment (Figure 2.1) with a drainage area of 800, 1,062, 1,888 and 25 km², respectively (Table 2.1). The daily storage volume and the flooded area for each strategic reservoir are derived from the monitoring of water levels. The dam constructions usually dispose of two different release facilities (Table 2.1): a drain unit with an adjustable clasp device and an uncontrolled spillway.

Time series of the controllable releases are available for the two of the strategic reservoirs (Poço da Pedra and Benguê). For Poço da Pedra no controllable released discharges occurred for the entire period. The records for Benguê showed some days, during which water was released. No regularity was discernible and the discharges were rather small (usually lower than 100 L/s). As the controllable released discharges are negligibly small compared to the observed streamflow and to the losses caused by lake evaporation (Güntner et al., 2004), they were disregarded for the calculation of reservoir water balance. Differently from the controllable water releases, the spillway overflow is quite relevant to estimate the reservoir water balance, since large flood events were recurrent during the study period.

Table 2.1 - Hydraulic structure of strategic reservoirs located in the study catchment.

Item	Dam			
	Poço da Pedra	**Do Coronel**	**Benguê**	**Mamoeiro**
Operation year	1958	1946	2000	2012
Drainage area [km²]	8,000	25	1,062	1,888
Capacity [hm³]	52.00	1.77	19.56	20.68
Flooded area at cap. [km²]	8.320	0.5	3.479	3.691
Spillway type	No Public Info	Concrete Sill	Type Creager	Type Creager
Spillway width (constant)	60	24	150	80
Height of spillway crest	22	13	18.54	18
Controllable outlet	yes	no	yes	yes

Source: Secretary of Water Resources of the Government of Ceará – SRH, 2021

2.2.2.2 Small reservoirs

For previous studies on the reservoir network in the UJB (Mamede et al., 2012; Peter et al., 2014, Simshäuser,), a total number of 230 reservoirs distributed over a total catchment area of 3,347 km² (1 reservoir per 14.5 km²) were registered in the Conceição River Catchment analyzing aerial images taken immediately after the rainy season of the three comparatively wet years 2004, 2008 and 2009. This analysis allowed the estimation of the maximum water surface and the corresponding perimeter of the lakes. In-situ measurements of volume, area and height of the small reservoirs are not available.

As the flooded areas represent a moisture state shortly after the rainy season of extremely wet years, it was assumed that they correspond to the maximum capacity, beyond which water is spilled from a reservoir (Mamede et al., 2012; Peter et al., 2014). Hence, an estimation of the storage volumes based on these surface areas was conducted to gain the input data required by the hydrological model. Simplified approaches to estimate the storage capacity and, additionally, the spillway width are shown as follows.

Storage capacity estimation:

Molle (1994) conducted an extensive field study on the geometry of reservoirs in four states of the semi-arid Northeast of Brazil, including the state of Ceará. Based on this work, he developed the following equations 2.1 and 2.2 describing the relation between surface area, height and volume of a reservoir as a function of two parameters:

$$V = k \cdot h^{\alpha} \tag{2.1}$$

$$A = k \cdot \alpha \cdot h^{(\alpha-1)} \tag{2.2}$$

V: estimated reservoir volume [m³]

k: aperture coefficient

h: reservoir height / water stage [m]

α: shape coefficient

A: surface area [m²]

When combining the two equations, one obtains an expression (equation 2.3) for the reservoir volume as a function of the surface area (Pereira, 2017):

$$V = k \cdot \left(\frac{A}{\alpha \cdot k}\right)^{\left(\frac{\alpha}{\alpha-1}\right)} \tag{2.3}$$

The two coefficients are site specific and vary depending on the prevailing topography. Molle (1994) determined these coefficients for a sample of 420 reservoirs in four states of the semi-arid of Brazil (Ceará, Rio Grande do Norte, Paraíba, and Pernambuco) with capacities ranging from 0.03 to 0.66 hm³. The mean value of the sample for α and the median for k amounted to 2.7 and 1500, respectively. Using these parameters, the equation has been commonly applied in many studies (e.g. Malveira et al. 2012, Peter et al. 2014).

In order to find mean values for the two coefficients of Molle's equation that are more representative for the reservoir dimensions found in the Conceição River Catchment (reservoirs with flooded area till 0.07 hm²), which are rather smaller than those from the sample of Molle (1994), a sub-sample of 21 reservoirs in the catchment from a database published by the Brazilian National Department of Constructions against Droughts (Departamento Nacional de Obras Contra as Secas - DNOCS) (Pinheiro, 2004) was taken at hand. The average value for

α, 2.7, and the median for k, 5046, of this sub-sample were determined and adopted for this work. The estimated storage capacity of the small reservoirs detected by aerial images in the catchment, based on Molle's equation, ranges from 2,362 to 1,939,301 m^3. The mean and median storage capacity of the small reservoirs are 80,335 and 23,700 m^3, respectively.

Spillway width estimation:

Not only the strategic reservoirs dispose of spillway structures, but the private non-operated dams as well, even though their flood water release is generated in different manners. The small reservoirs usually have a lowered sill made of compacted soil. Some reservoirs simply spill via a natural or excavated so-called preferential flow channel. No information is available on the width and the height of spillways of small reservoirs. So, in order to realize a broad-scale assessment of the small-reservoir spillway widths, measurements based on satellite images were conducted in Google Earth in cases where a spillway was clearly discernible from the flight perspective.

After the satellite image analysis (Google Earth Pro images ranging from 1985 to 2020), only 21 measurements were considered, because in the majority of cases no clear distinction between dam and spillway was discernible, mainly due to the fact that both structures are made of earth and hence no difference in depth was recognizable. Additionally, some of the larger reservoirs dispose of tubes integrated into the dam, which could also not be assessed in the imagery. Aiming the estimation of all spillway widths, it was assumed that the flood magnitude is related to the upstream drainage area. So, all 21 values of Google-Earth-based spillway width were plotted against the upstream drainage area of each dam obtained from a *geographic information system* (*GIS*). After removing three outliers, a linear function was fitted to the plot with a coefficient of determination of 0.88. Based on the thus obtained relationship, the width of the spillway of other small reservoirs could be approximately determined entering the respective drainage area. With this width, the released discharge based on the water stage over the spillway crest may be calculated. However, it must be stated that the relation between width and drainage area represent only a very rough estimation. It presents a source of uncertainty originating from the low resolution of the satellite images in some regions, the potential misinterpretation of them and measuring imprecision.

2.2.3 Model of the system of reservoirs and ponds

2.2.3.1 Catchment delineation including reservoirs

For simulating hydrological processes and reservoirs in the catchment, the model SWAT was used. The delineation of the watershed and the definition of its river network (Figure 2.1) were done in ArcSWAT based on a digital elevation model (DEM) with 90 m resolution. Outlets of strategic reservoirs were incorporated as nodes. In this section, the model development and parameterization of ponds and reservoirs is presented. Strategic reservoirs and main private reservoirs along the river network were implemented into the SWAT model as "Reservoir" during the watershed delineation, while the other small ones were added as "Pond" as they are situated on tributaries off the main river network (Figure 2.1).

The classification of small reservoirs as "Reservoirs" or as "Ponds" was done depending on their impact on the generated water runoff. Water impoundments were implemented as Reservoir, if they meet all of the following criteria:

i. The water impoundment is caused by a dam construction built across the main river reach;
ii. The upstream drainage area of the reservoir is substantially larger than the average design sub-basin area (~20 km^2);
iii. The estimated storage capacity of the water impoundment is larger than 0.01 hm^3.

In the special case that the water impoundment was complying with the first two criteria but not with the third one, it was assigned to the second category (Pond) for means of simplification, even though it was receiving water from upstream sub-basins. By implementing these water impoundments as Pond, as if they were located off the main channel, their water retaining effect was not completely neglected.

To implement the remaining reservoirs as Pond, the following criteria were checked:

i. The water impoundment is caused by a dam construction built across the river reach;

ii. The upstream drainage area of the reservoir is approximately equal or smaller than the average design sub-basin area (~20 km²).

Fulfilling these criteria, a water impoundment was considered a pond according to the SWAT definition. In case the upstream drainage area was larger than the designated minimum sub-basin area (5 km²), the outlet was placed on the stream just downstream of the lake, generating a sub-basin whose entire area drains into the pond allocated to it. Deliberately placing certain ponds at the outlet of sub-basins simplifies further calculations for the determination of their drainage fraction, which is a required input parameter for SWAT.

If no dam construction was detected, the water impoundment was disregarded in the model. During a flood event, depressions in the landscape or flood plains may be inundated and filled with water, being registered as a water impoundment through remote sensing. These inundation lakes were neglected in the model as they show different topographic characteristics than the lakes impounded by dams, which would lead to an overestimation of their storage volume when applying the general method for volume estimation from flooded surface area (see section 2.2.2.2). This would then cause a distorted impact on the surface runoff.

The model catchment delineation ended up with a total of 191 dams and 197 sub-basins (Figure 2.1). The average sub-basin size amounted to approximately 17 km². A total of 18 dams were implemented as Reservoir (4 strategic and 14 main private) and 79 sub-basins contained dams that were either individually assigned or aggregated as Pond.

2.2.3.2 Aggregation of small reservoirs into ponds

SWAT allows only one single pond to be allocated to each sub-basin. After the watershed delineation, however, many sub-basins ended up containing multiple small reservoirs, that was considered a reservoir system, in which it was distinguished between a cascade and a parallel arrangement of reservoirs (Figure 2.2). In the cascade arrangement, two or more reservoirs are located one behind the other on the same river reach. Water being released from the upstream reservoir will flow into the downstream reservoir. So, the filling of a downstream reservoir depends on the amount of water held up by reservoirs further upstream and thus on the storage capacities and drainage areas of all upstream reservoirs. In the case that two or more reservoirs are arranged parallel to each other, the filling and spilling processes are independent of each other. In the parallel arrangement, each reservoir is located on a separate

river branch of the same order. Water being released from one reservoir does not flow into the other. Each reservoir has a separate drainage area.

Based on the arrangement of small reservoirs and their drainage areas, certain calculation rules were applied for the determination of the aggregated reservoir volume. Drainage areas of downstream reservoirs were kept fixed, while the volumes were reduced if necessary. In that way, it was guaranteed that only a fraction of the sub-basin contributes to runoff production that actually does not drain into any reservoir. In the case that a pond is located directly at the outlet, no outflow from the sub-basin will occur until the storage capacity of the aggregated pond is exceeded.

Given the rarity and variability of runoff, it is reasonable to assume that in some dry years, even the smaller reservoirs may not overflow. Therefore, it was aimed at estimating the average storage volume required for water to begin flowing out of a network of small reservoirs. This volume will be referred to as the equivalent capacity, while the system's overall impact on hydrology will be termed the storage effect.

Figure 2.2 - Schematic illustration of a sub-basin containing two small reservoirs configured in a cascade (left) and a parallel (right) arrangement. DAtot: drainage area of the aggregated pond defining the total drainage fraction of the sub-basin; Rd/R1 (red squares): downstream/first reservoir; Ru/R2 (red squares): upstream/second reservoir; DAd/DA1 (not hatched): drainage area of downstream/first reservoir; DAu/DA2 (hatched in grey): drainage area of upstream/second reservoir; Blue line: river reaches.

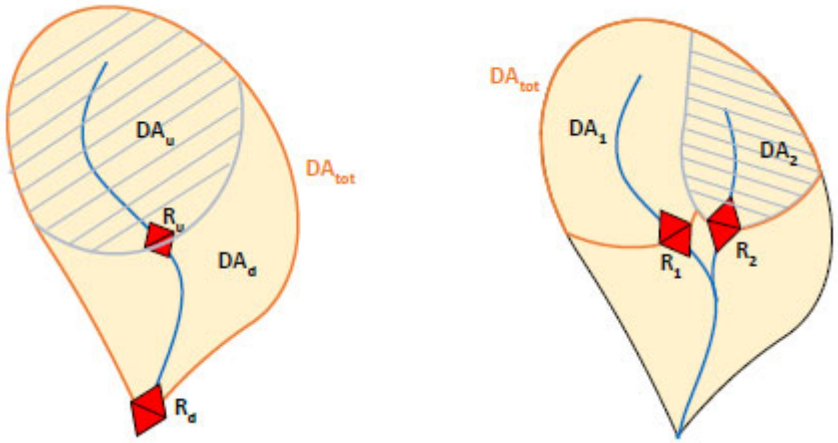

Source: The author

Two extreme states may be distinguished with regard to the storage effect:

i. The state when the entire amount of generated runoff in the system is stored so that no outflow occurs. This may be seen at the beginning of the rainy season. Only if a certain threshold water volume is exceeded the system spills. This threshold storage may be considered the effective capacity.
ii. The other state occurs after full saturation of the system (all reservoirs filled, high soil moisture) after some consecutive rainy days. At this point, the system only damps the outflow hydrograph, releasing the amount of water above the total storage capacity of the system.

In other words, the effective capacity of the reservoir network determines whether it spills, while the total storage capacity determines how much water is spilled. In order to simulate a storage effect that will match the one in reality on average, it was to set the equivalent storage capacity of the lumped pond to a value in between effective capacity and total storage capacity.

If the relation of capacity to drainage area of an upstream reservoir is equal to or smaller than that of the downstream reservoir (considering only the fraction of drainage area beneath the upstream reservoir), the upper dam will spill first. Hence, the equivalent storage capacity of the system amounts to the total capacity, the sum of both. This case corresponds to the assumption of a positively constant relation between capacity and drainage area made for other studies (e.g., Güntner et al., 2004; Zhang et al., 2012). In the case that this ratio is higher for the upstream reservoir, the downstream reservoir will spill first. When assuming the drainage area of the downstream reservoir, though, an addition of the single storage capacities would lead to a strong overestimation of the effective capacity. Spilling from the sub-basin would be simulated with delay or not at all. If only the downstream volume is considered the threshold storage for spilling of the system would be matched but the total capacity would be highly underestimated. In this case, the equivalent capacity is calculated as the sum between the full capacity of the reservoir with the larger specific drainage area and the other capacity reduced by the fraction of the two drainage areas.

$$if\ \frac{V(R_u)}{DA_u} \leq \frac{V(R_d)}{DA_d}:$$

$$V_{eq} = V(R_u) + V(R_d)$$

$$if\ \frac{V(R_u)}{DA_u} > \frac{V(R_d)}{DA_d}:$$

$$if\ DA_u > DA_d\colon\ V_{eq} = V(R_u) + \frac{DA_d}{DA_u} \cdot V(R_d)$$

$$if\ DA_u < DA_d\colon\ V_{eq} = V(R_d) + \frac{DA_u}{DA_d} \cdot V(R_u)$$

- Veq: equivalent storage capacity of aggregated pond
- V(Ru): storage capacity of upstream reservoir
- V(Rd): storage capacity of downstream reservoir
- DAu: drainage area of upstream reservoir
- DAd: drainage area of downstream reservoir

Accordingly, for a parallel arrangement of small reservoirs in the same sub-basin, if the relation of capacity to drainage area of two reservoirs is equal both will spill at the same time. Hence, the equivalent storage capacity of the system amounts to the total capacity, the sum of both. This case corresponds to the assumption of a positively constant relation between capacity and drainage area.

For the case that this relation is smaller for one of the reservoirs, this dam will spill before the other one. Assuming the sum of both drainage areas as an upstream basin for the lumped pond, the effective storage capacity would be overestimated. Considering only the drainage area and capacity of the reservoir with the smaller ratio the threshold storage for spilling would be matched, but the total capacity would be underestimated. In this case, the equivalent capacity is calculated in the same way as for the sequential configuration, as the sum of the full capacity of the reservoir with the larger specific drainage area and the other capacity reduced by the fraction of the two drainage areas.

$$if\ \frac{V(R_1)}{DA_1} \approx \frac{V(R_2)}{DA_2}:$$

$$V_{eq} = V(R_1) + V(R_2)$$

$$if\ \frac{V(R_1)}{DA_1} \neq \frac{V(R_2)}{DA_2}:$$

$$if\ DA_1 > DA_2\colon V_{eq} = V(R_1) + \frac{DA_2}{DA_1} \cdot V(R_2)$$

$$if\ DA_1 < DA_2\colon V_{eq} = V(R_2) + \frac{DA_1}{DA_2} \cdot V(R_1)$$

- Veq: equivalent storage capacity of aggregated pond
- V($R1$): storage capacity of first reservoir
- V($R2$): storage capacity of second reservoir
- $DA1$: drainage area of first reservoir
- $DA2$: drainage area of second reservoir

By these calculation rules, it was considered that if the combined drainage area is assumed, the storage effect of the reservoir with the larger drainage area is weighted higher for the estimation of the joint storage capacity. In case that multiple small reservoirs are arranged in the same configuration or that the two arrangements are combined in one sub-basin, it was started with the most upstream reservoirs. Their volumes were aggregated according to the respective rule, then this intermediate equivalent volume was again lumped with the small reservoir further downstream and so on.

2.2.3.3 Parameterization of strategic reservoirs

In SWAT, a reservoir is basically described by the principal volume (Vpr), the emergency volume (Vem) and the respective flooded surface areas (SApr and SAem). With these parameters the surface-area-volume curve is calculated and the water release is determined. The gradual flood water release from the strategic reservoirs may best be modeled in SWAT with the target release for controlled reservoir function (IRESCO = 2). The outflow routine allows a gradual spilling of the water volume above a certain target volume (Vtarg) and under the emergency volume (Vem). The maximum storage capacity of each reservoir, corresponding to a water level equal to the height of the weir crest, was set as Vpr. Considering that the spillways of all reservoirs in the catchment are uncontrollable free weirs, Vtarg was fixed as Vpr for all months. In order to guarantee a gradual water release over the spillway,

Vem must be set substantially higher than Vpr so that it is possibly never exceeded. Vem and SAem are available for strategic reservoirs by the state water agency.

The parameter NDTARG, representing the number of days required for releasing all excess water above Vtarg, determines the amount of water flowing out from the reservoir on each day. It depends on the type and the width of the spillways. In order to find a value for this parameter, daily spillway discharges for different excess volumes were calculated for each strategic reservoir. The discharge over the spillway in SWAT was calculated according to the commonly known weir overflow Poleni equation (Aigner, 2008), which depends on the width and the form of the spillway (Table 2.1). The weir-type-specific overflow coefficients were set according to the weir types: 2.1 for Benguê and Mamoeiro, 1.75 for Poço da Pedra and 1.6 for Do Coronel. Water levels were considered only up to a height slightly above the maximum observed elevation in the provided time series of the reservoirs: 1 m above the spillway crest for Benguê and Mamoeiro, 0.75 and 0.5 m for Do Coronel and Poço da Pedra, respectively. Excess volumes were also calculated for water stages at 0.01, 0.05, 0.10, 0.25 and 0.50 m above the spillway for all strategic reservoirs.

Therefore, the Poleni equation was solved for half-hourly time steps, readjusting the water stage after each step based on the specific volume-elevation-curve. The amounts of water released after each time step were added up, obtaining the total water volume released in one day. The values for the excess volume, i.e., the volume above reservoir capacity, were then plotted against the values for the calculated released water volume. Linear functions were fitted to the plots (Figure 2.3), with NDTARG equal to the inverse of the slopes of the straights. The straight lines presented high coefficients of determination ($R^2 > 0.9$), which led to the conclusion that the spilling behaviour of such reservoirs could be suitably represented by the function implemented in SWAT.

The obtained values for NDTARG reveal that all the excess water is released within slightly more than one day for the reservoirs Benguê and Do Coronel. Mamoeiro spills all the excess water in less than one day. For the excess water to be released from Poço da Pedra, however, it takes more than two days. These statements are only valid for the assumption that no water is entering the reservoir during this time. In reality, the spilling process is much more dynamic. A simulation on hourly time steps would be much more precise, but would lead to high computation time. As the simulation step in SWAT was set to one day due to data availability limitations, the approach presented here was considered the most appropriate way to estimate the daily released water volume.

Figure 2.3 - Excess volumes corresponding to certain water stages (0.01, 0.05, 0.10, 0.25, 0.50, 0.75 and 1.00 m) above the spillway crest plotted against calculated daily released volume with fitted straight line for Poço da Pedra (top left), Do Coronel (top right), Benguê (bottom left) and Mamoeiro (bottom right) Reservoir.

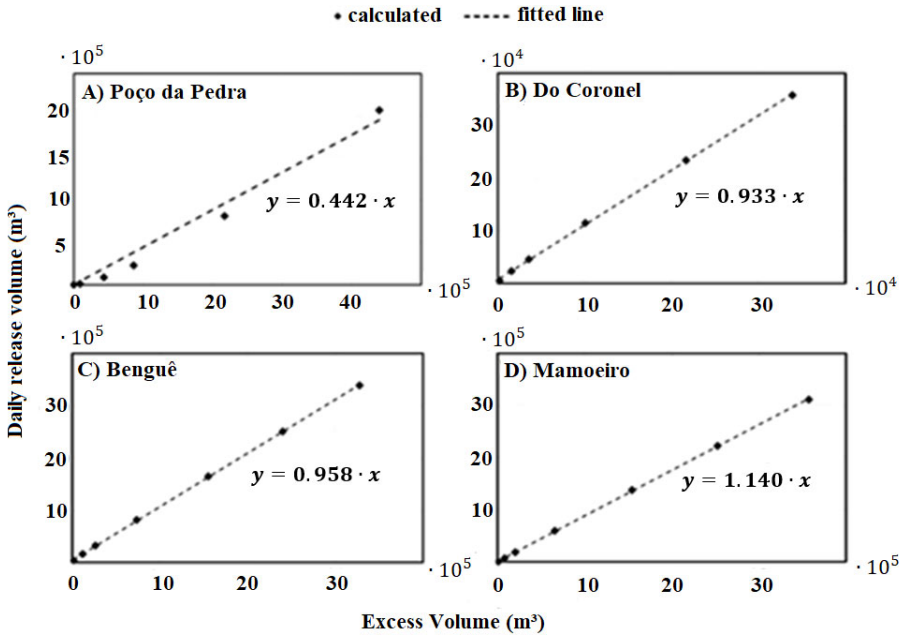

Source: The author

The parameters IYRES and MORES (year and month, in which the reservoir was built, respectively) were set according to the available information. The parameter EVRSV, the lake evaporation coefficient, was set to 1, which represents the maximum value, to guarantee high evaporation losses. The parameter RES_K represents the hydraulic conductivity of the reservoir bottom. It determines the losses through infiltration. Due to the professional planning and construction of the governmental reservoirs, it was assumed that these dams were sufficiently sealed and RES_K was set to 0.

The initial reservoir volume (parameter RES_VOL) for Benguê was obtained from recorded values shortly after the reservoir became operational in 2000. The initial storage volume represented about 4% of its capacity. For Mamoeiro, which became operational in 2012, the initial volume was also set to 4% of its capacity. However, no further time series were available for Mamoeiro. For Do Coronel, the observed storage volume on the first day of simulation in 1979 was obtained from the available records.

The time series for Poço da Pedra showed a gap for the years around 1979. The storage volume at that time was estimated based on all other values registered at the beginning

of January in the other years and based on the rainfall measured in 1978. The mean annual rainfall was calculated from five rain gauges inside the study catchment both for the year 1978 and for the entire simulation period. The annual rainfall in 1978 showed to be around 71% of the mean annual rainfall of the entire simulation period. The average of registered reservoir volumes at the beginning of January amounted to 46% of the total capacity. So, the initial storage for Poço da Pedra was estimated with these percentages: RES_VOL = 0.71 x 0.46 x capacity. Table 2.2 summarizes the parameterization of reservoirs, with a description of all parameters.

The representation of the withdrawal of water from the reservoirs was considered in the model in a simplified approach: urban water supply and irrigation were represented by a constant monthly water withdrawal based on state water agency data for each strategic reservoir. For the small reservoirs, as the withdrawals are negligibly small compared to the observed streamflow and to the losses caused by lake evaporation (Güntner et al., 2004), they were disregarded for the calculation of reservoir water balance.

2.2.3.4 Parameterization of main private reservoirs

Except for the flooded areas measured through remote sensing at the end of the flood season of extremely wet years, no data were available on the 14 main private reservoirs, which were implemented as Reservoir into the SWAT model. As they typically dispose of some type of spillway, it was assumed that the water storage effect of these dams was similar to that of the strategic reservoirs. So, their implementation followed the same principle.

The measured flooded area was set as SApr and the respective volume, which was therefore estimated using the Molle-based approach, was assumed as capacity and set as Vpr. Moreover, the volume corresponding to a water level of 1.5 m above the crest of the spillway was calculated and assumed as Vem. The height of 1.5 m was assumed as a reasonable value for the average height between spillway and dam crest.

Assuming the same procedure of overflow analysis that was followed for the strategic reservoirs and general simplifications of spillway geometric properties, it was found that the excess water is spilled within less than one day for almost all small reservoirs, i.e., less than the model calculation time step. The average NDTARG parameter was set as 1 for the main private reservoirs.

Table 2.2 - Parameterization of reservoirs (water impoundments implemented into the model as reservoirs). Reservoir numbers and sub-basin numbers correspond to the IDs given automatically in ArcGIS. Abbreviations B., dC., PP. and M. stand for Benguê, Do Coronel, Poço da Pedra and Mamoeiro, respectively

SWAT parameter		**MORES**	**IYRES**	**RES_ESA**	**RES_EVOL**	**RES_PSA**	**RES_PVOL**	**RES_VOL**	**RES_K**	**EVRSV**	**IRESCO**	**RES_TARG**	**NDTARGR**
				[10000 m²]	**[10000 m³]**	**[10000 m²]**	**[10000 m³]**	**[10000 m³]**	**[mm/h]**			**[10000 m³]**	**[d]**
Explanation		Month, in which reservoir became operational	Year, in which reservoir became operational	Surface area when reservoir filled to emergency spillway	Storage volume when reservoir filled to emergency spillway	Surface area when reservoir filled to principle spillway	Storage volume when reservoir filled to principle spillway	Initial reservoir storage volume	Hydraulic conductivity of reservoir bottom	Lake evaporation coefficient	Reservoir outflow simulation code	Manually set target volume (equal for each months)	No. of days to reach target storage from current reservoir storage
Res-No.	**SB-No.**												
2 (B.)	7	8	2000	438.00	2937.00	348.00	1956.00	85.80	0.0	1	2	1956.00	1.04
1 (dC.)	70	1	1979	100.00	300.00	50.00	177.00	46.80	0.0	1	2	177.00	1.08
0 (PP.)	108	11	1979	1639.00	14696.00	832.00	5200.00	1698.00	0.0	1	2	5200.00	2.25
174 (M.)	148	1	2012	454.00	2887.85	369.10	2068.30	82.73	0.0	1	2	2068.30	1.00
13	31	11	1994	22.56	66.91	15.89	38.19	0.00	0.1	1	2	38.19	1.01
17	57	11	2003	40.10	107.62	26.89	57.67	0.00	0.1	1	2	57.67	1.00
19	91	11	1999	23.13	63.44	15.77	34.66	0.00	0.1	1	2	34.66	1.00
24	54	1	1991	7.47	13.66	4.08	5.07	0.00	0.1	1	2	5.07	1.00
30	18	1	1979	21.93	62.36	15.17	34.66	3.47	0.1	1	2	34.66	1.00
32	39	1	1979	12.39	32.56	8.31	17.10	1.71	0.1	1	2	17.10	1.00
34	96	1	1979	10.96	24.59	6.82	11.34	1.13	0.1	1	2	11.34	1.00
46	118	1	1979	89.26	307.50	64.40	192.83	38.57	0.1	1	2	192.83	1.14
90	78	1	1979	14.75	37.03	9.71	18.78	1.88	0.1	1	2	18.78	1.00
123	165	1	1979	20.74	64.12	14.82	37.55	3.75	0.1	1	2	37.55	1.00
128	172	1	1979	4.19	12.91	2.97	7.56	0.00	0.1	1	2	7.56	1.00
146	89	1	1979	45.03	127.57	30.74	71.06	7.11	0.1	1	2	71.06	1.05
197	126	1	1979	8.91	18.15	5.25	7.60	0.00	0.1	1	2	7.60	1.00
203	170	1	1979	5.97	8.26	2.39	2.15	0.00	0.1	1	2	2.15	1.00

Source: The author

The application Google Timelapse was used to determine, in which year each reservoir was built, setting IYRES accordingly. This Google function provides satellite images of many regions from the years 1984 until 2017. If it was seen that a dam had been present since 1984, it was assumed that it had been existing since 1979. In these cases, MORES was set to January. In the other cases, MORES was set to November, the ending of the dry season, assuming that the dams are constructed during the dry season.

According to Molle (1989), seepage does not occur in the flooded area of the reservoir due to the underlying crystalline bedrock but rather underneath the dam along the original river bed. In the study, the insufficient sealing and compaction of the dam structures were concluded to be the principal reason for infiltration losses. So, the seepage process implemented in SWAT, assuming a loss through the flooded area (Neitsch et al., 2009), does not adequately represent the infiltration process happening in the field. In order not to neglect seepage losses from small reservoirs, however, the SWAT parameter RES_K (hydraulic conductivity of reservoir bottom) was set according to the average seepage rate found in Molle (1989), which amounted to 2.64 mm per day (0.1 mm per hour). For evaporation losses, the same value of 1 for EVRSV was defined, as described for strategic reservoirs.

Reservoirs that were built during the simulation period were assigned 0 as initial storage volume. For the other reservoirs, the initial storage was set according to the size class (same as used in the studies presented here). Micro-dams (capacity < 0.1 hm^3) were assumed to be empty before the flood season (in January), small-sized dams (0.1 hm^3 < capacity < 1 hm^3) were assumed to be at 10 % of their capacity and the medium-sized ones (1 hm^3 < capacity < 10 hm^3) were assumed to be at 20 % of their capacity. The remaining parameters were left as SWAT default. A summary of the main private reservoir parameters can be found in Table 2.2.

2.2.3.5 Parameterization of ponds

The obtained equivalent capacity of a system of small reservoirs was set as the Vpr of the aggregated pond of each sub-basin. The corresponding equivalent surface area was determined according to the same calculation rules, setting it as the SApr of the lumped pond of each sub-basin. With the single reservoir volumes corresponding to a water level of 1.5 m above the spillway Vem and SAem of the aggregated ponds were calculated using the same method.

In SWAT, it is not possible to set the date when a pond came into being. So, it had to be assumed that all ponds had been existing since the beginning of the simulation period,

which adds another source of uncertainty considering the transient nature of the micro-dams and looking at the development of dam construction in the region analysed in Malveira et al. (2012).

Based on the considerations made for reservoir bottom percolation, the respective parameter for infiltration through the pond bottom (K_POND) was set as 0.1 mm/h, too. From the investigation about the spilling behaviour, it was found that only above the threshold value of 0.01 for the ratio of capacity to drainage area of the single small reservoirs, it takes more than one day for the excess volume to be spilled (NDTARG > 1.0). From the highest value for NDTARG and the lowest one with the corresponding ratios, a linear relation was set up. Based on this equation the NDTARG parameter was determined for all the small ponds that showed a ratio higher than 0.01. In case the pond was located at the outlet of a sub-basin, the interpolated value for NDTARG was assumed for the aggregated pond in the respective sub-basin. For the remaining sub-basins with ponds, the parameter was set to 1.

Initial storages of the aggregated ponds were also set based on the single small reservoirs located in the sub-basin, following the reservoir-size class as aforementioned. If at least one small reservoir of a higher reservoir size-class (small- or medium-sized dam) is located in a sub-basin, the initial storage was set as a fraction of the capacity of this reservoir, accordingly. Table 2.3 summarizes the parameterization of ponds.

Table 2.3 - Parameterization of ponds (water impoundments implemented into the model as ponds). Sub-basin numbers correspond to the IDs given automatically in ArcGIS.

(continued)

SB No.	Drainage Fraction	Volume Principle (Vpr)	Surface Area Principle (SApr)	Volume Emergency (Vem)	Surface Area Emergency (SAem)	Initial Storage	NDTARG
	[-]	[10000 m³]	[10000 m²]	[10000 m³]	[10000 m²]	[10000 m³]	[d]
2	0.1407	7.5238	8.6954	19.8279	16.2424	0	1
3	1	180.773	57.3379	245.2304	71.9404	36	1.35
5	0.4696	0.8167	1.8449	4.2163	5.1859	0	1
6	1	7.5132	9.6866	24.3122	23.3748	0	1
8	0.0391	3.7472	4.8147	10.7188	9.3316	0	1.23
10	0.4067	4.9495	7.3037	13.0763	15.9801	0	1
13	1	5.1694	5.8958	13.3848	10.7323	0	1
19	0.1458	0.8939	2.2837	5.4764	7.2734	0	1
23	0.0763	0.9053	1.9686	4.4619	5.374	0	1
25	1	1.2363	3.0887	7.26	9.4324	0	1

Table 2.3 - Parameterization of ponds (water impoundments implemented into the model as ponds). Sub-basin numbers correspond to the IDs given automatically in ArcGIS.

(continued)

SB No.	Drainage Fraction	Volume Principle (Vpr)	Surface Area Principle (SApr)	Volume Emergency (Vem)	Surface Area Emergency (SAem)	Initial Storage	NDTARG
	[-]	[10000 m³]	[10000 m²]	[10000 m³]	[10000 m²]	[10000 m³]	[d]
27	1	1.3203	2.4965	5.5348	6.1549	0	1
28	0.6053	1.5654	3.311	7.7935	9.624	0	1
33	1	0.3281	1.0389	2.6666	3.8864	0	1
34	0.3461	1.0677	2.184	4.8947	5.6966	0	1
36	0.2796	2.7783	3.9881	8.7843	8.2325	0	1
40	0.2456	0.2206	0.8092	2.2375	3.4799	0	1
43	1	2.3644	3.6029	7.9147	7.7095	0	1
46	0.8	0.6155	1.2528	3.2769	4.3561	0	1
59	0.8349	1.3593	3.6802	9.2813	12.9686	0	1
60	0.1041	0.1517	0.6393	1.9212	3.1614	0	1
61	1	5.4467	7.7014	17.1033	16.0336	0	1
64	0.3512	13.3103	10.6946	26.894	16.6532	1.3	1
65	1	5.1583	6.819	15.6876	14.6899	0	1
69	1	1.5008	4.0274	9.7324	13.1594	0	1
71	0.3748	1.1897	2.5641	6.0043	7.4319	0	1
72	0.819	1.7086	3.3212	7.5068	8.6277	0	1
74	0.4773	2.6592	4.4424	10.284	9.7641	0	1.22
75	0.0524	0.2017	0.8205	2.4195	3.9328	0	1
77	0.3162	2.9359	5.4036	12.6029	14.5969	0	1
79	0.2002	0.8926	2.127	4.9608	6.3172	0	1.02
80	0.4298	0.2251	1.0437	3.4006	5.8433	0	1
81	0.8215	0.6982	1.7436	4.1308	5.3995	0	1
82	0.7291	0.4968	1.5373	4.1508	6.2157	0	1
85	1	3.6826	4.7623	10.5934	9.2627	0	1
87	0.4025	2.9633	5.2069	11.8974	13.1948	0	1.05
88	0.95	0.7407	1.8059	4.2567	5.5043	0	1
90	1	1.5455	3.1587	7.5267	9.2915	0	1
93	1	7.5586	8.8378	20.4257	17.3195	0	1.02
95	0.7517	0.6823	1.6475	3.829	4.8805	0	1
98	0.4006	1.031	2.8662	7.3597	10.478	0	1
99	0.1782	0.7418	2.1364	5.2665	7.3392	0	1
100	1	29.5171	26.1075	64.7025	45.078	2.95	1.02
102	1	5.2178	7.5602	16.7197	15.8657	0	1
106	1	4.6885	5.7291	12.9448	11.0297	0	1
107	1	16.1602	13.5462	34.7797	24.2638	0	1
110	0.6358	6.8338	7.2609	17.1445	13.7023	0	1.04
112	0.0922	0.3418	1.066	2.7175	3.9329	0	1
113	0.3669	2.3219	5.0349	11.6349	14.25	0	1

Table 2.3 - Parameterization of ponds (water impoundments implemented into the model as ponds). Sub-basin numbers correspond to the IDs given automatically in ArcGIS.

(conclusion)

SB No.	Drainage Fraction	Volume Principle (Vpr)	Surface Area Principle (SApr)	Volume Emergency (Vem)	Surface Area Emergency (SAem)	Initial Storage	NDTARG
	[-]	[10000 m³]	[10000 m²]	[10000 m³]	[10000 m²]	[10000 m³]	[d]
117	0.081	4.1549	5.797	12.799	11.7793	0	1
119	0.1587	2.3743	4.6125	10.3382	11.7731	0	1
120	1	6.3861	8.8767	19.733	18.2893	0	1.05
122	1	3.6661	6.3311	14.2447	15.3917	0	1
123	1	4.1293	6.2352	14.076	14.1237	0	1
124	0.9464	2.5164	4.4371	10.3236	11.7177	0	1
128	0.1765	0.3815	1.1425	2.8614	4.0627	0	1
131	0.1025	0.578	1.4841	3.5123	4.6224	0	1
132	0.191	2.0321	4.3421	9.9109	11.9397	0	1
134	1	9.3236	13.8683	31.2845	31.0957	0	1
135	1	31.3789	22.0259	59.2537	34.1384	3.14	1.02
137	0.2512	1.0437	2.5996	6.1387	7.9998	0	1
138	0.1997	0.4126	1.2002	2.9704	4.1595	0	1
139	1	3.279	4.4266	9.7989	8.819	0	1
142	1	3.8062	5.6076	12.4575	12.0347	0	1
144	0.9	0.7818	1.7949	4.1178	5.1092	0	1
149	0.2237	0.1046	0.5058	1.6715	2.8961	0	1
150	0.5671	0.3025	0.9872	2.5698	3.7969	0	1
153	0.1916	25.1365	15.9595	44.4581	22.853	2.51	1.15
154	0.0536	0.0951	0.4765	1.6162	2.8355	0	1
157	0.1087	0.6223	1.8313	4.6474	6.6331	0	1.05
159	1	0.304	0.9902	2.5753	3.802	0	1
168	0.3333	0.7133	1.6942	3.9201	4.9533	0	1.19
171	0.9508	3.1478	4.3143	9.5366	8.6696	0	1
173	0.1667	0.2131	0.7918	2.2051	3.4481	0	1
175	1	2.5427	3.7716	8.2931	7.9395	0	1
181	1	2.6293	3.852	8.4747	8.0486	0	1
183	0.0633	5.2966	5.9868	13.6159	10.8486	0	1.07
187	0.0855	0.3322	1.0472	2.6822	3.9006	0	1
193	1	2.8781	4.0776	8.9893	8.3529	0	1
195	1	1.0286	2.1333	4.7922	5.6212	0	1

Source: The author

2.2.4 Parameterization of dryland hydrology

2.2.4.1 Model calibration approach

The aim of the calibrated model is to describe the rainfall-runoff relationship of the catchment with the reservoir system as a base for further investigations and scenario simulations. Studying the sensitivity and uncertainty of hydrological parameters is not the subject of this study.

Climate data from 1979 to 2010 were collected from 38 FUNCEME rain gauges and 6 INMET meteorological stations, including daily precipitation, temperature, wind speed, humidity, and solar radiation. These variables were spatially interpolated using the inverse distance weighting method to generate inputs for 197 sub-basins. Detailed information about climate inputs can be found in Appendix A.

The soil map was provided as a polygon shapefile encompassing 109 soil association classes for the entire Jaguaribe River basin, following the soil classification system of Jacomine et al. (1973), which aligns with the coarser-scale soil map produced by FAO. Land use data were obtained from FUNCEME and provided as a polygon shapefile initially containing 26 land use classes. These land use classes were reclassified to match the default land use categories integrated into the SWAT model, with Caatinga being similar to Range, a vegetation from a semi-arid area in Texas, USA Brush (Scholz, 2015). Considerations regarding land use refinement were necessary due to the combination of different vegetation. Soil management information was not considered, only the land use patterns and native vegetation of the region. Detailed information on both land use and soil data is available in Appendix B.

Based on the available data, literature (Rocha et al., 2023) and the experience of the modelers, the following methods were chosen for the calculation of infiltration, evapotranspiration and channel routing, respectively: Curve Number Method, Plant Evaporation Method and Muskingum Method.

The parameters of the model were calibrated with a manual iterative trial and error procedure with the objective of maximizing statistical model performance – the Nash-Sutcliffe-Efficiency (NSE) and the Kling-Gupta-Efficiency (KGE) – and minimizing the percent bias (PBIAS) in stream flows comparison (observed vs. simulated), by keeping parameter values in a physically meaningful range. Initial values for the model parameters were derived from field data as much as possible. Then, where field data from the case study area were not sufficient,

values from literature about dryland catchments were chosen to represent the characteristics of the study catchment. Finally, remaining sensitive parameters were calibrated.

The model was calibrated separately for the sub-catchments of the three large strategic reservoirs Benguê, Poço da Pedra and Do Coronel. The simulated reservoir volume was compared to the time series for the strategic reservoirs. As the Mamoeiro reservoir became operational only in 2012, after the last year of the Malhada station available time series (1979 – 2010), it was disregarded for the presented analysis. The remaining sub-basins were sub-divided into three categories: upstream sub-basins with mountainous river reaches, transition sub-basins with medium-order river reaches and down-stream sub-basins. The sub-division was done by personal judgment with regard to the topography, slope classes and the order of the river reaches.

It is common in hydrological modeling to use warm-up periods, especially when the initial simulation conditions are not known. A warm-up is a sufficient period to run the model to initialize important variables or allow processes to reach a dynamic equilibrium. The complexity of watershed-scale processes impact the length of warm-up periods for hydrological models. However, two to four years are recommended by model developers due to having a complete hydrological cycling in the modeling. These periods are used by SWAT modelers in the arid and semiarid region for hydrological studies (Bressiani et al., 2015b; Daggupati et al., 2015; Jajarmizadeh et al., 2017; Zettam et al., 2017; Kim et al., 2018; Mendoza et al., 2021; Mengistu et al., 2021).

The manual calibration and validation of the model was performed using the technique of two-fold cross-validation. Considering the first two years as a warm up of the model simulation (1979 and 1980), the first half of the series (1981 - 1995) was used for calibration, while the second half (1996 - 2010) was used for validation, obtaining the statistical criteria for both series at the Malhada station. Subsequently, the second half of the series was used for calibration, while the first half was used for validation.

The reservoir volume simulation was evaluated for the whole series, but with a special highlight in the periods when each reservoir spilled out. These periods have a greater importance due to the spillway overflow directly influencing the streamflow at the outlet of the catchment. The simulated and observed time series of the reservoir's volume were overlain and their fitting was visually evaluated.

The years considered in the series for two-fold cross-validation have periods of flood and drought, such as 1985 and 2004 (rainy years) and 1993 and 2005 (drought years). These rainy years were extremely wet years, when all strategic reservoirs spilled out. Beyond

these extreme years, the preceding and following years were moderately wet to dry. In this way, the model could be evaluated for different extreme seasons and rainfall events.

For the calibration procedure, the daily simulated stream flow were tried to match the daily observed stream flow at Malhada gauging station, evaluating the plausibility of the magnitude and the duration of the uncontrolled released discharges by reservoirs with regard to the stage-discharge curves (i.e., excess-volume-to-released-volume-curves) developed in this work. To assess the fitting of daily streamflow hydrographs (observed vs. simulated), a combination of three quantitative statistical criteria commonly applied in hydrological modeling was used: the PBIAS, the NSE and the KGE.

2.2.4.2 Rainfall-runoff process, flood routing and channel transmission losses

The dominant vegetation Caatinga resembles the vegetation type rangeland. The Manning's roughness coefficient for overland flow for rangeland with 20% vegetation cover was provided in Neitsch et al. (2009). The maximum canopy storage (CANMX) was set to 1.5 mm as the average value for canopy storage in an arid environment stated in Attarod et al. (2015). The parameters SOL_AWC (available water capacity) and SOL_K (saturated hydraulic conductivity) were derived by applying pedo-transfer functions (PTF) based on Brazilian literature for each soil layer (Appendix B). Three soil types (Latosol Vermelho Amarelo, Bruno não-Calcio and Litolicos Eu Textura Arenosa) had characteristics of vertic soils. For them, the bypass flow function of SWAT was activated, to account for an additional water retention volume at the beginning of the rainy season due to the formation of cracks caused by shrinkage of the soil.

For a reach of the Middle Jaguaribe River, Costa et al. (2013) found that at the end of regular/moist rainy seasons, the river becomes a losing/gaining system, with its streamflow being sustained from base flow occurring in the underlying alluvium. The test reach represented a high order river in lower areas. As the principal rivers and tributaries in the study catchment are embedded in layers of alluvium as well, similar effects of streamflow being sustained by backflow from these alluvium bodies may also be expected. Therefore, river reaches were classified into three orders in the model: high order reach, medium order reach, and upstream tributary. SWAT allows to calculate water movement from the shallow aquifer to the root zone, which is controlled by the groundwater "revap" coefficient (GW_REVAP). For the respective sub-basins, the GW_REVAP was set accordingly to different values, decreasing in magnitude with increasing reach order.

According to the findings in Costa et al. (2013), transmission losses increase with increasing discharges due to a higher hydraulic head. In order to include a more appropriate approach for transmission losses on a catchment scale, the parameters CH_K2 (effective hydraulic conductivity of the channel alluvium in main river reaches) were set to different values depending on the topographic position of the sub-basins and the slope classes in the vicinity of the main river reaches.

The calibration of other parameters, such as CH_N2 (Manning's roughness coefficient for main channels), ESCO (soil evaporation compensation coefficient), ALPHA_BNK (bank flow recession coefficient), ALPHA_BF (base flow recession coefficient), GW_DELAY (delay time for aquifer recharge), GWQMN (threshold water level in shallow aquifer for base flow), REVAPMN (threshold water level in shallow aquifer for evaporation) and TRNSRCH (fraction of the transmission losses partitioned to the deep aquifer) can be seen in a summary in the Table 2.4, Table 2.5, and Table 2.6. Table 2.4 presents parameters set for the entire catchment.

Table 2.5 presents parameters set for specific sub-basins of the catchment, with distinction between sub-catchments of two strategic reservoirs and topographic position of sub-basins. Table 2.6 presents parameters set for specific zones in the catchment, with distinction between soil types.

Table 2.4 - Parameterization of calibrated model: Parameters set for the entire catchment.

Entire Catchment	
Calibrated Parameters	**Calibrated Value**
TRNSRCH	0.3
OV_N	0.6
CN2	57.34 to 92
CH_N1	0.065
CH_N2	0.05
CANMX	1.5
REVAPMN	265
CH_N2	0.05
SURLAG	4
ALPHA_BNK	0.6
ESCO	0.02
LAT_TTIME	0

Source: The author

Table 2.5 - Parameterization of calibrated model: Parameters set for specific sub-basins of the catchment. Distinction between sub-catchments of two strategic reservoirs and topographic position of sub-basins.

Item of Distinction	Sub-catchments		Specific Sub-basins			
Calibrated Parameters	Poço da Pedra Catchment	Benguê Catchment	Upstream SB	Transition SB/Medium-order Reaches	Downstream SB/High-order Reaches	Lowlands (incl. Do Coronel Sub-catchment)
	Calibrated Values					
GW_DELAY	12 and 30	12 and 30	30	12	12	12
GW_REVAP	0.15	0.15	0.25	0.15	0.1	0.25
GWQMN	700 and 1050	700 and 1050	1050	700	700	700
CH_K1	25	19	5	20	72	72
CH_K2	25	19	5	20	72	72
ALPHA_BF	0.6 and 0.8	0.6 and 0.8	0.6	0.8	0.8	0.8
RCHARG_DP	0.25 and 0.30	0.25	0.30	0.25	0.25	0.25

Source: The author

Table 2.6 - Parameterization of calibrated model: Parameters set for specific zones in the catchment. Distinction between soil types.

Item of Distinction	Soil Type				
Calibrated Parameters	Bruno	Latosol	LitolicosEu	Planosolos	Podisolico-EqEu
	Calibrated Values				
SOL_K	PTF results	PTF results	PTF results x 0.8	PTF results	PTF results
SOL_AWC	PTF results	PTF results	PTF results x 1.2	PTF results	PTF results
GW_REVAP	0.1 and 0.15	0.15	0.1, 0.15 and 0.25	0.25	0.1 and 0.15
SOL_CRK	0.3	0.4	0.3	0.01	0.01

Source: The author

2.2.5 Reservoir scenarios

One of the goals of this investigation is to assess the impact of the small reservoirs (ponds and main private reservoirs) on the model streamflow and volume series. As the estimate of those structures was made mainly with the help of aerial images, there is considerable uncertainty in this process.

Thus, in order to investigate different scenarios for the dimensions of the small reservoirs their volumes were multiplied by factor zero and the factor ten. These parameters represent areas and volumes that were estimated by the analysis of aerial images in the model (see section 2.2.2.2). “0 time” means the total absence of small reservoirs and was chosen to show how the model behaves without these small reservoirs. “10 times” means a ten times increase in the aforementioned parameters that represent the volumes of these small reservoirs. With these modifications, the model was run from 1979 to 2010 to assess their impact on the simulation of the streamflow at the Malhada station and of the volumes and the spillway overflows for the strategic reservoirs. We especially evaluated the peak values of the streamflow hydrograph at the Malhada station and the number of days of spillway overflow in the strategic reservoirs.

In addition, another scenario approach was performed to assess the impact of the reservoirs on the simulated streamflow at the outlet. The general influence of reservoirs was performed considering 4 scenarios: (i) considering all strategic reservoirs and small reservoirs (reference); (ii) removing all small reservoirs in the hydrological system, but keeping only the strategic reservoirs; (iii) removing all strategic reservoirs but keeping only the small reservoirs; (iv) removing all reservoirs. The model was run for the whole series with these hypothetical scenarios [(ii), (iii) and (iv)] and the streamflow at Malhada station was compared with the reference scenario (i).

Figure 2.4 illustrates the main flowchart of this study, with a summary of all methods applied.

Figure 2.4 - Flowchart of methods applied in the representation of reservoirs in the SWAT model and in the approaches to impact assessment of small reservoirs in the catchment.

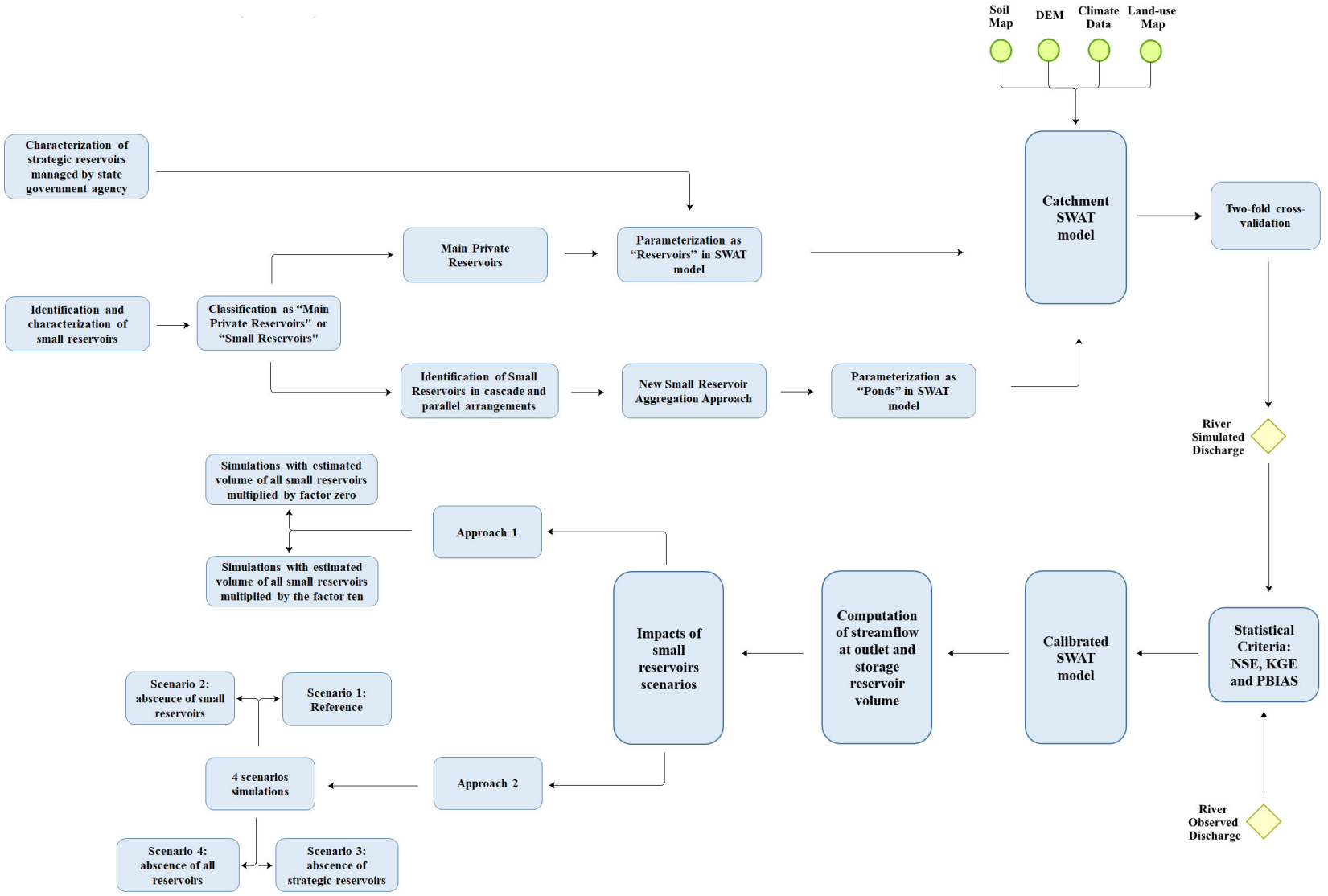

Source: The author

2.3 Results and discussion

2.3.1 Simulation of streamflow

The most relevant parameters in SWAT simulations in this study were identified as SOL_CRK, TRNSRCH, CH_K2, LAT_TIME, REVAPMN, GW_REVAP and CH_N1. It is worth mentioning that CN2 showed only low sensitivity even though it was often reported as very sensitive in other catchments. We explain that with the climatic and soil characteristics of the area, where soil moisture and infiltration processes more often underlie extreme dry or wet conditions than elsewhere. In this study, the first two years (1979 and 1980) were considered as warm-up period for adjustment of internal processes (e.g., soil moisture redistribution) that moves from an estimated initial condition to a realistic state. The model performance during the two-fold cross-validation periods was assessed with the three previously presented statistical performance criteria. Table 2.7 presents the obtained values for each for the calibration-validation periods. These values indicate a good model performance. The analysis of the values for both NSE and KGE attested a good overall fit of the simulated and observed hydrographs at Malhada station. The model simulated streamflow peaks with fairly high accuracy with regard to their dates of occurrence and their magnitudes. When calibrating the model with the first half of the series (1981-1995) the model overestimated streamflow values (highly negative PBIAS) for the second half (1996-2010); when calibrating the model with the second half of the series (1996-2010) the model underestimated the streamflow values (highly positive PBIAS) for the first half (1981-1995).

Table 2.7 - Evaluation of model performance in streamflow at Malhada gauging station with statistical methods for calibration period in 2-fold cross-validation of the series, where PBIAS is the percent bias, NSE is the Nash-Sutcliffe Efficiency and KGE is the Kling-Gupta Efficiency.

Performance criterion	Calibration Value (1981 – 1995)	Validation Value (1996 – 2010)	Calibration Value (1996 – 2010)	Validation Value (1981 – 1995)
PBIAS (%)	5.22	-38.93	2.29	33.55
NSE	0.65	0.56	0.65	0.65
KGE	0.81	0.53	0.82	0.55

Source: The author

Figure 2.5 depicts the observed and the simulated hydrographs for the calibration-validation periods, while Figure 2.6 depicts the log flow duration curve for these periods. For better display, Figure 2.7 shows close-ups of hydrographs with a logarithmic scale streamflow for the single years (1985 and 2004) during which relevant discharges were observed. These years were chosen because they represent the wettest years, allowing a full analysis of the hydrograph rising limb, the peak flow and the recession flow. For dry years, with low precipitations, and consequently low flows, the analysis of these hydrograph characteristics would be limited. Figure 2.5 (a, b), Figure 2.6 (a, b) and Figure 2.7 (a, b) present results for 1981-1995 calibration and 1996-2010 validation and (c) and (d) in both figures present results for 1996-2010 calibration and 1981-1995 validation. For Figure 2.7, only the first half of the year, the wet season period, is presented as for the rest of the year neither observed nor simulated discharges occur (the dry season). It is remarked that the scale of the vertical axis is adapted for each year.

Figure 2.5 - Comparison of observed and simulated daily discharges at Malhada gauging station for: (a) calibration in 1981 – 1995; (b) validation in 1996 – 2010; (c) calibration in 1996 – 2010; (d) validation in 1981 – 1995.

(a) Hydrograph for Malhada gauging station for the calibration period of 1981 - 1995

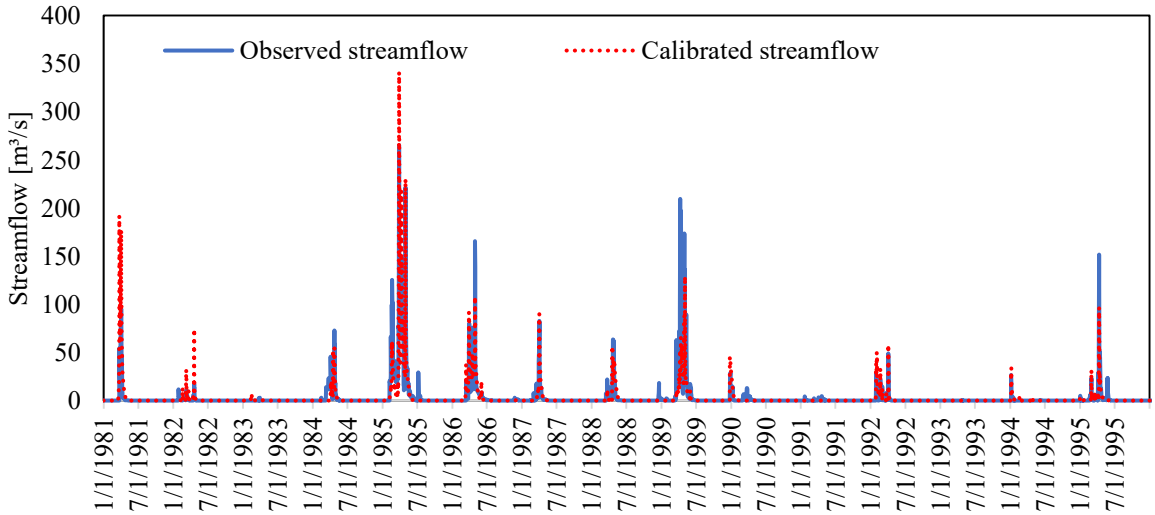

(b) Hydrograph for Malhada gauging station for the validation period of 1996 - 2010

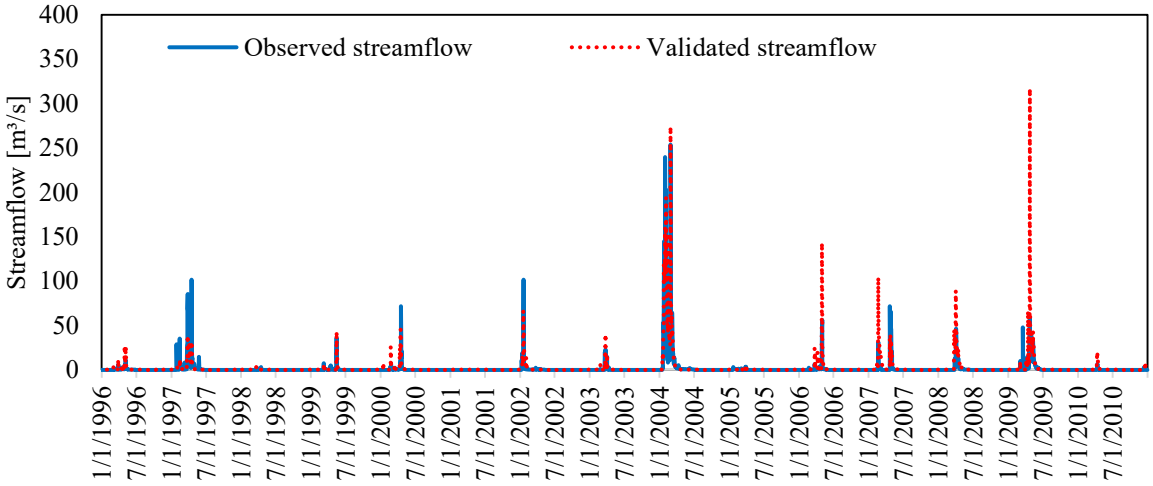

(c) Hydrograph for Malhada gauging station for the calibration period of 1996 - 2010

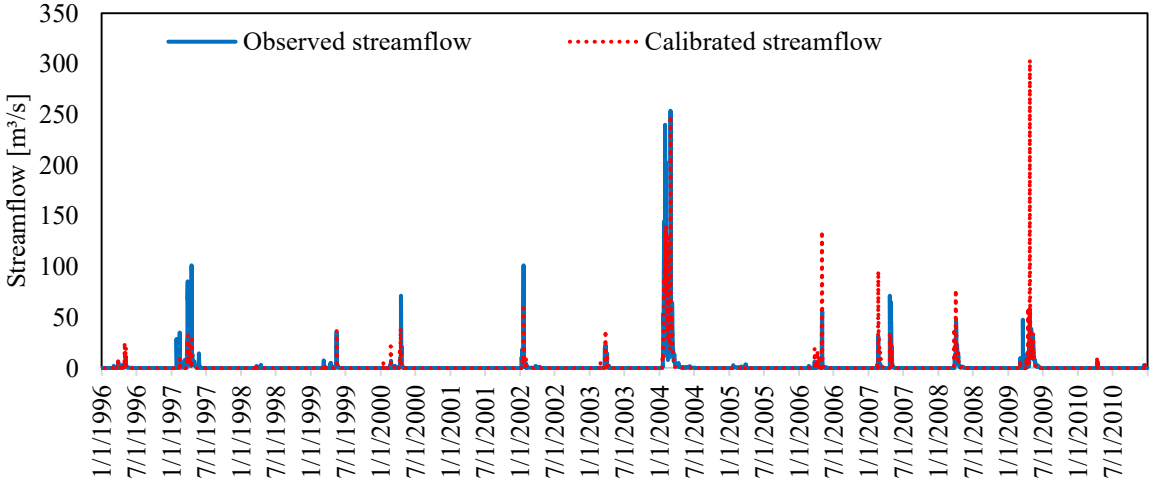

(d) Hydrograph for Malhada gauging station for the validation period of 1981 - 1995

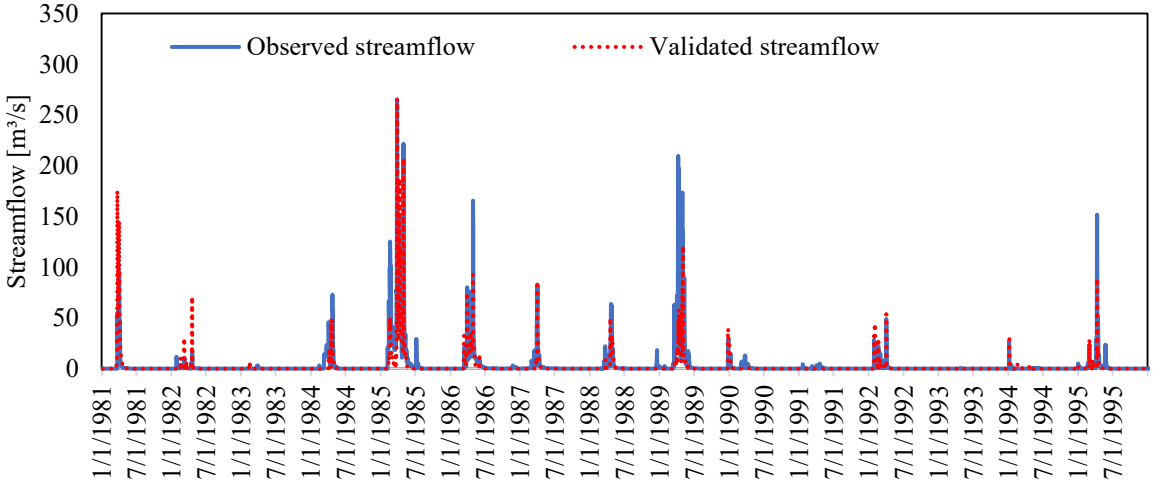

Source: The author

Figure 2.6 - Comparison of observed and simulated log flow duration curves for: (a) calibration in 1981 – 1995; (b) validation in 1986 – 2010; (c) calibration in 1986 – 2010; (d) validation in 1981 – 1995.

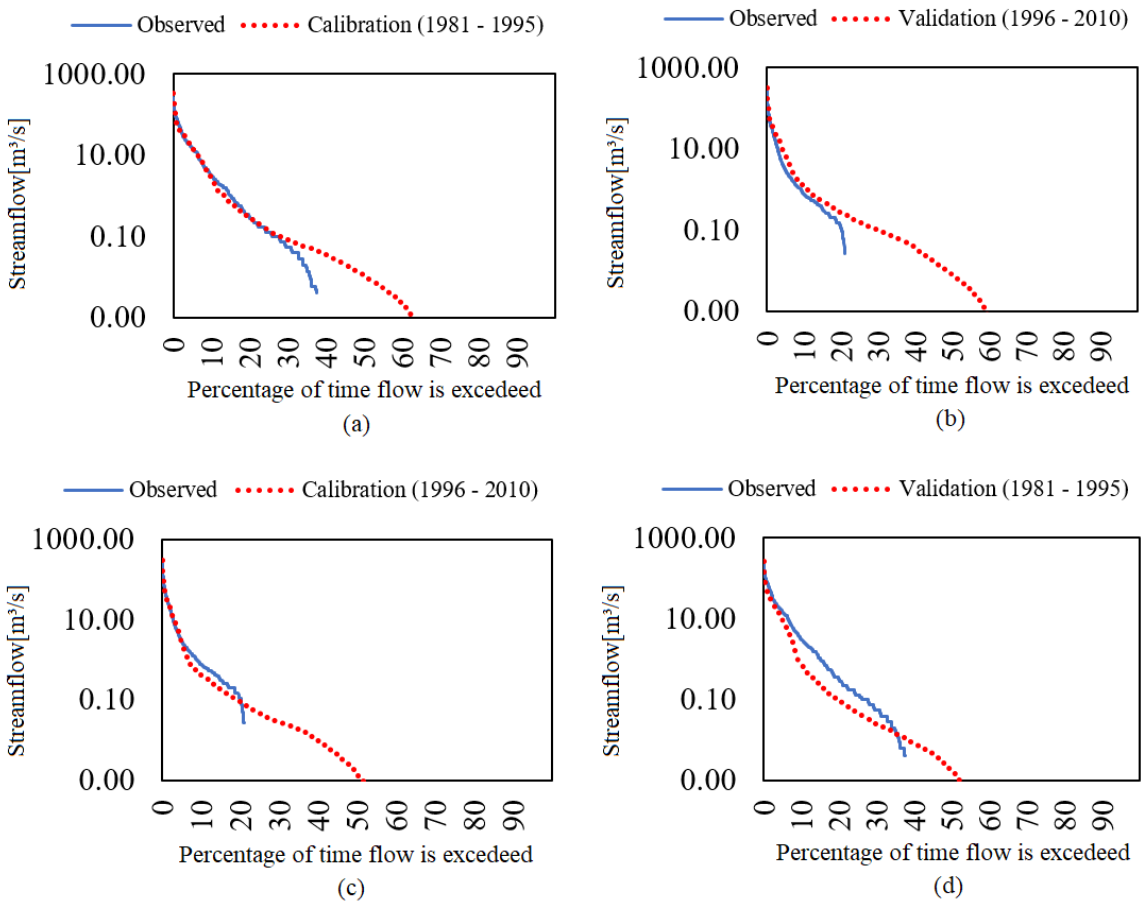

Source: The author

The results show that the model was able to simulate dry years in which no or only minor discharges are registered (1983, 1993, 2001 and 2005) at the Malhada gauging station. For these years no water reached the outlet of the catchment, so the hydrograph was not presented here. This indicates that both the storage capacity of the single reservoirs and the losses due to evapotranspiration and riverbed infiltration were estimated sufficiently high. For years with near-average water yield, the model accuracy was good for some years (1984, 1987-1988, 1990, 1992, 1994, 1996, 1999 and 2003), but was rather poor in others (1986, 1989, 1995, 1997, 2000, 2002 and 2006-2008). For these years with worse accuracy, until 2002 the peak streamflow was underestimated, which means that the observed streamflow has higher peaks and more water reaching the outlet. From 2006 to 2008 the model overestimated the peak

streamflow. These results can be seen in Figure 2.5. For 2009, the modeled peak was clearly overestimated.

Figure 2.7 - Comparison of observed and simulated hydrograph for daily discharges at Malhada gauging station for: (a) calibration year of 1985; (b) validation year of 2004; (c) calibration year of 2004; (d) validation year of 1985.

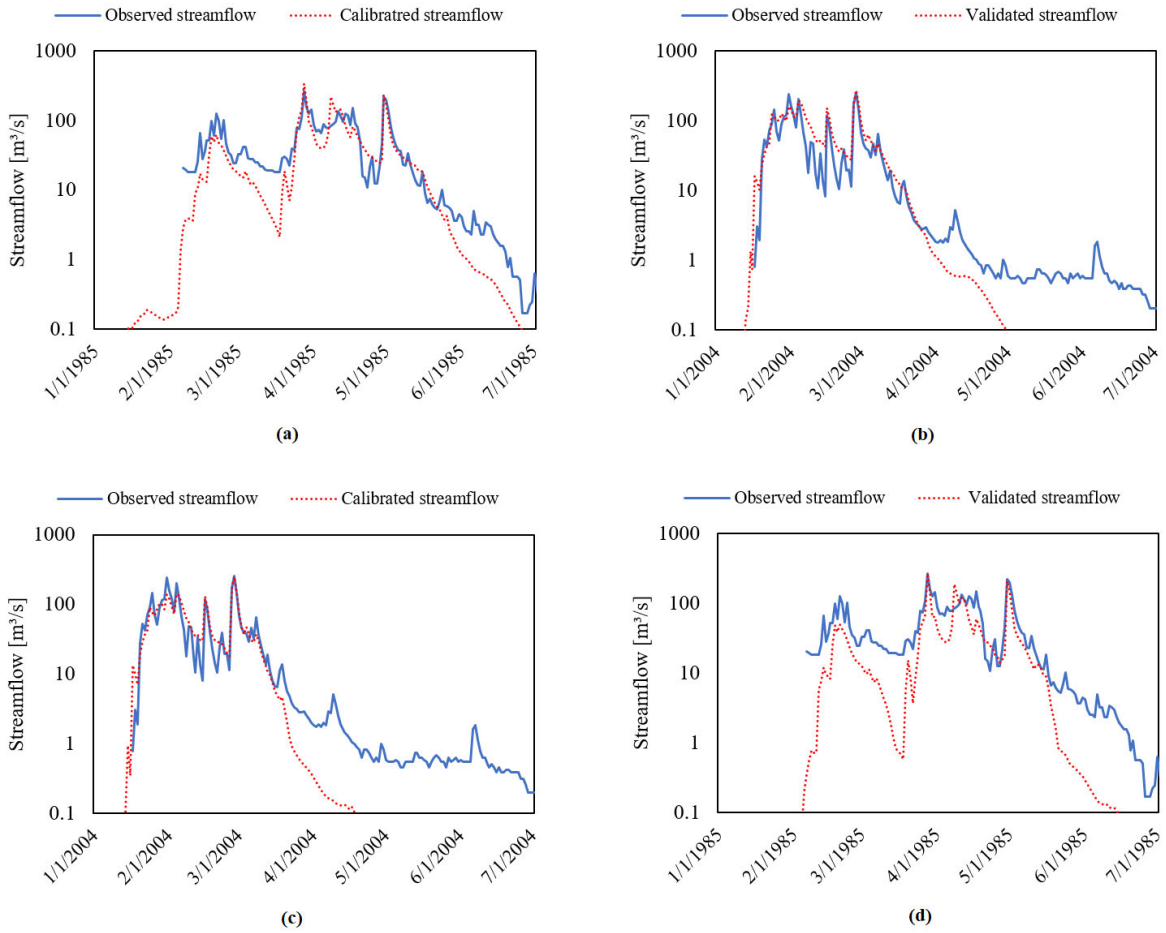

Source: The author

The graphs clarify that for wet years during which the large reservoirs spilled out (1985 and 2004) the days of extreme flood events (high peaks) were matched with high accuracy by the model. The magnitude of the simulated peaks was within a similar range than those of the observed ones. However, the flow recession was not well represented by the model. It was found that it is characteristic for the study area that the streamflow lasted for many days after strong consecutive rain events. The abrupt recession of the simulated hydrograph at the end of wet periods, with streamflow going down to zero just after a few days the peak occurred in all simulation results, while in the observed hydrograph the streamflow lasts for a few days.

After extremely rainy periods, water accumulates in the regions close to the river channel, forming flood plains. The river recharge process after this period is notably complex, with unsaturated seepage and vertical unsaturated subsurface water redistribution beneath the stream, lateral stream-aquifer interaction and groundwater flow, parallel to the river course, in unconfined aquifers. These processes and the channel transmission losses for arid and semi-arid watersheds are very simplified in the SWAT model and have a great influence on these basins (Costa et al., 2012).

Some of the years with moderate rain showed worse accuracy in peak streamflow, hydrographs limbs and recession flow, either with underestimation or with overestimation in the simulated values, depending on the year of analysis. Those years with near-average streamflow require attention in the hydrological simulations, mainly due to the possible unsaturated characteristics of the soil. Transmission losses are more complex in these years and the SWAT model equation is relatively simple, depending on hydraulic conductivity, flow translation time, wet perimeter and channel length. Uncertainties in the input data were one of the difficulties during modeling in this dryland catchment, mainly in the values of hydraulic conductivity. The values of hydraulic conductivity and transmission losses estimated also affected the recession flow, whose simulated values also showed streamflow results with sharper drops than the observed values in the hydrographs after the rainy season. In all cases, there is uncertainty in rainfall data (lack of continuous rain gauge monitoring in some days and human errors in measurements) although the 44 stations available in the catchment can reduce errors. No significant errors were found. Despite that, errors of rainfall data during storm events can significantly impact modeling. Even interpolation cannot compensate for gaps in the recording of the local variability of rain.

2.3.2 Simulation of reservoir volume

The simulated storage volumes during the cross-validation of the three strategic reservoirs Poço da Pedra, Benguê and Do Coronel are presented for comparing their values and temporal dynamics with the observed values based on data availability and operation periods (Figure 2.8). From the diagrams, it can be seen that the peaks during flood year 2004 were matched well for the three reservoirs. The model simulated the filling of the reservoir very well until the storage capacity was exceeded. For the other years, the model simulated that the capacity was exceeded for 1986, 1988-1990, 1997 and 2009-2010 for Poço da Pedra, 2006-

2009 for Benguê and 2009 for Do Coronel. Analyzing Figure 2.8, the storage volume in Poço da Pedra and Benguê reservoirs was higher overestimated in some years, besides the periods that the simulated storage of the reservoir reached the maximum volume (1988-1990, 1997 and 2009-2010 for Poço da Pedra and 2006-2007 for Benguê), when the observed data showed a value quite distant from that. The evolution of the hydrograph, however, was well represented by the model. For Do Coronel, the curve of simulated storage volume showed slightly overestimated values compared to the observed ones for the years after and before the flood years. The overall dynamics is better simulated than for the other two reservoirs.

Figure 2.8 - Comparison of observed by state water agency and simulated by SWAT daily storage volumes in the three strategic reservoirs for the calibration and validation periods: (a) Poço da Pedra (storage capacity 52 hm³, simulation 1986 - 2010) (b) Benguê (storage capacity 19.56 hm³, simulation 2000 - 2010), (c) Do Coronel (storage capacity 1.77 hm³, simulation 2004 - 2010).

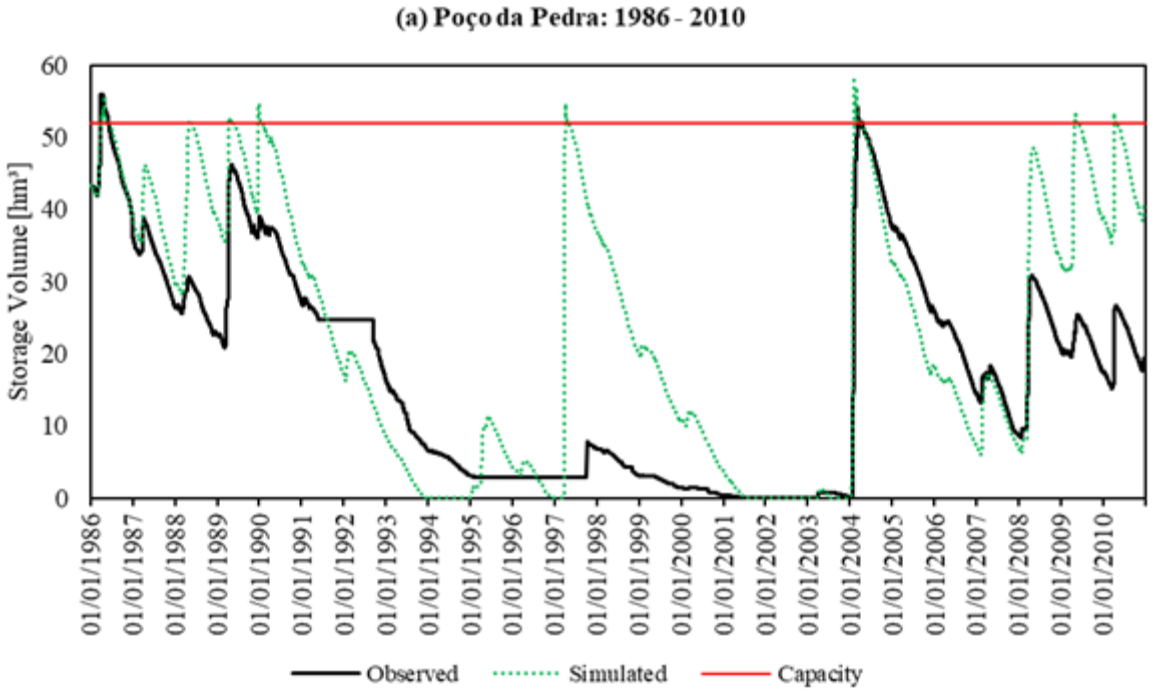

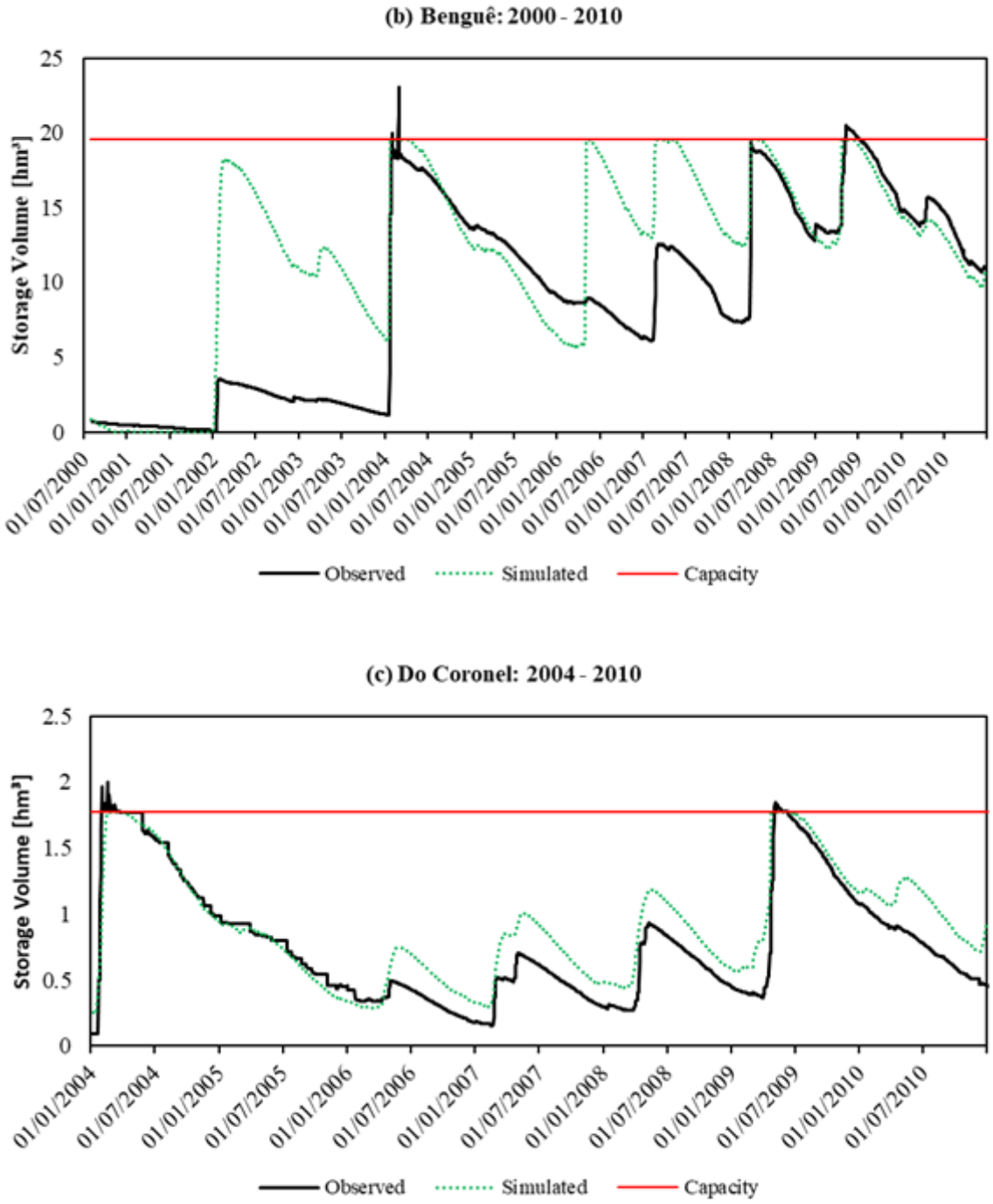

Source: The author

Despite these differences in storage volumes of Poço da Pedra and Benguê, we did not find any systematic error. The years of 1997, 2008 and 2009, for example, showed considerable streamflow at Malhada gauging station, while the years of 1998, 2001 and 2010 showed low streamflow. There were no direct discharge measurements upstream from the studied reservoirs. Storage volumes were used to validate the reservoir modeling approach. On the other hand, from 2008 to 2010 the model overestimated the storage volumes in Poço da

Pedra, as well as the streamflow at Malhada gauging station in these years, especially in 2009. Some characteristics of dryland environments cause uncertainties for modeling of rainfall-runoff processes, for example the nonlinear behavior of runoff generation and the irregular spatial patterns of soil properties (Rödiger et al., 2014; Mamede et al., 2018).

The fall of the storage volume during the dry period, too, was modeled very realistically. For the years before and after a flood year, the curves fitted very well for reservoirs. The slope of the curve after a rainy season was a little more pronounced in the model. This period is characterized by intense evaporation and a decrease in the volume of the reservoirs for semiarid sub-basins and the parameter that calculates the evaporation (EVRSV) in the reservoirs in the model was established at the highest possible value (see Table 2.2).

The catchment of Benguê reservoir was modeled by Mamede et al. (2018) using the WASA-SED model (Güntner et al., 2004; Bronstert et al., 2014) for the period 2000-2012. The WASA-SED model also simulates the impact of the small reservoirs on the generated catchment runoff as aforementioned. The WASA-SED results for the storage volumes of the Benguê reservoir were very similar to those produced by the SWAT model presented here, although the WASA-SED model was specifically adjusted only for the Benguê catchment.

Furthermore, it can be seen that the model simulated the release from the reservoir during flood events within the calibration and validation periods (Figure 2.9). Both the durations and the magnitudes of the overflow discharges seem plausible for all reservoirs. According to the specific stage-discharge curves edited for this study the simulated maximum discharge from Poço da Pedra corresponds to a water stage of about 60 cm above the spillway crest. The maximum simulated overflow discharge from Do Coronel would cause the water stage to reach a height of 40 cm above the spillway crest. The maximum discharge from Benguê corresponded to a water stage higher than 2 m above the spillway crest. 2.1 m is given as the maximum water level above the spillway. So, in this case it may be assumed that the model overestimated the outflow. But as the outflow from the spillway represents a dynamic process, depending on hourly flood events, the water stage may be kept constant during a longer time span, leading to higher discharges than the one predicted by the stage-discharge curves, which assume no further inflow to the reservoir. As no information was available regarding the spillway overflow from the reservoirs, no further comments on the plausibility of the outflow hydrographs were done. However, the results were an indication that the filling and emptying processes in reservoirs may be mimicked realistically with the SWAT model even on a daily time step, which was rarely shown before.

Figure 2.9 - Hydrographs of released discharge for simulated outflow over the spillway of the three strategic reservoirs for model simulations: (a) Poço da Pedra – 2004; (b) Poço da Pedra – 1986; (c) Benguê – 2004; (d) Benguê – 2009; (e) Do Coronel – 2004; (f) Do Coronel – 2009.

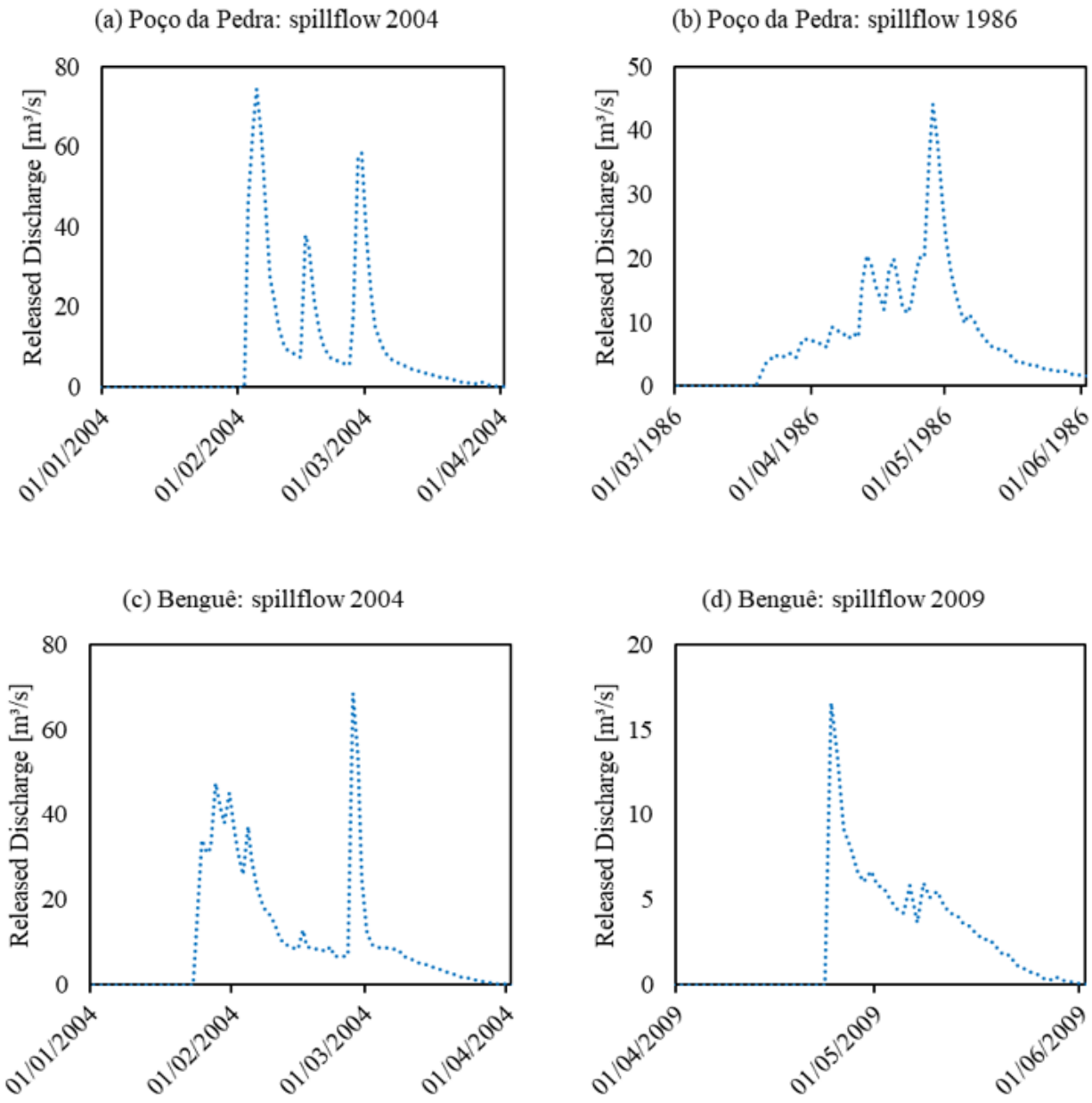

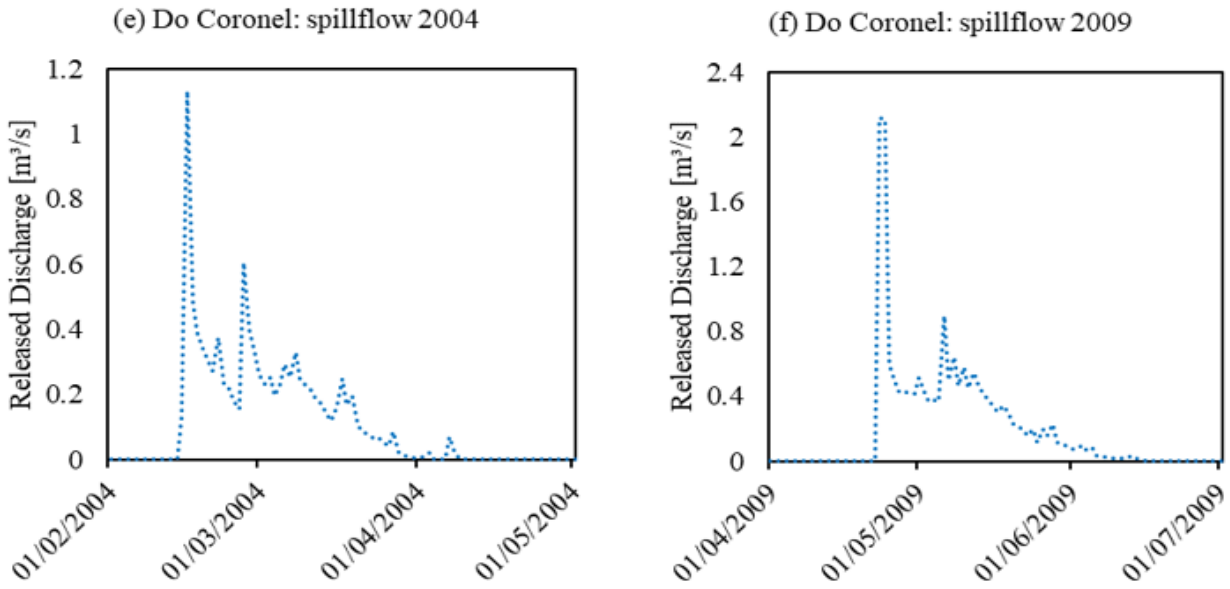

Source: The author

Beyond the results presented for reservoirs, an analysis was also made for the number of days on which the three reservoirs overflowed. These results were taken from analysis of the simulation, counting the days when each reservoir exceeded capacity resulting in spillway overflow during the simulation period (1979 – 2010). These values were compared with the number of spillway overflow days from the state water agency observed data for each reservoir. The results were presented in Table 2.8. The model greatly overestimated the number of days with spillway overflow, mainly for Poço da Pedra and Benguê. This is an expected result, since the hydrographs of these reservoirs for model simulation had several years reaching their capacities. On the other hand, for Do Coronel the results were very close. A greater number of days of spillway overflow from the reservoirs implies that more water reaches the outlet of the catchment, increasing the simulated streamflow values. This could be clearly seen in 2009, where all reservoirs overflowed and, consequently, the simulated peak flow at the Malhada station was much higher than the observed peak flow. Other years that also had simulated streamflow rates greater than those observed (2006, 2007, 2008 and 2010) coincided with the overflow of the reservoirs having a higher number of days in these years.

Figure 2.10 depicts the outflow hydrographs for four selected main private dams implemented as reservoirs for the entire simulation period (1979 – 2010). The two main private reservoirs with the largest drainage area and the largest storage volume (No. 46 and No. 146 respectively) and the largest main private reservoirs for Poço da Pedra catchment (No. 123) and Benguê catchment (No. 17) were chosen for presentation (see Figure 2.1), as they had the highest hydrological impact. The diagrams showed that water release from the reservoirs 17,

46 and 123 was simulated by the model only in some years, with the spilling lasting only for a couple of days. As presented before, it was expected that such medium-sized reservoirs spill out only in wet years after consecutive strong rain events. These results agree with this field observation. Hence, the spilling behavior seems realistic. With regard to the spillway outflow simulated for these main private reservoirs, the magnitude of the discharges were consistent considering the smaller drainage areas and the spillway widths estimated. Consequently, it may be stated that the estimation of the reservoir capacity and the model parameterization were reasonable. No other information nor observed data was available for these reservoirs. Therefore, the plausibility of the results may not be assessed more specifically.

The higher frequency and duration of spilling of reservoir number 146 simulated by the model were due to the fact that the soil type present in that area does not have any cracking potential. Therefore, the soil is saturated faster and more runoff is generated leading to a faster filling of the reservoir. As the spillway outflow magnitudes were consistent to the drainage area and the spillway width and the parametrization was based on the calibration of the volume of Do Coronel reservoir located nearby, it may be assumed that these results, too, were reasonable.

Table 2.8 - Comparison between the number of days with spillway outflow for observed data and the number of days with spillway outflow for model simulations during periods with data availability for reservoirs: 1986 - 2010 for Poço da Pedra, 2000 - 2010 for Benguê and 1998 - 2010 for Do Coronel.

Reservoir	**Number of days with spillway outflow observed**	**Number of days with spillway outflow simulated**
Poço da Pedra	97	316
Benguê	64	231
Do Coronel	93	110

Source: The author

Figure 2.10 - Hydrographs for simulated daily discharges released from the private reservoirs No. 17 (a), No. 123 (b), No. 46 (c) and No. 146 (d) via spillway for the years 2003-2010.

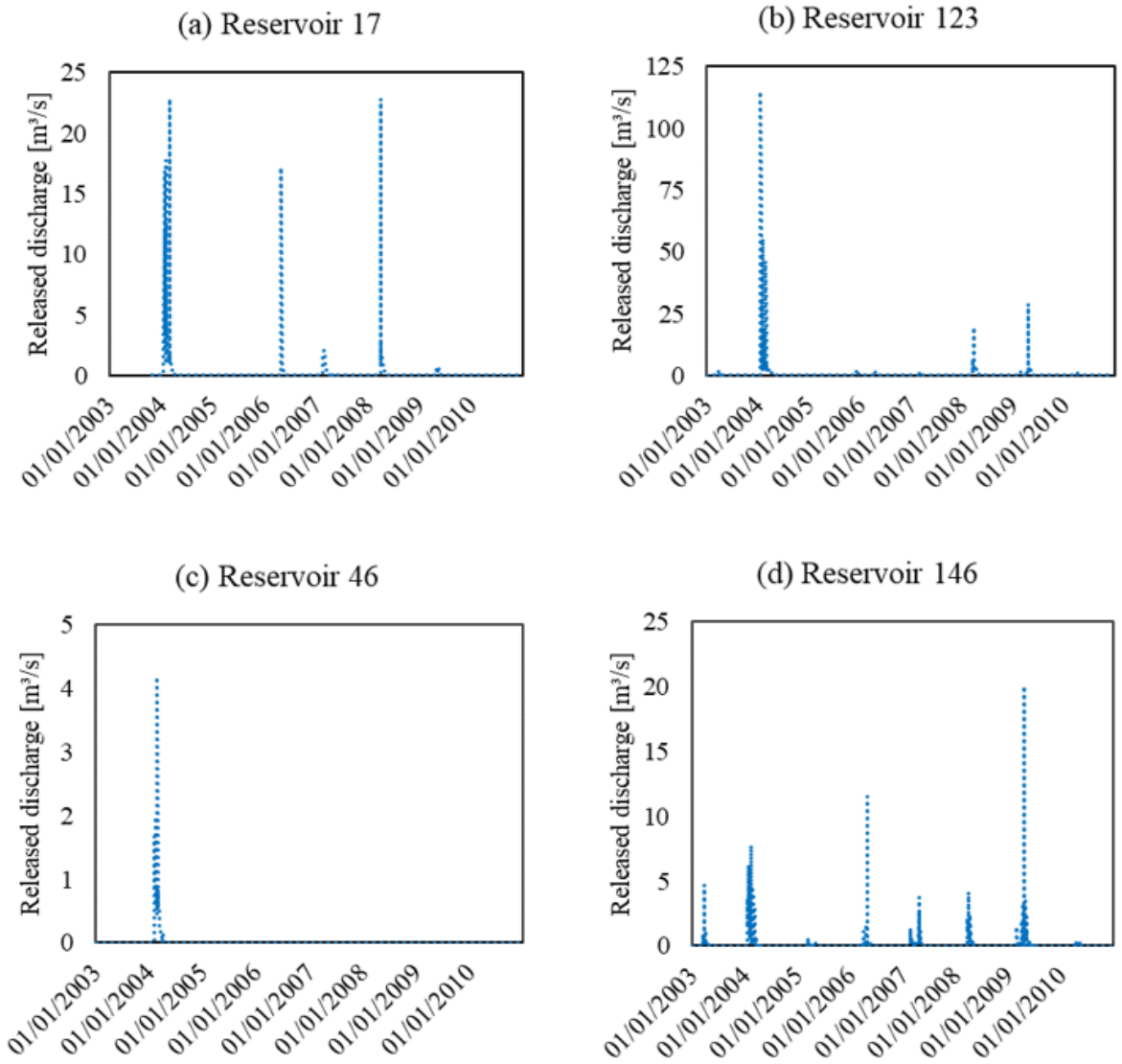

Source: The author

2.3.3 Impact of the reservoir network on streamflow and reservoir volume simulations

The influence of reservoirs on the outflow of the catchment was first investigated with the following four scenarios for the whole flow series (1979 – 2010): (i) considering all strategic reservoirs and small reservoirs (reference); (ii) removing all small reservoirs in the hydrological system, but keeping only the strategic reservoirs; (iii) removing all strategic reservoirs but keeping only the small reservoirs; (iv) removing all reservoirs. Table 2.9 presents a comparison for the model results criteria (PBIAS, NSE and KGE) between the four scenarios. The analysis of the statistical criteria in Table 2.9 showed that removing strategic reservoirs

significantly reduced the PBIAS, which means an increase in the simulated streamflow in the outlet. Also, NSE and KGE decreased. This result is in line with the expectations due to the decrease in retention by removing the reservoirs.

Table 2.9 - Comparison of model results in streamflow at Malhada gauging station for different reservoir scenarios (1979 - 2010).

Performance criterion	Scenario (i) (reference)	Scenario (ii) (only strategic reservoirs)	Scenario (iii) (only small reservoirs)	Scenario (iv) (no reservoirs)
PBIAS (%)	0.53	-2.76	-16.99	-20.30
NSE	0.63	0.61	0.51	0.48
KGE	0.81	0.80	0.70	0.66

Source: The author

Besides that, to illustrate the results obtained for wet years, the year of 2004 was chosen to show the comparison between the simulations, with the streamflow in the outlet at logarithmic scale (Figure 2.11). The streamflow hydrograph showed that, during the first increasing limb, the scenarios had a similar slope, but the scenarios (iii) and (iv) reached a higher peak flow. Scenarios (iii) and (iv) do not have strategic reservoirs, therefore water retention was lower in the catchment. After this point, all the scenarios showed similar results. As the differences between scenarios (i) and (ii) and between scenarios (iii) and (iv) were very small, this result also showed that the presence of small reservoirs did not significantly alter the streamflow during the rainy season. The water retention due to small reservoirs in wet years was 2%. The decreasing limb and the recession flow showed the same aspect observed in model calibration, with the end of wet periods to be abrupt, with streamflow going down to zero faster than the observed values, probably due to river-aquifer interaction processes that were not catched by SWAT as aforementioned. This behaviour is also seen in other wetted years, such as 1985 and 2009 (not shown here). Therefore, these results indicated that the basin under study is far from reaching its maximum water reserve capacity, especially considering the saturation of small reservoirs.

All scenarios overestimate the observed streamflow data, which can be seen more clearly on the cumulative streamflow representation (Figure 2.11). For the scenarios (i) and (ii), during the intermediate rainy season, the simulated recession flow was higher than the observed

one, mainly from 02/2004 to 03/2004. Furthermore, the scenarios (iii) and (iv) reached a higher peak flow at the beginning of the rainy season, due to the absence of the strategic reservoirs.

Figure 2.11 - Hydrographs and cumulative stream flow at Malhada station showing observed values and 4 scenarios of reservoirs during the year of 2004: scenario (i) considering all strategic reservoirs and small reservoirs (reference); (ii) removing all small reservoirs in the hydrological system, but keeping only the strategic reservoirs; (iii) removing all strategic reservoirs but keeping only the small reservoirs; (iv) removing all reservoirs.

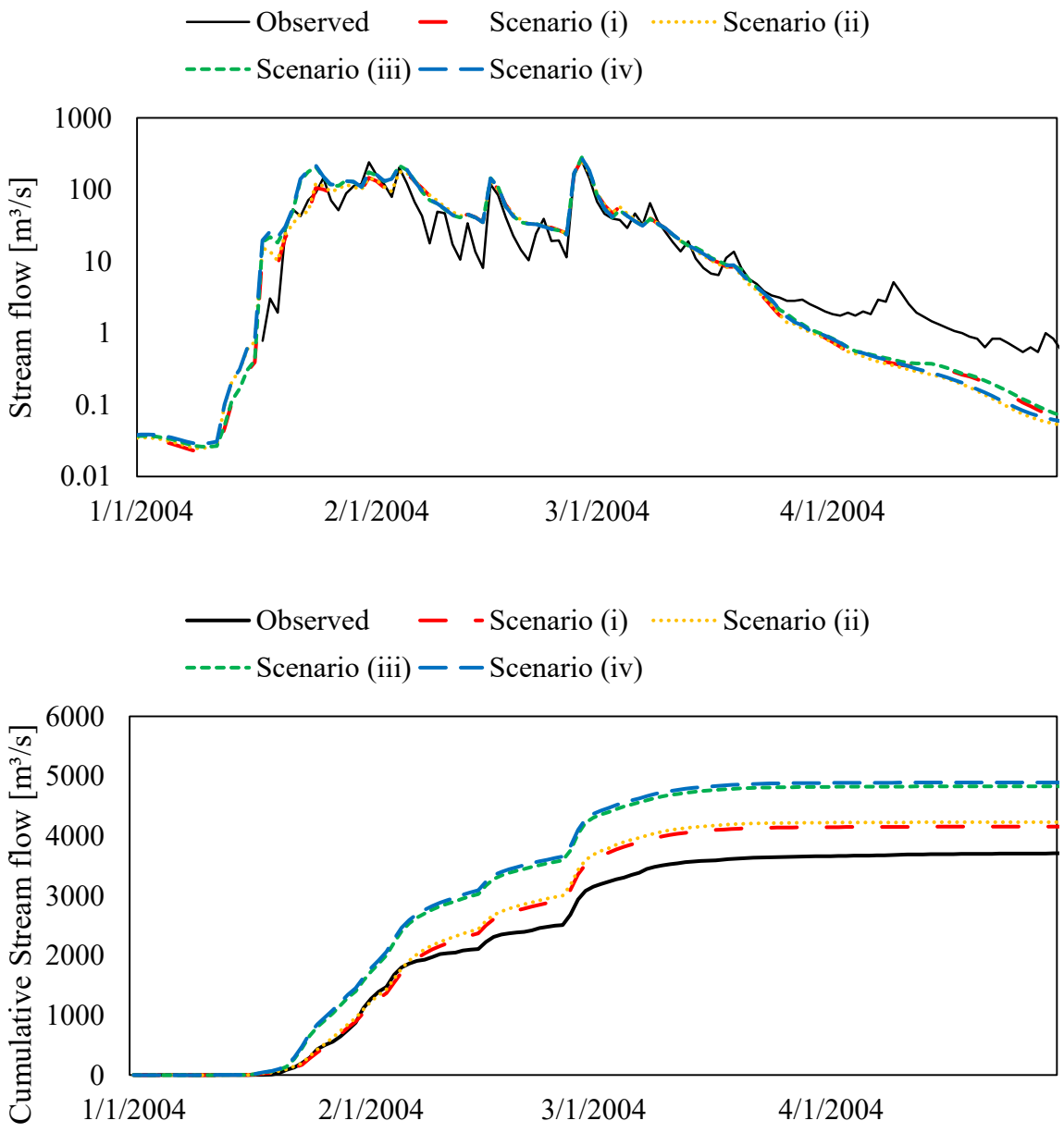

Source: The author

To illustrate the results obtained for dry years with low flows, the year of 2003 was chosen to show the comparison between the simulations and the observed data, with the streamflow in the outlet at logarithmic scale (Figure 2.12). The results were very similar to those obtained for wet years. All scenarios overestimate the observed streamflow data. However, the differences between scenarios (i) and (ii) and between scenarios (iii) and (iv) showed that the presence of small reservoirs is more significant for reducing the cumulative streamflow during a dry year. The water retention due to small reservoirs in dry years was 9%. Other studies have also shown that small reservoirs decrease low flows, with a more intense reduction in dry years (Perrin et al., 2012; Habets et al., 2018).

Now, modifying the dimensions of the small reservoirs ten times, we found a lower streamflow peak for the estimation with small reservoirs parameters ten times larger than the reference (original parameterization). This result was expected, because with more small reservoirs in the catchment, more water retention is observed, which means less outflow to the Malhada station. Despite this, the comparison of scenario simulations (the absence of small reservoirs, the reference and the larger dimensions of small reservoirs) for peak flow, increasing and decreasing limb were very close, with no considerable differences between the model scenarios for small reservoirs, even in dry years (not shown here).

The analysis of the reservoir volumes for the scenarios was carried out by a comparison of the time series of the storage volumes (

Figure 2.13,

Figure 2.14, and Figure 2.15). The results showed a small difference for the storage volume in the Poço da Pedra reservoir (

Figure 2.13) considering the changes in the dimensions of the small reservoirs. For the Benguê and Do Coronel reservoirs (

Figure 2.14 and Figure 2.15, respectively), the differences in the storage volume can be observed more clearly between 2002 and 2004, with larger volumes for the "0 times" simulation, which means the absence of small reservoirs, and slightly smaller volumes for the "10 times" simulation. Once again, this was an expected result, because by decreasing the small reservoirs more water can reach the strategic reservoirs, increasing the storage volumes. However, the differences between the simulations were not considerable to conclude for a relevant impact of small reservoirs on those catchments.

Figure 2.12 - Hydrographs and cumulative stream flow at Malhada station showing observed values and 4 scenarios of reservoirs during the year of 2003: scenario (i) considering all strategic reservoirs and small reservoirs (reference); (ii) removing all small reservoirs in the hydrological system, but keeping only the strategic reservoirs; (iii) removing all strategic reservoirs but keeping only the small reservoirs; (iv) removing all reservoirs.

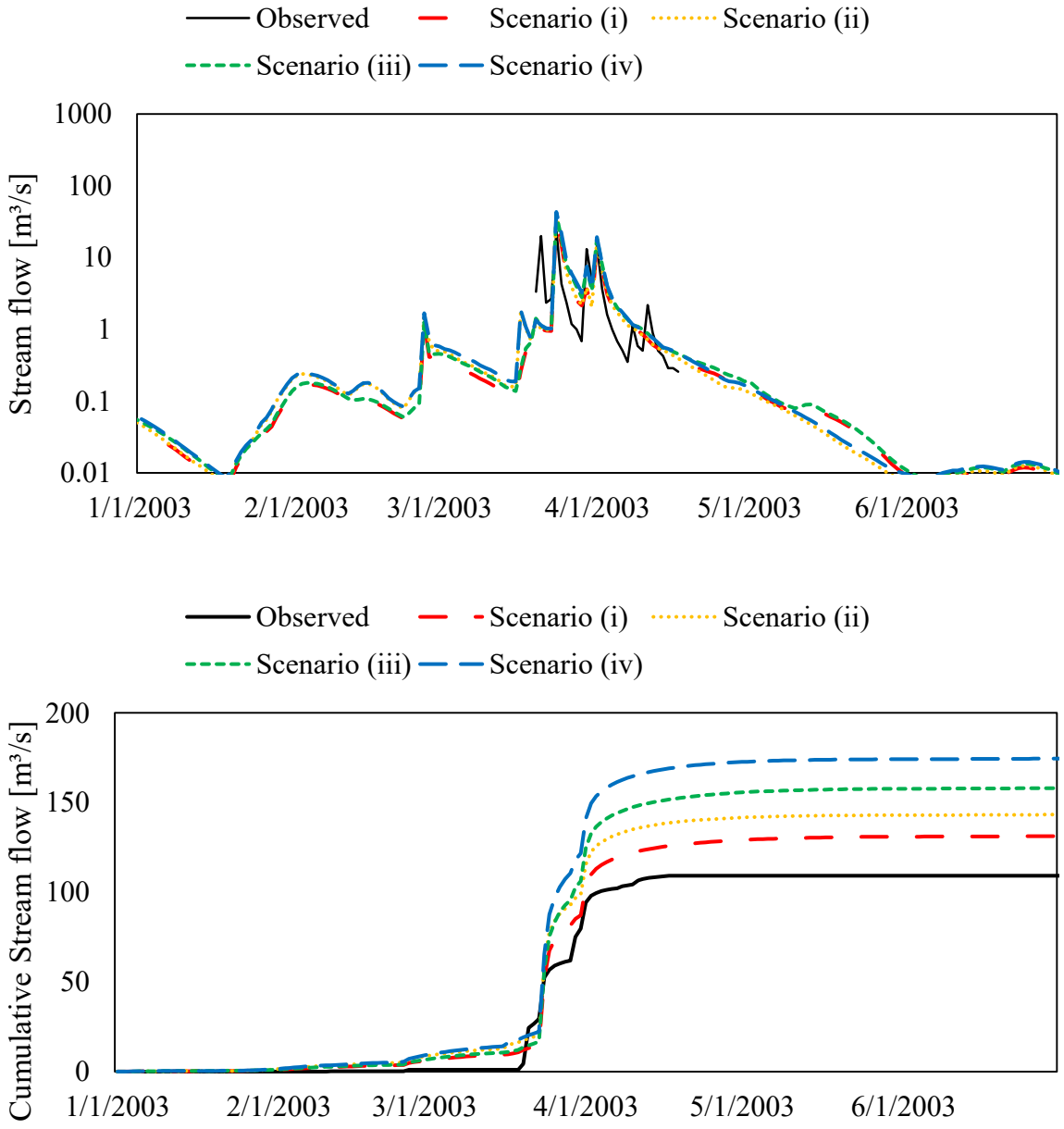

Source: The author

Figure 2.13 - Comparison for storage volumes in Poço da Pedra (2000 – 2010) with modifications in the dimensions of the small reservoirs in 0 and 10 times. “0 times” means the total absence of small reservoirs. “10 times” means a ten times increase in the parameters that represent the volumes of these small reservoirs. Model reference means the original parameterization.

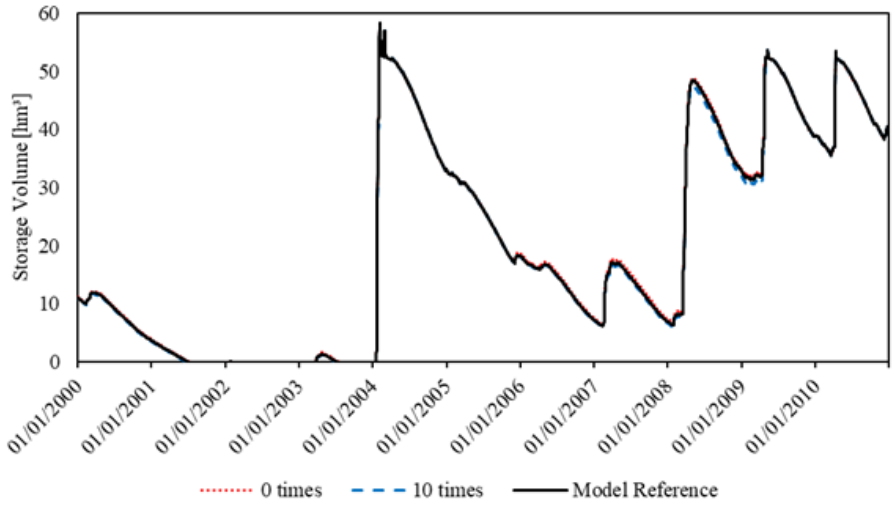

Source: The author

Figure 2.14 - Comparison for storage volumes in Benguê (2000 – 2010) with modifications in the dimensions of the small reservoirs in 0 and 10 times. “0 times” means the total absence of small reservoirs. “10 times” means a ten times increase in the parameters that represent the volumes of these small reservoirs. Model reference means the original parameterization.

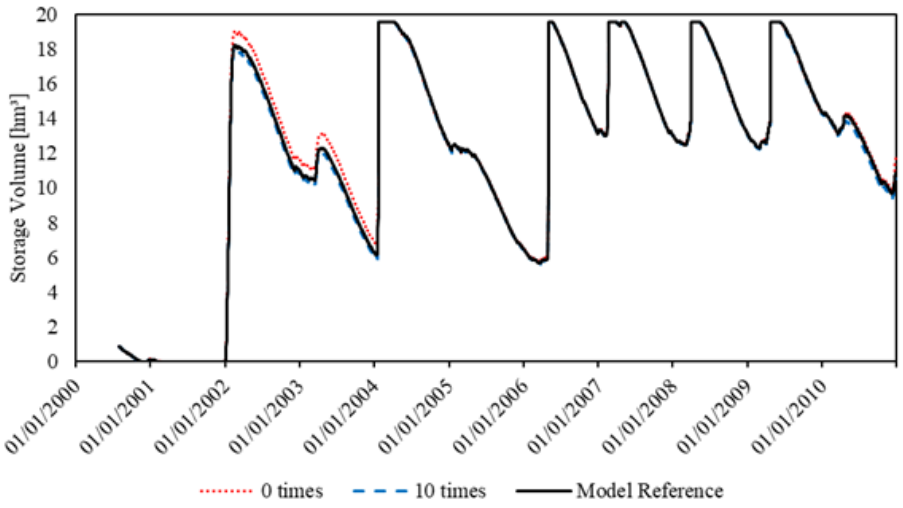

Source: The author

Figure 2.15 - Comparison for storage volumes in Do Coronel (2000 – 2010) with modifications in the dimensions of the small reservoirs in 0 and 10 times. “0 times” means the total absence of small reservoirs. “10 times” means a ten times increase in the parameters that represent the volumes of these small reservoirs. Model reference means the original parameterization.

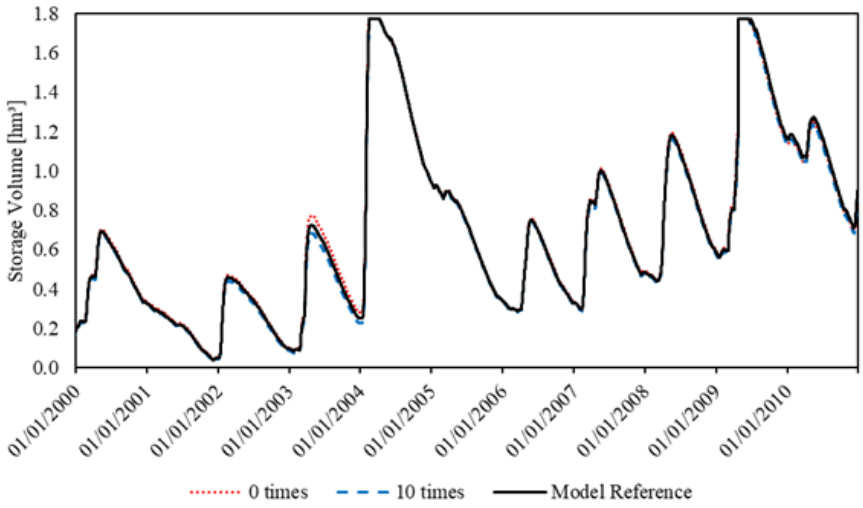

Source: The author

Previous studies suggested a relatively high impact of small reservoirs on the catchment water retention for the model aggregation of the small reservoirs in a lumped way - from 10% to 20% (Araújo and Medeiros, 2013; Peter et al., 2014; Mamede et al., 2018; Habets et al., 2018; Andrade Neto, 2022), while the present model with new representation of small reservoirs in SWAT showed a lower impact on the water inflow for strategic reservoirs (about 2% of water retention in wet years and about 9% in dry years). The study basin has an estimate of 230 reservoirs distributed over a total catchment area of 3,347 km², resulting in 1 reservoir per 14.5 km² (reservoir density). For semi-arid regions, the variability of spatial distribution and density of small reservoirs varies significantly, between 0 and 4.2 reservoirs per km² (Mady et al., 2020). In comparison with other dryland regions, the Conceição River Catchment reservoir density is 25 times bigger than reservoir density in California, USA, as reported by Minear and Kondolf (2009), for example. Despite the large number of reservoirs in the Upper Jaguaribe Basin (UJB), where the study area is located, we found a reservoir density 2.5 times smaller than that of the whole UJB, which is 1 reservoir per 6 km² (Lima Neto et al., 2011). This indicates that the study area can still be considered to have a high density of reservoirs, although it has a lower reservoir density than the average of the UJB. The impact of small reservoirs on water retention was also minimal in the Quaraí River basin, RS, South Brazil

(Collischonn, 2011). In this region, the number of small reservoirs is rapidly increasing due to the growing irrigation demand for annual crops, despite the catchment having a relatively low reservoir density.

Furthermore, considering the observed data from 1979 to 2010, the main hydrologic fluxes of the study are: annual precipitation, annual potential evapotranspiration and annual streamflow of 605 mm, 2,328 mm and 67.8 hm^3/year (20.3 mm), respectively. The total estimated reservoir capacity is 113.1 hm^3 (or 33.8 mm), of which 94.0 hm^3 (28.1 mm) comes from three strategic reservoirs. Ponds and main private reservoirs (226) have only 19.1 hm^3 (5.7 mm), on average 0.085 hm^3 (0.025 mm) per small reservoir. Even increasing the volume estimates of small reservoirs by ten times, the average volume per area of each small reservoir (0.25 mm) remains very small in comparison with strategic reservoirs and the aforementioned hydrologic fluxes. Moreover, as the stream flow are normally concentrated in a few days of the year in this catchment, the surface runoff has much more volume than the capacity of the small reservoirs, even for forcing moderate rainfall events.

Although the results obtained in this work represent hydrological aspects of a specific catchment in the Brazilian semiarid region, the methodology for assessing the impact of small reservoirs and the discussion of hydrological processes, such as peak flow and non-flow periods, channel transmission losses, analysis at the beginning and end of the rainy season in the streamflow gauge station hydrographs and in the storage volume of reservoirs, as well as the parameterization of the dense network of reservoirs, can also be applied to large-scale catchments located in other dryland regions. Some examples include semi-arid watersheds in Australia, United States, Mexico and South Asia, which present similar climate, hydrological and land-use characteristics.

2.4 Conclusions

In this study, we assessed the impact of small reservoirs on a dryland catchment with a high-density network of reservoirs and investigated the water routing dynamics and hydrological processes in the basin. For this purpose, a model was developed to simulate the catchment streamflow at the outlet, the storage volumes of large reservoirs and the water balance of lumped small-reservoirs at sub-basin scale. A methodology for the parameterization of the small reservoirs was developed to represent their integration into the catchment

hydrological modeling and to investigate their influence on the hydrological outputs (streamflow and reservoir volume storage) of the basin.

The main findings of our work can be described as follows:

1. The model proved to be well suited for simulating peak flow in wet years, the non-flow periods and the rising limb of the hydrograph with high reliability for the streamflow at the catchment outlet.

2. In the strategic reservoirs, wet and dry years were well represented, as well as the magnitude of spillway overflow of strategic and small reservoirs. On the other hand, the number of days with spillway overflow showed to be overestimated.

3. The proposed model presents an innovative way to represent a dense network of reservoirs in semi-arid basins in catchment hydrological models. The efforts in the parameterization and aggregation of ponds and reservoirs proved to be worthwhile, allowing a more accurate spatial representation of the strategic and small reservoirs in the SWAT model for high-density networks and improving the analysis of the hydrological processes and impacts in the basin.

4. The presence of small reservoirs decreased the stream flow and storage downstream reservoir volumes, with only 2% of water retention on average. Increasing the volumes of small reservoirs along the basin by ten times showed that the small ponds had a low influence on stream discharge. The catchment under study is far from reaching its maximum water reserve capacity, especially considering the current density of small reservoirs. However, in dry years, their impact can reach 9% of water retention, which may worsen periods of water scarcity in the large reservoirs.

For semi-arid catchments, the reliability of the results for peak flow in wet years, for non-flow periods and for the rising limb of the hydrograph is very important for the simulation of the stream flow reaching the large reservoirs and, consequently, for meeting the water demand at catchment scale. However future improvements should be done in the model for better representations in recession flow.

Since the results of the present study pointed to a low influence of the network of small reservoirs on the stream flow and strategic reservoir storages, the small reservoirs in the catchment might be an option to increase decentralized water access for small rural

communities, without competing with other water uses, such as large and medium-sized city sanitation demands and irrigation industry, from the strategic reservoirs.

The spatial representation of small reservoirs for a high-density network in the SWAT model and the results of the cumulative impact of small reservoirs presented in this study contributed to a better understanding of hydrology in dryland catchments, and can be applied to catchments in similar climatic and socio-economic environments. Further studies on the SWAT model in semi-arid regions will evaluate different arrangements for the increase of small reservoirs in the basin and their impact on reservoir water quality. Such studies should also be concerned with investigating channel transmission losses and river-aquifer interactions, based on comparison with additional (intermittent) groundwater data. The coupling of surface and groundwater models will potentially improve the understanding of dryland hydrology and integrated water resources management in semi-arid regions.

3 IMPACT OF DENSE NETWORKS OF RESERVOIRS ON STREAMFLOWS AT DRYLAND CATCHMENTS[2]

3.1 Introduction

Reservoirs are a worldwide used water infrastructure for compensating natural flow variability (Rabelo et al., 2021). In dry regions the water stored in reservoirs has fundamental importance to supply the population water demand during the dry seasons and droughts, as well as the use of water for industrial processes and for food production by irrigation (Samimi et al., 2020). The increase in population and the consequent growth in water demand, combined with climate and land use changes, have put pressure on water resources and increased the risk of severe hydrological droughts over the years in these dry regions (Ribeiro Neto et al., 2022). The combination of strategic reservoirs with many small reservoirs in dryland catchments generates a High-density Reservoirs Network (HdRN) that should improve water security but can modify streamflows during dry and wet periods.

The construction of public (strategic) reservoirs promoted by state water agencies was an important factor for population water security during the last century (de Araújo and Medeiros, 2013). Despite this, the hydraulic network for water distribution in many regions has several limitations, not reaching the population further away from urban centers, mainly in rural communities. Thus, the construction of small and medium-sized reservoirs has intensified in recent decades. These small reservoirs (below 1 million m^3) are often built by the population itself or by farmers, being essential for the availability of water in these rural communities. In addition to the importance of reducing inequality in the water distribution for water-scarcity regions these small reservoirs have low costs (Mady et al., 2020; Samimi et al., 2020).

On the other hand, the building of small reservoirs occurs most of the time without technical supervision, lacking hydrological studies and disregarding potential impacts on the availability of water for downstream regions (di Baldassarre et al., 2018; Rabelo et al., 2021). Usually, small reservoirs represent risks to the population downstream in the rainy season since many of these reservoirs do not have well-sized structures for flood control, with the risk of dam break during periods of more intense floods. Small reservoirs are often constructed in the

[2]A paper based on the content of this chapter has been accepted for publication in the Sustainability, MDPI, as Rabelo et al. (2022), and is available online at: https://doi.org/10.3390/su142114117.

cascade scheme along the rivers, so that the rupture of an upstream reservoir can cause the downstream reservoir to fail with catastrophic consequences for the population downstream (Cao et al., 2014, Oliveira and Lima Neto, 2020).

One of the reasons that makes it hard to estimate the cumulative impact of the HdRN on the hydrological processes of a region is the lack of data on small reservoirs, mainly information on storage capacity and surface area. Their mapping has grown a lot in recent years with the advancement of remote sensing techniques, which allow the acquisition of surface areas during rainy periods from satellite images combined with digital elevation models, and consequently the estimation of storage capacities (Avisse et al., 2017; Mady et al., 2020; Pereira et al., 2019; Ribeiro Neto et al., 2022). The spatial density of small reservoirs is quite different around the world, with densities ranging from 0.05 small reservoirs per km² in Nigeria to 0.4 small reservoirs per km² in Myanmar (Mady et al., 2020), for example. However, some specific dryland watersheds reach even higher values, as in India, 4.2 small reservoirs per km² (Paredes-Beltran et al., 2021), in Brazil, 7 small reservoirs per km² (Ribeiro Neto et al., 2022), and in Australia, 10 small reservoirs per km² (Nathan et al., 2015).

The understanding of small reservoirs' dynamics is extremely important for the management of water resources in dryland regions since their impacts on the hydrological network depend on their dimensions, uses and locations. Recent studies have been carried out to assess the cumulative impact of small reservoirs, such as the increase in evaporation losses (Althoff et al., 2019; Rodrigues et al., 2021) and the decrease of runoff generated in the catchment (de Araújo and Medeiros, 2013; Fowler et al., 2016; Habets et al., 2018; Lasage et al., 2015; Malveira et al., 2012; Rabelo et al., 2021). In addition, other studies have investigated the effect of small reservoirs on sediment retention dynamics (Bronstert et al., 2014; Mamede et al., 2018; Medeiros et al., 2014), in the reduction of energy demand for water pumping (Nascimento et al., 2019) and on the evolution and intensification of drought events (di Baldassarre et al., 2018; Ribeiro Neto et al., 2022; van Oel et al., 2018).

Another important effect of small reservoirs is on the water quality of the hydrological network, which is a risk associated with the misuse of small reservoirs. Many studies have been documented on the effects of nutrient accumulation in man-made reservoirs. For drylands, water supply reservoirs may be recurrently eutrophic or hypereutrophic, mainly due to phosphorus (P) and nitrogen (N) loads, which is a great concern for integrated water resources management. Sediment retention increases the amount of nutrients in small reservoirs, mainly P and N (Rocha and Lima Neto, 2021, 2022). Extended droughts may

intensify the eutrophication of these reservoirs. River streamflows carrying fertilizers and sewage provided by agricultural and urban practices may increase the number of pollutants in small reservoirs, such as pesticides, fecal coliforms, and even heavy metals. Furthermore, as the small reservoirs may be used for population supply, the increase in diseases associated with poor water quality can bring health risks to the population, such as diarrhea, schistosomiasis, and onchocerciasis (Cortez et al., 2022; Ignatius et al., 2016; Lima Neto et al., 2022; Moura et al., 2020; Owusu et al., 2022).

A system of small reservoirs can influence hydrological processes at catchment scale (Habets et al., 2018; Rabelo et al., 2021). However, most studies use highly simplified models to represent small reservoirs in hydrological networks. The storage capacities of small reservoirs, their horizontal connectivity, and their interaction with large strategic reservoirs are not represented in detail, which may lead to misinterpretation of the role of small reservoirs in simulating interannual variability of runoff. There is a gap in understanding the interannual variability of runoff retention, particularly during hydrologic extremes (floods and droughts), which complicates modeling the effects of future increases in the number of small reservoirs in drylands.

The eco-hydrological model SWAT (Soil and Water Assessment Tool) has been widely used for hydrological simulation in watersheds, obtaining good results for application in dryland regions (Andrade et al., 2019; Liu et al., 2014; Nguyen et al., 2017; Pathak et al., 2019; Shukla et al., 2020; Zhang et al., 2012). Despite this, even complex models such as SWAT need adjustments to modeling small reservoirs, since the large number of them usually has limitations to be implemented in the models.

A recent study using remote sensing in the State of Ceará, carried out by Research Institute of Meteorology and Water Resources of Ceará (FUNCEME), identified more than 105,000 dams with widths starting from 20 meters. The territorial area of the State of Ceará is approximately 150,000 km², with almost 87% of this area inside of the Brazilian semiarid. This distribution of small reservoirs is not uniform, so that some regions have very high densities of small reservoirs, especially in locations close to the largest strategic reservoirs in the State (FUNCEME, 2021). For these small reservoirs, water agencies in Ceará do not have information on systematic volume monitoring, only for strategic reservoirs. It is estimated that a recent drought in Ceará (2012-2017) caused losses of more than 6 billion dollars (Ribeiro Neto et al., 2022). These extended droughts encourage the construction of even more medium and small reservoirs to meet the water demand of small rural communities. The first studies

carried out by Ribeiro Neto et al. (2022) identified that small reservoirs can induce and modify drought events, extending hydrological droughts by an average of 30%. However, the influence of small reservoirs in the emergence, intensification, and propagation of droughts in drylands at watershed level still has few studies based on the modeling of these HdRN. Also considering the limitations in the data of the small reservoirs, the impact of small reservoirs in the annual streamflows at dryland catchments can still be better understood, such as the interannual influence that these HdRN have on the reduction of flows during wet and dry years.

The present study aims to determine the impact of the increase in the number of small reservoirs on dry hydrological networks, evaluating the annual flows generated at the outlet of a dryland watershed for scenarios with different densities of small reservoirs (number of reservoirs per area). To achieve this objective a detailed representation of a watershed, including large and small reservoirs, was modeled in SWAT. The study area was in the Brazilian semiarid region. The methodology generated a scenario approach for several hypotheses of growth in the density of small reservoirs in the catchment. The present study improves the understanding of the hydrology of dense reservoir networks and uses a modeling approach that can be applied to water resources management in drylands.

3.2 Materials and methods

3.2.1 Study area

The study was carried out in the Conceição catchment (3,347 km²), which is in the state of Ceará, northeast of Brazil (Figure 3.1). The Conceição River is a tributary of the Upper Jaguaribe River Basin (UJB), which is a sub-catchment of the Jaguaribe River basin (75,000 km²). The Jaguaribe River is the most important river in Ceará, and all over the river basin reservoirs were constructed to store water for agricultural, industrial and domestic use.

The climate in the region is classified as semiarid, “Bsh” according to the Köppen classification, characterized by a clear distinction between rainy and dry seasons. The rainy season occurs between the months of January and May concentrating approximately 80% of the annual rainfall. The period from June to December is characterized by a decrease in river streamflow (low flows) and high evapotranspiration rate. Annual precipitation in the region has an average around 600 mm, while annual potential evapotranspiration has an average around 2300 mm, which is almost four times greater than annual precipitation. The annual precipitation

and evapotranspiration provided by an interpolated series during the simulation period (1979 – 2010) are presented in Figure 3.2.

Figure 3.1 - Location of the study catchment with the main rivers and reservoirs. The red dots represent small reservoirs identified by remote sensing mapping of Funceme (2021). Main private reservoirs represent medium-sized reservoirs constructed by farmers.

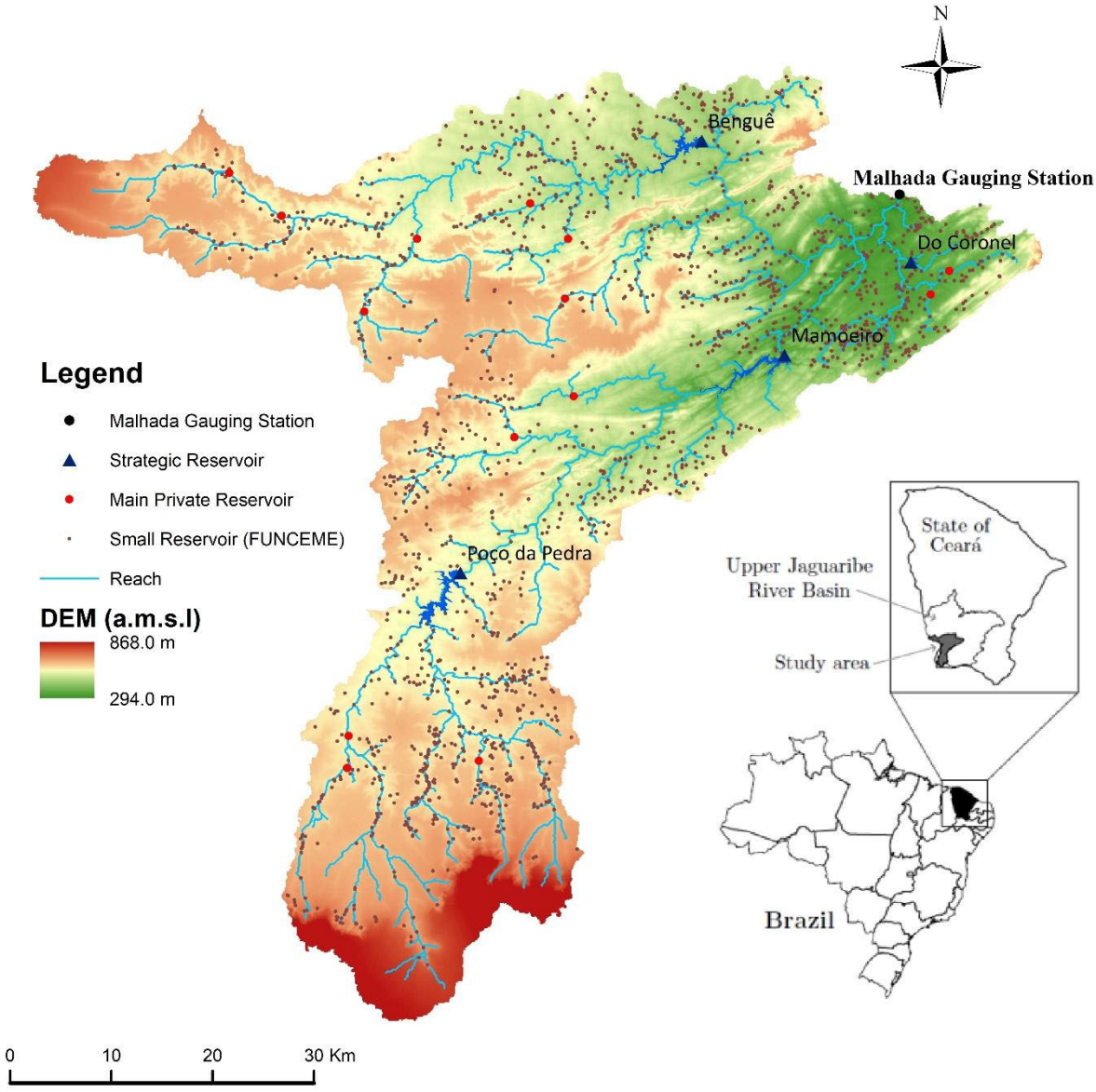

Source: The author

The soil of the region is characterized by being shallow, with low hydraulic conductivity and porosity. Geologically, 80% of the region is composed of a complex of crystalline rocks, with a low occurrence of aquifers. Consequently, the combination of soil-

related factors, high spatial and temporal variability in rainfall, and high annual evapotranspiration rates make the rivers of the region intermittent. Thus, the occurrence of droughts in the region is quite recurrent even in consecutive years, so called extended droughts.

Figure 3.2 - Average annual precipitation and average annual potential evapotranspiration in study catchment. Results provided by an interpolated series from 1979 to 2010 that represent the simulation period.

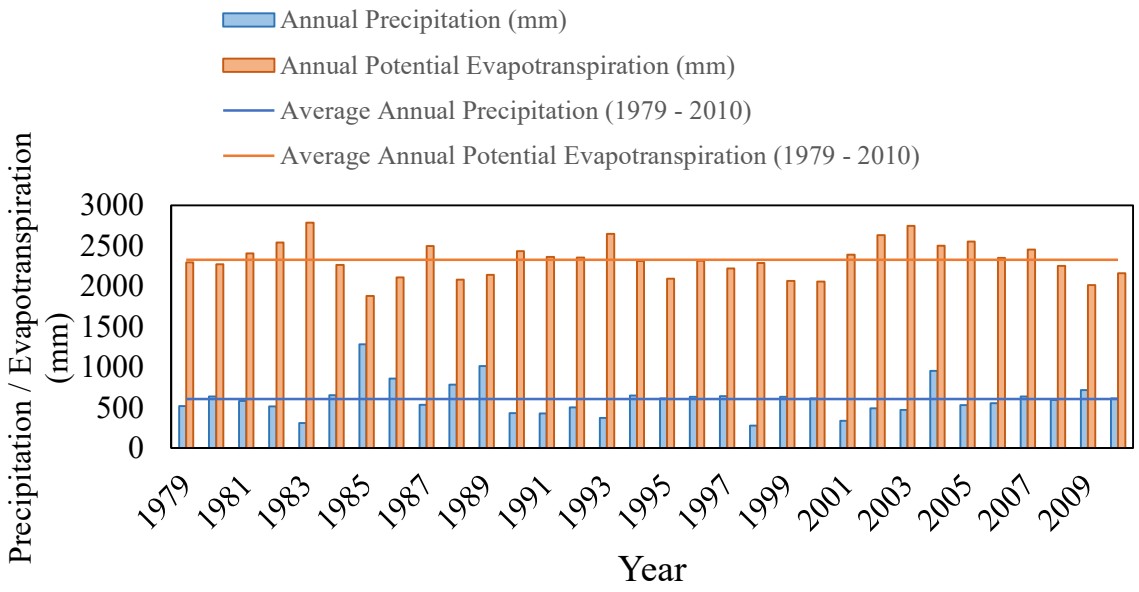

Source: The author

The streamflows at Conceição River catchment are monitored daily at the Malhada Station. Figure 3.1 presents Malhada Gauging Station and all reservoirs identified by FUNCEME (2021) for the catchment. There are 4 strategic reservoirs monitored by the Water Agency of the State of Ceará (COGERH): Poço da Pedra, Benguê, Do Coronel and Mamoeiro. The privately built reservoirs with different sizes and shapes (main private reservoirs and small reservoirs) are usually referred to as small reservoirs. Despite not being one of the regions in Ceará with the highest density of small reservoirs, this availability of flow data is critical to assess the impacts of human processes on the hydrological network, such as the increase of the construction of small reservoirs to supply rural communities. In addition, the study area was also chosen based on the frequent droughts that occur, thus representing a very dry region of the Brazilian semiarid.

3.2.2 Model parameterization

The SWAT model was used to model hydrological processes and reservoirs, and to simulate streamflows in the outlet of the catchment. The delineation of the watershed and its river network (Figure 3.1) were carried out based on a digital elevation model (DEM) with 90 m resolution. The climate data was made available by FUNCEME. All analyzed scenarios of small reservoirs were based on the SWAT model calibrated and validated for the Conceição River catchment available at Rabelo et al. (2021). To clarify the modeling processes carried out in SWAT, in the following sections the parameterization of large and small reservoirs and the calibration of the model are briefly presented.

3.2.2.1 Reservoir system

The modeling of reservoirs was carried out as follows: the analysis of aerial images in the Conceição River catchment identified 230 reservoirs after the rainy seasons in 2004, 2008 and 2009; the volume and area of these reservoirs were estimated using the Molle's equation (Molle, 1994) adapted by Pereira (2017); water impoundments caused by dam constructions built across the main river reach and with estimated storage capacity larger than 0.01 hm^3 were modeled in the "reservoir" structure of the SWAT model (strategic reservoirs and main private reservoirs); the remaining reservoirs were modeled in the "pond" structure of the SWAT model (small reservoirs); due to the large number of small reservoirs and the limitation of SWAT2012 in allowing only one "pond" per sub-basin, they were aggregated into a single "pond" for each sub-basin, by the cascade or parallel arrangement. A more detailed description of the methodology for aggregation of small reservoirs into ponds by cascade and parallel arrangement is available in sections 2.2.3.2 and 2.2.3.5. The results of the reservoir modeling in the contribution area can be summarized as follows: 230 reservoirs distributed in a total area of 3,347 km^2, with 4 strategic reservoirs (capacity = 73.33 hm^3), 14 private reservoirs (capacity = 5.28 hm^3) and 212 small reservoirs (capacity = 13.70 hm^3). The density of reservoirs in the region is estimated at 0.068 reservoirs per km^2 (about 1 reservoir per 14.81 km^2). However, Mamoeiro reservoir was disregarded in the analysis due to this strategic reservoir becoming operational only in 2012, after the last year of simulation (1979 – 2010). This model was considered in the study as a reference model.

3.2.2.2 Calibrated model

The parameterization of strategic reservoirs used information obtained from COGERH for the surface area when reservoir filled to emergency spillway (RES_ESA), storage volume when principal reservoir filled to emergency spillway (RES_EVOL), surface area when reservoir filled to emergency spillway (RES_PSA), storage volume when reservoir filled to principal spillway (RES_PVOL), initial reservoir storage volume (RES_VOL), target storage volume (RES_TARG), month in which reservoir became operational (MORES), year in which reservoir became operational (IYRES), hydraulic conductivity of reservoir bottom (RES_K), and lake evaporation coefficient (EVRSV). The number of days to reach target storage from current reservoir storage (NDTARGR) was defined for each reservoir using the Poleni equation (Aigner, 2008). The withdrawal of water from the strategic reservoirs was considered constant during all months, based on a simplified average approach measured by water agencies.

The parameterization of the main private reservoirs and of the ponds was done by defining the same model parameters as for the strategic reservoirs. However, no data was available for them from COGERH. The flooded areas were estimated by aerial images and the storage volumes were calculated by the adapted Molle's equation. The application Google Timelapse was used to determine the parameters MORES and IYRES of the main private reservoirs, while SWAT assumes that all ponds had been existing during the simulation period. The other parameters were defined following the same characteristics of the strategic reservoirs. Detailed information about main private reservoirs and ponds can be found in section 2.2.3. Table 2.2 presented in section 2.2.3.3 summarizes the parameterization of strategic reservoirs and main private reservoirs with a description of all parameters, while Table 2.3 presented in section 2.2.3.5 summarizes the parameterization of small reservoirs.

The calibration of the reference model was based on the available data, literature (Rocha et al., 2023), and experience of the modelers. The following methods were used by applying the curve number method, plant evaporation method and Muskingum method for the calculation of infiltration, evapotranspiration, and channel routing, respectively. The parameters to describe the rainfall-runoff relationship were calibrated with an iterative trial and error procedure, by keeping parameter values in a physically meaningful range. Initial values for the model parameters were derived from field data as much as possible. When field data were not available, dryland-based literature values were chosen for them. Table 2.4, Table 2.5,

and Table 2.6 presented in section 2.2.4 show parameters set to the entire catchment, parameters set for specific sub-basins of the catchment, and parameters set for specific soil zones, respectively. More detailed information about model parameterization and calibration can be found in section 2.2.4.

The main aim of this study is not to make an in-depth discussion of the calibration criteria of the River Conceição catchment model in SWAT. Some information is still important with regard to the calibration and validation of the model. The model parameters were calibrated by an manual iterative trial and error process, considering each sub-catchment of the three strategic reservoirs separately. The first two years (1979-1980) were considered warm up years in the simulation. A two-fold cross-validation was performed using both halves of the series (1981 - 1995 and 1996 - 2010). First the time series 1981 - 1995 was used for calibration while the second time series was used for validation. Subsequently, the process was inverted to consider the time series 1996 - 2010 as the calibration series and the time series 1981 - 1995 as the validation series. After the two-fold cross-validation process the parameters of the models were defined to maximize the Nash-Sutcliffe-Efficiency (NSE) and Kling-Gupta-Efficiency (KGE) statistical parameters and to minimize the percent bias (PBIAS) for the simulated streamflows in comparison with the daily observed streamflow at the basin outlet (Malhada Station). The reference model obtained good results for daily streamflows, with values of 0.63, 0.81 and 0.53% for NSE, KGE and PBIAS, respectively. A detailed description of the reference model and its results can be found in Chapter 2.

3.2.3 Scenarios approach for increase in the number of small reservoirs

To assess the impact of the increase in the number of small reservoirs in the watershed, eight scenarios with different numbers of small reservoirs were chosen, based on the technical report “Mapping of the dams of small reservoirs located in the State of Ceará” carried out by FUNCEME (2021), which identified reservoir densities with values distributed between 0 and 2 reservoirs per km² in Ceará territory. Thus, the scenarios of small reservoirs per km² in this study were chosen based on the classes defined by the assessment of FUNCEME, with the inclusion of one value above this range: 0.10 res/km²; 0.25 res/km²; 0.50 res/km²; 0.75 res/km²; 1.00 res/km²; 1.50 res/km²; 2.00 res/km²; 3.00 res/km².

The addition of small reservoirs in the model has the following methodology: for each value of reservoir density the number of reservoirs distributed in the total area of 3,347

km² of the catchment was calculated; the number of strategic reservoirs was kept constant in the modeling, so the number of reservoirs exceeding the reference model was due only to the addition of private reservoirs and small reservoirs. The calculation of the addition of these two types of reservoirs in the scenarios was done keeping the same proportion between main private reservoirs and small reservoirs of the reference model. This number of additional reservoirs was converted into volume using the average volume of private reservoirs and the average volume of small reservoirs in the watershed, and then distributed equally in the model. This methodology considered the hypothesis that the construction of new reservoirs in this region will be uniformly distributed along the catchment. In this way, the process of the increase in the number of small reservoirs was performed by the addition of these volumes in each pond and in each main private reservoir of the model, increasing the parameters RES_EVOL and RES_PVOL of the SWAT. These increases in SWAT parameters of small reservoirs were carried out for all scenarios of densities of small reservoirs as summarized in Table 3.1. It is important to note that none of the other SWAT parameters of the small reservoirs were changed, remaining equal to the values of the reference model.

The different scenarios of small reservoirs modeled in SWAT were simulated between 1979 and 2010. The results obtained from the simulations were the Flow Duration Curves (FDCs) for monthly flows, and the annual streamflow obtained at the basin outlet (Malhada Station) for each of the scenarios. The annual streamflows were compared between the data observed by COGERH, the previously calibrated model (reference model), and the different scenarios of the increase in small reservoirs. For this comparison we used the annual anomaly for precipitation (equation 3.1) and for discharge (equation 3.2) and the percentage of reduction of the annual discharge (equation 3.3) in the catchment, between the years 1981 and 2010 (the first two years were considered as model warm-up) for each scenario.

$$\text{Annual Anomaly (precipitation)} = \frac{P_y - P_a}{P_a} \ (\%), \tag{3.1}$$

$$\text{Annual Anomaly (discharge)} = \frac{Q_y - Q_{r,a}}{Q_{r,a}} \ (\%), \tag{3.2}$$

$$\text{Percentage Reduction of Annual Discharge} = \frac{Q_{s,y} - Q_{r,y}}{Q_{r,y}} \ (\%), \tag{3.3}$$

where: Py represents total precipitation in year “y”, Pa the average annual precipitation from 1981 to 2010, Qy the annual accumulated discharge in year “y”, Qr,a the

average annual discharge from 1981 to 2010 for reference model, Qs,y the annual discharge for different scenarios in year “y” and Qr,y the annual discharge for reference model in year “y”.

Table 3.1 - Volume increases for each density of small reservoirs in the model. The numbers with “*” represent the parameterization of total ponds, total main private reservoirs, and their respective volumes in the reference model.

Small Reservoirs Density (small reservoirs per km²)	**Reference Model (0.068)**	**0.10**	**0.25**	**0.50**	**0.75**	**1.00**	**1.50**	**2.00**	**3.00**
Number of total Small Reservoirs	226	335	837	1,674	2,510	3,347	5,021	6,694	10,041
Number of additional Small Reservoirs	-	109	611	1,448	2,284	3,121	4,795	6,468	9,815
Number of Ponds to be added	212*	102	573	1,358	2,143	2,928	4,497	6,067	9,207
Number of Main Private (MP) reservoirs to be added	14*	7	38	90	142	193	297	401	608
Total Volume of the new Ponds (hm³)	13.7*	7	37	88	138	189	291	392	595
Volume increase in each Pond of the model (hm³)	-	0.03	0.19	0.45	0.70	0.96	1.48	1.99	3.02
Total Volume of the new MP reservoirs (hm³)	5.3*	2.54	14.28	33.84	53.40	72.97	112.09	151.22	229.47
Volume increase in each MP reservoir of the model (hm³)	-	0.18	1.02	2.42	3.81	5.21	8.01	10.80	16.39

Source: The author

A new calibration and validation processes of the simulations were not necessary, since the model parameters were not changed, only the number of small reservoirs in each simulation.

Figure 3.3 illustrates the main flowchart of this study with a summary of all steps applied.

Figure 3.3 - Flowchart of steps applied in SWAT model and the approach to analyze the impact of the small reservoir increase in the catchment streamflow.

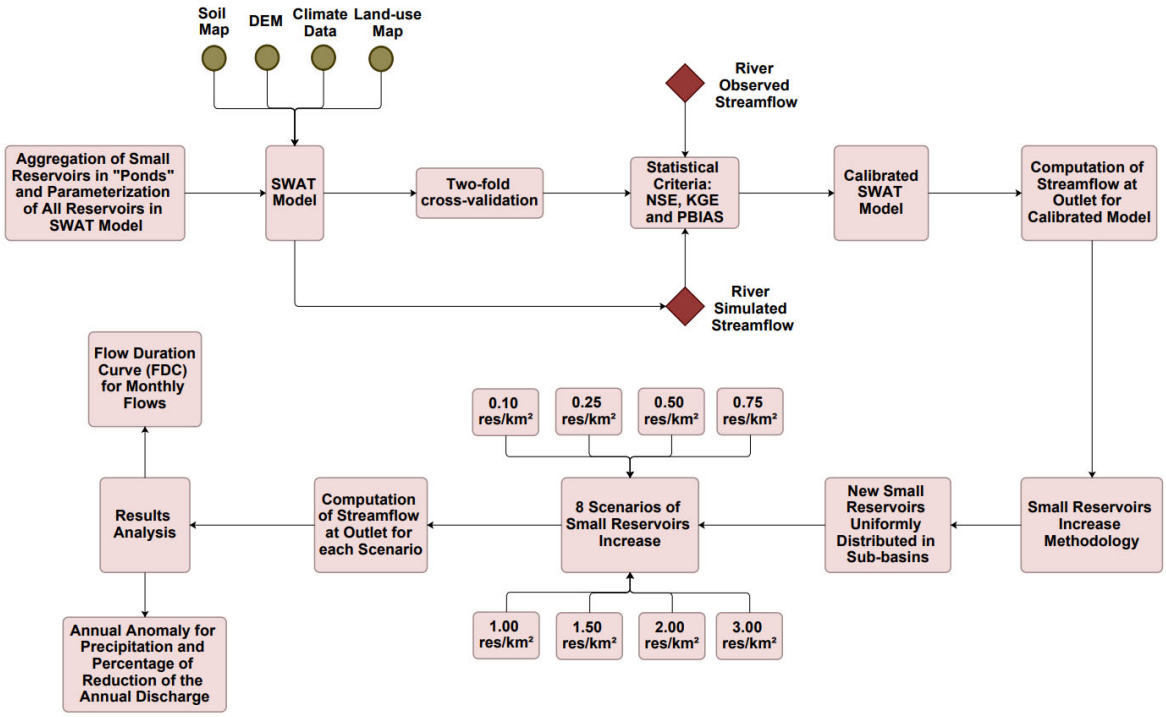

Source: The author

3.3 Results

3.3.1 Simulated impact of small reservoirs on streamflow

The first results were the duration curves on a monthly scale for the simulated flows at the outlet (Malhada station). Two FDC were initially defined as references to compare the results: the duration curve provided by the values measured by COGERH at Malhada station and the duration curve provided by the reference model (reservoir density = 0.068 res/km²). For a better graphical representation only the two extreme results of the simulations are presented in the duration curves (Figure 3.4): the scenario in which there is no reservoir and the scenario with the largest number of reservoirs in the simulation (3 res/km²). All other scenarios had intermediate values between these two. As the study area is in a semiarid region with ephemeral streamflow in the river, most of the time river flow becomes next to zero. To analyze the impact

of small reservoirs in the period that the flows are effective, the flow duration curves (Figure 3.4) were also presented showing only the first 20% of the time when the flow is exceeded. For 80% exceedance probability the remaining runoff in the catchment is almost zero, consequently with no significant differences between the simulated scenarios.

In Figure 3.4 we can observe the impact of the small reservoirs in the 20% of the time when the flows have relevant values. The simulation with the absence of reservoirs presents the highest values of monthly flow for the same percentage of time in which this flow is exceeded. For example, the monthly flow around 580 m^3/s is exceeded in 5% of the time for the simulation without reservoirs, while for the other three scenarios this monthly flow is about 420 to 460 m^3/s. For a 10% exceedance time the monthly flow is around to 150 m^3/s at no reservoir's scenario, while around 100 m^3/s at observed values by COGERH, around 130 m^3/s at calibrated model and around 110 m^3/s at 3 res/km^2 scenario. Differences can reach over 60% in some cases, such as for an exceedance probability of around 8%. The FDC for a density of small reservoirs equal to 3 res/km^2 is significantly below the FDC of 0 res/km^2 between 1% and 10% of time in which the monthly flows are exceeded. For values of exceedance probability next to 0%, the differences in monthly streamflow tend to decrease (a maximum value around 7%). These values of streamflow represent months with very high peaks of flow. In these situations, all reservoirs in the catchment (strategic and small reservoirs) tend to have spillway overflows and the impact of reservoirs on flow reduction diminishes during these periods (Rabelo et al., 2021; Ribeiro Neto et al., 2022).

The FDCs in Figure 3.4 show the impact of small reservoirs in the decrease of water during the rainy months is more intense with the increase in the number of small reservoirs. Although most studies in the literature focus on the decreased annual stream discharge, for peak flows the impact of these small reservoirs are estimated up to 45% of reduction (Habets et al., 2018; Ayalew et al., 2017). For flows next to zero a more detailed analysis is necessary and there is a limitation in the SWAT model for low flows in dryland catchments due to transmission losses (Rabelo et al., 2021).

The mapping of dams available by FUNCEME identified that the highest densities of small reservoirs occur in regions close to the largest strategic reservoirs. Thus, there is a tendency to build small reservoirs in these regions, mostly to take advantage of the regularization of water that strategic reservoirs provide to rivers. Despite this, as the study area does not have the highest densities of small reservoirs in the state, the assumption of adding

small reservoirs uniformly along the watershed was a simplification in the model to evaluate the impact of small reservoirs in the simulations.

Figure 3.4 - Monthly Flow Duration Curve (FDC) for streamflows at Malhada gauging station.

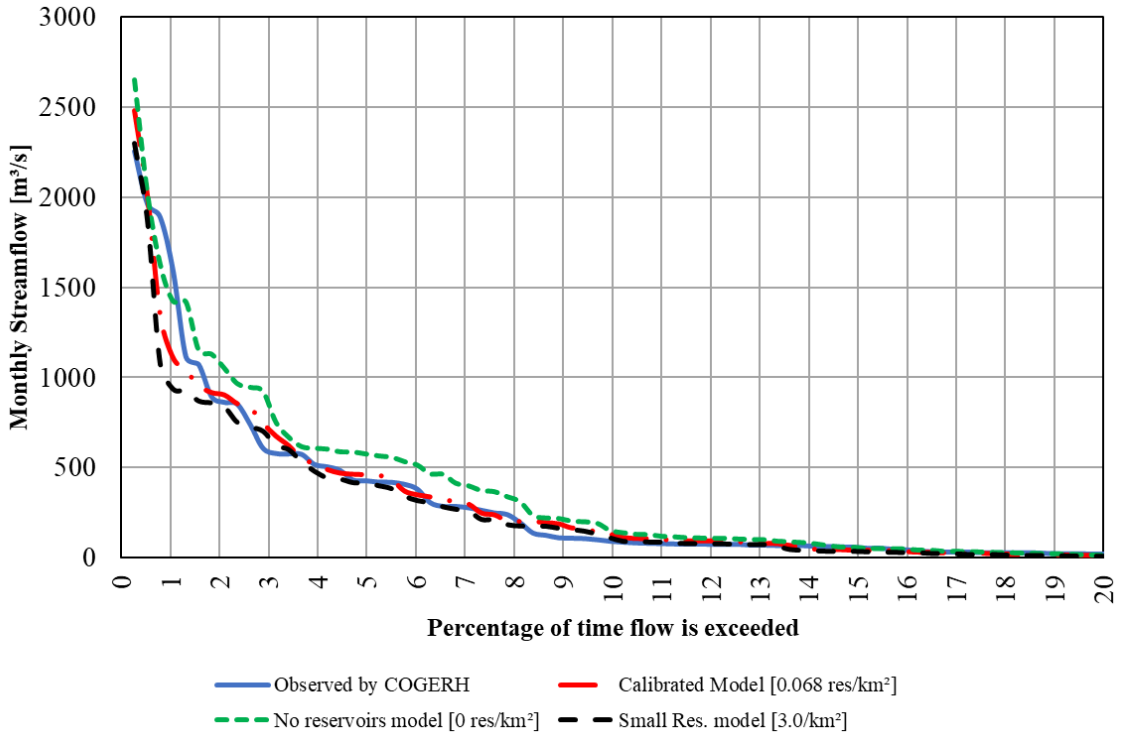

Source: The author

3.3.2 Annual streamflow anomaly

As a starting point for the study of annual flows for the study area three anomaly graphs were obtained: the first provided by the annual rainfall anomaly (precipitation anomaly); the second provided by the annual anomaly of the flows measured by COGERH (measured discharge anomaly); the third provided by the annual anomaly of the flows simulated by the reference model (simulated discharge anomaly). The objective of the anomaly graphs is to identify years with greater deviations in rainfall and runoff and to observe the behavior of precipitation and measured and simulated streamflows at Malhada gauging station during wet and dry years. Figure 3.5 shows the three annual anomaly graphs from 1981 to 2010.

The analysis of the anomaly graphs allows to identify high positive deviations for precipitation and for measured discharge in 1985, 1986, 1989 and 2004 (wet years), while high negative deviations for precipitation in 1983, 1990-1993, 1998 and 2001-2003 (dry years) and high negative deviations for measured discharge in 1982-1983, 1990-1994, 1996, 1998-2003,

2005-2008 and 2010. The other years had values close to the average. The pattern of positive deviations in precipitation implying positive deviations in streamflows is observed for other regions around the world for drought studies (Floriancic et al., 2020, 2021). However, this cause-and-effect relationship is not so clear for low precipitation and low flow years. In dryland catchments highly modified by human activities there is a strong nonlinear pattern between rainfall and runoff (Costa et al., 2021). This nonlinearity can be observed not only during dry years, but also during wet years, in which deviations in discharge are much greater than deviations in precipitation.

In order to understand the effects of the increase in the number of reservoirs on the streamflows, the total annual flows were obtained at the Malhada station in each year, and in each of the scenarios: reference model (0.068 res/km²); 0.10 res/km²; 0.25 res/km²; 0.50 res/km²; 0.75 res/km²; 1.00 res/km²; 1.50 res/km²; 2.00 res/km²; 3.00 res/km². In each year from 1981 to 2010 and in each of the simulated scenarios the differences between the total annual flows were calculated considering the flows in the reference model as base values. In this way, Table C.1 and Table D.1 presented in Appendix C and Appendix D show respectively the values of annual streamflows at Malhada gauging station and the percentage difference for streamflows in comparison to the flow obtained for the reference model in each scenario of increase in reservoir density and in each year. This percentage difference represents the annual reduction of flow due to the increase of small reservoirs in each scenario.

A combination between the anomaly graphs and the annual reduction of flow table (Table S8) was developed to analyze the influence of the increase in the number of small reservoirs in the streamflows for all years of the series, mainly wet and dry years. Figure 3.5 shows the three anomaly graphs, with an indication of their percentage on the left axis, and the annual reduction values for each simulated scenario, with an indication of their percentage on the right axis.

The annual streamflow reduction at Malhada gauging station for the scenario approach had values from 1% (0.1 res/km²) to 14% (3.0 res/km²) on average. The analysis of Figure 3.5 shows that the greatest ranges in flow reduction correspond to the years 1983 (1.6% to 21.5%), 1998 (2.0% to 30.3%), 1999 (0.8% to 23.5%) and 2005 (2.5% to 29.8%). Comparing with the anomaly graphs, we notice that these years correspond to dry years, with highest negative bias in precipitation, mainly in the years of 1983 and 1998, and negative bias in the runoff, mainly in the years of 1983, 1998 and 2005. Habets et al. (2018) point out that during dry years the reduction on annual discharge tends to be twice as high as in median years and

these results can be observed even without changes in the small reservoir network, just due to the seasonality of the climate. For dry years the reported decreases in the annual discharges have a high range, with values next from 0% to values up to 50% (Nathan et al., 2015; Perrin et al., 2012; Rabelo et al., 2021; Thompson, 2012). The results for dry years in our simulations suggest the increase in the number of small reservoirs leads to an intensification of the hydrological drought during the dry years, since these years have a higher percentage of flow reduction with the increase in the number of small reservoirs.

Figure 3.5 - Comparison between anomalies in precipitation and annual discharge versus annual streamflow reduction for different scenarios of small reservoirs per km².

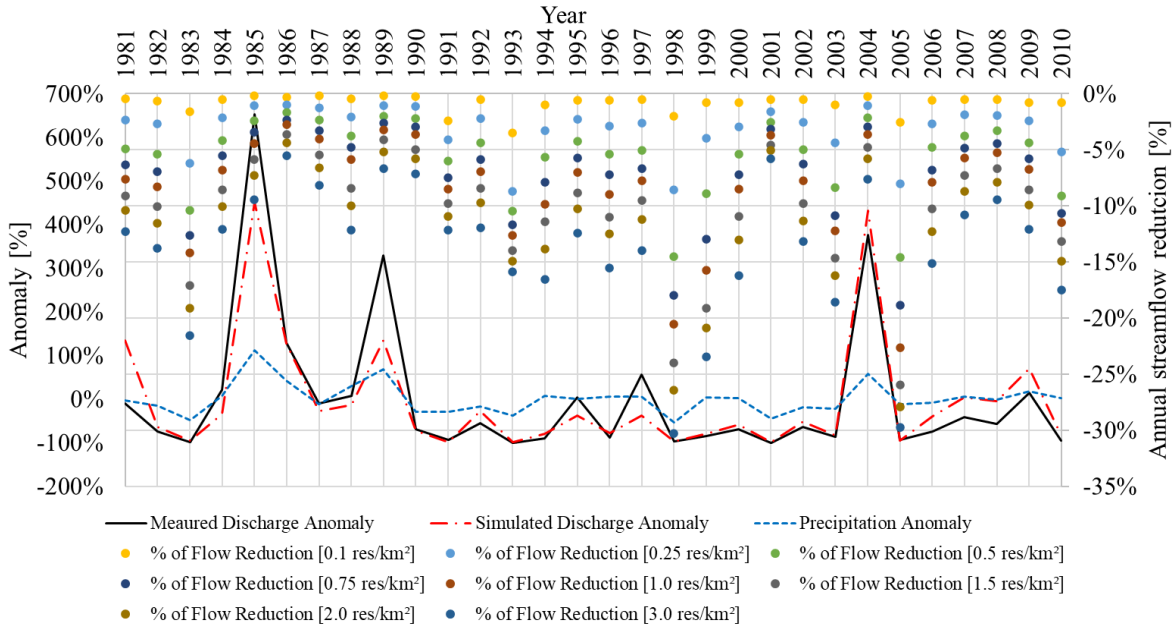

Source: The author

On the other hand, the smallest ranges in flow reduction occur in the years 1986 (0.3% to 5.5%), 1989 (0.2% to 6.7%) and 2004 (0.2% to 7.6%). The years 1986, 1989 and 2004 correspond to wet years with positive bias in rainfall and flows. The last two years have a large positive bias in the flows measured at the Malhada Station, while the first (1986) is the year following the year with the highest positive anomaly for the flows (1985). This result suggests that in rainy years the increase in the number of small reservoirs has less impact on the reduction of streamflow. As the small reservoirs have small capacities, their filling occurs quickly during the wettest years, making the network hydraulically connected, with excess overflows going more easily to downstream regions, and reducing the volume retained in each reservoir. Other

studies found that when storage capacities of all reservoirs are close to the maximum the impact of the small reservoirs are limited (Ribeiro Neto et al., 2022).

Another two years with low ranges in streamflow reduction, if individually observed, were 1990 and 2001. The year 1990 represents the beginning of an extended meteorological drought between 1990-1993, while the year 2001 represents the beginning of another extended meteorological drought between 2001-2003. In these cases, the reduction of flows intensified with the extension of the meteorological drought. For example, in 1990 the annual flow reduction due to the increase in the small reservoirs ranged from 0.3% to 7.1%, while in 1993 the annual flow reduction ranged from 3.5% to 15.9%. In 2001, the range was from 0.6% to 5.8%, while in 2003 the range was from 1.0% to 18.6%. These results suggest that the increase in the number of small reservoirs can intensify the period of extended droughts since the few flows generated in the catchment are retained by the small reservoirs. Ribeiro Neto et al. (2022) suggest that dense networks of small reservoirs can induce and intensify drought events, mainly causing the onset of hydrological drought earlier and extending the duration of this drought.

If in the year following an extended meteorological drought the precipitation occurs around the mean, the reduction of streamflows tends to remain high, since this average rainy season would not be able to fill all the reservoirs. We can observe this result in 1994, with a range in flow reduction between 1% and 16% for the scenarios, values close to the year 1993 (end of the meteorological drought). However, if in the year following an extended meteorological drought the precipitation occurs well above the average, the tendency is a small reduction of the annual runoff, since the reservoirs of the hydrological network would quickly become full. This result can be observed in 2004, with a range in flow reduction between 0.2% and 7.6%, almost half of the range observed in 2003 (end of the meteorological drought).

The analysis of Figure 3.5 also shows that the increase in flow reduction has a strong nonlinearity effect by the increase in the number of small reservoirs, even in dry or wet years. For dry years (1983, 1998 and 2003) different ranges were observed (up to 21.5% for 1983 and up to 30% for 1998 and 2003) although nearby anomalies for precipitation and streamflow. For wet years (1985, 1989 and 2004) the differences in the ranges were up to 9.4% in 1985, up to 6.7% in 1989 and up to 7.6% in 2004. The years with rainfall around the average also had average reduction values. In this situation, the reduction values for the scenario with 0.1 reservoir per km² ranged from 0.1% to 1.0%, while for the scenario with 3 reservoirs per km² ranged from 8.2% to 17.5%. Figure 3.5 shows that there is no linearity between the increase in

the small reservoirs and the streamflow reduction, as years with nearby anomalies for precipitation and streamflow have different ranges and peak values in annual flow reduction.

3.4 Discussion

The amount of water retained in small reservoirs is an important information for water resources management in regions with dense networks of reservoirs. These HdRN can be found in dry areas of different countries, such as Brazil, USA, West Africa, and Australia. Reservoir management is critical to water availability and sustainability in dry regions. The integration of the cumulative effect of small reservoirs must be considered in the hydrological network, either from models or from average estimates of accumulated volume and nutrient loads, mainly in dry years. The estimation of total volume of water accumulated in small reservoirs during dry or wet years is hampered by the lack of monitoring in them, which is hard to obtain due to the high number of small reservoirs. This is one of the main limitations for considering small reservoirs in water management (Habets et al., 2018; van Oel et al., 2018). Furthermore, with the prognosis of population growth, economic development, urbanization, and climate change in the future the increase in the number of small reservoirs can be a challenge for water agencies (Deitch et al., 2013; Owusu et al., 2022; Rabelo et al., 2021).

The impact of small reservoirs in streamflows is currently small compared to strategic reservoirs. For Conceição River catchment Rabelo et al. (2021) found on average a 2% of annual flow retention with the density of reservoirs equaling 0.068 res/km². However, the increase in the number of small reservoirs may increase the effects in the streamflows of the hydrological network. In this sense, scenarios with higher densities of small reservoirs can lead to cumulative impacts, increasing the flow retention to values close to those found for large reservoirs impacts (Deitch et al., 2013; Habets et al., 2018). This study obtained, on average, streamflow reductions from 1% to 14% in semiarid Brazil for densities of reservoirs from 0.1 res/km² to 3.0 res/km², while studies in semiarid West Africa obtained flow reductions of 14% in mean annual streamflow for scenarios with 0.08 res/km² (Owusu et al., 2022).

By an analysis of around 30 references, Habets et al. (2018) show that similar densities of small reservoirs can lead to different flow retentions (from 5.4% to 21.4%), as we see for semiarid Brazil and semiarid West Africa. The definition of a single indicator, as the density of small reservoirs in the area, to provide a first guess for the flow retention of small reservoirs has limitations due to the hydro-climatic conditions. The distribution of the reservoir

network in dryland catchments and the hydrological processes in these regions, such as transmission losses and increased evaporation by small reservoirs should be evaluated to understand better the streamflow reduction caused by small reservoirs (Owusu et al., 2022; Rabelo et al., 2021).

The impact of the increase in the number of small reservoirs on streamflow reduction occurs strongly during dry years, with low flows. The decrease in low flows also has a large range, between 0.3 to 60% in Australia, Brazil, New Zealand, South Africa, and the USA (Habets et al., 2018; Owusu et al., 2022; Rabelo et al., 2021). In addition, this research found values of up to 30% of streamflow retention for scenarios with densities of reservoirs until 3.0 res/km², while during extended drought years the values of retention ranged from 0.3% to 18.6%. These results lead to the intensification of droughts by the increase in the number of small reservoirs.

When a meteorological drought starts it is common an increase in well digging for water supply. In a region with low availability of underground water the construction of small reservoirs becomes a possibility for the local population to cope with droughts. The spatial distribution of reservoirs has a great impact on the occurrence of the hydrological drought. As streamflow drought responds more quickly than reservoir drought to a meteorological drought, the presence of water stored in small reservoirs can cause a delay between the beginning of the meteorological drought and the beginning of the hydrological drought, mainly in upstream regions. These small reservoirs dry up quickly in the dry season, consequently downstream reservoirs suffer the effects of droughts more quickly (He et al., 2017; van Langen et al., 2021; van Loon et al., 2022; van Oel et al., 2018; Vicente-Serrano et al., 2017). In dense networks of reservoirs this problem may be aggravated. As the presence of a dense network of reservoirs can lead to a 30% increase in the duration of hydrological droughts, the greater the number of small reservoirs, the greater the impact on water availability in the region (Ribeiro Neto et al., 2022). Despite those results, it is still hard to evaluate individually the impact of small reservoirs on the transition from meteorological drought to hydrological drought due to the complexity of the hydrological processes in the catchment. Many authors observed a clear nonlinear relationship of hydrological drought and meteorological drought in different regions, with nonlinear functions modeled to propagation threshold from meteorological drought to hydrological drought (Salimi et al., 2021; Wu et al., 2021; Zhou et al., 2021).

The impact of small reservoirs on streamflow reduction is smaller during rainy years. In these years, as the precipitations are high and the small reservoirs usually fill quickly,

the overflow of the spillways occurs in most of the small reservoirs also quickly. In this sense, for rainy years the hydraulic connectivity is achieved and the potential for water held in small reservoirs decreases, as they are already full (Rabelo et al., 2021; Ribeiro Neto et al., 2022).

The accumulation of water in small reservoirs during rainy years has an important social and economic function for rural communities. Not only in the Conceição River catchment, but also in several other watersheds in regions with a semiarid climate, small reservoirs act as an important structure to increase water access to the population (Rabelo et al., 2021; Owusu et al., 2022).

One of the main benefits is the use of this available water for irrigation and food production, bringing food security to these communities. Both small families and farmers in these regions also may use agricultural activities, fishing, and aquaculture as a source of income. As the water infrastructure to transport water to the population far from urban centers is often expensive, these small reservoirs are invaluable for the livelihoods of rural communities. In addition to the small reservoirs, the population of these regions usually uses wells for supply. The impact of small reservoirs on groundwater recharge is still unknown for dense networks of reservoirs at dryland catchments (Casadei et al., 2019; Cecchi et al., 2020).

3.5 Conclusions

This study analyzed the impact of the increase in the number of small reservoirs in large-scale dryland catchments. We used a SWAT model to simulate the streamflows for the Conceição River catchment (semiarid of Brazil) and applied a methodology to represent the increase in the number of small reservoirs per square kilometers in the catchment.

The main findings of this study are:

1. The impact of reservoirs on flow reduction is very small for periods of extreme high flows. In this period, the comparison of monthly streamflows between the reference model and scenarios with and without reservoirs have approximately a maximum difference of 7%.
2. The influence of the dense network of reservoirs on streamflow reduction mostly occurs for a probability of exceedance between 1% and 10% for Conceição River catchment.
3. There is a strong nonlinear effect for the increase in the number of small reservoirs at the annual streamflow reduction. For different dry years with the same

precipitation pattern, the streamflow reduction has different ranges. The ranges of streamflow reduction have no linearity even for wet and normal years.

4. The impact of the increase in the number of small reservoirs on flow reduction occurs strongly during dry years, with values up to 30% for the higher density of small reservoirs (3 res/km²).

5. The streamflow reduction tends to increase in years with consecutive lack of rains. In extended droughts, flow reduction is from about 7% in the first year to about 20% in the last year of the worst scenario. The increase in the number of small reservoirs may intensify the period of extended droughts.

This research provides insights about the influence of the increase in the number of small reservoirs at dryland catchments. However, as a starting point for the scenario approach, the increase in small reservoirs was evenly distributed across the catchment. For future studies, a more realistic scenario approach should be adopted, with a higher increase of small reservoirs in regions close to large strategic reservoirs and higher population densities.

Since small reservoirs on minor tributaries are largely unregulated in most countries, especially in drylands due to water scarcity, yet there is the potential for them to have significant impacts on water availability, with both positive effects and many potential negative impacts. In this sense, the methodology proposed in this study is highly transferable for different catchments worldwide. Moreover, as the population growth coupled with climate change trends may intensify the construction of small reservoirs to meet water demand of rural communities, the future scenarios of growth in the number of small reservoirs and the understanding of their influence on streamflow reduction may help water resources agencies to better prepare for future periods of droughts and extended droughts.

4 SEMI-DISTRIBUTED HYDROLOGICAL MODEL PERFORMANCE DECREASES DRASTICALLY DURING EXTREME DROUGHT AND HYDROLOGICAL RECOVERY [3]

4.1 Introduction

Climate change and global warming have raised alarms in the international community due to their potential to intensify the hydrological cycle through long-term alterations in climate patterns and increases in the planet's average temperature (Ju et al., 2021). Recent climate research has identified that the increase of global temperature may escalate the magnitude and frequency of extreme droughts, thereby reducing water availability (Allan et al., 2020; Asif et al., 2023; Hattermann et al., 2018; Konapala et al., 2020; Qiu et al., 2023; Salehi, 2022; Tzanakakis et al., 2020).

Drought typically begins with a lack of precipitation in the catchment area, commonly defined as meteorological drought, which leads to decreased streamflow in rivers, and consequently, reduced volumes in reservoirs, usually defined as hydrological drought. Drought propagation plays an important role in determining different drought impacts across catchments, with its effects being more or less pronounced depending on the region's vulnerability. Recent studies have identified that the transition from meteorological to hydrological drought is influenced by climate factors, catchment properties and human activities (Apurv et al., 2017; Colombo et al., 2024; Wu et al., 2022; Zhang et al., 2022). As a result, similar meteorological droughts can propagate differently across catchments, leading to varied eco-socio-economic impacts (Bradford et al., 2020; Crausbay et al., 2020; Shi et al., 2022; Wang et al., 2024). Understanding the hydrological impacts of climate change and human activities in regions susceptible to extreme droughts is fundamental to meeting water demands in these areas. In this sense, the need for robust hydrological models for future climate impact assessments is a key element for effective water management.

Conceptual rainfall-runoff models have been commonly employed to assess the impacts of climate change on water resources, as these models have demonstrated satisfactory performance under modified climate conditions. However, during extremely dry periods,

[3]A paper based on the content of this chapter has been submitted for publication in the Journal Hydrological Processes, Wiley.

especially severe and multi-annual droughts, these models experience a decline in performance, particularly in catchments where changes in the rainfall-runoff relationship are identified (Saft et al., 2016; Trotter et al., 2023).

On the other hand, different models have been employed to simulate hydrological processes at various catchment scales, particularly distributed and semi-distributed models. Several studies have investigated hydrological impacts due to land use changes (Kibii et al., 2021; Serrão et al., 2022; Zhang et al., 2020b), the cumulative influence of High-density Reservoirs Networks (HdRN) (Colombo et al., 2024; Lima et al., 2023; Rabelo et al., 2022), pollutant propagation (Dogan and Karpuzcu, 2023; Noori et al., 2020), sediment retention (Mamede et al., 2018), changes in cropping patterns (Akbari et al., 2022; Shaabani et al., 2024), and the hydrodynamics and thermal stratification of reservoirs (Larabi et al., 2022; Mesquita et al., 2020; Rocha et al., 2022). One model that has gained significant prominence and has been widely used in catchments worldwide is the SWAT/SWAT+ (Soil and Water Assessment Tool), which is one of the best suited models for agro-hydrological studies at catchment scale (Uniyal et al., 2019), thus can be used for studying agricultural droughts on larger scale. Also, the SWAT model has achieved satisfactory results in reproducing both wet and dry periods within catchments, particularly when parameter calibration is well executed. The SWAT model is also currently being used to investigate the impact of climate change on water resources (Li and Fang, 2021; Saade et al., 2021), but there is still room for further exploration of the model's performance during recent extreme drought events (Tan et al., 2020) and subsequent periods of hydrological recovery, especially for catchments with HdRN.

One of the limitations reported by authors regarding the use of hydrological models to investigate future scenarios is related to the sensitivity of calibration periods to climatic conditions. Depending on the available meteorological series, severe and multi-annual droughts are frequently absent from the calibration dataset, which introduces uncertainty in the model’s application to future climate change scenarios. Bruno et al. (2024) argue that including droughts in the calibration process may enhance model performance for streamflow simulations; however, the results from Vaze et al. (2010) suggest that models calibrated using more than 20 years of data can generally be employed for climate impact studies where the future mean annual rainfall does not deviate by more than 15% drier or 20% wetter than the mean annual rainfall during the calibration period. Conversely, the findings of Trotter et al. (2021) indicate that the "naïve" approach of extending calibration sequences to encompass as much climate

diversity as possible is not sufficient to significantly improve model reliability when addressing future climate uncertainty and recent shifts in the hydrological behavior of natural watersheds.

The effect of parameter value changes is often neglected post-calibration, resulting in a validation and prediction process that utilizes a calibrated model, extending the simulation by only considering the new climate projection. Merz et al. (2011) concluded that there is strong evidence of correlations between model parameters and climatic variables, and time-varying parameter methods for hydrological simulations are being employed to capture the dynamic nature of hydrological processes in changing environments (Liu et al., 2024; Zhang et al., 2024). However, Merz et al. (2011) also stated that, in addition to parameter variability, changes in the representation of processes within models are also necessary. For instance, the authors suggested that vegetation might transpire more efficiently than models would predict based solely on air temperature, as observed when comparing conditions between the late 1970s and the early twenty-first century, leading to model runoff overestimation. Incorporating these dynamic processes could also help reduce biases.

Regarding the evaluation of model output quality, many studies still rely on traditional criteria, such as the Nash-Sutcliffe coefficient (NSE) or the Kling-Gupta coefficient (KGE). For the specific case of assessing low-flow periods, applying logarithmic or inverse transformations to the simulated and observed discharge time series can put more weight on low flows and mitigate the influence of error range distortions (Pushpalatha et al., 2012; Santos et al., 2018b).

Another issue that deserves attention in hydrological models is the transmission losses in drylands, especially during severe droughts and subsequent hydrological recovery. Some researchers have observed that channel transmission losses increase during higher stream discharges, attributed to enhanced infiltration due to elevated hydraulic heads at the surface (Costa et al., 2012, 2013). Conversely, Jarihani et al. (2015) found that channel transmission losses were higher during low flows (up to 68%) compared to high flows (up to 24%) in a dryland catchment in Australia. Moreover, runoff transmission losses are intricate in dryland catchments, influenced by features such as pools, subsidiary channels, floodplain areas, clogging layers, and high hydraulic conductivity heterogeneity, resulting in varied loss values along river lengths (Costa et al., 2023; McMahon and Nathan, 2021). The SWAT model's approach to simulate channel transmission losses is relatively straightforward, relying on parameters like hydraulic conductivity, flow translation time, wet perimeter, and channel length. During periods of severe droughts, groundwater dynamics can vary greatly, so that

hydrological processes and the values of these parameters can change significantly (Costa et al., 2013; McMahon and Nathan, 2021).

Furthermore, the behavior of watersheds in the face of historical severe droughts remains under investigation. Peterson et al. (2021) suggest that hydrological recovery following an extreme drought event can be uncertain and may require an extended wet period, rather than occurring within a fixed period with regular rainfall post-drought. Recent observations show that prolonged droughts can cause unexpectedly reductions in rainfall-runoff relationship in regions such as Australia (Saft et al., 2016), the USA (Avanzi et al., 2020), China (Tian et al., 2018), Chile (Alvarez-Garreton et al., 2021), and Italy (Massari et al., 2022). Some studies have been conducted to assess the persistence of watersheds alternative state after droughts (Grafton et al., 2019), yet there remains scope to evaluate the impact of human-induced changes on the hydrological recovery of watersheds following severe droughts. Whether or not watersheds consistently recover from prolonged droughts has relevant implications for long-term global water resource planning and aquatic environments, particularly under changing climate conditions.

To contribute to the discussion on the limited performance of hydrological models during severe droughts and their hydrological recovery, this research aims to promote a broader scientific discourse on the need to enhance hydrological modeling during extreme drought events and hydrological recovery afterwards. The present research evaluated the runoff performance of a large-scale semi-distributed hydrological SWAT model, previously calibrated from 1981 to 2010, in a later drier and warmer climate decade from 2011 to 2022. This period includes the prolonged drought (from 2012 to 2017) in the study region, which was initially analyzed through precipitation and maximum and minimum temperature trends. The decade of 2011 – 2020 was the warmest on record, with a global mean temperature 1.10 °C ± 0.12 °C above 1850 – 1900 average (WMO, 2023). A new sensitivity analysis was done to the most sensitive parameters, with meaningful ranges based on typical values used in scientific literature, to assess their impact on streamflow model performance during the prolonged drought. Also, to investigate the rainfall-runoff patterns before and after the prolonged drought, correlation graphs were developed for precipitation and observed and simulated runoff in the catchment.

4.2 Methods

4.2.1 Study area

The study area is the Riacho Conceição catchment (3,347 km²), in the Upper Jaguaribe Basin, State of Ceará, Brazil. The runoff of the catchment is measured in the outlet by the Malhada fluviometric gauging station. Riacho Conceição is a tributary of the Jaguaribe River, the largest river in Ceará. The climate is semi-arid, with the rainy season occurring between January and May, and the annual precipitation has an average of 583.5 mm. The dry period is characterized by a lack of rain and high evaporation rates. Potential evapotranspiration reaches annual values up to four times greater than precipitation rates. These climatic conditions provide regular droughts in the region, which can even occur in many consecutive years (Cunha et al., 2019; Pontes Filho et al., 2020).

The study area has four strategic reservoirs to supply water demand for urban areas, agriculture, and industries. The four strategic reservoirs are monitored by the Water Agency of the State of Ceará (COGERH): Poço da Pedra, Mamoeiro, Benguê and Do Coronel, with the respective drainage areas equal to 800 km², 1,888 km², 1,062 km² and 25 km² and the respective capacities equal to 52 million m³, 20.68 million m³, 19.56 million m³ and 1.77 million m³. Additionally, there are small reservoirs that supply water to rural communities and farmers. An analysis of aerial images identified 230 reservoirs in the area following the rainy periods of 2004, 2008, and 2009 (Rabelo et al., 2021). Figure **4.1** illustrates the location of the study area and the reservoir system, comprising the strategic reservoirs and the small reservoirs aggregated in ponds within the model.

4.2.2 SWAT model

The SWAT2012 model was used to represent hydrological processes and to simulate streamflows for the catchment outlet (Malhada gauging station). The definition of the watershed and the drainage network was carried out with a 90 m resolution digital elevation model (DEM), in a semi-distributed model with 197 sub-basins.

The climate data were obtained between the years 1979 and 2022 as follows: daily precipitation data were collected from 38 rain gauges maintained by the Foundation for Meteorology and Water Resources of the State of Ceará (FUNCEME), and 6 meteorological

stations maintained by the National Institute of Meteorology (INMET); daily temperature, wind speed, and humidity data were obtained from the 6 INMET meteorological stations; and daily solar radiation data were sourced from the Xavier et al. (2022) database. To achieve daily climatic input variables for the 197 sub-basins of the model, these climatic variables were estimated through interpolation of the measured data, taking the centroids of the sub-basins as reference points. The inverse distant weighing method was used for the spatial interpolation. Detailed information about climate inputs can be found in Appendix A.

Figure 4.1 - Modeling catchment with representation of river and reservoir networks

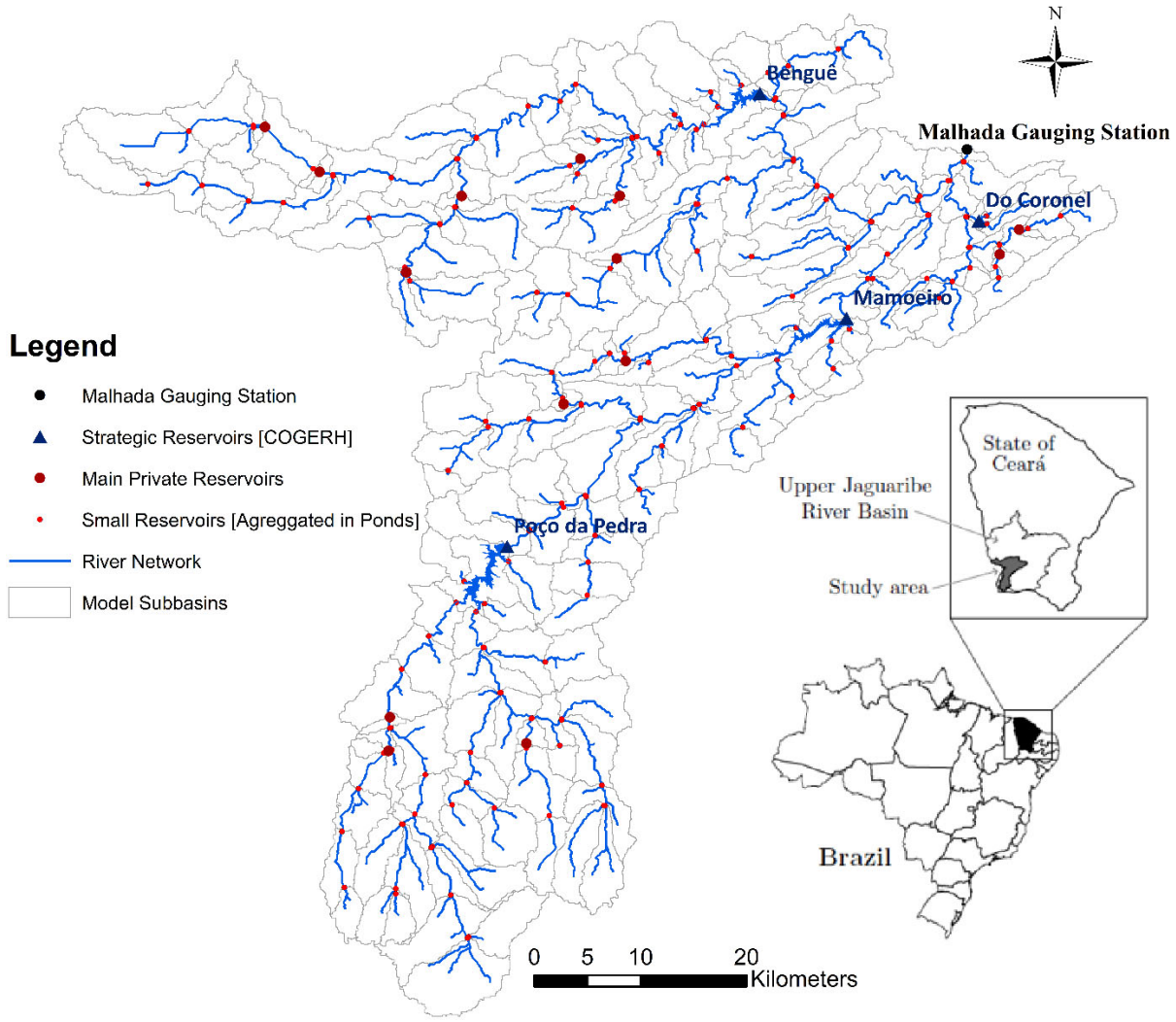

Source: The author

The soil map, provided as a polygon shapefile, includes 109 soil association classes based on Jacomine et al. (1973) and FAO classifications. Land use data from FUNCEME,

initially containing 26 classes, were reclassified to align with the SWAT model's default categories. Further details on soil and land use data are available in Appendix B.

One of the main challenges of modeling in dry regions with dense reservoir networks is the representation of the complex hydrological network, with the presence of strategic reservoirs and small reservoirs. The four strategic reservoirs and the small reservoirs with capacities greater than 0.01 million m³ (main private reservoirs) were modeled in the SWAT using the "reservoir" structure, while the smaller reservoirs were modeled in the SWAT "pond" structure. Due to a limitation of SWAT2012, only one pond can be used in each sub-basin, so small reservoirs that share the same sub-basin had to be aggregated into a single "pond". To simulate the average water retention effect for cascade or parallel arrangement, an equivalent reservoir capacity was set between the effective and the total accumulation capacity of the reservoir system. Detailed information about the methodology of small reservoirs aggregation into ponds can be found in section 2.2.3.2.

In the study area, 79 of the 197 sub-basins were identified with one or more reservoirs, making it necessary to apply the reservoir aggregation methodology. In the case of multiple reservoirs with cascade and parallel arrangements in the same sub-basin, the methodology must begin by applying it to the most upstream reservoirs, generating equivalent intermediate reservoirs and consequently new applications of the reservoir aggregation methodology downstream.

The final modeling of the reservoirs resulted in 230 reservoirs distributed over a total area of 3,347 km² (0.07 res/km²), with four strategic reservoirs (total capacity = 73.33 million m³) and 14 main private reservoirs (total capacity = 5.28 million m³, resulting in 18 "reservoirs" in the model and 212 small reservoirs (total capacity = 13.70 million m³) aggregated into 79 "ponds". The reservoir system is illustrated in Figure **4.1**.

4.2.3 Parameterization of the reference model

The parameterization of the model in SWAT was divided into 2 stages: parameterization of the reservoirs and parameterization of the hydrological processes of the model.

The parameters for the strategic reservoirs were sourced directly from COGERH, supplemented by the application of the Poleni equation (Aigner, 2008) to estimate the number of days required to achieve the target storage volume (volume of the reservoir when reaching

the main spillway). For the main private and small reservoirs, the parameters had to be estimated using Molle equation (1994) for areas and volumes, Molle (1989) for hydraulic conductivity of the bottom, and Google Timelapse application for year in which the reservoir became operational. A complete description with the presentation of tables with the values of these parameters in SWAT for each reservoir in the study area can be found in section 2.2.3.

The manual calibration of the hydrological processes was carried out based on data available in literature and authors' experience. It is noteworthy that the parameter values used in calibration fall within the typical range observed for dryland watersheds, as indicated by Rocha et al. (2023). The methods used to calculate evapotranspiration, rainfall-runoff process, and runoff propagation were respectively: the Penman-Monteith method, the CN method, and the Muskingum method. The flood routing simulation was performed using a modified SWAT version (Nguyen et al., 2018), incorporating the corrected Muskingum subroutine proposed by the authors. The model parameterization used an iterative trial and error process, using parameter values in a range with hydrological meaning for the study area. The parameters were divided into three main groups during the calibration process: parameters set for the entire catchment, parameters set for specific sub-basins of the catchment, such as those delimited by the main reservoirs, and parameters set by the different soil types in the catchment. The calibrated values for some of the main sensitive parameters were resumed at

Table **4.1**. A detailed explanation with all the hydrological parameters and the calibrated values can be found in section 2.2.4.

The calibration and validation were conducted using a 2-fold cross-validation approach between the streamflow simulated by the model and the streamflow measured at the Malhada gauging station, from 1979 to 2010. The first two years of simulation (1979 and 1980) were considered as model warm-up. The statistical parameters used in the comparison of simulated and measured streamflows were the Nash-Sutcliffe coefficient (NSE), the Kling-Gupta coefficient (KGE), and the percentage of bias (PBIAS). The calibrated model obtained good results for daily streamflows, with values of 0.63, 0.81 and 0.53% for NSE, KGE and PBIAS, respectively. From this point forward, this model covering the period from 1981 to 2010 will be referred to as the reference model. A detailed description of the reference model and its results can be found in Chapter 2.

Table 4.1 – Parameterization of the Main Parameters of the Reference Model

Parameter	Definition	Calibrated Value	Spatial Distribution
CH_K1	Effective hydraulic conductivity in tributary channel alluvium	5 mm/h to 72 mm/h	Set by sub-basin
CH_K2	Effective hydraulic conductivity in main channel	5 mm/h to 72 mm/h	Set by sub-basin
CH_N2	Manning's "n" value for the main channel	0.05	Set for the whole catchment
CN2	Curve number for the day	57.34 to 92	Set by sub-basin
ESCO	Soil evaporation compensation factor	0.02	Set for the whole catchment
GW_DELAY	Groundwater delay time	12 days and 30 days	Set by sub-basin
GW_REVAP	Groundwater "revap" coefficient	0.10 to 0.25	Set by soil type
GWQMN	Threshold depth of water in the shallow aquifer required for return flow to occur	700 and 1050	Set by soil type
RCHARG_DP	Deep aquifer percolation fraction	0.25 and 0.30	Set by sub-basin
REVAPMN	Threshold depth of water in the shallow aquifer required for "revap" or percolation to the deep aquifer to occur	265	Set for the whole catchment
SOL_CRK	Potential or maximum crack volume of the soil profile expressed as a fraction of the total soil volume	0.01, 0.03, and 0.4	Set by soil type
TRNSRCH	Fraction of transmission losses partitioned to the deep aquifer	0.3	Set for the whole catchment

Source: The author

4.2.4 Analysis of Precipitation and Temperatures from 1979 to 2022 and Drought Characterization

Climate variability in the study area (Malhada catchment) was analyzed using measurements of precipitation, maximum temperatures, and minimum temperatures, which were transformed from daily to annual values to verify climate trends over the years and plotted together with the annual average. The average annual values of precipitation and maximum and minimum temperatures were obtained for 5 periods: 1979 – 2022 (complete climate series), 1981 – 2010 (reference period), 2011 – 2022 (extension of the period), 2012 – 2017 (prolonged drought period), and 2018 – 2022 (drought recovery period).

The trends in the annual series of precipitation, maximum, and minimum temperatures were assessed using the Mann-Kendall test at a 5% significance level (Kendall and Gibbons, 1990; Mann, 1945), as presented in equations from 4.1 to 4.6.

$$S = \sum_{k=1}^{n-1} \sum_{j=k+1}^{n} \text{sgn}\left(x_j - x_k\right) \tag{4.1}$$

Where:

$$sgn\left(x_j - x_k\right) = \begin{cases} 1, & if\ x_k < x_j \\ 0, & if\ x_k = x_j \\ -1, & if\ x_k > x_j \end{cases} \tag{4.2}$$

And the variance including the correction term for ties is:

$$\sigma^2 = \{n(n-1)(2n+5) - \sum_{j=1}^{p} t_j(t_j-1)(2t_j+5)\}/18 \tag{4.3}$$

“p” is the number of the tied groups in the data set and tj is the number of data points in the j-th tied group.

The standardized test statistic (z) of the Mann-Kendall test and the corresponding p-value (p) for the one-tailed test are respectively given by:

$$z = \begin{cases} \frac{S-1}{\sqrt{Var(S)}}, & if\ S > 0 \\ 0, & if\ S = 0 \\ \frac{S+1}{\sqrt{Var(S)}}, & if\ S < 0 \end{cases} \quad (4.4)$$

$$p = 0.5 - \varphi(|z|) \quad (4.5)$$

$$\varphi(|z|) = \frac{1}{\sqrt{2\pi}} \int_0^{|z|} e^{-t^2/2} dt \quad (4.6)$$

Positive z values indicate an upward trend, while negative z values denote a downward trend. At a 0.05 significance level, if $p \leq 0.05$, the trend is considered statistically significant. To deal with the effect of serial correlation on the Mann-Kendall test, a modified Mann-Kendall test (modified MK test) was applied using the Yue and Wang (2004) Effective Sample Size (ESS) approach.

To obtain trendlines for maximum and minimum temperatures, Sen's slope was applied, as presented in the equation 4.7 (Sen, 1968):

For the time series T = {temp1, temp2, …, temp$n$}, where "temp" represents the maximum or the minimum temperatures, the Sen's slope can be calculated:

$$Sen's\ Slope = Median\left(\frac{temp_j - temp_i}{j - i}\right) for\ all\ 1 \leq i < j \leq n \quad (4.7)$$

To characterize the drought that occurred from 2012 to 2017 in the region, its duration and magnitude were evaluated using monthly potential evaporation and precipitation data from the complete climate series (1979–2022). This analysis was conducted with the Standardized Precipitation Evapotranspiration Index (SPEI) at a 12-month time scale, referred to hereafter as SPEI12. The 12-month time scale was selected because it encompasses the entire rainy season within each time step, which is particularly relevant to the study area. SPEI procedure involves converting the log-logistic distribution into the standard normal distribution. The analysis of drought severity was conducted based on the wet and dry period criteria presented in Table **4.2** (Ribeiro Neto et al., 2022; Xu et al., 2022). Further, details of the SPEI methodology can be found in the study of Vicente-Serrano et al. (2010).

Table 4.2 – Classification of Drought Severity by SPEI Index

Range	Categories
SPEI ≤ -2	Extreme dry
-2 < SPEI ≤ -1.5	Severe dry
-1.5 < SPEI ≤ -1	Moderate dry
-1 < SPEI ≤ - 0.5	Mild dry
-0.5 < SPEI < 0.5	Normal
SPEI ≥ 0.5	Wet

Source: The author

4.2.5 Evaluation of the Model by the Extension of the Climate Data

Based on the reference model described in Section 4.2.3, the daily climate series for precipitation, maximum and minimum temperatures, solar radiation, air humidity, and wind speed were extended to include data from 2011 to 2022.

To analyze the performance during the prolonged meteorological drought and its drought recovery, the NSE, lnNSE, and KGE were obtained for three distinct periods: 1981–2022, 2012–2017 (drought period), and 2018–2022 (recovery period). These metrics were derived using daily simulated and observed runoff data and were compared against the reference model results (1981-2010). The year 2011 was excluded from all analyses since no field streamflows measurements were available for that year.

The NSE and KGE are the most widely used statistical indices in hydrology for the evaluation of the performance of simulated values in a model in comparison with observed values. Traditionally, the NSE metric is widely used because it normalizes model performance on an interpretable scale. However, the KGE has gained prominence in recent hydrological modeling literature for model calibration, as it provides a more balanced evaluation by combining correlation, bias, and the coefficients of variation of NSE (Knoben et al., 2019; Liu, 2020).

NSE is calculated by equation 4.8, and the KGE is calculated by equation 4.9, for daily streamflow.

$$NSE = 1 - \frac{\sum_{t=1}^{n}({Q_o}^t - {Q_s}^t)^2}{\sum_{t=1}^{n}({Q_o}^t - \overline{Q_o})^2} \quad (4.8)$$

Where Q_o^t is the observed discharge at time t, Q_s^t is the simulated discharge at time t and $\overline{Q_o}$ is the mean of observed discharges.

$$KGE = 1 - \sqrt{(\beta - 1)^2 + (\alpha - 1)^2 + (\rho - 1)^2} \quad (4.9)$$

Where β is the ration between standard deviation of simulated and observed values, α is the ratio between the mean of simulated and observed values, and ρ is the correlation coefficient between simulated and observed values.

Additionally, considering that the new periods analyzed predominantly exhibits low flows, a common approach to better focus on specific flow ranges involves applying prior transformations to the simulated and observed runoff time series (Santos et al., 2018b). To this end, a logarithmic transformation will be applied to the NSE criterion, resulting in the lnNSE metric, calculated according to equation 4.10. To address the effect of daily zero-flow values, a small constant equivalent to 1/100 of the mean observed runoff will be added to all values (Pushpalatha et al., 2012). This approach is widely used, and Pushpalatha et al. (2012) demonstrated the lnNSE metric remains relatively insensitive to this constant as long as it is sufficiently small compared to the flow values. The logarithmic transformation will not be applied to the KGE metric because it may cause numerical issues, potentially leading to a biased evaluation of model performance (Santos et al., 2018b).

$$lnNSE = 1 - \frac{\sum_{t=1}^{n}\left[\ln\left({Q_o}^t + \varepsilon\right) - \ln\left({Q_s}^t + \varepsilon\right)\right]^2}{\sum_{t=1}^{n}\left[ln\left({Q_o}^t + \varepsilon\right) - \overline{ln\left(Q_o + \varepsilon\right)}\right]^2} \quad (4.10)$$

Where Q_o^t is the observed discharge at time t, Q_s^t is the simulated discharge at time t, $\overline{Q_o}$ is the mean of observed discharges, and ε is the small constant equivalent to 1/100 of the mean observed runoff.

To better understand the hydrological processes and the model's results, the values for precipitation, evapotranspiration, surface runoff, lateral flow, baseflow, and percolation, alongside the percentage metrics were obtained for the four analyzed periods (1981-2010, 1981-2022, 2012-2017, and 2018-2022). These metrics provide insight into the distribution of precipitation into evapotranspiration, runoff components, and percolation, offering a detailed evaluation of water balance and flow dynamics in the watershed across different hydrological periods.

To verify the results obtained by the model, the hydrographs of the rainy season (from January to June) of 2016 and 2020 were chosen to represent the years during the

prolonged meteorological drought and the drought recovery, respectively. In addition, hydrographs were also obtained during the rainy season of the years 1983 and 1985, 1993 and 1995, 1998 and 2000, and 2001 and 2004, to compare the results of the reference model for other notable drought years and following drought recovery years. The hydrographs were used to analyze the patterns of peak flow and runoff duration, based on the rise and depletion of the hydrograph between the simulated model and the observed values.

Additionally, to examine the rainfall-runoff relationship across the calibration period (1981–2010), during the prolonged drought (2012–2017), and after the drought (2018–2022), correlation plots of annual precipitation and rainfall were generated to assess potential shifts, as suggested by Saft et al. (2016) and Peterson et al. (2021). Annual rainfall data were assumed to approximate a normal distribution, whereas annual runoff data, which are typically skewed, were transformed using a Box-Cox transformation (Box and Cox, 1964). This transformation adjusted the runoff data to approximate a normal distribution and linearized the rainfall-runoff relationship, thereby enhancing the applicability of various parametric statistical techniques.

4.2.6 Sensitivity Analysis for the Extension of the Climate Data

To investigate the impact of parameter changes on model performance during the extended period, including the prolonged drought and its recovery (2012–2022), box plots of NSE and lnNSE were generated for different parameter simulations. The parameter values employed in the sensitivity analysis are summarized in Table **4.3**.

To extend the sensitivity analysis, an in-depth evaluation was carried out for four of the most sensitive parameters (CH_K2, CN2, RCHRG_DP, and TRNSRCH) during the extended period, as summarized in Table **4.4**. To verify the performance of the model during the period of prolonged drought and its recovery from drought, the model was simulated on a daily step time, obtaining the KGE, NSE, and lnNSE for the values of the four parameters for two periods: 1981-2022 and 2012-2022.

Table 4.3 – Range of SWAT Parameters Values for Sensitivity Analysis During the Extended Period (2012-2022)

Parameter	Range of Parameters Values
ALPHA_BF	0 to 1
CH_K1	Spatial calibrated values ± 50%
CH_K2	Spatial calibrated values ± 50%
CH_N2	0.015 to 0.15
CN2	Spatial calibrated values from -50% to +20%
ESCO	Spatial calibrated values from -50% to +20%
GW_DELAY	0.01 to 1
GW_REVAP	0.02 to 0.2
GWQMN	0 to 2000
RCHRG_DP	0 to 1
REVAPMN	0 to 800
SOL_CRK	0 to 1 (only in vertic soils)
TRNSRCH	0 to 1

Source: The author

Table 4.4 – Methodology for Sensitivity Analysis of the Most Sensitive Parameters (CH_K2, CN2, RCHRG_DP, and TRNSRCH)

Parameter	What this parameter does	Why it was chosen for an in-depth sensitivity analysis	Sensitivity analysis process
CH_K2	During periods when the groundwater has no contribution to streamflow, water can be lost from the channel through the side and bottom, a process called transmission losses. SWAT estimates transmission losses as follows: $T_{loss} = CH\_K2 \cdot TT \cdot P_{ch} \cdot L_{ch}$ Where Tloss is the channel transmission losses (m^3), CH_K2 is the effective hydraulic conductivity of the channel alluvium (mm/hr), TT is the travel time of the flow (hr), Pch is the wetted perimeter (m), and Lch is the channel length (km).	CH_K2 is the main parameter to calibrate channel transmission losses.	For the reference model (1981-2010), the CH_K2 parameter was defined individually for each sub-basin. During the new sensitivity analysis, CH_K2 values were incrementally increased and decreased by 5%, up to a maximum change of ±50% relative to the reference values, to account for variations in the catchment's hydraulic conductivity—from low to high—while preserving the spatial distribution defined in the reference model.

Parameter	What this parameter does	Why it was chosen for an in-depth sensitivity analysis	Sensitivity analysis process
CN2	The CN method is a runoff generation method to obtain the precipitation excess as a function of soil cover, land use, and antecedent soil moisture. The retention parameter (S) varies spatially due to changes in soils, land use management, and slope and temporally due to changes in soil water content. The retention parameter is defined as: $$S = 25.4 \cdot \left(\frac{1000}{CN} - 10\right)$$ Where CN is the curve number for the day.	The curve number is a function of soil's permeability, land use, and antecedent soil water conditions. The CN is a major parameter to calculate the retention parameter, which estimates infiltration during the precipitation event.	For the reference model, the CN2 parameter was defined individually for each sub-basin, with different values in each hydrological response unit (HRU) of the model. During the new sensitivity analysis, the CN2 values were incrementally increased and decreased by 5%, up to a maximum change of +20% and a minimum change of -50%, preserving the spatial distribution defined in the reference model.

Parameter	What this parameter does	Why it was chosen for an in-depth sensitivity analysis	Sensitivity analysis process
RCHRG_DP	A fraction of the total daily recharge can be routed to the deep aquifer. The amount of water than will be diverted from the shallow aquifer due to percolation to the deep aquiver on a given day is: $$w_{deep} = RCHRG\_DP \cdot w_{rchrg}$$ Where wdeep is the amount of water moving into the deep aquifer on day (mm), RCHRG_DP is the aquifer percolation coefficient, and wrchrg is the amount of recharge entering both aquifers on day (mm).	The partitioning of groundwater between the shallow and the deep aquifer is only governed by the RCHRG_DP.	The value of RCHRG_DP was simulated at the maximum and minimum limits allowed by the model (0.00 ≤ RCHRG_DP ≤ 1.00), with a gradual increase of 0.10. The value of RCHRG_DP in the reference model was 0.25.

Parameter	What this parameter does	Why it was chosen for an in-depth sensitivity analysis	Sensitivity analysis process
TRNSRCH	In the model SWAT, the transmission losses from the channel alluvium are assumed to enter the bank storage. Model SWAT estimates the amount of water entering bank storage on a given day as following equation: $$bnk_{in} = T_{loss} \cdot (1 - TRNSRCH)$$ Where bnkin is the amount of water entering bank storage (m^3), Tloss is the channel transmission losses (m^3), and TRNSRCH is the fraction of transmission losses partitioned to the deep aquifer.	The bank storage can contribute to the flow at main channel from a recession curve, that depends directly on bnkin. In addition to Tloss, TRNSRCH is a main parameter to calibrate the flow at main channel from the bank storage in the model SWAT.	The value of TRNSRCH was simulated at the maximum and minimum limits allowed by the model ($0.00 \leq TRNSRCH \leq 1.00$), with a gradual increase of 0.10. The value of TRNSRCH in the reference model was 0.3. The TRNSRCH parameter is defined in the SWAT model for the entire watershed.

Source: The author

4.3 Results

4.3.1 Precipitation and temperature trends and drought characterization

Figure **4.2** illustrates annual precipitation and the average precipitation from 1979 to 2022. Additionally, Figure **4.2** displays the annual average values of maximum and minimum temperatures, along with the Sen's Slope trendline for each temperature series.

Figure 4.2 - Precipitation (a) and maximum (b) and minimum (c) temperature in the study area catchment (1979 – 2022)

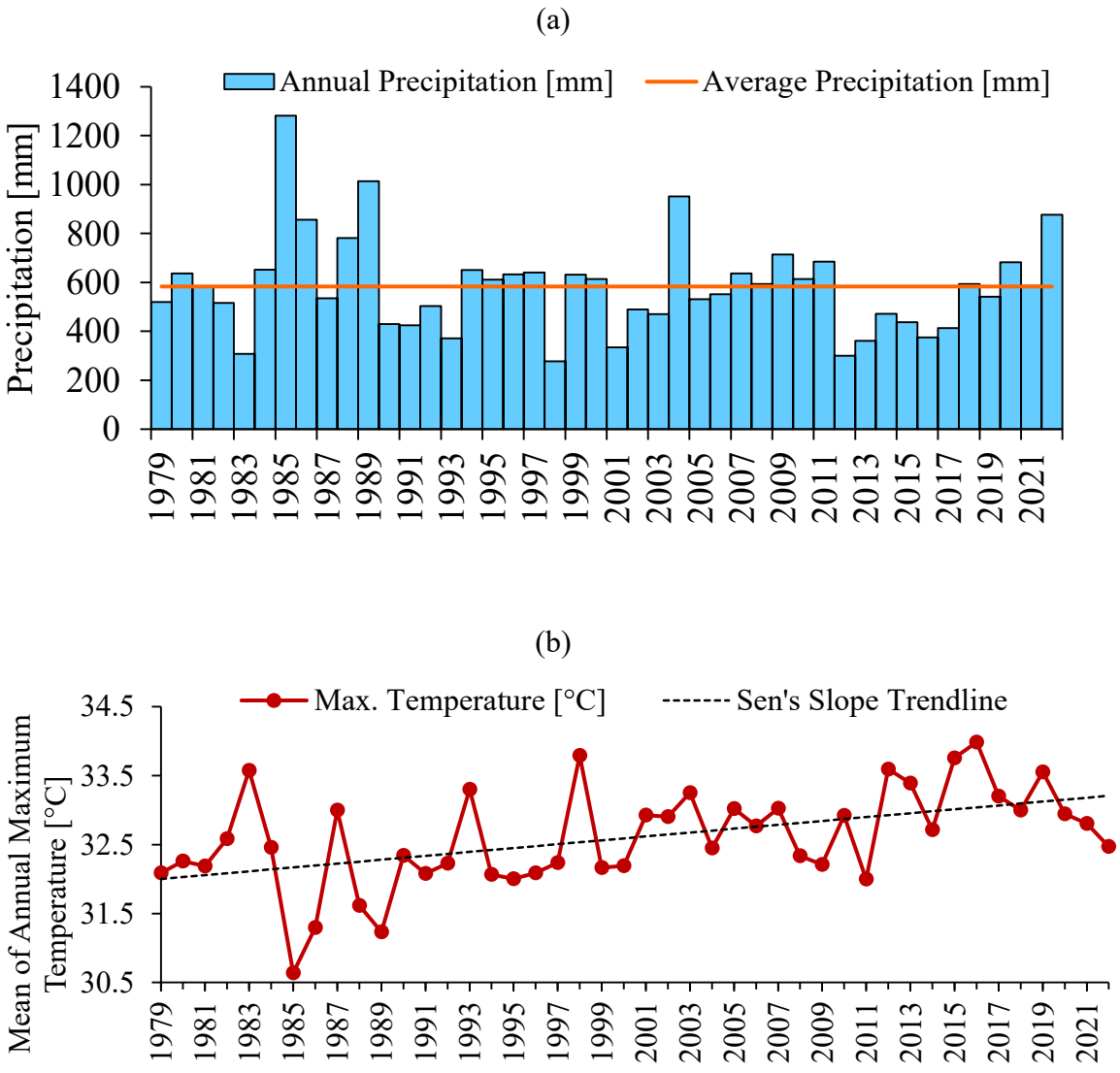

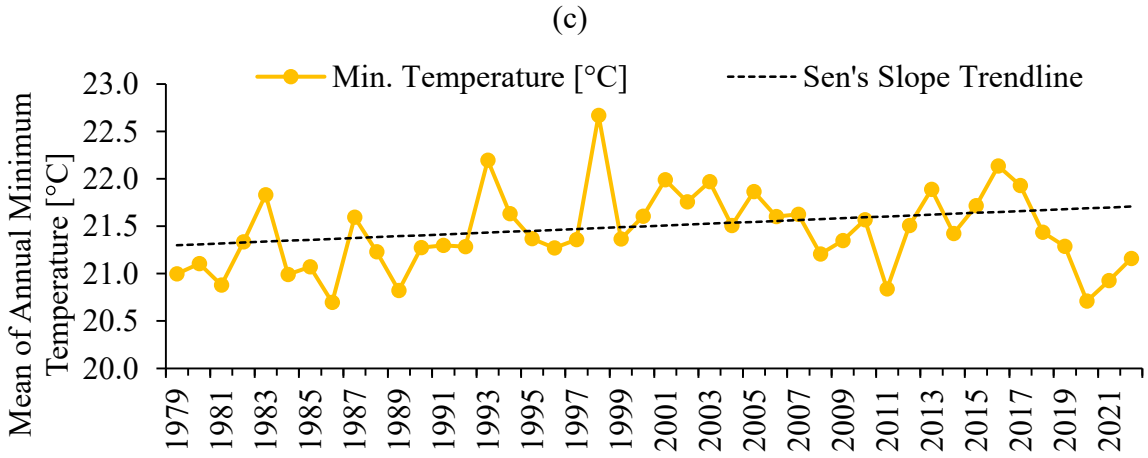

Source: The author

Table **4.5** compares the average annual precipitation, maximum temperatures and minimum temperatures across five study periods in the region: (1979 – 2022, 1981 – 2010, 2011 – 2022, 2012 – 2017 and 2018 – 2022).

Table 4.5 - Comparison of annual average precipitation and annual average maximum and minimum temperature for different periods in the study area catchment

Years	Definition	Average Precipitation [mm]	Average Maximum Temperature [°C]	Average Minimum Temperature [°C]
1979 - 2022	Full period	583.5	32.61	21.44
1981 - 2010	Calibrated period	606.6	32.43	21.45
2011 - 2022	Extended period	526.7	33.12	21.41
2012 - 2017	Prolonged drought period	392.9	33.44	21.77
2018 - 2022	Drought recovery period	655.8	32.96	21.10

Source: The author

Table **4.5** presents an analysis of average precipitation and temperatures for different periods in the Malhada Catchment. Between 2012 and 2017, the average precipitation was only 392.9 mm, approximately 33% below the total annual average precipitation for the entire series (1979-2022), and approximately 35% below the reference period (1981-2010). The climate series used for the reference model (1981-2010) had an average annual precipitation of

606.6 mm, while the extended series (2011-2022) averaged 526.7 mm annually. Regarding temperatures, Table **4.5** shows that during the period 2012-2017, both the average maximum temperature (33.44 °C) and average minimum temperature (21.77 °C) were higher than the overall series (1979-2022) averages by 0.83 °C and 0.33 °C, respectively. The reference model (1981-2010) had average annual maximum and minimum temperatures of 32.43 °C and 21.47 °C, while the extended series (2011-2022) averaged 33.12 °C and 21.41 °C annually. Furthermore, applying the modified MK test at a 5% significance level to the climate data revealed a positive trend for maximum temperature ($z = 9.74$, p-value ≈ 0.000, Sen's slope = 0.0281 °C/year) and for minimum temperature ($z = 2.09$, p-value = 0.037, Sen's slope = 0.0095 °C/year), and no significative trend for annual precipitation ($z = -1.38$, p-value = 0.167).

Analysis of Figure **4.3** reveals that the years 1985, 1989, and 2004 were the wettest, characterized by the highest total annual precipitation and SPEI-12 values. Conversely, 1983 and 1998 stand out as severe dry years, while the periods from 1992 to 1993 and 2001 to 2003 are classified as moderate dry periods. The 2012–2017 period is the only one with months classified as extreme dry, with three consecutive months in 2013 and one month in 2017 meeting this classification. Additionally, this period is marked by extended severe dry periods, occurring from October 2012 to January 2014 (16 months) and from April 2016 to February 2017 (11 months).

Figure 4.3 – 12-month SPEI for Malhada Catchment from 1980 to 2022

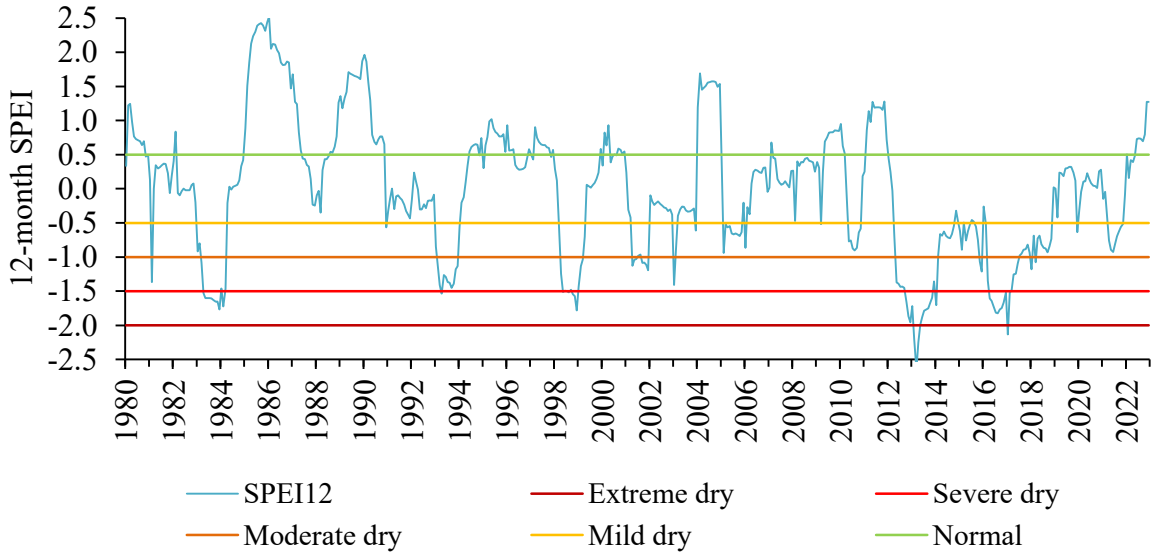

Source: The author

4.3.2 Performance of the model during extreme drought and its hydrological recovery

Figure 4.4 presents the daily streamflow results at the Malhada gauging station (catchment outlet), and displays the results obtained for NSE, KGE, and lnNSE for the four evaluated periods: 1981-2010 (reference period), 1981-2022 (total series), 2012-2017 (prolonged drought), and 2018-2022 (recovery period).

The results of NSE and KGE reveal a marked decline in the model's performance over the extended period, particularly between 2012 and 2017 (prolonged drought) and during the subsequent drought recovery phase from 2018 to 2022. The reference model struggled to accurately estimate daily flows throughout these periods. Moreover, the model exhibited an even more pronounced decline in performance during the hydrological recovery period, emphasizing the model's limitations in accurately representing runoff conditions following a severe prolonged drought.

The lnNSE results demonstrated satisfactory performance during both the reference period and the total series. However, the model's performance according to lnNSE also drastically declined during the prolonged drought and its recovery, though the values were less negative compared to those obtained with NSE and KGE. Remarkably, lnNSE pointed to poorer performance during the prolonged drought, while NSE indicated worse performance during the drought recovery period.

To better understand the hydrological processes and the model's results, Table 4.6 presents the values for annual average precipitation (P), evapotranspiration (ET), surface runoff (SUR Q), lateral flow (LAT Q), baseflow (GW Q), and percolation (PERCO), alongside the percentage metrics ET / P, PERCO / P, TOT Q / P, SUR Q / TOT Q, LAT Q / TOT Q, and GW Q / TOT Q for the four analyzed periods.

During the prolonged drought (2012–2017), the average annual precipitation of 392.9 mm was consumed primarily by evapotranspiration, accounting for 93.7%. Additionally, 6.4% of the precipitation contributed to percolation, while only 1.2% was converted into runoff. Of this runoff, 48.9% originated from surface runoff and 51.1% from lateral flow. Notably, there was no baseflow simulated by the model during this period.

Figure 4.4 - Daily streamflow at catchment outlet (Malhada Station) during calibration, extreme drought and drought recovery periods

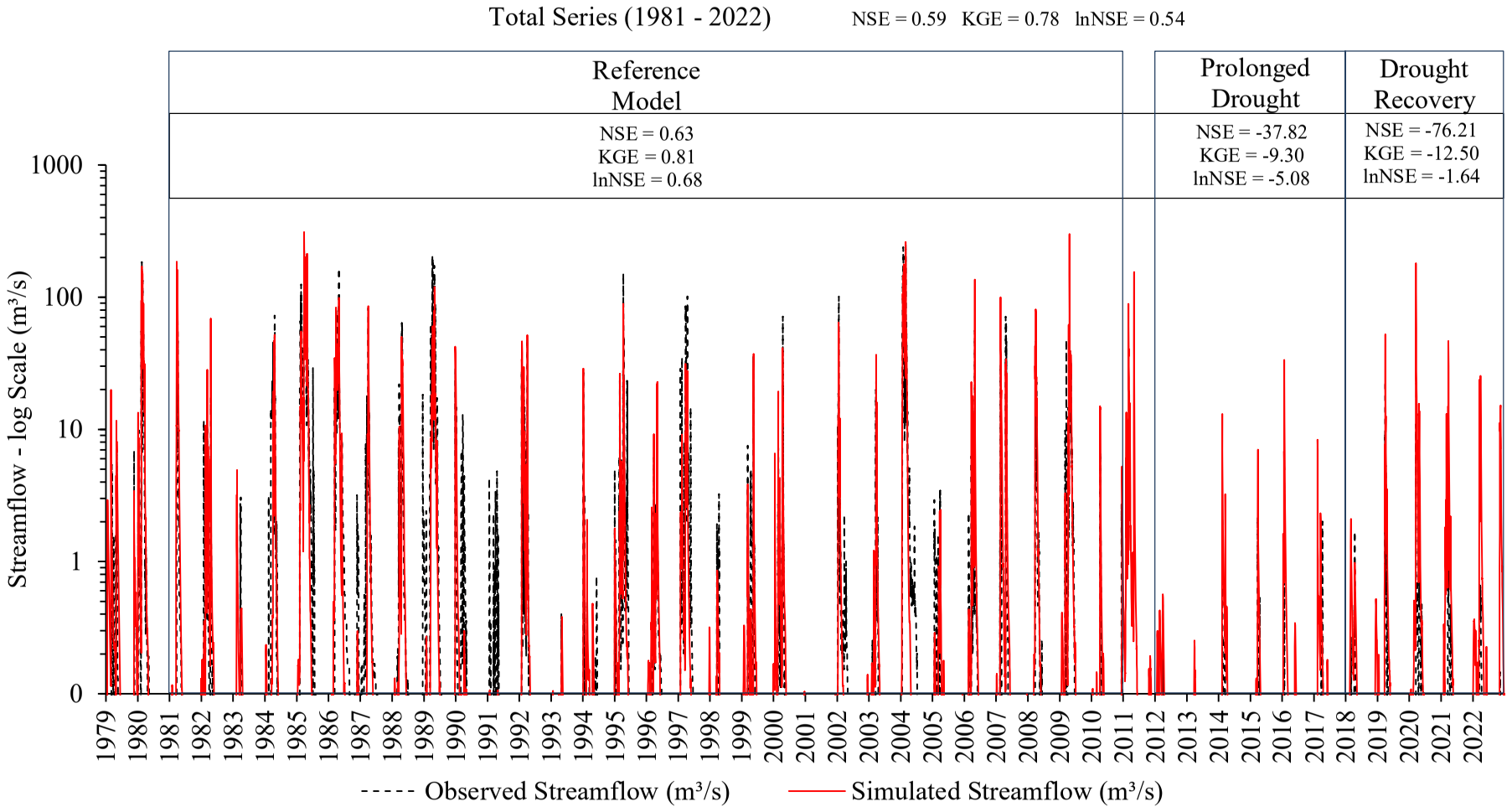

Source: The author

In contrast, during the hydrological recovery period (2018–2022), the average annual precipitation increased to 655.8 mm, with 83.6% consumed by evapotranspiration. Percolation accounted for 11.6% of the total precipitation, while 3.1% of the total precipitation was converted into total runoff. Of this runoff, 69.2% originated from surface runoff and 30.8% from lateral flow. Similar to the drought period, no baseflow was simulated by the model during this recovery phase.

Table 4.6 – Results of Water Balance of the Model (annual average of precipitation (P), evapotranspiration (ET), surface runoff (SUR Q), lateral flow (LAT Q), baseflow (GW Q), and percolation (PERCO)) (a) and the Percentage Metrics (ET / P, PERCO / P, TOT Q / P, SUR Q / TOT Q, LAT Q / TOT Q, and GW Q / TOT Q) (b) for the four analyzed periods

(a)

Periods	P (mm)	PET (mm)	SUR Q (mm)	LAT Q (mm)	GW Q (mm)	TOT Q (mm)	PERCO (mm)
1981 – 2010 (reference)	606.6	489.7	21.6	6.2	0.6	28.4	87.2
1981 - 2022	583.8	481.7	18.3	5.7	0.4	24.4	77.0
2012 - 2017	392.9	368.0	2.3	2.4	0.0	4.6	25.1
2018 - 2022	655.8	548.5	13.9	6.2	0.0	20.1	76.0

(b)

Periods	ET / P	PERCO / P	TOT Q / P	SUR Q / TOT Q	LAT Q / TOT Q	GW Q / TOT Q
1981 – 2010 (reference)	80.7%	14.4%	4.7%	76.1%	21.8%	2.1%
1981 - 2022	82.5%	13.2%	4.2%	75.0%	23.2%	1.8%
2012 - 2017	93.7%	6.4%	1.2%	48.9%	51.1%	0.0%
2018 - 2022	83.6%	11.6%	3.1%	69.2%	30.8%	0.0%

Source: The author

To elucidate the hydrological outcomes derived from the model, we analyzed the hydrographs of two pivotal years: 2016, which falls within the extreme dry period, and 2020, representing the middle of the catchment's drought recovery phase. Figure 4.5 illustrates the hydrographs for 2016 (a) and 2020 (b) during the wet season in the region (from January to June). Between July and December, precipitation is scarce, resulting in negligible flows during this period.

Figure 4.5 - Comparison of streamflows at Malhada gauging station (model x observed by State agency) during the years of 2016 (a) and 2020 (b)

(a)

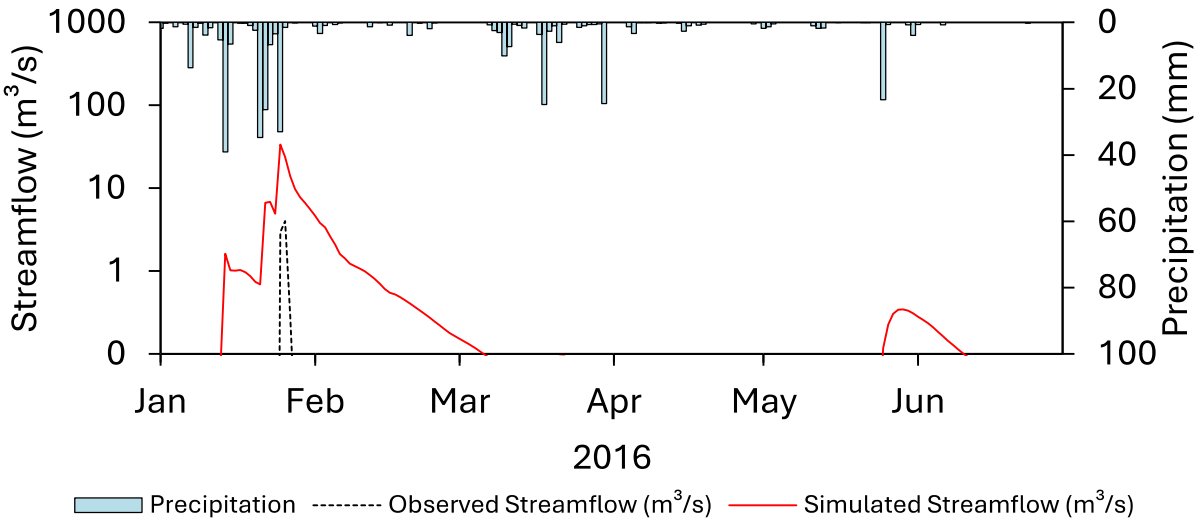

(b)

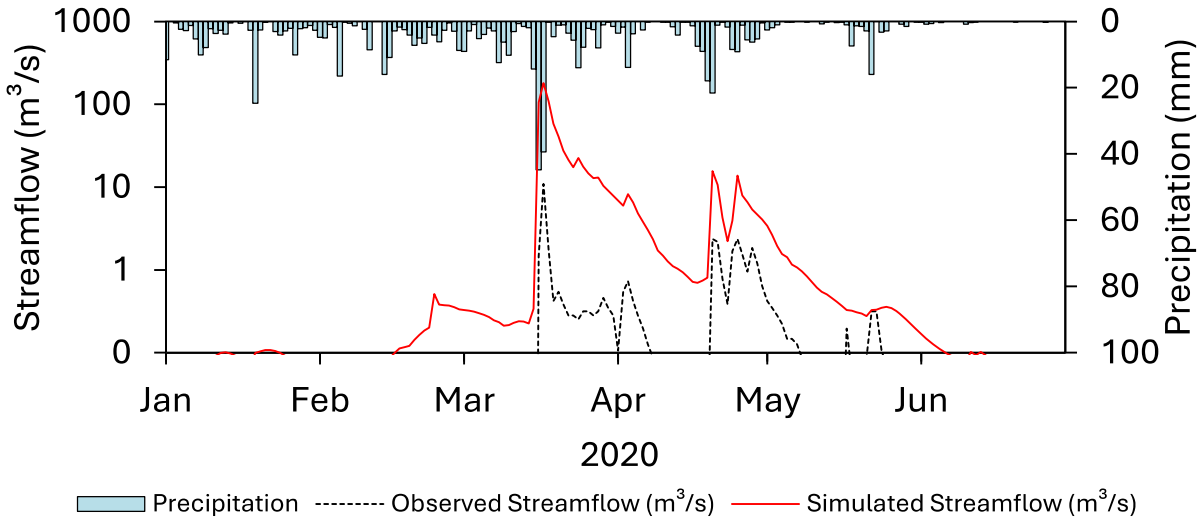

Source: The author

The findings depicted in Figure 4.5 indicate that the model consistently overestimated streamflow within the catchment during both the prolonged drought and subsequent recovery periods. In Figure 4.5a, the hydrograph illustrates that the peak flow simulated by the model in 2016 was 33.5 m³/s, whereas the observed value at the Malhada Gauging Station was 4.0 m³/s. While the model successfully reproduced the day of peak flow

occurrence (January 25, 2016), it overestimated both the rise and recession phases, resulting in a simulated hydrograph lasting 52 days compared to the observed hydrograph's duration of 3 days. Similar behavior was observed in the hydrographs for other years during the prolonged drought period (2012-2017), where the simulated hydrographs consistently overestimated peak flows and the duration of flow, while observed hydrographs exhibited quicker rises and falls in flow rates.

The analysis of Figure 4.5b reveals that during the drought recovery period in the region, the model continued to overestimate peak flow values. The simulation indicated a peak flow of 180.0 m^3/s, while the observed peak flow at the Malhada station was 10.9 m^3/s on March 17, 2020. During this rainy season, the model depicted a hydrograph resembling the observed, with peak flow occurring on the same day, however a longer duration of measurable flow days. Furthermore, the model simulated additional peaks in streamflow during subsequent rainfall events, such as those occurring on April 20, 2020, April 25, 2020, and May 23, 2020 (Figure 6b). However, it still exhibited limitations in accurately predicting the magnitude of peak flows and the rate of flow recession.

To compare the results obtained by the reference model during different years of meteorological drought and hydrological recovery periods afterwards, Figure **4.6** presents the hydrographs of 1983 and 1985 (a), 1993 and 1995 (b), 1998 and 2000 (c), and 2001 and 2004 (d).

In 1983 (Figure **4.6**a), the reference model estimated a peak flow value of 4.9 m^3/s, slightly higher than the observed value of 3.0 m^3/s. However, the model indicated two runoff periods (from February to March and in April), whereas observed streamflow occurred only in April. For 1993 (Figure **4.6**b), the reference model's peak flow (Qpeak = 0.38 m^3/s) was nearly identical to the observed value (Qpeak = 0.40 m^3/s), with flow predominantly in May. In 1998 (Figure **4.6**c), the reference model underestimated the peak flow (Qpeak = 0.84 m^3/s) compared to the observed peak (Qpeak = 3.24 m^3/s). The duration of the hydrograph was similar, but differences were noted in the rise and recession phases. For 2001 (Figure **4.6**d), the reference model did not simulate any flows, which corresponds accurately to observations at the Malhada gauging station where no flows were recorded during that year. In this year, the model effectively captured the sparse distribution of precipitation throughout the rainy season, which was insufficient to generate streamflow.

Figure 4.6 – Comparison of Streamflows at Malhada Gauging Station (Simulated x Observed by State Agency) during droughts/recovery periods of 1983/1985 (a), 1993/1995 (b), 1998/2000 (c), and 2001/2004 (d)

(a)

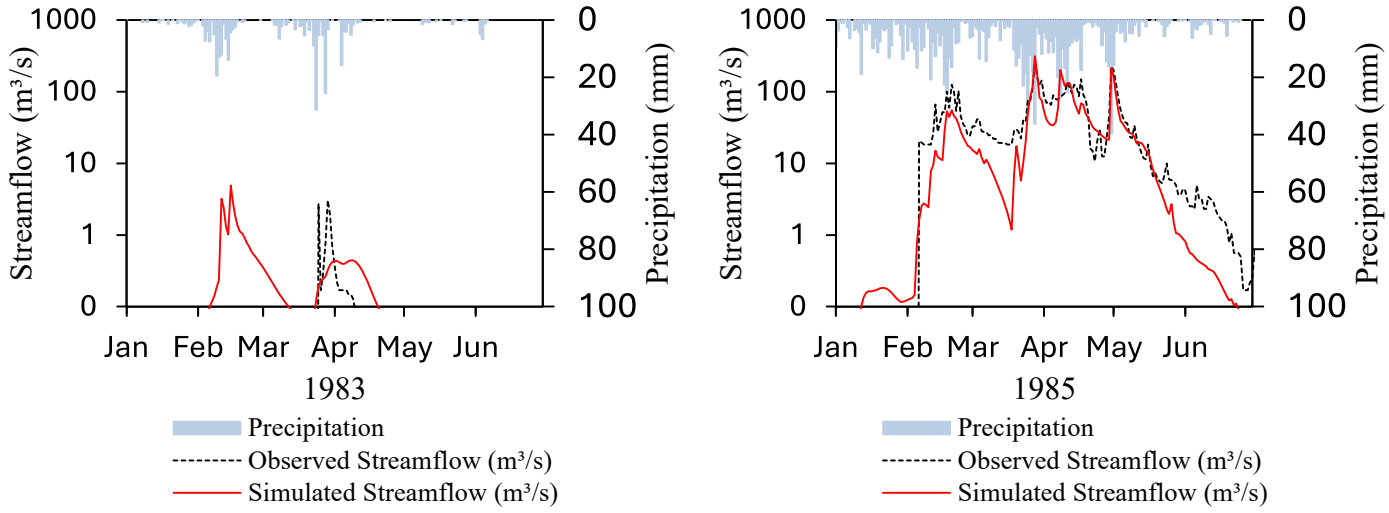

(b)

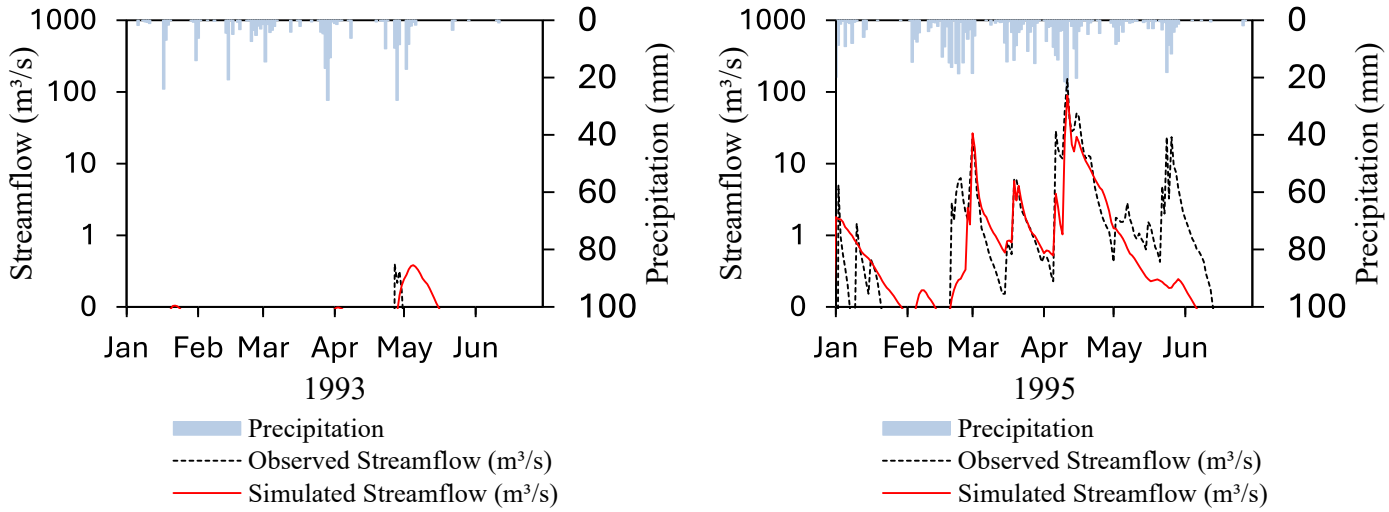

(c)

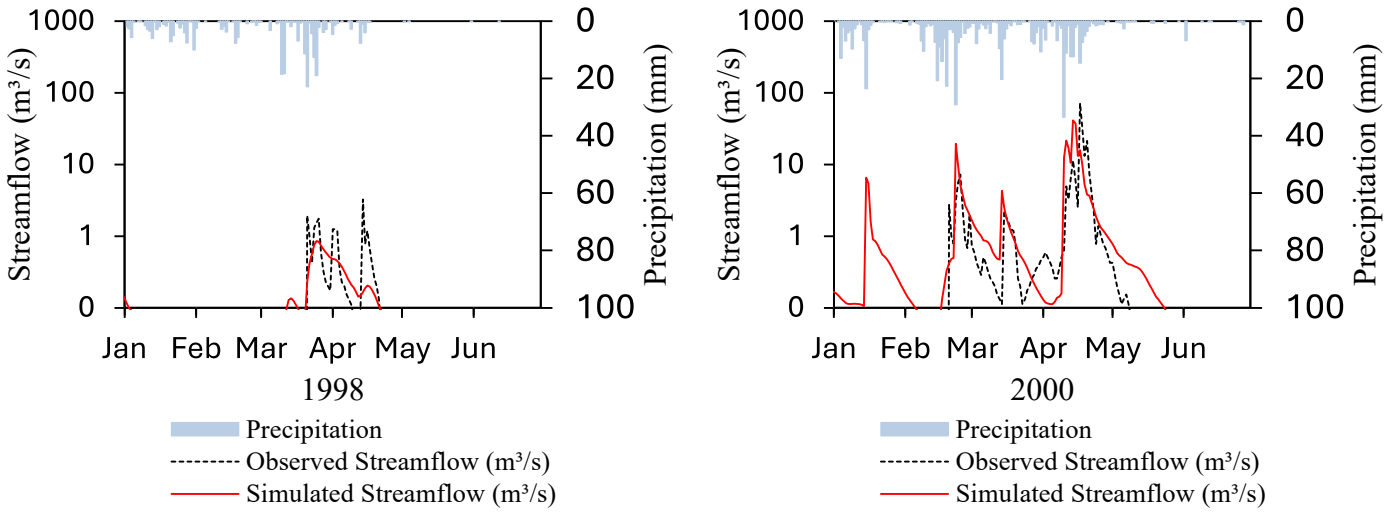

(d)

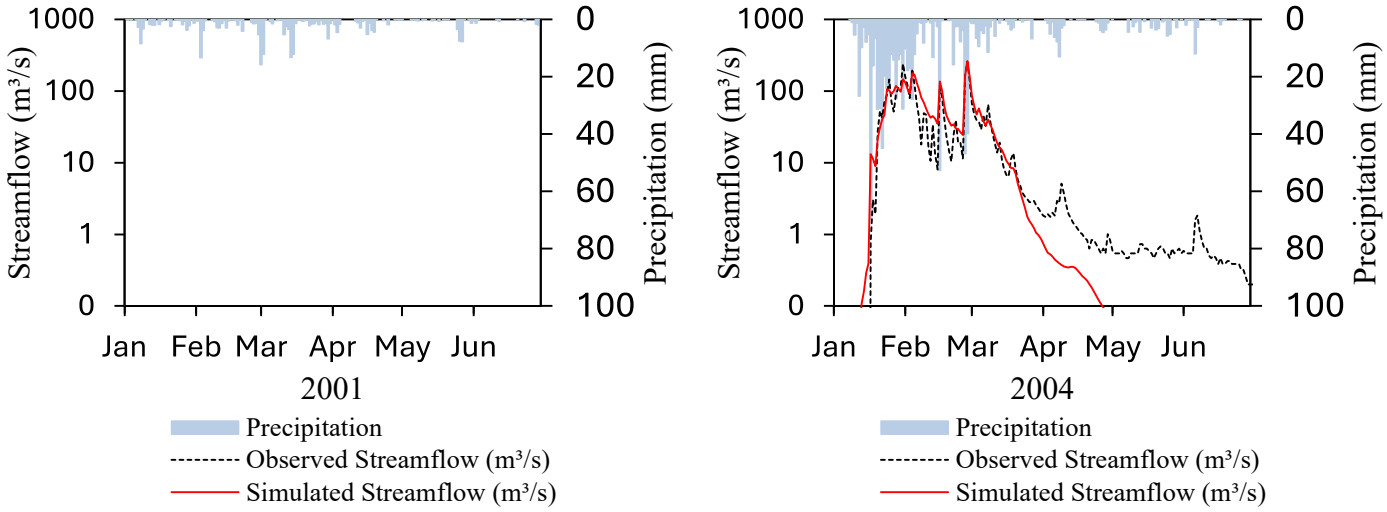

Source: The author

For the hydrological recovery periods, the reference model satisfactorily captured the runoff rates, especially in terms of peaks and hydrograph shapes. The peaks match well in the years 1985 (Figure **4**.**6**a), 1995 (Figure **4**.**6**b), 2000 (Figure **4**.**6**c), and 2004 (Figure **4**.**6**d), indicating the model's capability to represent the return of flows within the catchment, despite some discrepancies, such as an unidentified peak in June 1995 (Figure **4**.**6**b) and an overestimated peak in February 2000 (Figure **4**.**6**d). However, the model continued to present challenges in accurately representing recession flow during these analyzed years of hydrological recovery.

The performance of the reference model during previous drought events in the calibration period was notably better than during the subsequent prolonged drought period (2012 – 2017). Importantly, the model exhibited varying behaviors during drought events, demonstrating both overestimation and underestimation of peak flows and hydrograph durations.

To illustrate the lack of hydrological recovery after the extreme drought period, Figure **4**.**7**a presents a correlation graph between precipitation and observed runoff (box-cox transformed) in the Malhada catchment. It can be observed that during the drought recovery period, runoff not only decreased but also ceased to respond to higher precipitation events. This finding suggests that the watershed undergoes a substantial shift in the rainfall-runoff process, reaching probably a new equilibrium state during this period.

The correlation graph between precipitation and simulated runoff (box-cox transformed) in Malhada catchment, as presented in Figure **4**.**7**b, shows that the model, characterized as a HdRN, exhibited a decline in rainfall-runoff during the prolonged drought period, which persisted even after the hydrological recovery phase. Although the SWAT model results reproduce a scenario of reduced rainfall-runoff relationships during both the drought period and the hydrological recovery phase, the observed decline in the rainfall-runoff relationship within the Malhada catchment during the same period was greater than that simulated by the model. This limitation suggests that SWAT may lack mechanisms to account for such non-linear changes in watershed response under extreme drought conditions.

Figure 4.7 – Relation Between Annual Precipitation and Runoff for Observed (a) and Simulated (b) Values

(a)

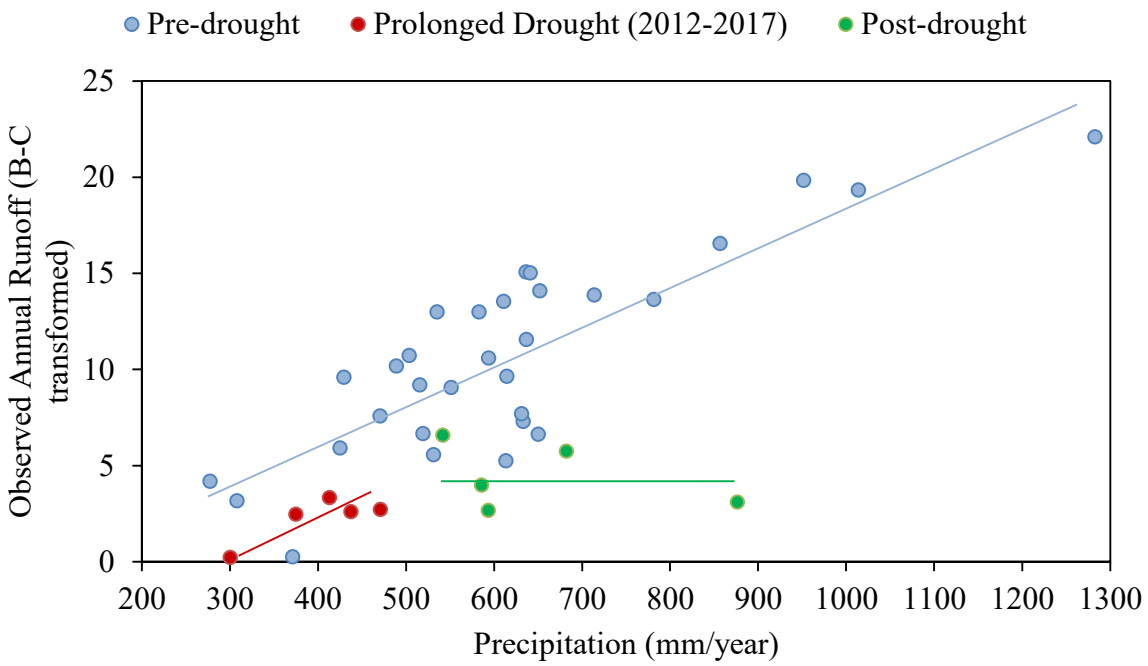

(b)

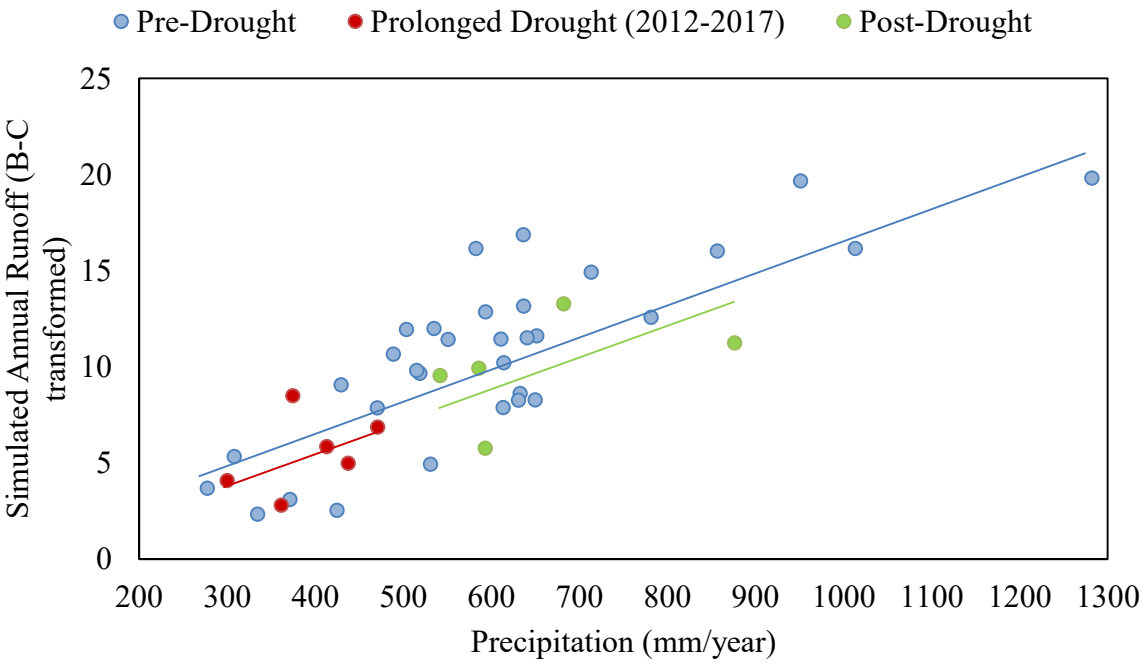

Source: The author

4.3.3 Sensitivity analysis for changes in SWAT parameters

To further assess the impact of the model parameters during the extended period (2012-2022), Figure **4.8** depict ranges of NSE (a) and lnNSE (b) for SWAT parameters governing hydrological processes in the soil, groundwater, subsurface and surface flow (CH_K1, CH_K2, CH_N2, CN2, ESCO, GW_DELAY, GW_REVAP, GWQMN, RCHRG_DP, REVAPMN, SOL_CRK, and TRNSRCH.

The analysis of Figure **4.8** shows that parameter variations consistently led to negative NSE and lnNSE values. Exceptions were observed with an increase in TRNSRCH values from 0.3 to 0.7–0.9, which resulted in positive lnNSE values (up to 0.46), and a decrease in RCHRG_DP from 0.25 to 0, which resulted in lnNSE values approximating zero. Other notable improvements in model performance were associated with increases in CH_K2 and decreases in CN2 values; however, these adjustments were insufficient to achieve positive lnNSE values. These parameter values suggest increased runoff losses, implying that channel transmission losses or infiltration into soils were likely underestimated by the model during the prolonged drought and its recovery period.

Figure 4.8 – Sensitivity Analysis of the Model in Malhada Catchment by NSE Range (a) and lnNSE Range (b) During the Drought Period (2012-2022)

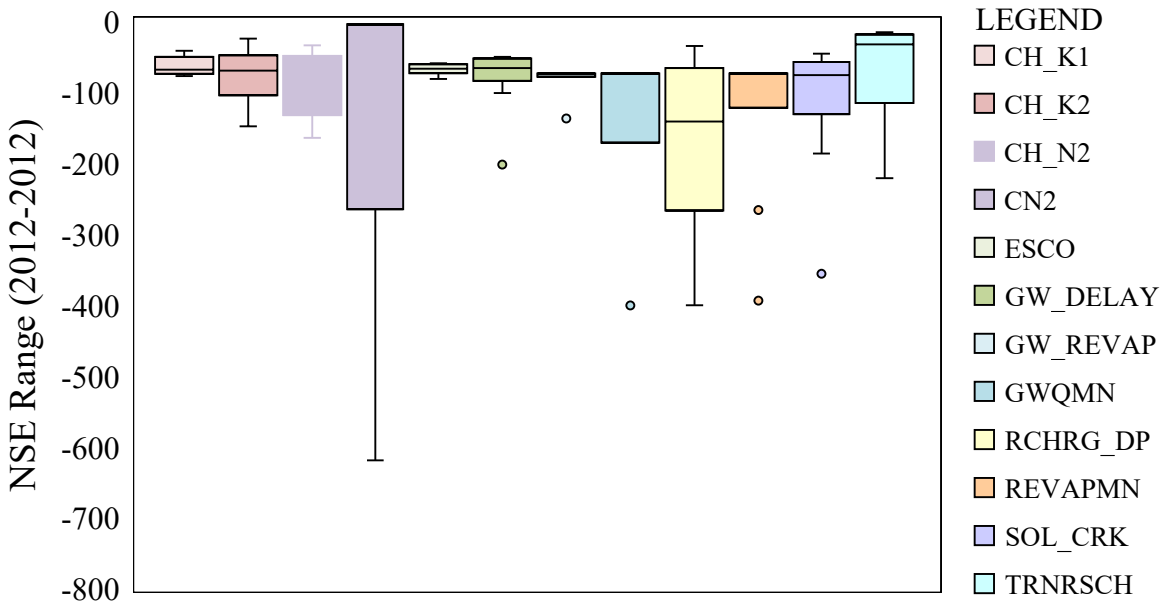

(a)

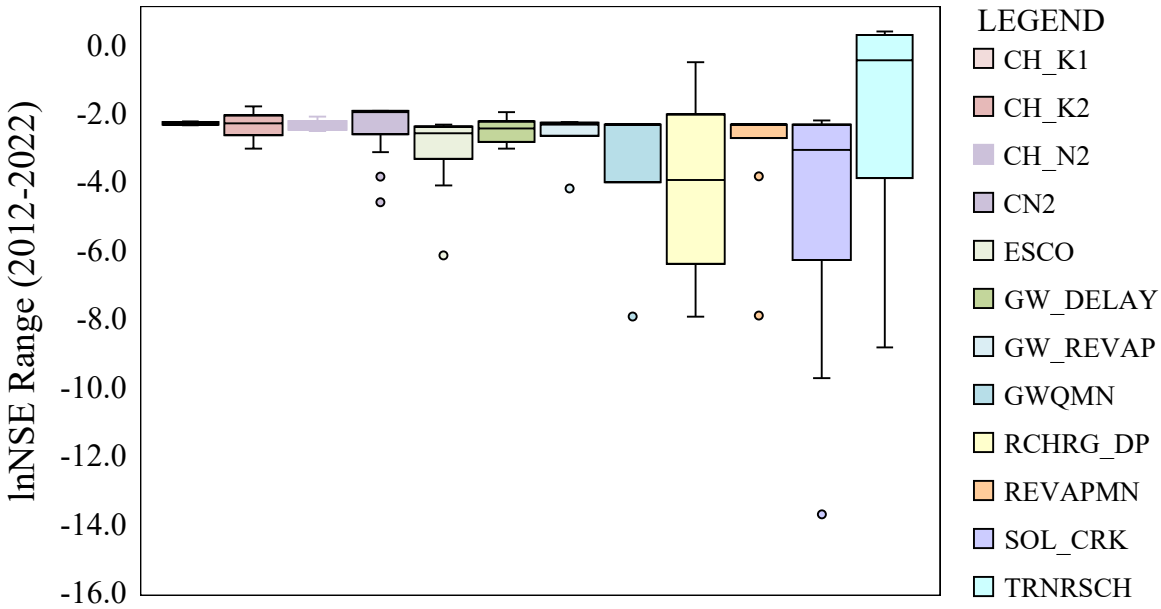

(b)

Source: The author

To analyze the impact of runoff transmission losses during the simulation period (1981 – 2010) and during the period of prolonged drought and its recovery (2012 – 2022), the performance results of the sensitivity analysis of parameters CH_K2, CN2, RCHRG_DP, and TRNSRCH were illustrated in Figure **4.9**, Figure **4.10**, Figure **4.11**, and Figure **4.12** for KGE, NSE, and lnNSE, respectively. The analysis of KGE and NSE indicate that the optimal CH_K2, CN2, RCHRH_DP, and TRNRSCH values for the Malhada catchment from 1981 to 2022 is similar to the values obtained during the calibration of the reference model. However, these values do not adequately represent the period from 2012 to 2022. Incremental increases in CH_K2 and TRNSRCH values and incremental decreases in CN2 and RCHRG_DP values tended to enhance model performance, yet not enough for the results to be considered a good fit.

In addition, analyzing the model's behavior using the lnNSE, it is possible to observe improved performance with incremental increases in CH_K2 and TRNSRCH values, as well as incremental decreases in CN2 and RCHRG_DP, for both the 1981–2022 and 2012–2022 periods.

Figure 4.9 – KGE, NSE, and lnNSE in Malhada Catchment for Changes in CH_K2 from 1981-2022 and 2012-2022 Periods

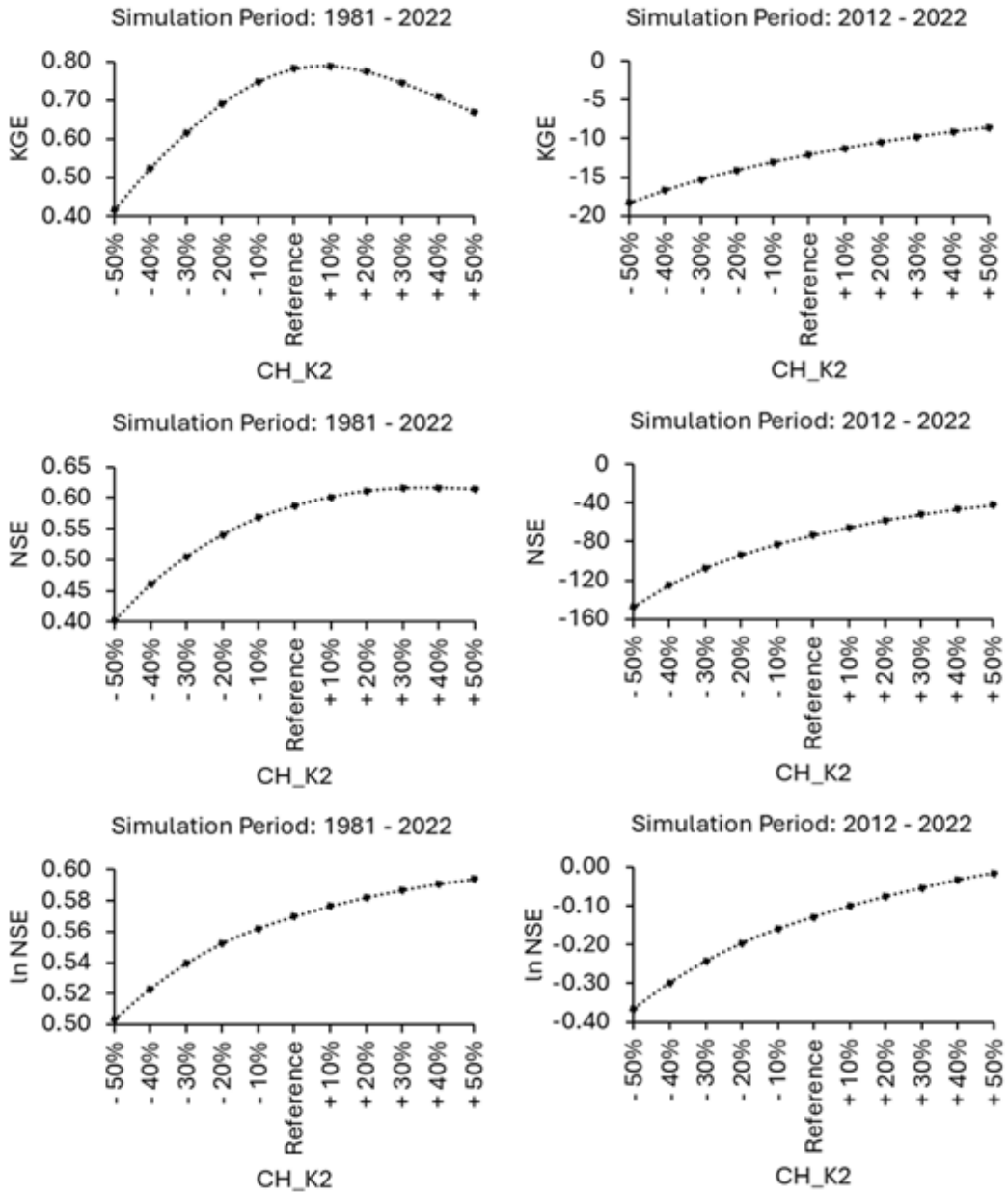

Source: The author

Figure 4.10 – KGE, NSE, and lnNSE in Malhada Catchment for Changes in CN2 from 1981-2022 and 2012-2022 Periods

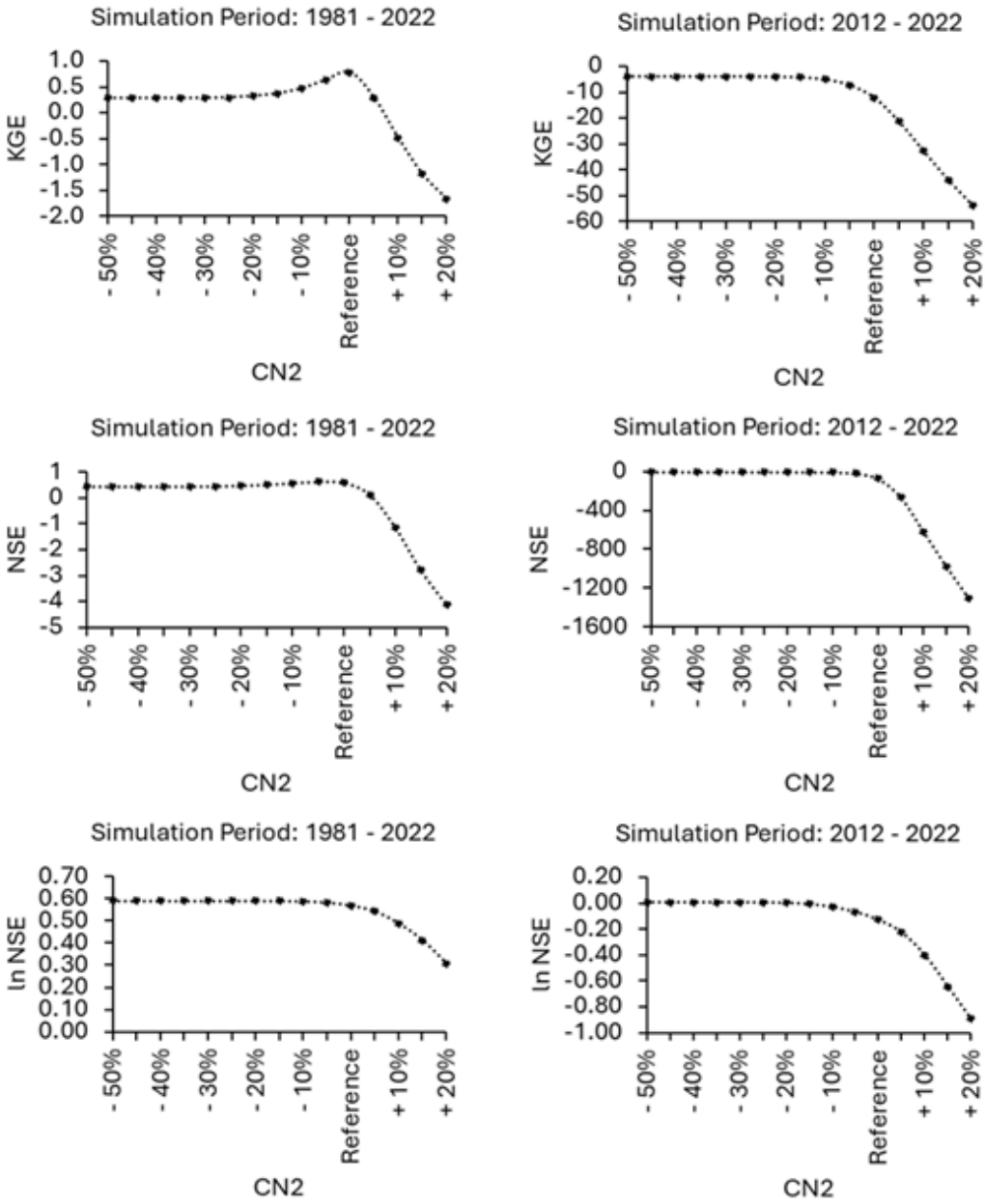

Source: The author

Figure 4.11 – KGE, NSE, and lnNSE in Malhada Catchment for Changes in RCHRG_DP from 1981-2022 and 2012-2022 Periods

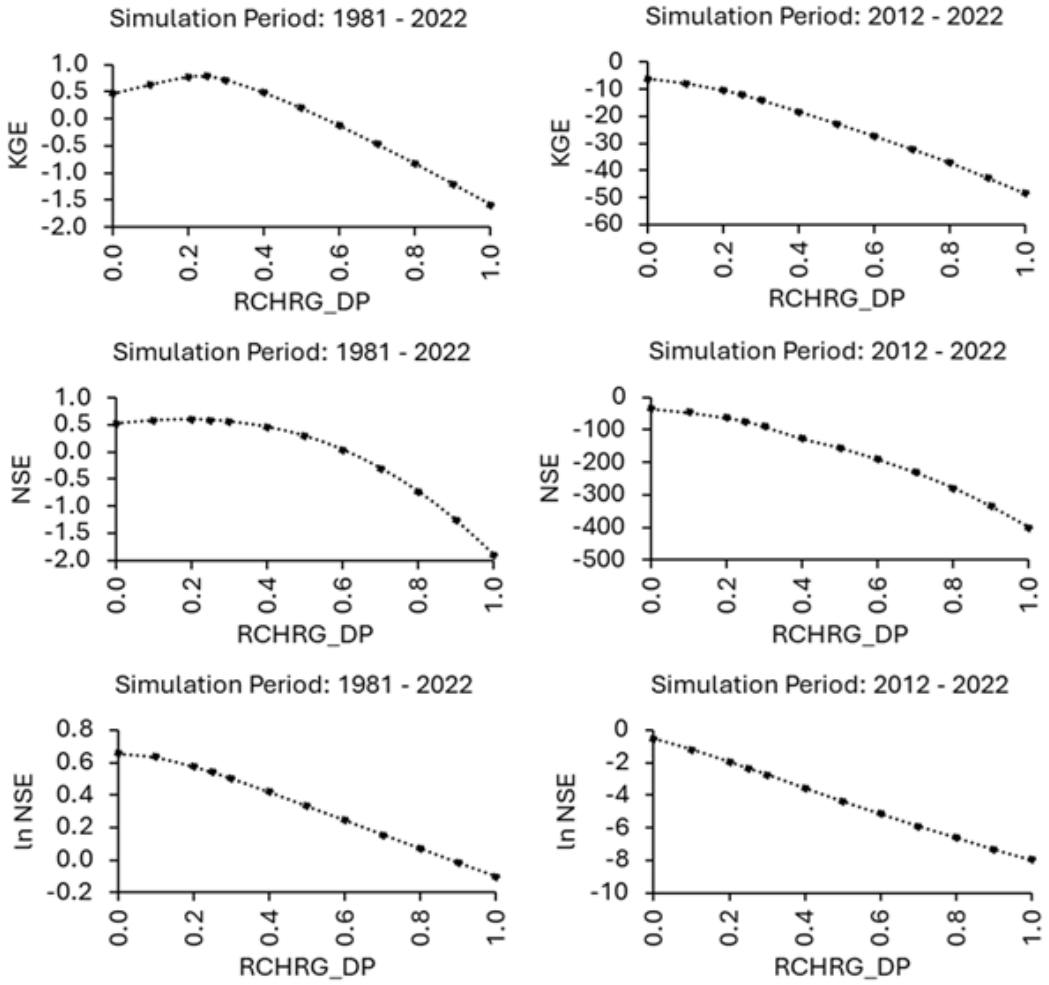

Source: The author

Figure 4.12 – KGE, NSE, and lnNSE in Malhada Catchment for Changes in TRNSRCH from 1981-2022 and 2012-2022 Periods

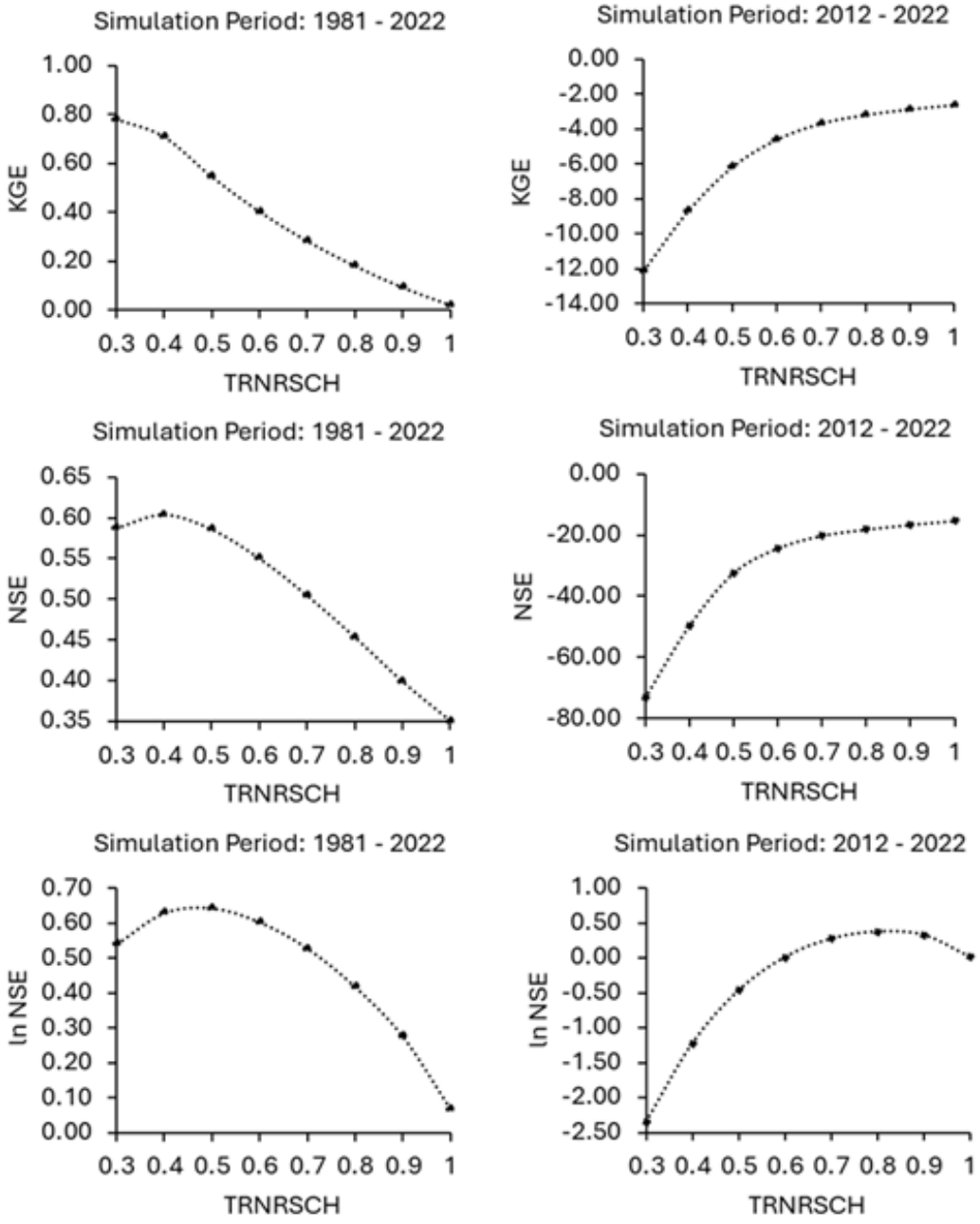

Source: The author

In general, the results indicated that the model performs well in terms of NSE, lnNSE, and KGE when considering the entire time series from 1981 to 2022. However, the model did not effectively represent the periods of prolonged drought and subsequent recovery, whether using the previous parameterization (1981 – 2010) or adjusting sensitive parameters.

4.4 Discussion

The results presented for the interannual and interdecadal climate variations are typical of drylands worldwide. However, the period 2012-2017 represents a critical event for the study area, with consecutive years of severe drought and two years with periods of extreme drought (2013 and 2017) evaluated by the SPEI12 index. The period is also characterized by average precipitation that is 35% lower and maximum temperatures that are 3.11% higher compared to those observed during the reference period (1981–2010). Moreover, both maximum and minimum temperatures exhibited positive trends. This pattern aligns with future projections of global warming and climate change, and other climate regions may experience the same characteristics and challenges of drylands, such as the Amazon basin, where traditional communities are now regularly facing water shortness due to recurrent, prolonged drought events (Lima et al., 2024; Marengo et al., 2024; Wunderling et al., 2022).

The modeling provided important insights into the performance of a semi-distributed model during and after a prolonged drought in a semi-arid region. The results obtained with the SWAT model in this study demonstrated a decline in performance when applying the previously calibrated model for a prolonged drought, even though the model performance was acceptable for past droughts. Similar limitations in model performance and lack of sensitivity to extreme events were observed when applying the continental-scale MGB model in South Brazil (Miranda et al., 2023a, 2023b).

During the hydrological recovery period after the prolonged drought, unlike recovery periods during the calibration period, the model overestimated streamflows significantly. These results of overestimation are similar to those found by Trotter et al. (2023) for conceptual rainfall-runoff models and by Deb and Kiem (2020) in a comparison of the IHACRES, HEC-HMS, and SWATgrid models under different climatic conditions, both studies in Australian catchments, and by Cai et al. (2023) for SWAT model in an arid region in Northwestern China.

The results of KGE, NSE, and lnNSE reveal satisfactory model performance for the reference period and the total climate series. However, while the analysis focusing more on mid and low flows also showed a decline in model performance (negative lnNSE values from 2012 to 2017 and from 2018 to 2022), the results were slightly better compared to NSE, since lnNSE is better to determine low flows model's efficiency (Castellanos-Osorio et al., 2023; Zhang et al., 2018). The lnNSE results being less negative than NSE suggest that the model can at least

capture the relative dynamics of the low flows during the prolonged drought period, although it still has limitations in representing the specific precipitation events, especially the peaks and the hydrographs duration. Notably, lnNSE indicated poorer performance during the prolonged drought, whereas the other three statiscal parameters showed worse performance during the drought recovery period. Since the overestimation of the model was higher during the recovery period, the traditional indexes were more impacted by the overestimated streamflow peaks simulated during the hydrological recovery period, showing a worst performance during this period than the drought period. For the lnNSE, the effect of peak streamflows is attenuated, leading to a daily evaluation of mid and low flows that is more balanced and closer to the average than during the drought period.

Although our model accounted for the drought years of 1990–1993 and 2001–2003 during calibration, their inclusion was insufficient to enhance the model's streamflow estimates for the period from 2012 to 2022. This result aligns with the discussions by Trotter et al. (2021), who argued that including a range of climate periods in the calibration process does not necessarily improve model reliability for future uncertainties. Similarly, the findings of Bruno et al. (2024) demonstrated that even adding a moderate drought to the calibration period did not lead to an improvement in streamflow estimates during a subsequent severe drought. Our findings complement these discussions, demonstrating that even a model calibrated with 30 years of climatic data, including periods of severe drought, could be insufficient to provide accurate streamflow estimates during an extreme and prolonged drought period.

The analysis of the components of the water balance showed that the percentage of evapotranspiration relative to precipitation increased during the prolonged drought period but returned to a percentage value close to the calibrated model after the drought. This result, combined with the temperature increase trends in the region, suggests that the model underestimated evapotranspiration after the prolonged drought. This finding is consistent with Bruno et al. (2024), who identified evapotranspiration underestimation as a contributing factor to decreased performance in modeling across droughts of varying severity in an Italian catchment with Continuum model. As Peterson et al. (2021) suggested, biophysical adaptations, such as increased transpiration in response to disturbances, can create positive feedback mechanisms that are not yet accounted for in current rainfall-runoff models. Regarding the results for subsurface flow, the simulated percentages relative to total flow during the prolonged drought and its recovery period were both higher than those observed during the calibration period. This suggests a greater contribution of this hydrological component during the

prolonged drought and subsequent hydrological recovery, as well as an indication of underestimation of channel and landscape transmission losses by the model, which led to an overestimation of streamflow values during these periods.

During the sensitivity analysis for the extended period, the most notable improvements in model performance were observed with an increase in TRNSRCH from 0.3 to 0.7-0.9 and decreases in RCHRG_DP from 0.25 to 0, suggesting a shift in these parameter values during the prolonged drought and its hydrological recovery period. The increase in the TRNSRCH parameter suggests higher transmission losses during the prolonged drought period, while reducing RCHRG_DP to zero indicates no water transfer between the shallow and deep aquifers, implying a disconnection between both aquifers, which is common during extreme drought periods. These results align with the findings of Merz et al. (2011) and Meles et al. (2024), who identified a correlation between model parameters and climatic variables, as well as with the conclusions of Liu et al. (2024) and Zhang et al. (2024), who demonstrated that time-varying parameter methods for hydrological simulations can better capture the dynamic nature of hydrological processes in changing environments.

However, even with the changes in the parameters of the model, the performance did not reach satisfactory levels during the prolonged drought period and its recovery, even when evaluated using the lnNSE metric. According to Rabelo et al. (2021), the SWAT model tends to struggle particularly during the flow recession period, where streamflow decreases more slowly in the model compared to field observations. Avanzi et al. (2020) and Bruno et al. (2024) suggested that overestimation of simulated terrestrial water storage, coupled with underestimated river-aquifer interactions and transmission losses during extreme droughts, may contribute to model inaccuracies. The results of the sensitivity analysis combined with the water balance and the hydrographs results during the prolonged drought and its hydrological recovery suggest that subsurface runoff was overestimated by the model. The linear functions applied in the model were insufficient to capture the interactions between groundwater and surface water under prolonged drought conditions in semi-arid catchments, suggesting that changes in the representation of the hydrological processes are also necessary for the model to accurately represent real conditions during a prolonged drought and the subsequent recovery period. Future studies could investigate the integration of surface and subsurface flows' processes, for instance, by utilizing MODFLOW or groundwater modules, to evaluate the behavior of coupled SWAT models during the prolonged drought period in the region.

The runoff results in the Malhada catchment during the prolonged drought of 2012-2017 indicated a shift in the rainfall-runoff relationship. Furthermore, during the drought recovery period of 2018-2022, runoff not only decreased but also ceased to respond to higher precipitation events. This finding suggests that the watershed undergoes a substantial shift in the rainfall-runoff process, reaching probably a new equilibrium state during this period. Recent studies have shown that rainfall-runoff transformation patterns can shift significantly following severe droughts, as demonstrated in the studies by Saft et al. (2016) and Peterson et al. (2021) on the millennial drought in Australia, by Alvarez-Garreton on the megadrought in Chile, and by Avanzi et al. (2020) on California's multi-year droughts.

No relevant land-use alterations occurred during the period of prolonged drought and hydrological recovery afterwards, as suggested by the analysis of land-use changes within the watershed (Appendix E). Land-use changes progressed gradually until 2010, which was captured by the reference model, with a trend toward stabilization afterward, except for high increases in temporary crop areas during the prolonged drought period. The expansion of agricultural areas, such as pasture and temporary crops, leads to alterations in evapotranspiration patterns, and consequently can lead to abrupt shifts in watershed behavior, as suggested by Fowler et al. (2022), and observed in the correlation between precipitation and runoff results of the Malhada catchment. For future scenarios of extreme or prolonged droughts, population behavior may respond adaptively to climatic events, often resulting in changes in watersheds to cope with dry conditions. Thus, the human-water dynamics in the catchments should be better represented in the models, to include social processes that affect the hydrological responses during extreme drought events.

4.5 Conclusions

In this study, we assessed the performance in streamflow results obtained by a calibrated SWAT model from the extrapolation of meteorological data to include a prolonged drought on a dryland catchment. The model performance for the previously unobserved drought period was not acceptable even though the model was before well calibrated, indicating room for improvement of parameters or problems of the model structure to simulate an extreme drought event. Model parameters did not result in a better parameterization of the model within meaningful ranges.

The main findings of our work can be described as follows:

1. The calibrated model had an acceptable performance from 1981 to 2010, but did not perform well for daily streamflow during the prolonged meteorological drought (2012 – 2017) and the hydrological recovery period afterward (2018 – 2022). The results of NSE, lnNSE, and KGE showed a drastic reduction in the model's performance during these two specific periods, with an even more pronounced decline in performance during the hydrological recovery period, emphasizing the model's limitations in accurately representing runoff conditions following a severe prolonged drought.

2. In general, the calibrated model presented higher streamflows than measured in the catchment during these periods, suggesting that water losses during hydrological processes were lower in the reference model during the prolonged drought and recovery. The gradual increase in the values of runoff transmission losses parameters tended to improve the model's performance, but not enough for the results to be considered a good fit.

3. The correlation graph between precipitation and simulated runoff showed that the HdRN model exhibited a decline in rainfall-runoff slope during the prolonged drought period, which increased during the hydrological recovery phase. Although the SWAT model managed to simulate a non-recovery scenario in runoff during the recovery period, the observed level of non-recovery in the catchment was even more pronounced, a state that the model was unable to fully capture.

This study could contribute to a more careful consideration of the reliability of streamflow prediction results during severe hydrological events, given that there is a rapid trend of increasing intensity and frequency of extreme climatic events, such as severe droughts, governed by climate change, but also influencing human adaptation measures.

A suggested future study is to evaluate the impact of the model's low performance on water resources management, particularly in the operation of strategic reservoirs with multiple uses. In terms of drought period modeling, a considerable error in statistical parameters may not necessarily translate into a significant difference in water availability for both people and the environment, given that water supply is naturally low during these periods. Future investigations could provide a more practical approach to this issue.

To better represent the accelerated extreme events caused by climate change, the traditional methodology of calibration based on past time series has important limitations. Modeling during extreme drought events would require an adaptation of the models, so the models need to consider the socio-hydrological processes during periods of extreme events. There is an important gap for improving hydrological models considering the dynamic changes in catchment, in which hydrological and social processes and parameters can be represented according to the climate event and not just as a calibrated and parameterized stationary model with different ranges in future climate projections.

5 GENERAL CONCLUSION AND RECOMMENDATIONS

This thesis has made a substantial contribution to our understanding of hydrological modeling in drylands, particularly through the application of the SWAT model across various simulation scenarios. The study highlights the model's capability to effectively represent dense reservoir networks and to analyze streamflow under diverse conditions, including average rainfall, periods of high flow, and extended droughts and its subsequential drought recovery.

Additionally, three specific objectives were pursued: (1) to develop a modeling methodology with a detailed representation of both large and small reservoirs in the SWAT model, and to conduct an extensive analysis of the cumulative impact of small reservoirs on horizontal hydrological connectivity in large-scale dryland catchments; (2) to assess the influence of high-density reservoir networks on interannual runoff variability; and (3) to evaluate the model's performance during extreme droughts and the subsequent hydrological recovery. In the preceding three chapters, each of these objectives is addressed as an independent paper, utilizing the same SWAT model as the basis for analysis.

The first paper introduced an innovative approach to incorporating a dense-reservoir network into the SWAT model, featuring a detailed representation of both large and small reservoirs. It also provided an extensive analysis of the cumulative impact of small reservoirs on horizontal hydrological connectivity in large-scale dryland catchments. Despite uncertainties in the input data, the model's daily performance was deemed acceptable, demonstrating good reliability in predicting peak flows during wet years, non-flow periods, and the rising limb of the hydrograph. The results indicated that while small reservoirs reduced streamflow, their overall impact on catchment retention was minimal, with only 2% of water being retained in wet years, and 9% in dry years. The proposed analysis significantly enhanced our understanding of hydrology in dryland catchments and the methodology approach to incorporate high-dense reservoirs networks can be applied to catchments in similar climatic and socio-economic contexts.

The second paper aimed to assess the potential impact of an increasing number of small reservoirs on dry hydrological networks, focusing on the annual flows generated at the outlet of the watershed under various small reservoir density scenarios (number of reservoirs per unit area, with densities ranging from 0.1 res/km² to 3.0 res/km², underscoring the tendency for small reservoir construction to increase in more remote areas as a strategy to mitigate drought impacts. The results indicated that the influence of the High-density Reservoir Network

(HdRN) on runoff reduction is most pronounced for a probability of exceedance between 1% and 10% of monthly flows and is minimal for months with very high flow peaks. The reduction in outlet flow due to the increased number of small reservoirs was found to be more significant during dry years (increases up to 30%) compared to wet years (increases up to 8%). This reduction also tends to escalate in consecutive years of drought, increasing from about 7% in the first year to around 20% in the final year under the worst-case scenario (3.0 res/km²), potentially exacerbating the effects of extended droughts. These results agreed with the results in the first paper, that small reservoirs has more influence during dry periods, however extend the discussion for consecutive dry years, which has the retention effect increased over the years. The results contribute to water resource management by highlighting the varying effects of small reservoirs during consecutive years of drought. This understanding is crucial for developing adaptive water management practices that account for the cumulative influence of small reservoirs, particularly in regions prone to extended dry periods.

In the third paper the model previously calibrated from 1981 to 2010 was employed to simulate streamflow in a subsequent, drier, and warmer decade (2011 to 2022), including the record drought from 2012 to 2017 within the study area. The findings indicate that, despite the model's acceptable performance over a 30-year climate series that included severe drought periods, it struggled to accurately predict streamflow during the record drought and the subsequent recovery phase, showing a marked decline in performance during these critical periods. Even after adjusting the most sensitive parameters related to key hydrological processes - a standard practice in hydrological research and modeling - the model's performance did not significantly improve. The results highlight the importance of viewing catchments as non-stationary systems, suggesting that model calibration and parameterization should be refined to incorporate improvements in hydrological process representation and consider human adaptive responses, integrating both physical and social factors to ensure more reliable flow predictions under future extreme scenarios.

In summary, the key innovations presented in this thesis are: (1) the first paper introduced a novel approach for integrating high-density reservoir networks into the SWAT model and demonstrated the model's strong performance in representing semi-arid catchments, making a technological contribution; (2) the second paper offered new insights into the cumulative impact of small reservoirs over a multi-year analysis, revealing an amplified effect on runoff reduction during consecutive dry years; and (3) the third paper contributed to the

broader scientific discussion on the necessity of enhancing hydrological models calibration and parameterization for more accurate streamflow simulations during extreme drought events.

For future work, each study offers its own set of recommendations.

In Chapter 2, the flow recession was not accurately represented by the model. The simulated hydrograph exhibited an abrupt recession at the end of wet periods, with streamflow dropping to zero just a few days after the peak. After periods of heavy rainfall, water tends to accumulate in areas near the river channel, forming floodplains. The river recharge process following this period is notably complex, involving unsaturated seepage, vertical unsaturated subsurface water redistribution beneath the stream, lateral stream-aquifer interactions, and groundwater flow parallel to the river course in unconfined aquifers. These processes, which are critical in arid and semi-arid watersheds, are overly simplified in the SWAT model, significantly impacting its accuracy in these basins. Future enhancements should focus on improving the model's representation of recession flows. Additionally, enhancements in reservoir outflow inputs could better capture the variable aspect of water withdrawals due to negotiated allocations. In the specific case of the represented catchment, water withdrawals from reservoirs are determined through discussions with all water users in the watershed, leading to significant variability throughout the year. It is crucial that the model allows for the inclusion of a historical series of reservoir withdrawals to achieve more accurate modeling.

In Chapter 3, the initial scenario approach involved an even distribution of small reservoirs across the catchment. However, for future studies, a more realistic scenario approach should be considered. This would involve a targeted increase in the number of small reservoirs in regions near large strategic reservoirs and in areas with higher population densities. This refined approach would better reflect the likely patterns of reservoir construction and their potential impact on hydrological processes and water management within the catchment.

In Chapter 4, to enhance modeling accuracy during extended droughts, it is recommended that models incorporate human adaptive measures into the calibration process, allowing catchment parameters to be flexible and responsive to climatic events. By integrating both physical and social processes in response to climate events, the model's reliability in predicting streamflows under extreme future scenarios can be significantly improved.

Overall, this thesis has provided valuable insights to enhance dryland modeling. By bridging the gap between science, modeling and management, these advancements in modeling are crucial for improving the accuracy of scenario predictions and, consequently, for enhancing water resource management strategies in regions vulnerable to scarcity.

REFERENCES

ABEL, C.; ABDI, A.M.; TAGESSON, T.; HORION, S.; FENSHOLT, R. **Contrasting ecosystem vegetation response in global drylands under drying and wetting conditions.** Global Change Biolology, v. 29, n. 14, p. 3954–3969, 2023.

ABOUABDILLAH, A.; WHITE, M.; ARNOLD, J.G.; DE GIROLAMO, A.M.; OUESLATI, O.; MAATAOUI, A.; LO PORTO, A. **Evaluation of soil and water conservation measures in a semi-arid river basin in Tunisia using SWAT.** Soil Use and Management, v. 30, n. 4, p. 539–549, 2014.

AGHAKOUCHAK, A.; FELDMAN, D.; HOERLING, M.; HUXMAN, T.; LUND, J. **Water and climate: Recognize anthropogenic drought.** Nature, v. 524, p. 409–411, 2015.

AIGNER, D. **Dresdner Wasserbauliche Mitteilungen Heft 36**: Überfälle. Dresden: Technische Universität Dresden, 2008. p. 162-176. Available online at: http://rcswww.urz.tu-dresden.de/~daigner/pdf/ueberf.pdf. Accessed on: 10 mar. 2021.

AKBARI, F.; SHOURIAN, M.; MORIDI, A. **Assessment of the climate change impacts on the watershed-scale optimal crop pattern using a surface-groundwater interaction hydro-agronomic model.** Agricultural Water Management, v. 265, n. 107508, 2022.

ALLAN, R.P.; BARLOW, M.; BYRNE, M.P.; CHERCHI, A.; DOUVILLE, H.; FOWLER, H.J.; GAN, T.Y.; PENDERGRASS, A.G.; ROSENFELD, D.; SWANN, A.L.S.; WILCOX, L.J.; ZOLINA, O. **Advances in understanding large-scale responses of the water cycle to climate change.** Annals of the New York Academy of Sciences, v. 1472, n. 1, p. 49-75, 2020.

ALTHOFF, D.; RODRIGUES, L.N.; DA SILVA, D.D.; BAZAME, H.C. **Improving Methods for Estimating Small Reservoir Evaporation in the Brazilian Savanna.** Agricultural Water Management, v. 216, p. 105–112, 2019.

ALVAREZ-GARRETON, C.; PABLO BOISIER, J.; GARREAUD, R.; SEIBERT, J.; VIS, M. **Progressive water deficits during multiyear droughts in basins with long hydrological memory in Chile.** Hydrology and Earth System Sciences, v. 25, n. 1, p. 429–446, 2021.

ANDARYANI, S.; TROLLE, D.; NIKJOO, M.R.; MOGHADAM, M.H.R.; MOKHTARI, D. **Forecasting near-future impacts of land use and climate change on the Zilbier river hydrological regime, northwestern Iran.** Environmental Earth Sciences, v. 78, n. 188, p. 1-14, 2019.

ANDRADE, C.W.L. DE; MONTENEGRO, S.M.G.L.; MONTENEGRO, A.A.A.; LIMA, J.R. DE S.; SRINIVASAN, R.; JONES, C.A. **Soil moisture and discharge modeling in a representative watershed in northeastern Brazil using SWAT.** Ecohydrology & Hydrobiology, v. 19, n. 2, p. 238–251, 2019.

ANDRADE NETO, J. V. **Simulação hidrológica de grandes bacias semiáridas com densas redes de açudes e poucos dados.** 2022. Dissertação (Mestrado em Recursos Hídricos), Universidade Federal do Rio Grande do Sul (UFRGS), Porto Alegre, 2022.

APURV, T.; SIVAPALAN, M.; CAI, X. **Understanding the Role of Climate Characteristics in Drought Propagation.** Water Resources Research, v. 53, n. 11, p. 9304–9329, 2017.

ARNOLD, J.G.; MORIASI, D.N.; GASSMAN, P.W.; ABBASPOUR, K.C.; WHITE, M.J.; SRINIVASAN, R.; SANTHI, C.; HARMEL, R.D.; VAN GRIENSVEN, A.; VAN LIEW, M.W.; KANNAN, N.; JHA, M.K. **SWAT: Model Use, Calibration, and Validation.** Transactions of ASABE, v. 55, n. 4, p. 1491–1508, 2012.

ASIF, Z.; CHEN, Z.; SADIQ, R.; ZHU, Y. **Climate Change Impacts on Water Resources and Sustainable Water Management Strategies in North America.** Water Resources Management, v. 37, p. 2771–2786, 2023.

ATTAROD, P.; SADEGHI, S.M.M.; PYPKER, T.G.; BAGHERI, H.; BAGHERI, M.; BAYRAMZADEH, V. **Needle-leaved trees impacts on rainfall interception and canopy storage capacity in an arid environment.** New Forests, v. 46, p. 339–355, 2015.

AVANZI, F.; RUNGEE, J.; MAURER, T.; BALES, R.; MA, Q.; GLASER, S.; CONKLIN, M. **Climate elasticity of evapotranspiration shifts the water balance of Mediterranean climates during multi-year droughts.** Hydrology and Earth System Sciences, v. 24, n. 9, p. 4317–4337, 2020.

AVISSE, N.; TILMANT, A.; FRANÇOIS MÜLLER, M.; ZHANG, H. **Monitoring Small Reservoirs' Storage with Satellite Remote Sensing in Inaccessible Areas.** Hydrology and Earth System Sciences, v, 21, p. 6445–6459, 2017.

AYALEW, T. B., KRAJEWSKI, W. F., MANTILLA, R., WRIGHT, D. B., & SMALL, S. J. **Effect of Spatially Distributed Small Dams on Flood Frequency: Insights from the Soap Creek Watershed.** Journal of Hydrologic Engineering, v. 22, n. 7, 2017.

BENITES, V.M.; MACHADO, P.O.A.; FIDALGO, E.C.C.; COELHO, M.R.; MADARI, B.E.; LIMA, C.X. **Funções de Pedotransferência para Estimativa da Densidade dos Solos Brasileiros.** Boletim de Pesquisa e Desenvolvimento, Ministério da Agricultura, Pecuária e Abastecimento, Empresa Brasileira de Pesquisa Agropecuária. ISSN: 1678-0892, 2006.

BERG, M.D.; POPESCU, S.C.; WILCOX, B.P.; ANGERER, J.P.; RHODES, E.C.; MCALISTER, J.; FOX, W.E. **Small farm ponds: overlooked features with important impacts on watershed sediment transport.** Journal of the American Water Resources Association, v. 52, n. 1, p. 67–76, 2016.

BERHANE, G.; GEBREYOHANNES, T.; MARTENS, K.; WALRAEVENS, K. **Overview of micro-dam reservoirs (MDR) in Tigray (northern Ethiopia): Challenges and benefits.** Journal of African Earth Science, v. 123, p. 210–222, 2016.

BOX, G.E.P.; COX, D.R. **An Analysis of Transformations.** Journal of the Royal Statistical Society: Series B (Methodological), v. 26, n. 2, p. 211–243, 1964.

BRADFORD, J.B.; SCHLAEPFER, D.R.; LAUENROTH, W.K.; PALMQUIST, K.A. **Robust ecological drought projections for drylands in the 21st century.** Global Change Biology, v. 26, n.7, p. 3906–3919, 2020.

BRESSIANI, D.A.; GASSMAN, P.W.; FERNANDES, J.G.; HAMILTON, L.; GARBOSSA, P.; SRINIVASAN, R.; BONUMÁ, N.B.; MENDIONDO, E.M. **Review of Soil and Water Assessment Tool (SWAT) applications in Brazil: challenges and prospects.** International Journal of Agricultural and Biological Engineering, v. 8, n. 3, p. 9–35, 2015a.

BRESSIANI, D.A.; SRINIVASAN, R.; JONES, C.A.; MENDIONDO, E.M. **Effects of spatial and temporal weather data resolutions on streamflow modeling of a semi-arid basin, Northeast Brazil.** International Journal of Agricultural and Biological Engineering, v. 8, n. 3, p. 125–139, 2015B.

BRONSTERT, A.; DE ARAÚJO, J.C.; BATALLA, R.J.; COSTA, A.C.; DELGADO, J.M.; FRANCKE, T.; FOERSTER, S.; GUENTNER, A.; LÓPEZ-TARAZÓN, J.A.; MAMEDE, G.L.; ET AL. **Process-Based Modelling of Erosion, Sediment Transport and Reservoir Siltation in Mesoscale Semi-Arid Catchments.** Journal of Soils and Sediments, v. 14, p. 2001–2018, 2014.

BRUNO, G.; AVANZI, F.; ALFIERI, L.; LIBERTINO, A.; GABELLANI, S.; DUETHMANN, D. **Hydrological model skills change with drought severity; insights from multi-variable evaluation.** Journal of Hydrology, v. 634, n. 131023, 2024.

CAI, Y.; ZHANG, F.; SHI, J.; CARL JOHNSON, V.; AHMED, Z.; WANG, J.; WANG, W. **Enhancing SWAT model with modified method to improve Eco-hydrological simulation in arid region.** Journal of Cleaner Production, v. 403, n. 136891, 2023.

CALLOW, J.N.; SMETTEM, K.R.J. **The effect of farm dams and constructed banks on hydrologic connectivity and runoff estimation in agricultural landscapes.** Environmental Modelling & Software, v. 24, n. 8, p. 959–968, 2009.

CAO, Z.; HUANG, W.; PENDER, G.; LIU, X. **Even More Destructive: Cascade Dam Break Floods.** Journal of Flood Risk Management, v. 7, n. 4, p. 357–373, 2014.

CARLUER N.; BABUT M.; BELLIARD J.; BERNEZ I.; BURGER-LEENHARDT D.; DORIOZ J.M.; DOUEZ O.; DUFOUR S.; GRIMALDI C.; HABETS F.; LE BISSONNAIS Y.; MOLÉNAT J.; ROLLET A.J.; ROSSET V.; SAUVAGE S.; USSEGLIO-POLATERA P.; LEBLANC B. **Expertise scientifique collective sur l'impact cumulé des retenues.** Rapport de synthèse, 2016. p. 82 + annexes.

CASADEI, S.; DI FRANCESCO, S.; GIANNONE, F.; PIERLEONI, A. **Small reservoirs for a sustainable water resources management.** Advances in Geosciences, v. 49, p. 165–174, 2019.

CASTELLANOS-OSORIO, G.; LÓPEZ-BALLESTEROS, A.; PÉREZ-SÁNCHEZ, J.; SENENT-APARICIO, J. **Disaggregated monthly SWAT+ model versus daily SWAT+ model for estimating environmental flows in Peninsular Spain.** Journal of Hydrology, v. 623, n. 129837, 2023.

CEARÁ. Secretaria dos Recursos Hídricos. **Sistema de Informaçõs dos Recursos Hídricos do Ceará**. Fortaleza: SEINFRA/SRH, 2024. Available online at: http://atlas.srh.ce.gov.br/. Accessed on: 10 mar.2024.

CEARÁ. Secretaria Executiva do CSBHAJ. **Comitê da sub-bacia hidrografica do Alto Jaguaribe.** Iguatu: COGERH - Gerência da Bacia do Alto Jaguaribe, 2024. Available online at: http://www.csbhaj.com.br/comissoesgestoras/comissao-gestora-do-acude-bengue/?pagina=regimento. Accessed on: 10 mar. 2024.

CECCHI, P.; FORKUOR, G.; COFIE, O.; LALANNE, F.; POUSSIN, J. C.; JAMIN, J. Y. **Small Reservoirs, Landscape Changes and Water Quality in Sub-Saharan West Africa.** Water, v. 12, n. 7, 2020.

CHIMWAMUROMBE, P.M.; MATARANYIKA, P.N. **Factors influencing dryland agricultural productivity.** Journal of Arid Environments, v. 189, n. 104489, 2021.

COLARES, J.Q.D.S.; FEITOSA F.A.C. **Diagnóstico do Município de Campos Sales.** Fortaleza: Ministério de Minas e Energia; Serviço Geológico do Brasil, 1998. (Programa de Recenseamento de Fontes de Abastecimento por Água Subterrânea no Estado do Ceará)

COLLISCHONN, B.; PAIVA, R. C. D. D.; COLLISCHONN, W.; MEIRELLES, F. S. C.; CAMAÑO SCHETTINI, E. B.; FAN, F. M. **Modelagem hidrológica de uma bacia com uso intensivo de água: Caso do Rio Quaraí-RS.** RBRH: Brazilian Journal of Water Resources, Porto Alegre, v. 16, n. 4, p. 119-133, 2011.

COLOMBO, P.; RIBEIRO NETO, G.G.; COSTA, A.C.; MAMEDE, G.L.; VAN OEL, P.R. **Modeling the influence of small reservoirs on hydrological drought propagation in space and time.** Journal of Hydrology, v. 629, n. 130640, 2024.

CORTEZ, F.; MONICELLI, F.; CAVALCANTE, H.; BECKER, V. **Effects of prolonged drought on water quality after drying of a semiarid tropical reservoir, Brazil.** Limnologica, v. 93, n. 125959, 2022.

COSTA, A. C.; ESTACIO, A. B. S.; SOUZA FILHO, F. DE A. DE; LIMA NETO, I. E. **Monthly and seasonal streamflow forecasting of large dryland catchments in Brazil.** Journal of Arid Land, v. 13, n. 3, p. 205–223, 2021.

COSTA, A.C.; BRONSTERT, A.; DE ARAÚJO, J.C. **A channel transmission losses model for different dryland rivers.** Hydrology and Earth System Sciences, v. 16, n. 4, p. 1111–1135, 2012.

COSTA, A.C.; DUPONT, F.; BIER, G.; VAN OEL, P.; WALKER, D.W.; MARTINS, E.S.P.R. **Assessment of aquifer recharge and groundwater availability in a semiarid region of Brazil in the context of an interbasin water transfer scheme.** Hydrogeology Journal, v. 31, p. 751–769, 2023.

COSTA, A.C.; FOERSTER, S.; DE ARAÚJO, J.C.; BRONSTERT, A. **Analysis of channel transmission losses in a dryland river reach in north-eastern Brazil using streamflow series, groundwater level series and multi-temporal satellite data.** Hydrological Processes, v. 27, n. 7, p. 1046–1060, 2013.

CRAUSBAY, S.D.; BETANCOURT, J.; BRADFORD, J.; CARTWRIGHT, J.; DENNISON, W.C.; DUNHAM, J.; ENQUIST, C.A.F.; FRAZIER, A.G.; HALL, K.R.; LITTELL, J.S.; LUCE, C.H.; PALMER, R.; RAMIREZ, A.R.; RANGWALA, I.; THOMPSON, L.; WALSH, B.M.; CARTER, S. **Unfamiliar Territory: Emerging Themes for Ecological Drought Research and Management.** One Earth, v. 3, n. 3, p. 337-353, 2020.

CUNHA, A.P.M.A.; ZERI, M.; LEAL, K.D.; COSTA, L.; CUARTAS, L.A.; MARENGO, J.A.; TOMASELLA, J.; VIEIRA, R.M.; BARBOSA, A.A.; CUNNINGHAM, C.; CAL GARCIA, J.V.; BROEDEL, E.; ALVALÁ, R.; RIBEIRO NETO, G. **Extreme drought events over Brazil from 2011 to 2019.** Atmosphere (Basel), v. 10, n. 11, 2019.

DAGGUPATI, P.; PAI, N.; ALE, S.; DOUGLAS-MANKIN, K.R.; ZECKOSKI, R.W.; JEONG, J.; PARAJULI, P.B.; SARASWAT, D.; YOUSSEF, M.A. **A Recommended Calibration and Validation Strategy for Hydrologic and Water Quality Models.** Transactions of the ASABE, v. 58, n. 6, p. 1705–1719, 2015.

DE ARAÚJO, J.C.; MEDEIROS, P.H.A. **Impact of Dense Reservoir Networks on Water Resources in Semiarid Environments.** Australasian Journal of Water Resources, v. 17, n. 1, p. 87–100, 2013.

DE FIGUEIREDO, J.V.; DE ARAÚJO, J.C.; MEDEIROS, P.H.A.; COSTA, A.C. **Runoff initiation in a preserved semiarid Caatinga small watershed, Northeastern Brazil**. Hydrological Processes, v. 30, n. 13, p. 2390–2400, 2016.

DEB, P.; KIEM, A.S. **Evaluation of rainfall–runoff model performance under non-stationary hydroclimatic conditions.** Hydrological Sciences Journal, v. 65, n. 10, p. 1667–1684, 2020.

DEITCH, M. J.; MERENLENDER, A. M.; FEIRER, S. **Cumulative Effects of Small Reservoirs on Streamflow in Northern Coastal California Catchments.** Water Resources Management, v. 27, n. 15, p. 5101–5118, 2013.

DI BALDASSARRE, G.; WANDERS, N.; AGHAKOUCHAK, A.; KUIL, L.; RANGECROFT, S.; VELDKAMP, T.I.E.; GARCIA, M.; VAN OEL, P.R.; BREINL, K.; VAN LOON, A.F. **Water Shortages Worsened by Reservoir Effects.** Nature Sustainability, v. 1, p. 617–622, 2018.

DOGAN, F.N.; KARPUZCU, M.E. **Modeling fate and transport of pesticides from dryland agriculture using SWAT model.** Journal of Environmental Management, v. 334, n. 117457, 2023.

DUETHMANN, D.; SMITH, A.; SOULSBY, C.; KLEINE, L.; WAGNER, W.; HAHN, S.; TETZLAFF, D. **Evaluating satellite-derived soil moisture data for improving the internal consistency of process-based ecohydrological modelling.** Journal of Hydrology, v. 614(A), n. 128462, 2022.

EUDORO, W.S. **Caderno Regional da Sub-bacia do Alto Jaguaribe.** Fortaleza: Assembleia Legislativa do Estado; Conselho de Altos Estudos e Assuntos Estratégicos, INESP, 2009. (Coleção Cadernos Regionais do Pacto das Águas - Volume 5)

FEITOSA, F.A.C. **Diagnóstico do Município de Aiuaba.** Fortaleza: Ministério de Minas e Energia; Serviço Geológico do Brasil, 1998. (Programa de Recenseamento de Fontes de Abastecimento por Água Subterrânea no Estado do Ceará)

FEITOSA, F.A.C.; OLIVEIRA, F.V.C. DE. **Diagnóstico do Município de Salitre.** Fortaleza: Ministério de Minas e Energia; Serviço Geológico do Brasil, 1998. (Programa de Recenseamento de Fontes de Abastecimento por Água Subterrânea no Estado do Ceará)

FLORIANCIC, M. G.; BERGHUIJS, W. R.; JONAS, T.; KIRCHNER, J. W.; MOLNAR, P. **Effects of climate anomalies on warm-season low flows in Switzerland.** Hydrology and Earth System Sciences, v. 24, n. 11, p. 5423–5438, 2020.

FLORIANCIC, M. G.; BERGHUIJS, W. R.; MOLNAR, P.; KIRCHNER, J. W. **Seasonality and Drivers of Low Flows Across Europe and the United States.** Water Resources Research, v. 57, n. 9, 2021.

FOWE, T.; KARAMBIRI, H.; PATUREL, J.E.; POUSSIN, J.C.; CECCHI, P. **Water balance of small reservoirs in the Volta basin: A case study of Boura reservoir in Burkina Faso.** Agricultural Water Management, v. 152, p. 99–109, 2015.

FOWLER, K.; MORDEN, R.; LOWE, L.; NATHAN, R. **Advances in assessing the impact of hillside farm dams on streamflow.** Australasian Journal of Water Resources, v. 19, n. 2, p. 96–108, 2016.

FOWLER, K.; PEEL, M.; SAFT, M.; PETERSON, T.J.; WESTERN, A.; BAND, L.; PETHERAM, C.; DHARMADI, S.; TAN, K.S.; ZHANG, L.; LANE, P.; KIEM, A.; MARSHALL, L.; GRIEBEL, A.; MEDLYN, B.E.; RYU, D.; BONOTTO, G.; WASKO, C.; UKKOLA, A.; STEPHENS, C.; FROST, A.; GARDIYA WELIGAMAGE, H.; SACO, P.; ZHENG, H.; CHIEW, F.; DALY, E.; WALKER, G.; VERVOORT, R.W.; HUGHES, J.; TROTTER, L.; NEAL, B.; CARTWRIGHT, I.; NATHAN, R. **Explaining changes in rainfall-runoff relationships during and after Australia's Millennium Drought: a community perspective.** Hydrology and Earth System Sciences, v. 26, n. 23, p. 6073–6120, 2022.

FUNDAÇÃO CEARENSE DE METEOROLOGIA E RECURSOS HÍDRICOS DO ESTADO DO CEARÁ. **Mapeamento das barragens dos pequenos reservatórios d'água situados no Estado do Ceará.** Fortaleza, 2021. p. 10.

GATTO, L.C.S. **Diagnóstico Ambiental da Bacia do Rio Jaguaribe. Diretrizes Gerais para a Ordenação Territorial.** Salvador: Fundação Instituto Brasileiro de Geografia e Estatística (IBGE); Diretoria Geociências, 1999.

GHORABA, S.M. **Hydrological modeling of the Simly Dam watershed (Pakistan) using GIS and SWAT model.** Alexandria Engineering Journal, v. 54, n. 3, p. 583–594, 2015.

GRAFTON, R.Q.; DOYEN, L.; BÉNÉ, C.; BORGOMEO, E.; BROOKS, K.; CHU, L.; CUMMING, G.S.; DIXON, J.; DOVERS, S.; GARRICK, D.; HELFGOTT, A.; JIANG, Q.; KATIC, P.; KOMPAS, T.; LITTLE, L.R.; MATTHEWS, N.; RINGLER, C.; SQUIRES, D.; STEINSHAMN, S.I.; VILLASANTE, S.; WHEELER, S.; WILLIAMS, J.; WYRWOLL, P.R. **Realizing resilience for decision-making.** Nature Sustainability, v. 2, p. 907–913, 2019.

GUAN, X.; HUANG, J.; ZHANG, Y.; XIE, Y.; LIU, J. **The relationship between anthropogenic dust and population over global semi-arid regions.** Atmospheric Chemistry Physics, v. 16, n. 8, p. 5159–5169, 2016.

GUDMUNDSSON, L.; BREMNES, J.B.; HAUGEN, J.E.; ENGEN-SKAUGEN, T. **Technical Note: Downscaling RCM precipitation to the station scale using statistical transformations - a comparison of methods.** Hydrology and Earth System Sciences, v. 16, n. 9, p. 3383–3390, 2012.

GÜNTNER, A. **Large-Scale Hydrological Modelling in the Semi-Arid North-East of Brazil.** 2002. Dissertation (Doctor of Natural Sciences) – Faculty of Mathematics and Sciences, University of Potsdam, Potsdam, Germany, 2002.

GÜNTNER, A.; KROL, M.S.; DE ARAÚJO, J.C.; BRONSTERT, A. **Simple water balance modelling of surface reservoir systems in a large data-scarce semiarid region.** Hydrological Sciences Journal, v. 49, n. 5, 2004.

GUPTA, H. V.; RAZAVI, S. **Revisiting the Basis of Sensitivity Analysis for Dynamical Earth System Models.** Water Resources Research, v. 54, n. 11, p. 8692–8717, 2018.

GUTIÉRREZ, A.P.A.; ENGLE, N.L.; DE NYS, E.; MOLEJÓN, C.; MARTINS, E.S. **Drought preparedness in Brazil.** Weather and Climate Extremes, v. 3, p. 95–106, 2014.

HABETS, F.; MOLENAT, J.; CARLUER, N.; DOUEZ, O.; LEENHARDT, D. **The cumulative impacts of small reservoirs on hydrology: A review.** Science of the Total Environment, v. 643, p. 850-867, 2018.

HATTERMANN, F.F.; VETTER, T.; BREUER, L.; SU, B.; DAGGUPATI, P.; DONNELLY, C.; FEKETE, B.; FLORKE, F.; GOSLING, S.N.; HOFFMANN, P.; LIERSCH, S.; MASAKI, Y.; MOTOVILOV, Y.; MULLER, C.; SAMANIEGO, L.; STACKE, T.; WADA, Y.; YANG, T.; KRYSNAOVA, V. **Sources of uncertainty in hydrological climate impact assessment: A cross-scale study.** Environmental Research Letters, v. 13, n. 1, 2018.

HE, X.; WADA, Y.; WANDERS, N.; SHEFFIELD, J. **Intensification of hydrological drought in California by human water management.** Geophysical Research Letters, v. 44, n. 4, p. 1777–1785, 2017.

HUANG, J.; LI, Y.; FU, C.; CHEN, F.; FU, Q.; DAI, A.; SHINODA, M.; MA, Z.; GUO, W.; LI, Z.; ZHANG, L.; LIU, Y.; YU, H.; HE, Y.; XIE, Y.; GUAN, X.; JI, M.; LIN, L.; WANG, S.; YAN, H.; WANG, G. **Dryland climate change: Recent progress and challenges.** Reviews of Geophysics, v. 55, n. 3, p. 719–778, 2017.

HUANG, J.; YU, H.; GUAN, X.; WANG, G.; GUO, R. **Accelerated dryland expansion under climate change.** Nature Climate Change, v. 6, p. 166-171, 2015.

HUGHES, D.A.; MANTEL, S.K. **Estimating the uncertainty in simulating the impacts of small farm dams on streamflow regimes in South Africa.** Hydrological Sciences Journal, v. 55, n. 4, p. 578–592, 2010.

IGNATIUS, A. R.; RASMUSSEN, T. C. **Small reservoir effects on headwater water quality in the rural-urban fringe, Georgia Piedmont, USA.** Journal of Hydrology: Regional Studies, v. 8, p. 145–161, 2016.

JACOMINE, P.K.T.; ALMEIDA, J.C.; MEDEIROS, L.A.R. **Levantamento Exploratório - Reconhecimento de Solos do Estado do Ceará.** Recife: Divisão de Pesquisa Pedológica; Divisão de Agrologia; Ministério da Agricultura; Ministério do Interior, 1973. (Convênio de Mapeamento de Solos)

JAJARMIZADEH, M.; SIDEK, L.M.; HARUN, S.; SALARPOUR, M. **Optimal Calibration and Uncertainty Analysis of SWAT for an Arid Climate.** Air, Soil and Water Research, v. 10, 2017.

JARIHANI, A.A.; LARSEN, J.R.; CALLOW, J.N.; MCVICAR, T.R.; JOHANSEN, K. **Where does all the water go? Partitioning water transmission losses in a data-sparse, multi-channel and low-gradient dryland river system using modelling and remote sensing.** Journal of Hydrology, v. 529 (3), p. 1511–1529, 2015.

JU, J.; DAI, H.; WU, C.; HU, B.X.; YE, M.; CHEN, X.; GUI, D.; LIU, H.; ZHANG, J. **Quantifying the Uncertainty of the Future Hydrological Impacts of Climate Change: Comparative Analysis of an Advanced Hierarchical Sensitivity in Humid and Semiarid Basins.** Journal of Hydrometeorology, v. 22, n. 3, p. 601–621, 2021.

KENDALL, M.; GIBBONS, J.D. **Rank Correlation Methods.** 5th Ed. London: Edward Arnold, 1990.

KIBII, J.K.; KIPKORIR, E.C.; KOSGEI, J.R. **Application of soil and water assessment tool (SWAT) to evaluate the impact of land use and climate variability on the kaptagat catchment river discharge.** Sustainability, v. 13, n. 4, p. 1–19, 2021.

KIM, K.B.; KWON, H.H.; HAN, D. **Exploration of warm-up period in conceptual hydrological modelling.** Journal of Hydrology, v. 556, p. 194–210, 2018.

KNOBEN, W.J.M.; FREER, J.E.; WOODS, R.A. **Technical note: Inherent benchmark or not? Comparing Nash-Sutcliffe and Kling-Gupta efficiency scores.** Hydrology and Earth System Sciences, v. 23, n. 10, p. 4323–4331, 2019.

KONAPALA, G.; MISHRA, A.K.; WADA, Y.; MANN, M.E. **Climate change will affect global water availability through compounding changes in seasonal precipitation and evaporation.** Nature Communications, v. 11, n. 3044, 2020.

KUMAR, A.; GOSLING, S.N.; JOHNSON, M.F.; JONES, M.D.; ZAHERPOUR, J.; KUMAR, R.; LENG, G.; SCHMIED, H.M.; KUPZIG, J.; BREUER, L.; HANASAKI, N.; TANG, Q.; OSTBERG, S.; STACKE, T.; POKHREL, Y.; WADA, Y.; MASAKI, Y. **Multi-model evaluation of catchment- and global-scale hydrological model simulations of drought characteristics across eight large river catchments.** Advances in Water Resources, v. 165, n. 104212, 2022.

LAM, K.C.; BRYANT, R.G.; WAINRIGHT, J. **Application of spatial interpolation method for estimating the spatial variability of rainfall in Semiarid New Mexico, USA.** Mediterranean Journal of Social Sciences, v. 6, n. 4, p. 108–116, 2015.

LARABI, S.; SCHNORBUS, M.A.; ZWIERS, F. **A coupled streamflow and water temperature (VIC-RBM-CE-QUAL-W2) model for the Nechako Reservoir.** Journal of Hydrology: Regional Studies, v. 44, n. 101237, 2022.

LASAGE, R.; AERTS, J.C.J.H.; VERBURG, P.H.; SILESHI, A.S. **The Role of Small Scale Sand Dams in Securing Water Supply under Climate Change in Ethiopia.** Mitigation and Adaptation Strategies for Global Change, v. 20, p. 317–339, 2015.

LI, C.; FANG, H. **Assessment of climate change impacts on the streamflow for the Mun River in the Mekong Basin, Southeast Asia: Using SWAT model.** Catena, v. 201, n. 105199, 2021.

LIMA NETO, I. E.; MEDEIROS, P. H. A.; COSTA, A. C.; WIEGAND, M. C.; BARROS, A. R. M.; BARROS, M. U. G. **Assessment of phosphorus loading dynamics in a tropical reservoir with high seasonal water level changes.** Science of the Total Environment, v. 815, n. 152875, 2022.

LIMA NETO, I.E.; WIEGAND, M.C.; DE ARAÚJO, J.C. **Sediment redistribution due to a dense reservoir network in a large semi-arid Brazilian basin.** Hydrological Sciences Journal, v. 56, n. 2, p. 319–333, 2011.

LIMA, L.S.; SILVA, F.E.O.; ANASTÁCIO, P.R.D.; KOLANSKI, M.M. DE P.; PEREIRA, A.C.P.; MENEZES, M.S.R.; CUNHA, E.L.T.P.; MACEDO, M.N. **Severe droughts reduce river navigability and isolate communities in the Brazilian Amazon.** Communications Earth and Environment, v. 5, n. 370, p. 1–12, 2024.

LIMA, T.B.R.; MEDEIROS, P.H.A.; MAMEDE, G.L.; DE ARAÚJO, J.C. **Impact of intensive water use from farm dams on the storage dynamics in strategic reservoirs.** Hydrological Sciences Journal, v. 68, n.16, p. 2422–2434, 2023.

LIU, D. **A rational performance criterion for hydrological model.** Journal of Hydrology, v. 590, n. 125488, 2020.

LIU, R.; LUO, Y.; WANG, Q.; WANG, Y.; LIU, Y.; XIA, X.; JIANG, E. **Time-varying parameters of the hydrological simulation model under a changing environment.** Journal of Hydrology, v. 643, n. 131943, 2024.

LIU, Y.; YANG, W.; YU, Z.; LUNG, I.; YAROTSKI, J.; ELLIOTT, J.; TIESSEN, K. **Assessing Effects of Small Dams on Stream Flow and Water Quality in an Agricultural Watershed.** Journal of Hydrologic Engineering, v. 19, n. 10, 2014.

LÓPEZ-RAMÍREZ, S.M.; MAYER, A.; SÁENZ, L.; MUÑOZ-VILLERS, L.E.; HOLWERDA, F.; LOOKER, N.; SCHÜRZ, C.; BERRY, Z.C.; MANSON, R.; ASBJORNSEN, H.; KOLKA, R.; GEISSERT, D.; LEZAMA, C. **A comprehensive calibration and validation of SWAT-T using local datasets, evapotranspiration and streamflow in a tropical montane cloud forest area with permeable substrate in central Veracruz, Mexico.** Journal of Hydrology, v. 603 (A), n. 126781, 2021.

LUO, K.; TAO, F.; DENG, X.; MOIWO, J.P. **Changes in potential evapotranspiration and surface runoff in 1981-2010 and the driving factors in Upper Heihe River Basin in Northwest China.** Hydrological Processes, v. 31, n.1, p. 90–103, 2016.

MADY, B.; LEHMANN, P.; GORELICK, S.M.; OR, D. **Distribution of small seasonal reservoirs in semi-arid regions and associated evaporative losses.** Environmental Research Communications, v. 2, n. 061002, 2020.

MALLAKPOUR, I.; SADEGH, M.; AGHAKOUCHAK, A. **A new normal for streamflow in California in a warming climate: Wetter wet seasons and drier dry seasons.** Journal of Hydrology, v. 567, p. 203–211, 2018.

MALVEIRA, V.T.C.; DE ARAÚJO, J.C.; GÜNTNER, A. **Hydrological Impact of a High-Density Reservoir Network in Semiarid Northeastern Brazil.** Journal of Hydrologic Engineering, v. 17, n. 1, p. 109–117, 2012.

MAMEDE, G.L.; ARAÚJO, N.A.M.; SCHNEIDER, C.M.; DE ARAÚJO, J.C.; HERRMANN, H.J. **Overspill avalanching in a dense reservoir network.** Proceedings of the National Academy of Sciences (U.S.A.), v. 109, n. 19, p. 7191–7195, 2012.

MAMEDE, G.L.; GUENTNER, A.; MEDEIROS, P.H.A.; DE ARAÚJO, J.C.; BRONSTERT, A. **Modeling the Effect of Multiple Reservoirs on Water and Sediment Dynamics in a Semiarid Catchment in Brazil.** Journal of Hydrologic Engineering, v. 23, n. 12, 2018.

MANN, H.B. **Nonparametric Tests Against Trend.** Econometrica, v. 13, n. 245, 1945.

MAPBIOMAS. **MapBiomas General "Handbook**": Algorithm Theoretical Basis Document (ATBD). Brazil: Collection 9, v. 1, 2024. Available online at: https://brasil.mapbiomas.org/wp-content/uploads/sites/4/2024/08/ATBD-Collection-9-v2.docx.pdf. Accessed on: 10 mar. 2024.

MARAUN, D. **Bias correction, quantile mapping, and downscaling: Revisiting the inflation issue.** Journal of Climate, v. 26, n. 6, p. 2137–2143, 2013.

MARENGO, J.A.; CUNHA, A.P.; ESPINOZA, J.-C.; FU, R.; SCHÖNGART, J.; JIMENEZ, J.C.; COSTA, M.C.; RIBEIRO, J.M.; WONGCHUIG, S.; ZHAO, S. **The Drought of Amazonia in 2023-2024.** American Journal of Climate Change, v. 13, n. 3, p. 567–597, 2024.

MASSARI, C.; AVANZI, F.; BRUNO, G.; GABELLANI, S.; PENNA, D.; CAMICI, S. **Evaporation enhancement drives the European water-budget deficit during multi-year droughts.** Hydrology and Earth System Sciences, v. 26, n. 6, p. 1527–1543, 2022.

MCMAHON, T.A.; NATHAN, R.J. **Baseflow and transmission loss: A review.** Wiley Interdisciplinary Reviews Water, v. 8, n. 4, 2021.

MEDEIROS, P.H.A.; DE ARAÚJO, J.C.; MAMEDE, G.L.; CREUTZFELDT, B.; GÜNTNER, A.; BRONSTERT, A. **Connectivity of Sediment Transport in a Semiarid Environment: A Synthesis for the Upper Jaguaribe Basin, Brazil.** Journal of Soils and Sediments, v. 14, p. 1938–1948, 2014.

MELES, M.B.; GOODRICH, D.C.; UNKRICH, C.L.; GUPTA, H. V.; BURNS, I.S.; HIRPA, F.A.; RAZAVI, S.; GUERTIN, D.P. **Rainfall distributional properties control hydrologic model parameter importance.** Journal of Hydrology: Regional Studies, v. 51, n. 101662, 2024.

MENDOZA, J.A.C.; ALCAZAR, T.A.C.; MEDINA, S.A.Z. **Calibration and Uncertainty Analysis for Modelling Runoff in the Tambo River Basin, Peru, Using Sequential Uncertainty Fitting Ver-2 (SUFI-2) Algorithm.** Air, Soil and Water Research, v. 14, 2021.

MENGISTU, A.G.; VAN RENSBURG, L.D.; WOYESSA, Y.E. **Techniques for calibration and validation of SWAT model in data scarce arid and semi-arid catchments in South Africa.** Journal of Hydrology: Regional Studies, v. 25, n. 100621, 2019.

MERZ, R.; PARAJKA, J.; BLÖSCHL, G. **Time stability of catchment model parameters: Implications for climate impact analyses.** Water Resources Research, v. 47, n. 2, 2011.

MESQUITA, J.B. DE F.; LIMA NETO, I.E.; RAABE, A.; DE ARAÚJO, J.C. **The influence of hydroclimatic conditions and water quality on evaporation rates of a tropical lake.** Journal of Hydrology, v. 590, n. 125456, 2020.

MINEAR, J.T.; KONDOLF, G.M. **Estimating reservoir sedimentation rates at large spatial and temporal scales: A case study of California.** Water Resources Research, v. 45, n. 12, 2009.

MIRANDA, P. T.; PAIVA, R. C. D. D.; COLLISCHONN, W.; FAGUNDES, H. D. O.; RIBEIRO, L. D. C.; ROSSI, J. B.; FERNANDEZ, G. M. R. **Falta de sensibilidade a extremos na modelagem hidrológica.** In: Encontro Nacional de Desastres – END, III, 2023, Niterói. Anais [Eventos extremos e sociedade sob a perspectiva das mudanças climáticas]. Porto Alegre: ABRHidro, 2023.

MIRANDA, P. T.; PAIVA, R. C. D. D.; COLLISCHONN, W.; SIQUEIRA, V. A. **Limitações da modelagem hidrológica na avaliação de impactos de mudanças climáticas.** In: Simpósio Brasileiro de Recursos Hídricos – SBRH, XXV, 2023, Aracaju. Anais [Detecção e estudo da origem de variabilidade e tendências em séries hidrológicas]. Porto Alegre: ABRHidro, 2023.

MOLINA-NAVARRO, E.; HALLACK-ALEGRÍA, M.; MARTÍNEZ-PÉREZ, S.; RAMÍREZ-HERNÁNDEZ, J.; MUNGARAY-MOCTEZUMA, A.; SASTRE-MERLÍN, A. **Hydrological modeling and climate change impacts in an agricultural semiarid region. Case study: Guadalupe River basin, Mexico.** Agricultural Water Management, v. 175, p. 29–42, 2016.

MOLLE, F. **Geometria Dos Pequenos Açudes.** Recife: Superintendência do Desenvolvimento do Nordeste (SUDENE), 1994. Available online at http://horizon.documentation.ird.fr/exl-doc/pleins_textes/pleins_textes_7/divers2/010033411.pdf. Accessed on: 20 jan. 2021. (Série Hidrologia 29).

MOLLE, F. **Perdas por Evaporação e Infiltração em Pequenos Açudes**. Recife: Superintendência do Desenvolvimento do Nordeste (SUDENE), 1989. Available online at http://horizon.documentation.ird.fr/exldoc/pleins_textes/pleins_textes_7/b_fdi_03_01/33854.pdf. Accessed on: 20 jan. 2021. (Série Hidrologia 25)

MOURA, D. S.; LIMA NETO, I. E.; CLEMENTE, A.; OLIVEIRA, S.; PESTANA, C. J.; APARECIDA DE MELO, M.; CAPELO-NETO, J. **Modeling phosphorus exchange between bottom sediment and water in tropical semiarid reservoirs.** Chemosphere, v. 246, n. 125686, 2020.

NASCIMENTO, A.T.P. DO; CAVALCANTI, N.H.M.; CASTRO, B.P.L. DE; MEDEIROS, P.H.A. **Decentralized water supply by reservoir network reduces power demand for water distribution in a semi-arid basin.** Hydrological Sciences Journal, v. 64, n. 1, p. 80-91, 2019.

NASCIMENTO, F.R. **Water Management in Drylands**: Susceptibility and Risk of Desertification**.** SpringerBriefs in Latin American Studies: Global Environmental Changes, Desertification and Sustainability, 2023. p. 61–73.

NATHAN, R.; JORDAN, P.; MORDEN, R. **Assessing the impact of farm dams on streamflows, Part I: Development of simulation tools.** Australasian Journal of Water Resources, v. 9, n. 1, p. 1–12, 2015.

NATHAN, R.; LOWE, L. **The Hydrologic Impacts of Farm Dams.** Australasian Journal of Water Resources, v. 16, n. 1, p. 75-83, 2012.

NEAL, B.; NATHAN, R.J.; SCHREIDER, S.; JAKEMAN, A.J. **Identifying the Separate Impact of Farm Dams and Land Use Changes on Catchment Yield.** Australasian Journal of Water Resources, v. 5, n. 2, p. 165–176, 2002.

NEITSCH, S.L.; ARNOLD, J.G.; KINIRY, J.R.; WILLIAMS J.R. **Soil and Water Assessment Tool - Theoretical Documentation.** Texas: Texas Water Resource Institute: Grassland, Soil and Water Research Laboratory - Agricultural Research Service; Blackland Research Center - Texas AgriLife Research; Texas A&M University System, 2009. Available online at http://swat.tamu.edu/media/99192/swat2009-theory.pdf. Accessed on: 26 jan. 2019.

NGUYEN, H.H.; RECKNAGEL, F.; MEYER, W.; FRIZENSCHAF, J. **Analysing the Effects of Forest Cover and Irrigation Farm Dams on Streamflows of Water-Scarce Catchments in South Australia through the SWAT Model.** Water, v. 9, n. 33, 2017.

NGUYEN, V.; DIETRICH, J.; UNIYAL, B.; TRAN, D. **Verification and Correction of the Hydrologic Routing in the Soil and Water Assessment Tool.** Water, v. 10, n. 1419, 2018.

NOORI, N.; KALIN, L.; ISIK, S. **Water quality prediction using SWAT-ANN coupled approach.** Journal of Hydrology, v. 590, n. 125220, 2020.

OLIVEIRA, L.B.; RIBEIRO, M.R.; JACOMINE, P.K.T.; RODRIGUES, J.J.V.; MARQUES, F.A. **Funções de pedotransferência para predição da umidade retida a potenciais específicos em solos do estado de Pernambuco.** Revista Brasileira de Ciências do Solo, v. 26, n. 2, p. 315–323, 2002.

OLIVEIRA, L.C.S.; LIMA NETO, I.E. **Simulation of cascade dam break in a semiarid watershed.** Revista DAE, v.70, n. 235, p. 203-216, 2020.

OWUSU, S.; COFIE, O.; MUL, M.; BARRON, J. **The Significance of Small Reservoirs in Sustaining Agricultural Landscapes in Dry Areas of West Africa: A Review.** Water, v. 14, n. 1440, 2022.

PAREDES-BELTRAN, B.; SORDO-WARD, A.; GARROTE, L. **Dataset of Georeferenced Dams in South America (DDSA).** Earth System Science Data, v. 13, n. 2, p. 213–229, 2021.

PATHAK, S.; OJHA, C. S. P.; SHUKLA, A. K.; GARG, R. D. **Assessment of Annual Water-Balance Models for Diverse Indian Watersheds.** Journal of Sustainable Water in the Built Environment, v. 5, n. 3, 2019.

PEREIRA, B.; MEDEIROS, P.; FRANCKE, T.; RAMALHO, G.; FOERSTER, S.; DE ARAÚJO, J.C. **Assessment of the geometry and volumes of small surface water reservoirs by remote sensing in a semi-arid region with high reservoir density.** Hydrological Sciences Journal, v. 64, n. 1, p. 66–79, 2019.

PEREIRA, B.S. **Estimativa de Volumes de Reservatórios de Região Semiárida com Alta Densidade de Resevatórios por Sensoriamento Remoto.** 2017. Dissertação (Mestrado em Tecnologia e Gestão Ambiental), Instituto Federal de Educação, Ciência e Tecnologia do Ceará (IFCE), Fortaleza, 2017.

PERRIN, J.; FERRANT, S.; MASSUEL, S.; DEWANDEL, B.; MARÉCHAL, J. C.; AULONG, S.; AHMED, S. **Assessing water availability in a semi-arid watershed of southern India using a semi-distributed model.** Journal of Hydrology, v. 460–461, p. 143–155, 2012.

PETER, S.J.; DE ARAÚJO, J.C.; ARAÚJO, N.A.M.; HERRMANN, H.J. **Flood avalanches in a semiarid basin with a dense reservoir network.** Journal of Hydrology, v. 512, p. 408–420, 2014.

PETERSON, T.J.; SAFT, M.; PEEL, M.C.; JOHN, A. **Watersheds may not recover from drought.** Science, v. 372, n. 6543, p. 745–749, 2021.

PINHEIRO, F.D. **Açudagem particular em cooperação no Ceará.** Fortaleza: Departamento Nacional de Obras Contra a Seca (DNOCS), 2004. (Série conViver)

PONTES FILHO, J.D.; SOUZA FILHO, F.A.; MARTINS, E.S.P.R.; STUDART, T.M.C. **Copula-Based Multivariate Frequency Analysis of the 2012–2018 Drought in Northeast Brazil.** Water, v. 12, n. 834, 2020.

POST, D.F.; FIMBRES, A.; MATTHIAS, A.D.; SANO, E.E.; ACCIOLY, L.; BATCHILY, A.K.; FERREIRA, L.G. **Predicting Soil Albedo from Soil Color and Spectral Reflectance Data.** Soil Science Society of America Journal, v. 64, n. 3, p. 1027–1034, 2000.

PUSHPALATHA, R.; PERRIN, C.; LE MOINE, N.; ANDRÉASSIAN, V. **A review of efficiency criteria suitable for evaluating low-flow simulations.** Journal of Hydrology, v. 420–421, p. 171–182, 2012.

QADER, S.H.; DASH, J.; ALEGANA, V.A.; KHWARAHM, N.R.; TATEM, A.J.; ATKINSON, P.M. **The Role of Earth Observation in Achieving Sustainable Agricultural Production in Arid and Semi-Arid Regions of the World.** Remote Sensing, v. 13, n. 3382, 2021.

QIU, J.; SHEN, Z.; XIE, H. **Drought impacts on hydrology and water quality under climate change.** Science of the Total Environment, v. 858, n. 159854, 2023.

RABELO, U.P.; COSTA, A.C.; DIETRICH, J.; FALLAH-MEHDIPOUR, E.; VAN OEL, P.; LIMA NETO, I.E. **Impact of Dense Networks of Reservoirs on Streamflows at Dryland Catchments.** Sustainability, v. 14, n. 14117, 2022.

RABELO, U.P.; DIETRICH, J.; COSTA, A.C.; SIMSHÄUSER, M.N.; SCHOLZ, F.E.; NGUYEN, V.T.; LIMA NETO, I.E. **Representing a dense network of ponds and reservoirs in a semi-distributed dryland catchment model**. Journal of Hydrology, v. 603, n. 127103, 2021.

RIBEIRO NETO, G.G.; MELSEN, L.A.; MARTINS, E.S.P.R.; WALKER, D.W.; VAN OEL, P.R. **Drought Cycle Analysis to Evaluate the Influence of a Dense Network of Small Reservoirs on Drought Evolution.** Water Resources Research, v. 58, n. 1, 2022.

ROCHA, A.K.P.; SOUZA, L.S.B.; MONTENEGRO, A.A.A.; SOUZA, W.M.; SILVA, T.G.F. **Revisiting the application of the SWAT model in arid and semi-arid regions: a selection from 2009 to 2022.** Theoretical and Applied Climatology, v. 154, p. 7-27, 2023.

ROCHA, M. DE J. D.; LIMA NETO, I. E. **Internal phosphorus loading and its driving factors in the dry period of Brazilian semiarid reservoirs.** Journal of Environmental Management, v. 312, n. 114983, 2022.

ROCHA, M. DE J. D.; LIMA NETO, I. E. **Modeling flow-related phosphorus inputs to tropical semiarid reservoirs.** Journal of Environmental Management, v. 295, n. 113123, 2021.

ROCHA, S.M.G.; DA SILVA, J.V.B.; LEMOS, W.E.D.; SOUZA FILHO, F. DE A.; LIMA NETO, I.E. **Two-Dimensional Modelling of the Mixing Patterns in a Tropical Semiarid Reservoir.** Sustainability, v. 14, n. 16051, 2022.

ROCHA, S.M.G.; MOLINAS, E.; RODRIGUES, I.S.; LIMA NETO, I.E. **Assessment of total evaporation rates and its surface distribution by tridimensional modelling and remote sensing.** Journal of Environmental Management, v. 327, n. 116846, 2023.

RÖDIGER, T.; GEYER, S.; MALLAST, U.; MERZ, R.; KRAUSE, P.; FISCHER, C.; SIEBERT, C. **Multi-response calibration of a conceptual hydrological model in the semiarid catchment of Wadi al Arab, Jordan.** Journal of Hydrology, v. 509, p. 193–206, 2014.

RODRIGUES, I.S.; COSTA, C.A.G.; LIMA NETO, I.E.; HOPKINSON, C. **Trends of Evaporation in Brazilian Tropical Reservoirs Using Remote Sensing.** Journal of Hydrology, v. 598, n. 126473, 2021.

SAADE, J.; ATIEH, M.; GHANIMEH, S.; GOLMOHAMMADI, G. **Modeling impact of climate change on surface water availability using swat model in a semi-arid basin: Case of el Kalb river, Lebanon.** Hydrology, v. 8, n. 134, 2021.

SAFT, M.; WESTERN, A.W.; ZHANG, L.; PEEL, M.C.; POTTER, N.J. **The influence of multiyear drought on the annual rainfall-runoff relationship: An Australian perspective.** Water Resources Research, v. 51, n. 4, p. 2444–2463, 2016.

SALEHI, M. **Global water shortage and potable water safety; Today's concern and tomorrow's crisis.** Environment International, v. 158, n. 106936, 2022.

SALIMI, H.; ASADI, E.; DARBANDI, S. **Meteorological and hydrological drought monitoring using several drought indices.** Applied Water Science, v. 11, n. 11, p. 1–10, 2021.

SAMIMI, M.; MIRCHI, A.; MORIASI, D.; AHN, S.; ALIAN, S.; TAGHVAEIAN, S.; SHENG, Z. **Modeling arid/semi-arid irrigated agricultural watersheds with SWAT: Applications, challenges, and solution strategies.** Journal of Hydrology, v. 590, n. 125418, 2020.

SANTOS, C.; ALMEIDA, C.; RAMOS, T.; ROCHA, F.; OLIVEIRA, R.; NEVES, R. **Using a Hierarchical Approach to Calibrate SWAT and Predict the Semi-Arid Hydrologic Regime of Northeastern Brazil.** Water , v.10, n. 1137, 2018a.

SANTOS, L.; THIREL, G.; PERRIN, C. **Technical note: Pitfalls in using log-transformed flows within the KGE criterion.** Hydrology and Earth System Sciences, v. 22, n. 8, p. 4583–4591, 2018b.

SCHOLZ, F. E. **Influence of Reservoirs and Transmission Losses on the Hydrological Modelling of the Semi-arid Jaguaribe River Basin, Brazil.** 2015. Thesis (Master in Water Resources and Environmental Management), Leibniz University of Hannover (LUH), Hannover, 2015.

SCHREIDER, S.Y.; JAKEMAN, A.J.; LETCHER, R.A.; NATHAN, R.J.; NEAL, B.P.; BEAVIS, S.G. **Detecting changes in streamflow response to changes in non-climatic catchment conditions: Farm dam development in the Murray-Darling basin, Australia.** Journal of.Hydrology, v. 262, n. 1-4, p. 84–98, 2002.

SEN, P.K. **Estimates of the Regression Coefficient Based on Kendall's Tau.** Journal of the American Statistical Association, v. 63, n. 324, p. 1379–1389, 1968.

SERRÃO, E.A.O.; SILVA, M.T.; FERREIRA, T.R.; PAIVA DE ATAIDE, L.C.; ASSIS DOS SANTOS, C.; MEIGUINS DE LIMA, A.M.; DE PAULO RODRIGUES DA SILVA, V.; DE ASSIS SALVIANO DE SOUSA, F.; CARDOSO GOMES, D.J. **Impacts of land use and land cover changes on hydrological processes and sediment yield determined using the SWAT model.** International Journal of Sediment Research, v. 37, n. 1, p. 54–69, 2022.

SHAABANI, M.K.; ABEDI-KOUPAI, J.; ESLAMIAN, S.S.; GOHARI, S.A.R. **Simulation of the effects of climate change, crop pattern change, and developing irrigation systems on the groundwater resources by SWAT, WEAP and MODFLOW models: a case study of Fars province, Iran.** Environment, Development and Sustainability, v. 26, p. 10485–10511, 2024.

SHI, H.; ZHAO, Y.; LIU, S.; CAI, H.; ZHOU, Z. **A New Perspective on Drought Propagation: Causality.** Geophysical Research Letters, v. 49, n. 2, 2022.

SHUKLA, A. K.; OJHA, C. S. P.; GARG, R. D.; SHUKLA, S.; PAL, L. **Influence of Spatial Urbanization on Hydrological Components of the Upper Ganga River Basin, India.** Journal of Hazardous, Toxic, and Radioactive Waste, v. 24, n. 4, 2020.

SIMSHÄUSER, M. N. **Modelling of Small Reservoirs in the Semi-arid Jaguaribe River Basin, Brazil**. 2018. Thesis (Master in Water Resources and Environmental Management). Leibniz University of Hannover, Hannover, 2018.

SILVA, F.J.A., ARAÚJO, A.L., SOUZA, R.O. **Águas subterrâneas no Ceará - poços instalados e salinidade.** Revista Tecnologia (UNIFOR), v. 28, n.2, p. 136–159, 2007.

SIMMERS, I. **Understanding water in a dry environment. Hydrological processes in arid and semi-arid zones.** IAH - International Contributions to Hydrogeology, v. 23, London: A.A. Balkema Publisher, 2003.

SIQUEIRA, M.S.; DE ALCÂNTARA, H.M.; RIBEIRO, G.N.; MEDEIROS, P.C.; AFONSO, J.P.S.D.; DE MEDEIROS, A.C.; MARACAJÁ, P.B. **Influence of the scale effect on the sediment yield in not instrumented basins in the semiarid zone.** Revista Brasileira de Gestão Ambiental, v. 11, n. 1, p. 99–105, 2016.

SONG, Y.H.; CHUNG, E.S.; SHAHID, S. **Differences in extremes and uncertainties in future runoff simulations using SWAT and LSTM for SSP scenarios.** Science of the Total Environment, v. 838, n. 156162, 2022.

STAVI, I.; PASCHALIDOU, A.; KYRIAZOPOULOS, A.P.; HALBAC-COTOARA-ZAMFIR, R.; SIAD, S.M.; SUSKA-MALAWSKA, M.; SAVIC, D.; DE PINHO, J.R.; THALHEIMER, L.; WILLIAMS, D.S.; HASHIMSHONY-YAFFE, N.; VAN DER GEEST, K.; CORDOVIL, C.M.D.S.; FICKO, A. **Multidimensional food security nexus in drylands under the slow onset effects of climate change.** Land, v. 10, n. 1350, 2021.

SUKHBAATAR, C.; SAJJAD, R.U.; LUNTEN, J.; YU, S.-H.; LEE, C.-H. **Climate Change Impact on the Tuul River Flow in a Semiarid Region in Mongolia.** Water Environment Research, v. 89, n. 6, p. 527–538, 2017.

SUN, C.; FENG, X.; FU, B.; MA, S. **Desertification vulnerability under accelerated dryland expansion.** Land Degradation and Development, v. 34, n. 7, p. 1991–2004, 2022.

SUN, L.; YANG, L.; HAO, L.; FANG, D.; JIN, K.; HUANG, X. **Hydrological Effects of Vegetation Cover Degradation and Environmental Implications in a Semiarid Temperate Steppe, China.** Sustainability, v. 9, n. 281, 2017.

TAN, M.L.; GASSMAN, P.W.; YANG, X.; HAYWOOD, J. **A review of SWAT applications, performance and future needs for simulation of hydro-climatic extremes.** Advances in Water Resources, v. 43, n. 103662, 2020.

THOMPSON, J.C. **Impact and Management of Small Farm Dams in Hawke's Bay, New Zealand.** 2012. Thesis (Doctor of Philosophy in Physical Geography), Victoria University of Wellington, New-Zealand, 2012.

TIAN, W.; LIU, X.; LIU, C.; BAI, P. **Investigation and simulations of changes in the relationship of precipitation-runoff in drought years.** Journal of Hydrology, v. 565, p. 95–105, 2018.

TOMASELLA, J.; HODNETT, M.G. **Estimating unsaturated hydraulic conductivity of Brazilian soils using soil-water retention data.** Soil Science, v. 162, n. 10, p. 703-712, 1997.

TROTTER, L.; SAFT, M.; PEEL, M.C.; FOWLER, K.J.A. **'"Naïve" Inclusion of Diverse Climates in Calibration Is Not Sufficient to Improve Model Reliability under Future Climate Uncertainty'.** In: International Congress on Modelling and Simulation, 24th, 2021, Sydney. Proceedings [Modelling for action with a flood of data and a cloud of uncertainty]. Sydney, 2021. p. 588-594.

TROTTER, L.; SAFT, M.; PEEL, M.C.; FOWLER, K.J.A. **Symptoms of Performance Degradation During Multi-Annual Drought: A Large-Sample, Multi-Model Study.** Water Resources Research, v. 59, n. 2, 2023.

TZANAKAKIS, V.A.; PARANYCHIANAKIS, N. V.; ANGELAKIS, A.N. **Water supply and water scarcity.** Water, v. 12, n. 2347, 2020.

UNIYAL, B.; DIETRICH, J.; VU, N.Q.; JHA, M.K.; ARUMÍ, J.L. **Simulation of regional irrigation requirement with SWAT in different agro-climatic zones driven by observed climate and two reanalysis datasets.** Science of the Total Environment, v. 649, p. 846–865, 2019.

VAN LANGEN, S.C.H.; COSTA, A.C.; RIBEIRO NETO, G.G.; VAN OEL, P.R. **Effect of a reservoir network on drought propagation in a semi-arid catchment in Brazil.** Hydrological Sciences Journal, v. 66, n. 10, p. 1567–1583, 2021.

VAN LOON, A.F.; RANGECROFT, S.; COXON, G.; WERNER, M.; WANDERS, N.; DI BALDASSARRE, G.; TIJDEMAN, E.; BOSMAN, M.; GLEESON, T.; NAUDITT, A.; AGHAKOUCHAK, A.; BREÑA-NARANJO, J.A.; CENOBIO-CRUZ, O.; COSTA, A.C.; FENDEKOVA, M.; JEWITT, G.; KINGSTON, D.G.; LOFT, J.; MAGER, S.M.; VAN LANEN, H.A.J. **Streamflow droughts aggravated by human activities despite management.** Environment Research Letters, v. 17, n. 4, 2022.

VAN OEL, P.R.; MARTINS, E.S.P.R.; COSTA, A.C.; WANDERS, N.; VAN LANEN, H.A.J. **Diagnosing Drought Using the Downstreamness Concept: The Effect of Reservoir Networks on Drought Evolution.** Hydrological Sciences Journal, v. 63, n. 7, p. 979–990, 2018.

VAZE, J.; POST, D.A.; CHIEW, F.H.S.; PERRAUD, J.M.; VINEY, N.R.; TENG, J. **Climate non-stationarity – Validity of calibrated rainfall–runoff models for use in climate change studies.** Journal of Hydrology, v. 394, n. 3-4, p. 447–457, 2010.

VICENTE-SERRANO, S. M.; ZABALZA-MARTÍNEZ, J.; BORRÀS, G.; LÓPEZ-MORENO, J. I.; PLA, E.; PASCUAL, D.; SAVÉ, R.; BIEL, C.; FUNES, I.; AZORIN-MOLINA, C.; SANCHEZ-LORENZO, A.; MARTÍN-HERNÁNDEZ, N.; PEÑA-GALLARDO, M.; ALONSO-GONZÁLEZ, E.; TOMAS-BURGUERA, M.; EL KENAWY, A. **Extreme hydrological events and the influence of reservoirs in a highly regulated river basin of northeastern Spain.** Journal of Hydrology: Regional Studies, v. 12, p. 13–32, 2017.

WADA, Y.; BIERKENS, M.F.P.; DE ROO, A.; DIRMEYER, P.A.; FAMIGLIETTI, J.S.; HANASAKI, N.; KONAR, M.; LIU, J.; SCHMIED, H.M.; OKI, T.; POKHREL, Y.; SIVAPALAN, M.; TROY, T.J.; VAN DIJK, A.I.J.M.; VAN EMMERIK, T.; VAN HUIJGEVOORT, M.H.J.; VAN LANEN, H.A.J.; VÖRÖSMARTY, C.J.; WANDERS, N.; WHEATER, H. **Human-water interface in hydrological modelling: Current status and future directions.** Hydrology and Earth System Sciences, v. 21, n. 8, p. 4169–4193, 2017.

WANG, H.; LIU, Y.; WANG, Y.; YAO, Y.; WANG, C. **Land cover change in global drylands: A review.** Science of the Total Environment, v. 863, n. 160943, 2023.

WANG, Y.; WANG, J.; ZHANG, Q. **Analysis of ecological drought risk characteristics and leading factors in the Yellow River Basin.** Theoretical and Applied Climatology, v. 155, p. 1739–1757, 2024.

WEB OF SCIENCE. **Main Collection (Clarivate Analytics / Thomson Reuters).** Available through Coordination of Superior Level Staff Improvement (CAPES) Journals Portal, 2025.

WORLD METEOROLOGICAL ORGANIZATION. **The Global Climate 2011-2020. A decade of accelerating climate change.** WMO-No. 1338, 2023.

WU, J.; CHEN, X.; YAO, H.; ZHANG, D. **Multi-timescale assessment of propagation thresholds from meteorological to hydrological drought.** Science of the Total Environment, v. 765, n. 144232, 2021.

WU, J.; YAO, H.; CHEN, X.; WANG, G.; BAI, X.; ZHANG, D. **A framework for assessing compound drought events from a drought propagation perspective.** Journal of Hydrology, v. 604, n. 127228, 2022.

WUNDERLING, N.; STAAL, A.; SAKSCHEWSKI, B.; HIROTA, M.; TUINENBURG, O.A.; DONGES, J.F.; BARBOSA, H.M.J.; WINKELMANN, R. **Recurrent droughts increase risk of cascading tipping events by outpacing adaptive capacities in the Amazon rainforest.** Proceedings of the National Academy of Sciences (U.S.A.), v. 119, n. 32, 2022.

XAVIER, A.C.; SCANLON, B.R.; KING, C.W.; ALVES, A.I. **New improved Brazilian daily weather gridded data (1961–2020).** International Journal of Climatology, v. 42, n. 16, p. 8390–8404, 2022.

XU, D.; ZHANG, Q.; DING, Y.; ZHANG, D. **Application of a hybrid ARIMA-LSTM model based on the SPEI for drought forecasting.** Environmental Science and Pollution Research, v. 29, p. 4128–4144, 2022.

YAEGER, M.A.; REBA, M.L.; MASSEY, J.H.; ADVIENTO-BORBE, M.A.A. **On-Farm Irrigation Reservoirs in Two Arkansas Critical Groundwater Regions: A Comparative Inventory.** Applied Engineering in Agriculture, v. 33, n. 6, p. 869–878, 2017.

YAO, J.; LIU, H.; HUANG, J.; GAO, Z.; WANG, G.; LI, D.; YU, H.; CHEN, X. **Accelerated dryland expansion regulates future variability in dryland gross primary production.** Nature Communications, v. 11, n. 1665, 2020.

YUE, S.; WANG, C.Y. **The Mann-Kendall test modified by effective sample size to detect trend in serially correlated hydrological series.** Water Resources Management, v. 18, p. 201–218, 2004.

ZAHABIYOUN, B.; GOODARZI, M.R.; BAVANI, A.R.M.; AZAMATHULLA, H.M. **Assessment of Climate Change Impact on the Gharesou River Basin Using SWAT Hydrological Model.** Clean - Soil, Air, Water, v. 41, n. 6, p. 601–609, 2013.

ZETTAM, A.; TALEB, A.; SAUVAGE, S.; BOITHIAS, L.; BELAIDI, N.; SÁNCHEZ-PÉREZ, J. **Modelling Hydrology and Sediment Transport in a Semi-Arid and Anthropized Catchment Using the SWAT Model: The Case of the Tafna River (Northwest Algeria).** Water, v. 9, n. 216, 2017.

ZHANG, C.; PENG, Y.; CHU, J.; SHOEMAKER, C.A.; ZHANG, A. **Integrated hydrological modelling of small-and medium-sized water storages with application to the upper fengman reservoir basin of China.** Hydrology and Earth System Sciences, v. 16, n. 11, p. 4033–4047, 2012.

ZHANG, H.; WANG, B.; LIU, D.L.; ZHANG, M.; LESLIE, L.M.; YU, Q. **Using an improved SWAT model to simulate hydrological responses to land use change: A case study of a catchment in tropical Australia.** Journal of Hydrology, v. 585, n. 124822, 2020b.

ZHANG, R.; LIU, J.; GAO, H.; MAO, G. **Can multi-objective calibration of streamflow guarantee better hydrological model accuracy?** Journal of Hydroinformatics, v. 20, n. 3, p. 687–698, 2018.

ZHANG, S.; FOERSTER, S.; MEDEIROS, P.; DE ARAÚJO, J.C.; MOTAGH, M.; WASKE, B. **Bathymetric survey of water reservoirs in north-eastern Brazil based on TanDEM-X satellite data.** Science of the Total Environment, v. 571, p. 575–593, 2016.

ZHANG, X.; HAO, Z.; SINGH, V.P.; ZHANG, Y.; FENG, S.; XU, Y.; HAO, F. **Drought propagation under global warming: Characteristics, approaches, processes, and controlling factors.** Science of the Total Environment, v. 838, n. 156021, 2022.

ZHANG, X.; LIU, P.; CHENG, L.; ZHOU, L.; LIU, W.; LUO, X. **Time-varying parameters from the same period in previous years to improve runoff forecasting.** Journal of Hydrology, v. 631, n. 130685, 2024.

ZHANG, X.; XU, Y.P.; FU, G. **Uncertainties in SWAT extreme flow simulation under climate change.** Journal of Hydrology, v. 515, p. 205–222, 2014.

ZHANG, Z.; LIU, J.; HUANG, J. **Hydrologic impacts of cascade dams in a small headwater watershed under climate variability.** Journal of Hydrology, v. 590, n. 125426, 2020a.

ZHOU, Z.; SHI, H.; FU, Q.; DING, Y.; LI, T.; WANG, Y.; LIU, S. **Characteristics of Propagation From Meteorological Drought to Hydrological Drought in the Pearl River Basin.** Journal of Geophysical Research: Atmospheres, v. 126, n. 4, 2021.

APPENDIX A – CLIMATE DATA FOR MODELING

Precipitation data

In comparison with other semi-arid regions (also in Brazil), the density of rain gauges in Ceará may be considered relatively high (1 rain gauge to 250 km). In total, there are 44 rainfall gauges, mainly from FUNCEME, located inside and in the immediate vicinity of the study catchment (Figure S.1). Spatially and temporally, the gauges were not evenly distributed. In the more urbanized parts and around the large reservoir Poço da Pedra, gauge density is rather high, while the rural areas are hardly gauged. Regarding temporal records, the data is more complete for more recent times (much more complete from 2000 on), i.e., for these periods gauge density is higher as well.

Other meteorological forcings

When the Penman-Monteith-Method is selected for the calculation of evapotranspiration in SWAT as the case here, the required meteorological input data include maximum, minimum and mean temperatures, mean wind velocity, total daily solar radiation and mean relative humidity. However, the density of meteorological stations is much smaller than that of the rain gauges. Only one meteorological station is located inside the catchment (in Campos Sales). Therefore, the five closest surrounding stations (distances from the stations to the borders of the catchment are in the range of approximately 70 to 110 km) were also taken into account (Figure S.1). Additionally, a record with sub-daily measurements from an automatic station in Campos Sales (at a different location than the conventional station) was acquired. Meteorological data was taken from the Brazilian National Institute of Meteorology (INMET).

All time series of the conventional stations started before the year of 1979 and ended in 2015. However, they all presented large continuous gaps of several years within the period of 1981 until 1994, so that for a certain time span (from 1986 until 1989) no meteorological data was available for any station. The automatic stations started recording only in 2009. In order to complement those time series, weather data from the Climate Forecast System Reanalysis (CFSR) conducted by the National Centers for Environmental Predictions (NCEP) was used. The CFSR weather data was downloaded from the website for global weather data

of SWAT (https://globalweather.tamu.edu/) for one raster point only, the one closest to the climatic stations at Campos Sales situated inside the catchment (distance both to the conventional and the automatic station ca. 8 km) (Figure A.1). Then, the CFSR records were checked against the ground measurements to identify potential biases of the data. Only relative humidity showed considerable differences (about 20 % on average). The bias correction method used in this case was the so-called non-parametric quantile mapping (Maraun 2013; Gudmundsson et al. 2012).

Figure A.1 - Distribution of all 44 included rain gauges and meteorological stations located in and around the study catchment.

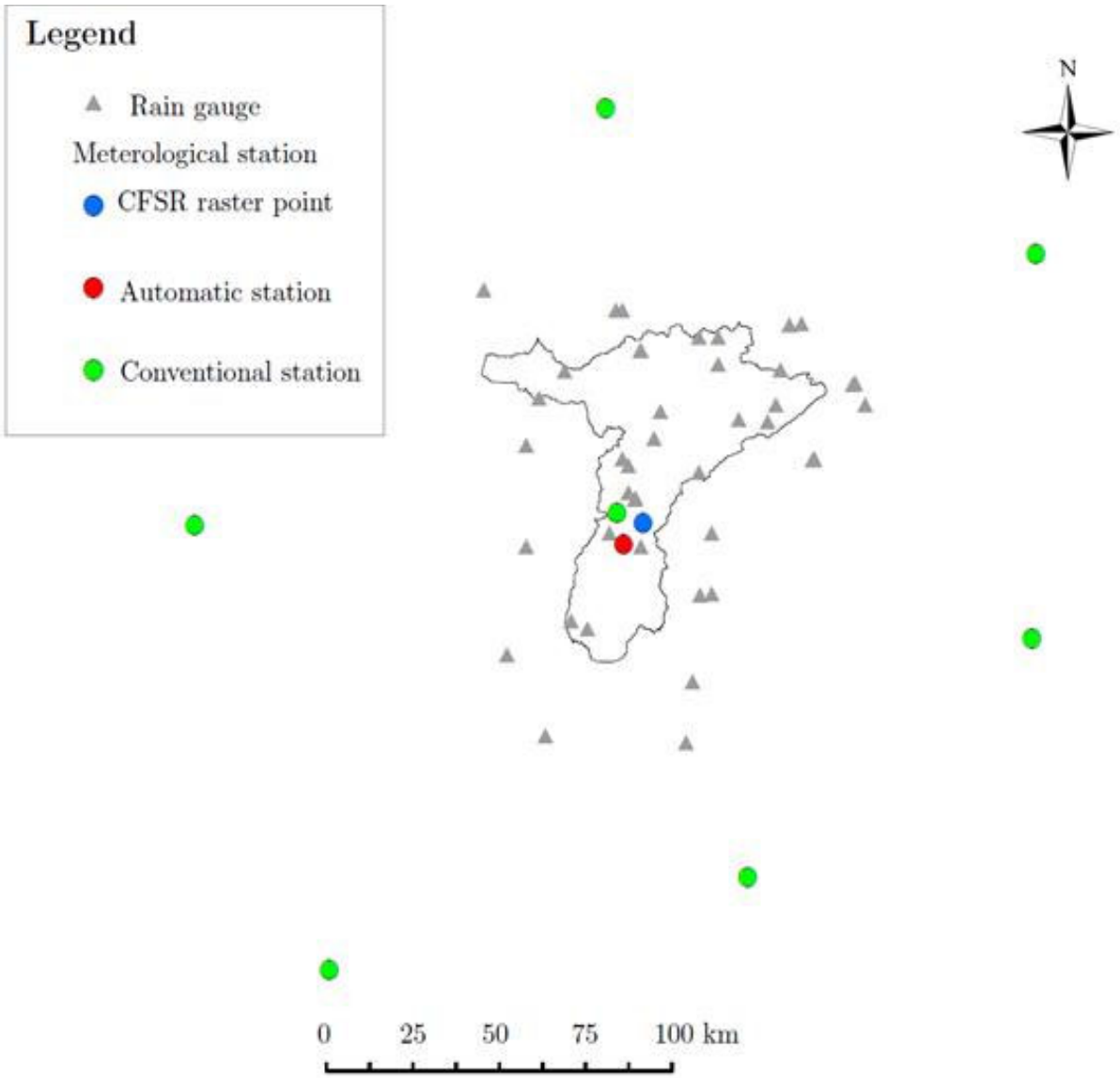

Source: The author

Interpolation

The watershed delineation subdivides the main catchment into numerous sub-basins, which require daily climatic input variables. Therefore, these variables were estimated through interpolation of the measured data obtained from rain gauges and meteorological stations, taking the centroids of the sub-basins as reference points. The inverse distant weighing method was used for the spatial interpolation. It is commonly applied in scientific research and hydrological modelling to interpolate rainfall distributions, having proved to produce good results even in a semi-arid environment (Lam et al. 2015). Figure A.2 shows the average monthly precipitation and the average monthly potential evapotranspiration in the study catchment and Figure A.3 shows the average annual precipitation and the average annual potential evapotranspiration in study catchment.

Figure A.2 - Average monthly precipitation and average monthly potential evapotranspiration in study catchment. Results provided by measured series for 1979 to 2010 that represent simulation period.

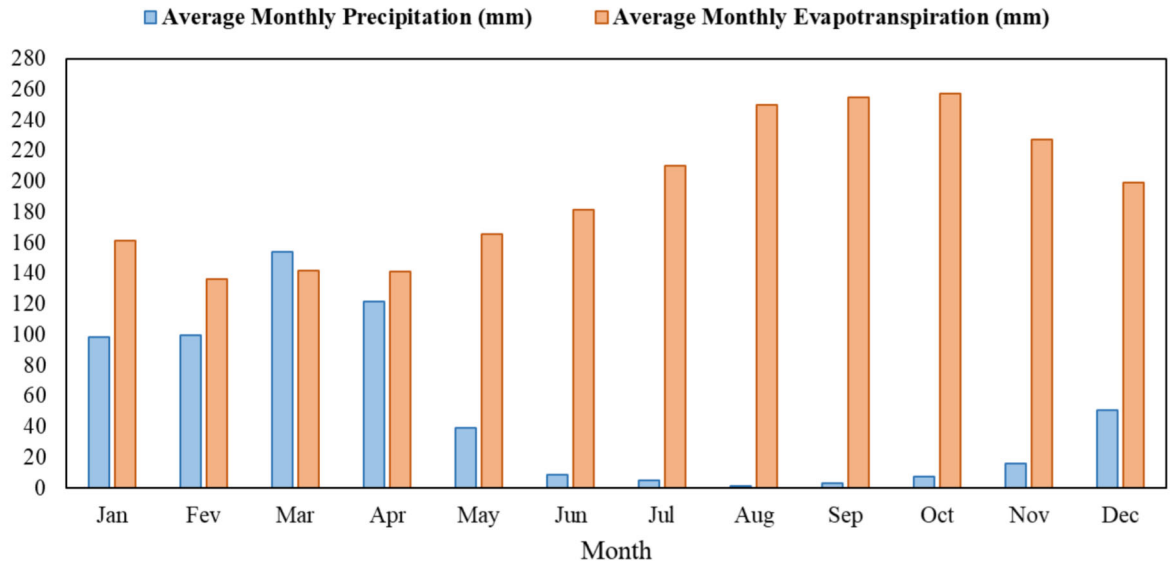

Source: The author

Figure A.3 - Average annual precipitation and average annual potential evapotranspiration in study catchment. Results provided by measured series for 1979 to 2010 that represent simulation period.

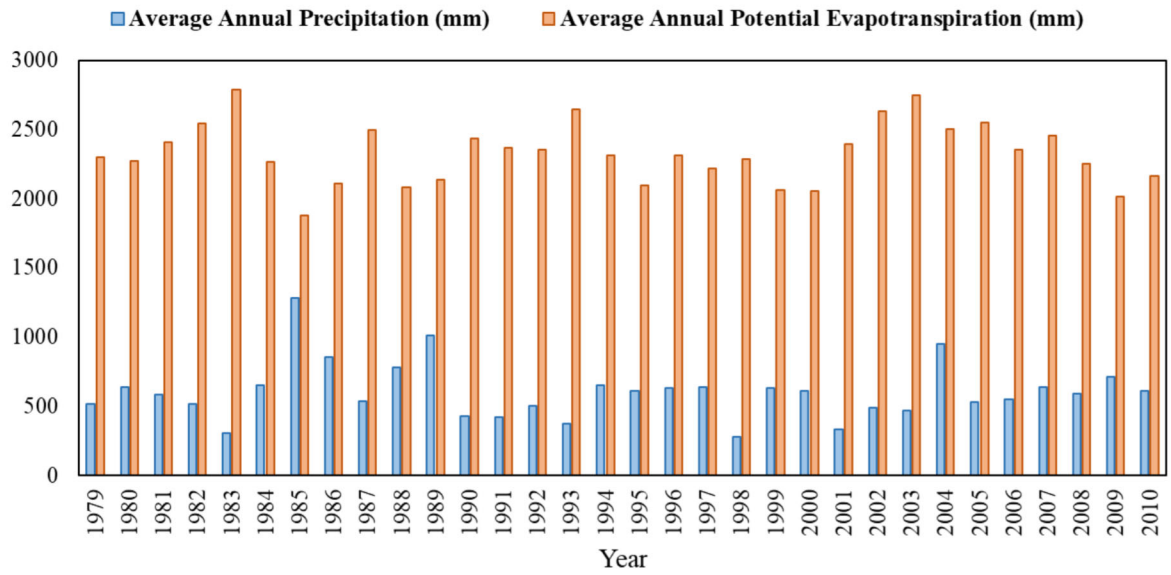

Source: The author

APPENDIX B - SOIL AND LAND USE PARAMETERIZATION FOR MODELING

The soil map was provided as a polygon shapefile encompassing 109 soil association classes for the whole Jaguaribe River basin and adapted for the Conceição River catchment (Figure B.1) according to the soil classification of Jacomine et al. (1973), which also showed consistency with the coarser soil map of FAO.

Parameters were generated for each soil class according to profiles. Some parameters could be directly taken from Jacomine et al. (1973), such as: a) Number of soil layers in soil profile; b) Depth of soil layers; c) Percentage of silt in soil layers; d) Percentage of clay in soil layers; and e) Organic carbon content in soil layers. In contrast, the missing parameters listed below (items “q” to “y”) had to be indirectly generated by means of pedo-transfer functions and other soil characteristics from Jacomine et al. (1973), such as: f) Percentage of gravel of soil layer; g) Percentage of stones of soil layer; h) Percentage of Coarse Sand of soil layer; i) Percentage of Fine Sand of soil layer; j) Value of Munsell colour system of moist soil of soil layer; k) Humidity equivalent; l) Texture of soil layer; m) Drainage capacity of soil profile; n) CA++; o) Mg++; and p) K++.

q) Maximum rooting depth of soil profile

The soil survey cited the quantity of roots in the soil layers using the words “abundant”, “many”, “some”, “a few” and “rare”. The maximum considered rooting depth was the one above the profile where above roots were rarely found. In the cases where all soil layers had roots, the total depth of soil profile was attributed to maximum soil rooting depth.

r) Percentage of sand in soil layers

The percentage of sand was calculated by the sum of fine and coarse sand. The Brazilian soil particle size classification of soils slightly differs from the American classification in terms of grain size. However, this difference was neglected.

s) Percentage of rock in soil layers

The percentage of rock was calculated by the sum of gravels and stones. Again, the difference between the Brazilian and the American grain size classification was neglected.

t) Moist soil albedo of soil layer

The colour of each soil layer was recorded for wet and dry conditions according to the Munsell colour system. It is possible to predict the soil albedo from the value dimension of the Munsell colour system. The following pedo-transfer function is a result of a linear regression and has a coefficient of determination of 0.93 reported by Post et al. (2000) and is given as follows:

$$Y = -0.11 + 0.07X \quad \text{(B.1)}$$

Y = soil albedo
X = value dimension of the Munsell colour system of wet soil

u) Moist bulk density of soil layer

The moist bulk density was calculated in two steps. First, the bulk density was calculated according to a pedo-transfer function. This function results from a regression model with a coefficient of determination of 0.66 and a standard error of the mean of 0.11 (Benites et al., 2006), given as follows:

$$Bd = 1.56 - 0.0005Cl - 0.01COT - 0.0075SB \quad \text{(B.2)}$$

Bd = bulk density (g/cm^3)
Cl = clay content (%)
COT = organic carbon content (g/kg)
SB = sum of bases (cmol/kg)

$$SB = CA + MG + K \quad \text{(B.3)}$$

CA = CA2+ content (cmol/kg)

MG = Mg2+ content (cmol/kg)

K = K+ content (cmol/kg)

Afterwards, the moist bulk density was calculated as follows:

$$Bdm = Bd + \frac{Eqh}{100} \quad \text{(B.4)}$$

Bdm = moist bulk density (g/cm^3)

Bd = bulk density (g/cm^3)

Eqh = humidity equivalent (%)

v) Available water capacity of soil layer

The available water capacity was calculated using the pedotransfer function reported by Oliveira et al. (2002). This function is the result of a regression model and has a coefficient of determination of 0.89 and a standard error of the mean of 0.0244.

$$AWCo = 0.000021Sa + 0.000203Si + 0.000054Cl - 0.021656Bd \quad \text{(B.5)}$$

$AWCo$ = available water capacity in (kg/kg)

Sa = sand content (g/kg)

Si = silt content (g/kg)

Cl = clay content (g/kg)

Bd = bulk density (g/cm^3)

$$AWC = AWCo \cdot Bd \quad \text{(B.6)}$$

AWC = available water capacity in (mm of water/mm)

w) Saturated hydraulic conductivity of soil layer

The saturated hydraulic conductivity was calculated using the pedo-transfer function reported by Tomasella and Hodnett (1997). The function is a regression model with a coefficient of determination of 0.903:

$$Ksat = 56540 \emptyset e^{4.5359} \quad \text{(B.7)}$$

Ksat = saturated hydraulic conductivity (mm/h)

$\emptyset e$ = effective porosity (%)

For Latossol Amarelo soil, the equation differs from other soil due to its particular behaviour. For this soil, the regression model has a coefficient of determination of 0.915:

$$Ksat = 29158 \emptyset e^{2.4734} \quad \text{(B.8)}$$

The effective porosity was assumed to be the same as the normal porosity, neglecting the clay-bound water in the soil:

$$\emptyset e = 1 - \frac{Bd}{Pb} \quad \text{(B.9)}$$

Bd = bulk density (g/cm^3)

Pb = particle density (2.65 g/cm^3)

x) Soil hydrologic group

In the soil survey, the soil drainage capacity was classified into 8 classes, which could be related to the four hydrologic groups: A (Excessively, strongly or pronouncedly drained), B (Well drained), C (Moderately drained) and D (Imperfectly, badly or very badly drained).

y) USLE equation soil erodibility (k) factor

The USLE equation soil erodibility (k) factor was calculated as the mean of the resulting values according to two different methods: the Wischmeier Method and the Smith and Williams Method (Arnold, et al., 2012).

Figure B.1 Soil map for Conceição river catchment. The soil classification in 5 soil types was generated according to the Ceará Soil Survey made and reported by Jacomine et al. (1973)

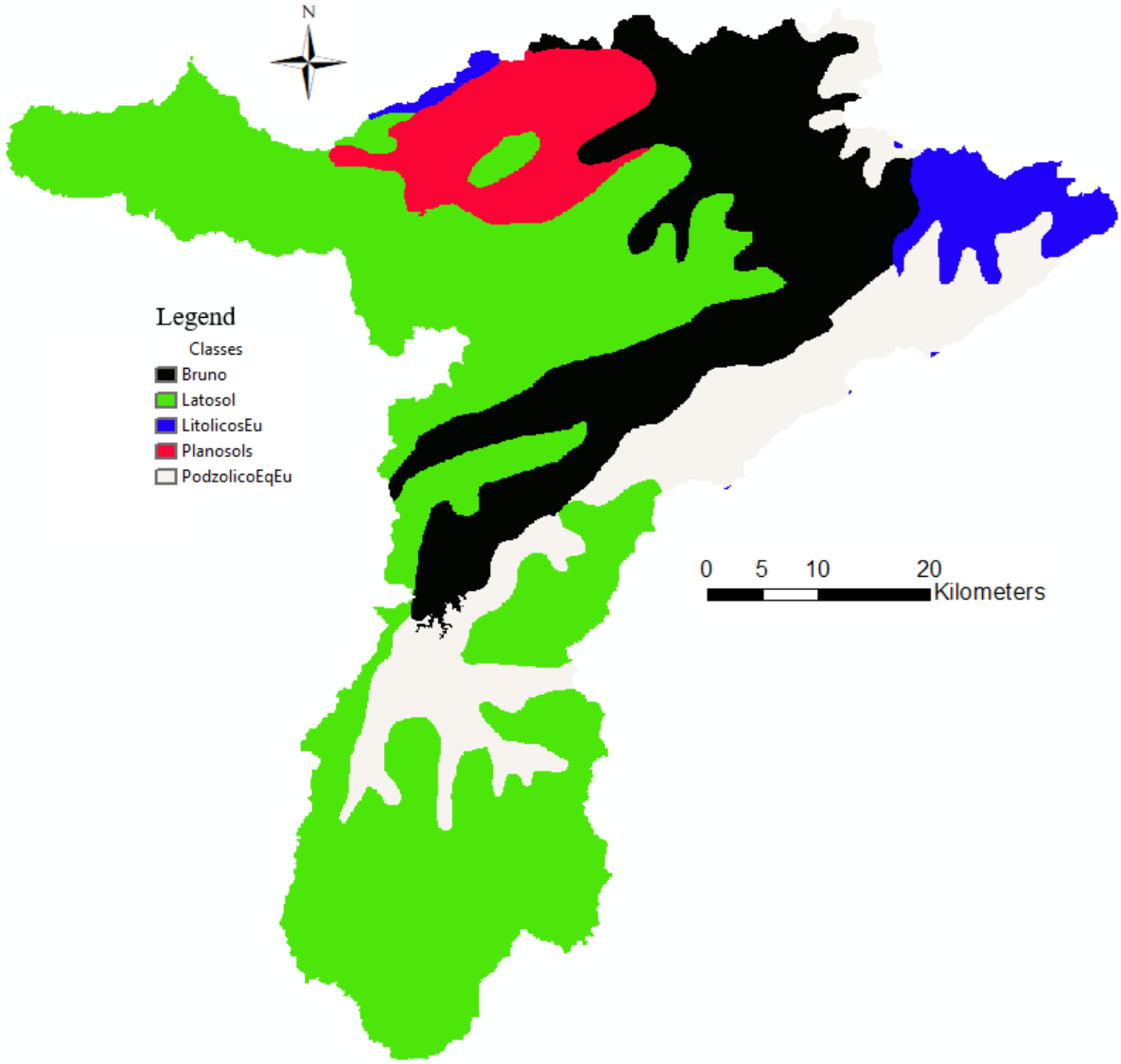

Source: Adapted by Scholz (2015)

The land use map was reclassified according to the default land use dataset integrated in SWAT and is presented in Table B.1 and in Figure B.2.

Table B.1 – Reclassification of land use dataset integrate in SWAT for Conceição river catchment

Old Classification	**New Classification**					
Given Land Use Data	**Code**	**SWAT Land Use Data**				
Water	WATR	Water				
Urban Area	URHD	Residential-High Density				
Maize/Beans	COBE	Corn	Pinto Beans			
Maize/Beans/Rice/Banana/Cashews	CBRC	Corn	Pinto Beans	Rice	Banana	Cashew
Grassland with Trees	RNGE	Range Grasses				
Open Tree Caatinga	RNGB	Range Brush				
Pasture	PAST	Pasture				
Transition Shrub Caatinga-Open Tree Caatinga	RNGB	Range Brush				

Source: The author

Figure B.2 Land use map for Conceição river catchment. The land use classification in 7 types was generated according to FUNCEME database

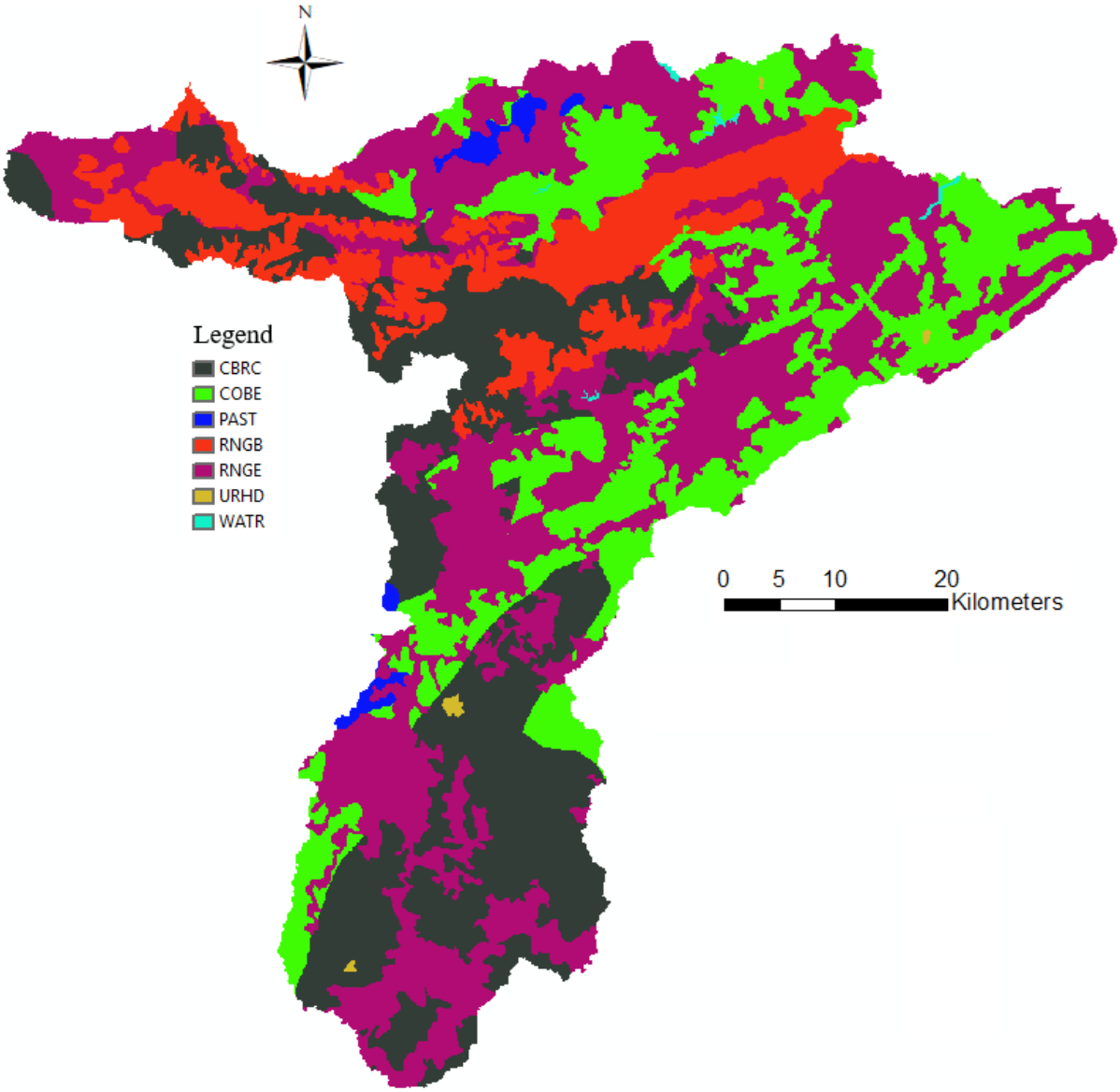

Source: Adapted by Scholz (2015)

APPENDIX C - ANNUAL STREAMFLOW AT MALHADA STATION FOR EACH INCREASE IN THE NUMBER OF SMALL RESERVOIRS PER YEAR OF SIMULATION

Table C.1 - Annual streamflow in m³/s at Malhada Station for each increase in the number of small reservoirs per year of simulation

Annual Streamflow [m³/s]										
Year	**Observed by COGERH**	**Reference model**	**Simulation models - Small reservoirs per area of catchment**							
			0.1/km²	**0.25/km²**	**0.5/km²**	**0.75/km²**	**1.0/km²**	**1.5/km²**	**2.0/km²**	**3.0/km²**
1981	699.5	1828.8	1820.8	1786.5	1739.5	1712.3	1689.0	1661.9	1638.2	1604.6
1982	204.9	275.9	274.1	268.5	261.0	256.7	253.0	248.0	244.0	237.8
1983	11.9	41.6	40.9	39.0	37.3	36.4	35.7	34.5	33.6	32.6
1984	951.3	507.1	504.6	496.3	486.1	479.2	472.7	463.7	456.0	445.9
1985	5905.2	4303.6	4295.6	4257.2	4200.7	4155.6	4113.5	4052.6	3990.6	3897.3
1986	1791.5	1771.4	1765.4	1753.3	1741.2	1730.4	1722.8	1707.4	1694.4	1673.2
1987	699.8	571.4	570.6	564.4	558.2	552.5	548.5	540.2	533.8	524.6
1988	839.4	680.8	677.8	666.8	655.3	648.1	640.9	623.5	612.8	598.1
1989	3373.2	1830.7	1827.1	1811.3	1793.7	1783.0	1772.3	1756.2	1736.2	1708.3
1990	236.2	209.9	209.3	207.6	205.2	203.8	202.3	199.5	197.7	194.9
1991	52.5	8.1	7.9	7.7	7.6	7.5	7.4	7.3	7.2	7.1
1992	347.7	560.3	557.3	547.8	536.0	527.4	521.4	512.8	505.8	493.3
1993	1.3	11.7	11.3	10.7	10.5	10.3	10.2	10.0	9.9	9.8
1994	73.3	154.4	152.8	149.3	145.7	142.2	139.2	136.8	133.0	128.8
1995	816.0	478.8	476.1	467.8	458.6	451.4	445.1	436.6	429.5	419.4
1996	97.1	175.9	174.9	170.8	166.5	163.2	160.2	156.6	153.9	148.5
1997	1219.2	486.0	483.5	473.1	461.5	453.5	448.1	439.8	431.6	418.0
1998	21.7	16.7	16.4	15.3	14.3	13.7	13.3	12.7	12.3	11.7
1999	115.1	154.3	153.2	148.2	140.6	134.3	130.0	124.8	122.1	118.1
2000	240.4	316.8	314.4	307.5	299.9	294.0	289.9	282.3	275.5	265.4
2001	0.0	7.0	7.0	6.9	6.9	6.8	6.8	6.7	6.7	6.6
2002	288.4	369.7	367.7	360.2	351.2	346.4	341.0	333.6	327.7	321.1
2003	109.1	131.5	130.2	125.8	120.5	117.2	115.5	112.2	110.2	107.1
2004	3741.3	4157.2	4147.6	4112.1	4066.7	4033.0	4006.5	3959.5	3915.8	3841.6
2005	44.7	33.9	33.0	31.2	28.9	27.5	26.2	25.1	24.4	23.8
2006	195.0	476.8	474.0	463.9	454.0	444.5	439.1	428.0	418.3	404.7
2007	454.8	814.5	810.3	799.2	784.1	774.8	767.7	755.4	743.4	726.7
2008	332.9	743.9	740.1	729.7	719.4	711.1	704.8	694.5	685.4	673.4
2009	895.9	1334.6	1324.2	1302.7	1276.3	1257.6	1244.9	1220.2	1202.2	1173.6
2010	38.1	130.4	129.4	123.7	118.6	116.5	115.5	113.2	110.9	107.6

Source: The author

APPENDIX D - PERCENTAGE OF ANNUAL STREAMFLOW REDUCTION AT MALHADA STATION FOR EACH INCREASE IN THE NUMBER OF SMALL RESERVOIRS PER YEAR OF SIMULATION

Table D.1 - Percentage of annual streamflow reduction at Malhada Station for each increase in the number of small reservoirs per year of simulation

Annual Percentage of Flow Reduction									
Year	Reference model	Simulation models - Small reservoirs per area of catchment							
		0.1/km²	0.25/km²	0.5/km²	0.75/km²	1.0/km²	1.5/km²	2.0/km²	3.0/km²
1981	-	-0.4%	-2.3%	-4.9%	-6.4%	-7.6%	-9.1%	-10.4%	-12.3%
1982	-	-0.6%	-2.7%	-5.4%	-6.9%	-8.3%	-10.1%	-11.6%	-13.8%
1983	-	-1.6%	-6.2%	-10.4%	-12.6%	-14.2%	-17.1%	-19.2%	-21.5%
1984	-	-0.5%	-2.1%	-4.1%	-5.5%	-6.8%	-8.6%	-10.1%	-12.1%
1985	-	-0.2%	-1.1%	-2.4%	-3.4%	-4.4%	-5.8%	-7.3%	-9.4%
1986	-	-0.3%	-1.0%	-1.7%	-2.3%	-2.7%	-3.6%	-4.3%	-5.5%
1987	-	-0.1%	-1.2%	-2.3%	-3.3%	-4.0%	-5.5%	-6.6%	-8.2%
1988	-	-0.4%	-2.1%	-3.7%	-4.8%	-5.9%	-8.4%	-10.0%	-12.2%
1989	-	-0.2%	-1.1%	-2.0%	-2.6%	-3.2%	-4.1%	-5.2%	-6.7%
1990	-	-0.3%	-1.1%	-2.2%	-2.9%	-3.6%	-5.0%	-5.8%	-7.1%
1991	-	-2.4%	-4.1%	-6.0%	-7.5%	-8.5%	-9.8%	-10.9%	-12.1%
1992	-	-0.5%	-2.2%	-4.3%	-5.9%	-6.9%	-8.5%	-9.7%	-12.0%
1993	-	-3.5%	-8.7%	-10.5%	-11.7%	-12.6%	-14.0%	-14.9%	-15.9%
1994	-	-1.0%	-3.3%	-5.6%	-7.9%	-9.8%	-11.4%	-13.8%	-16.6%
1995	-	-0.6%	-2.3%	-4.2%	-5.7%	-7.0%	-8.8%	-10.3%	-12.4%
1996	-	-0.6%	-2.9%	-5.4%	-7.2%	-9.0%	-11.0%	-12.5%	-15.6%
1997	-	-0.5%	-2.6%	-5.0%	-6.7%	-7.8%	-9.5%	-11.2%	-14.0%
1998	-	-2.0%	-8.6%	-14.5%	-18.0%	-20.6%	-24.0%	-26.4%	-30.3%
1999	-	-0.8%	-4.0%	-8.9%	-13.0%	-15.8%	-19.2%	-20.9%	-23.5%
2000	-	-0.8%	-2.9%	-5.4%	-7.2%	-8.5%	-10.9%	-13.0%	-16.2%
2001	-	-0.6%	-1.6%	-2.5%	-3.2%	-3.7%	-4.5%	-5.1%	-5.8%
2002	-	-0.5%	-2.6%	-5.0%	-6.3%	-7.8%	-9.8%	-11.4%	-13.2%
2003	-	-1.0%	-4.4%	-8.4%	-10.9%	-12.2%	-14.7%	-16.2%	-18.6%
2004	-	-0.2%	-1.1%	-2.2%	-3.0%	-3.6%	-4.8%	-5.8%	-7.6%
2005	-	-2.5%	-8.1%	-14.6%	-18.9%	-22.6%	-26.0%	-27.9%	-29.8%
2006	-	-0.6%	-2.7%	-4.8%	-6.8%	-7.9%	-10.3%	-12.3%	-15.1%
2007	-	-0.5%	-1.9%	-3.7%	-4.9%	-5.7%	-7.3%	-8.7%	-10.8%
2008	-	-0.5%	-1.9%	-3.3%	-4.4%	-5.3%	-6.6%	-7.9%	-9.5%
2009	-	-0.8%	-2.4%	-4.4%	-5.8%	-6.7%	-8.6%	-9.9%	-12.1%
2010	-	-0.8%	-5.2%	-9.1%	-10.6%	-11.5%	-13.2%	-14.9%	-17.5%

Source: The author

APPENDIX E - ANALYSIS OF LAND USE CHANGES BEFORE AND AFTER DROUGHT PERIOD (2012-2017)

Human-induced land use changes were evaluated using data from the MapBiomas project, which leverages satellite imagery—specifically from Landsat—to produce annual land cover and land use (LCLU) maps spanning from 1985 to 2023 in its latest version (collection 9). The project's methodology combines remote sensing data with advanced machine learning algorithms to classify various land cover types, including forests, agriculture, urban areas, water bodies, and others. The base data, derived from Landsat sensors, is processed to achieve high accuracy in detecting land use changes over time. Figure E.1 illustrates the general methodology steps of MapBiomas algorithms.

MapBiomas' approach involves collaboration with experts across fields such as ecology, geology, and computer science to refine its classification algorithms. The data undergoes validation through field surveys, high-resolution imagery, and cross-referencing with other datasets. The output includes detailed maps and time series that monitor the conversion of natural landscapes into agricultural or urban areas, deforestation rates, and the expansion of water bodies (MapBiomas, 2024).

The data provided by the MapBiomas project modules was intersected with the shapefile of the Malhada catchment to generate annual land use maps. Since no data is available for 1979, the analysis began with the 1985 land use map, representing the early years of simulation. An intermediate map was obtained for 2010, marking the end of the calibration period, and a final map for 2022, marking the end of the extended simulation period. These three maps were combined into a single figure to enable a visual analysis of spatial changes within the Malhada catchment across the time points of 1985, 2010, and 2022. The land uses identified in the catchment include a kind of savanna formation (Caatinga, the Brazilian dry forest), grassland, pasture, mosaic of uses (areas where it is not possible to distinguish between pasture and agriculture), urban areas, water bodies, and temporary crops.

Figure E.1 – General Methodology Steps of MapBiomas Project

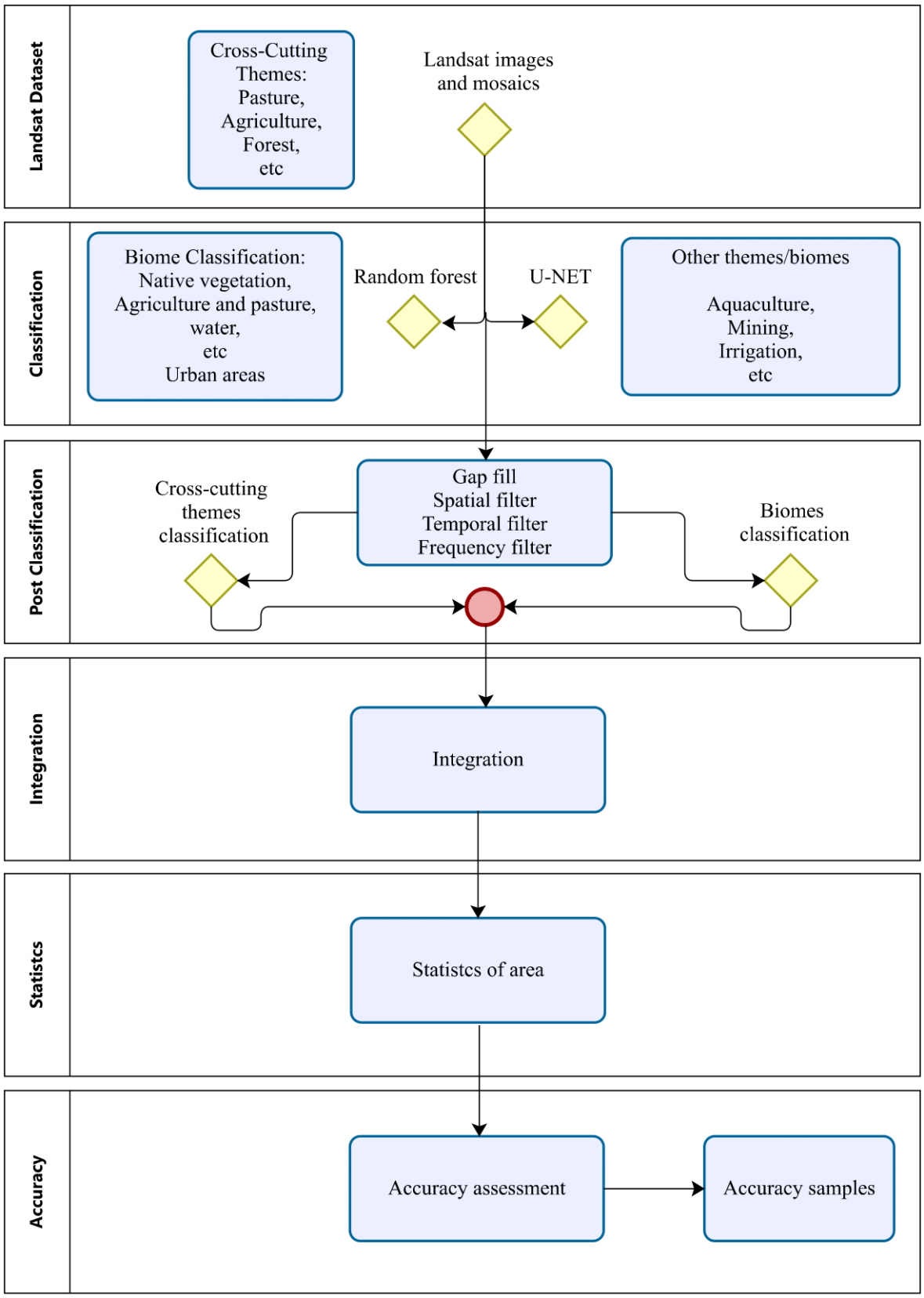

Source: The author

Additionally, quantitative data on land use areas for each year is also available from the MapBiomas project, allowing for a graphical analysis of the evolution of these areas (in hectares) from 1985 to 2022. This graphical analysis was divided into two charts due to differences in area magnitudes: the first chart includes information on savanna formation, pasture, and mosaic of uses, while the second covers water bodies, urban areas, and grasslands. Temporary crops appear on both charts to highlight the point of abrupt growth in this land use, transitioning from one scale to another.

To quantify the analysis of the increase and decrease in savanna formation, pasture, and water body areas, Sen's slope was applied, associated with the modified MK test (Yue and Wang, 2004). This approach was used to evaluate the trends in savanna formation, from 1985 to 2010, and from 2011 to 2022; pasture, from 1985 to 2010, and from 2011 to 2022; temporary crops, from 1999 to 2010, and from 2011 to 2017; water body areas decrease from 1985 to 2000, and from 2010 to 2017; and water body areas increase from 2001 to 2004, and from 2018 to 2022.

To analyze human-induced modifications in the study area, Figure E.2 presents land use maps of 1985, 2010, and 2022 within the Malhada catchment. The analysis of Figure E.2 suggests that in 1985 the catchment was predominantly covered by Caatinga, with small areas of pasture concentrated near urban zones. By 2010, an expansion in pasture areas, mosaic of uses, and temporary crops—mainly in the upper watershed—became evident. Pasture areas significantly increased in regions close to the area’s watercourses. Finally, in the 2022 map, a trend toward stabilization in pasture areas is observed, though there is a continued increase in areas dominated by temporary crops.

The comparison between maps allows for an assessment of spatial changes, indicating an advancement in the degradation of natural vegetation within the catchment (Caatinga savanna formations), accompanied by agricultural expansion, particularly in regions demarcated by the watercourses, as well as urban growth in nearby cities. This progressive modification can alter evapotranspiration and infiltration patterns, and an extreme drought may abruptly drive the catchment toward a new stable state. This trend is illustrated in Figure E.3, which shows the evolution of areas dominated by each land use type.

Figure E.2 – Land Use Maps of Malhada Catchment in 1985, 2010, and 2022

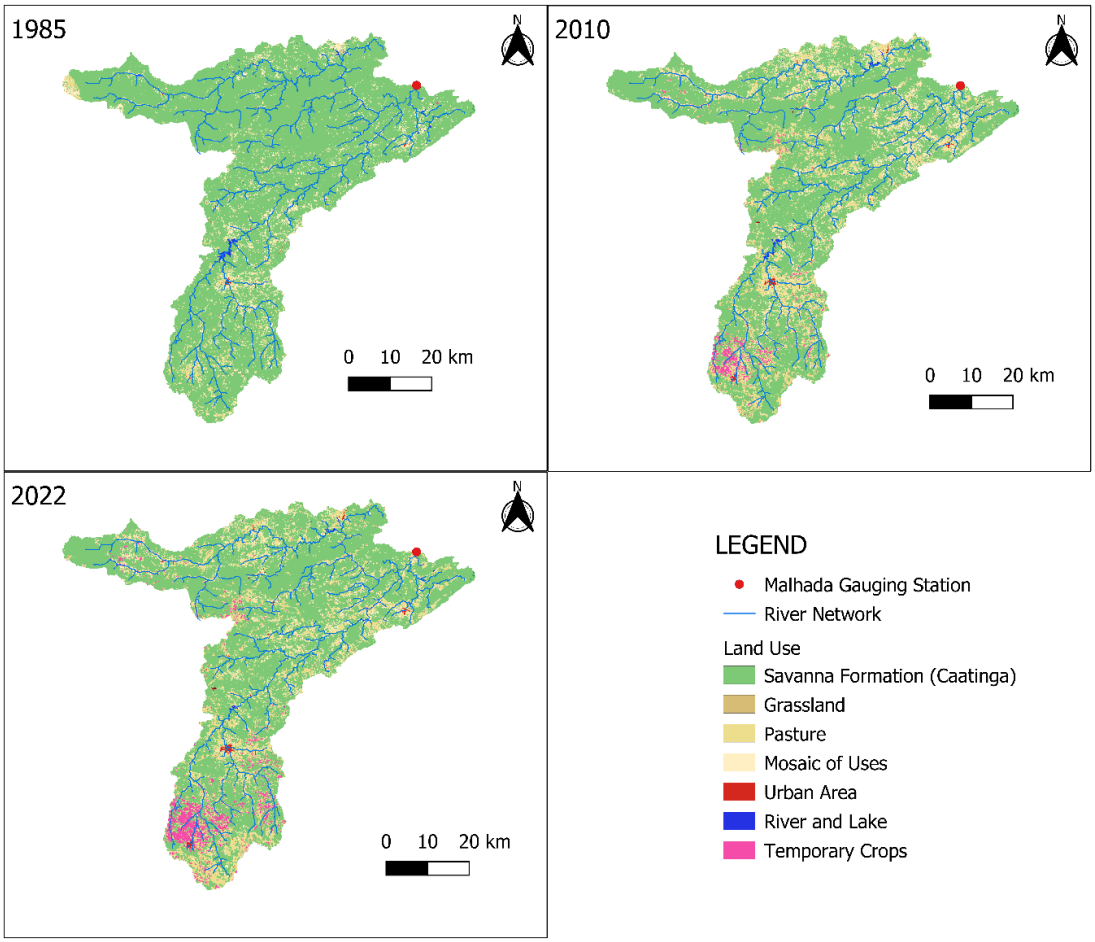

Source: The author

The analysis of Figure E.3 reveals a clear trend of degradation in the Caatinga area, which decreased from approximately 400,000 hectares in 1985 to around 317,000 hectares in 2010 ($z = -10.93$, p-value ≈ 0.000, Sen's slope = -3488.54 ha/year). This reduction process in Caatinga area appears to slow after 2010, with the area totaling about 309,000 hectares by the end of 2022 ($z = -0.57$, p-value = 0.570, Sen's slope = -119.27 ha/year). A similar trend is observed in the sharp increase in pasture, which expanded from approximately 13,000 hectares in 1985 to around 80,000 hectares in 2010 ($z = 10.29$, p-value ≈ 0.000, Sen's slope = 3440.59 ha/year), ultimately reaching about 86,000 hectares in 2022 ($z = 1.80$, p-value = 0.071, Sen's slope = 541.90 ha/year). Notably, temporary crops had two increase periods, the first one from 1999 to 2010 ($z = 6.37$, p-value ≈ 0.000, Sen's slope = 522.89 ha/year), and the second one from 2011 to 2017 ($z = 5.22$, p-value ≈ 0.000, Sen's slope = 1615.83 ha/year), as graphically presented in Figures E.3 and E.4.

Figure E.4 illustrates the evolution of surface areas identified as water bodies, specifically rivers and reservoirs within the study area. A reduction in water areas is observed from 1985 to 2000 (Z = -5.64, p-value ≈ 0.000, Sen's slope = -108.36 ha/year), with an increase from 2001 to 2004 (z = 3.14, p-value = 0.002, Sen's slope = 433.28 ha/year). From 2010 to 2017, there is a marked reduction in water areas (z = -5.29, p-value ≈ 0.000, Sen's slope = -155.96 ha/year), corresponding to the prolonged drought. A slight recovery occurred from 2018 to 2022 (z = 5.39, p-value ≈ 0.000, Sen's slope = 83.32 ha/year), consistent with the hydrological recovery phase. Given the absence of abrupt land-use changes during the drought, continuous degradation combined with the abrupt post-2010 drought may lead to a non-linear shift in the watershed's hydrological behavior, potentially resulting in a slower hydrological recovery. Urban areas showed continuous growth during the period analyzed, while grasslands showed two notable periods of increase, the first from 1992 to 1999, between the drought period of 1990 – 1993 and the extreme dry year of 1998, and the second one from 2012 to 2017, corresponding to the recent drought.

Figure E.3 – Evolution of Savanna Formation (Caatinga), Pasture, Mosaic of Uses, and Temporary Crops from 1985 to 2022

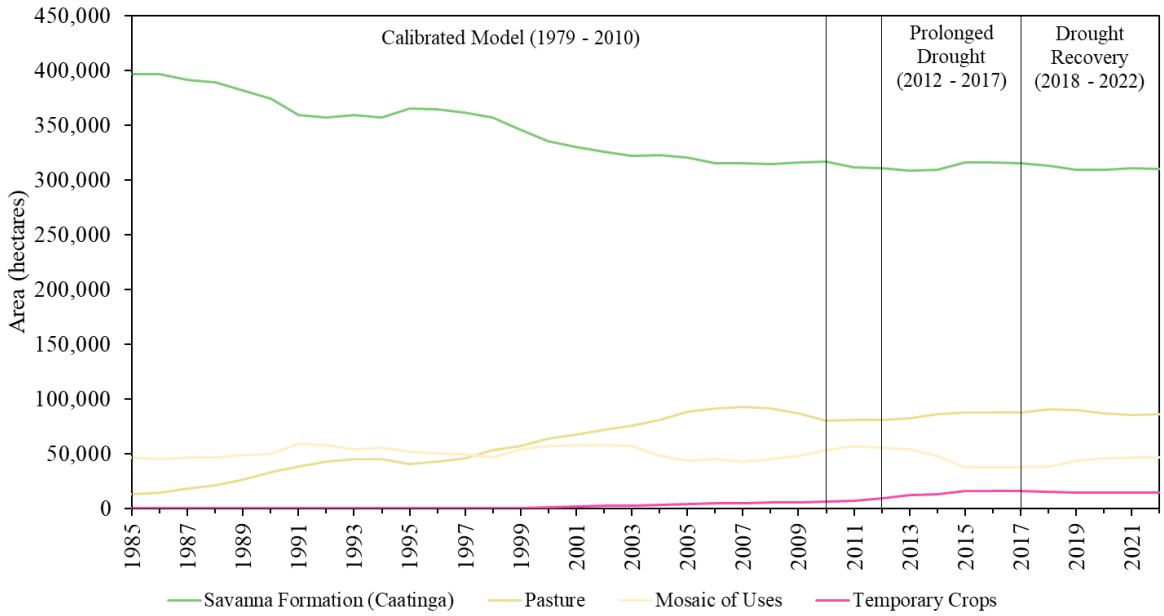

Source: The author

Figure E.4 – Evolution of Water Bodies Areas, Grasslands, Urban Areas, and Temporary Crops from 1985 to 2022

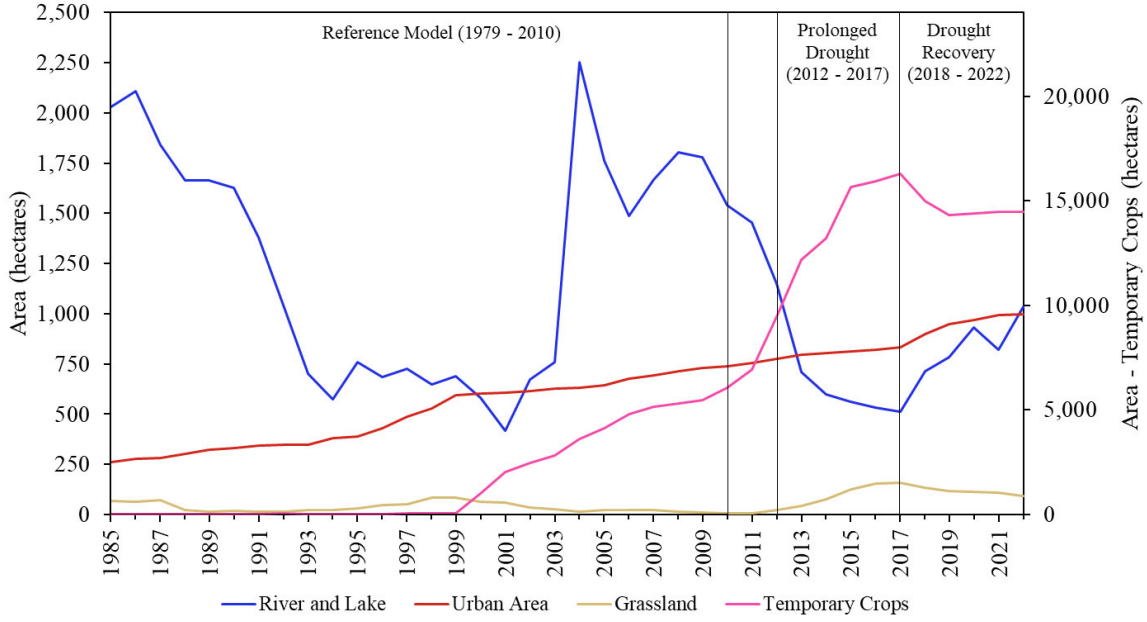

Source: The author